The University of Aston in Birmingham

Damage Analysis of Bridge Structures Using Vibrational Techniques

Michael George Wood

Doctor of Philosophy

October 1992

The University of Aston in Birmingham

Damage Analysis of Bridge Structures Using Vibrational Techniques

by

Michael George Wood

Doctor of Philosophy

October 1992

Much research is currently centred on the detection of damage in structures using vibrational data. The work presented here examined several areas of interest in support of a practical technique for identifying and locating damage within bridge structures using apparent changes in their vibrational response to known excitation. The proposed goals of such a technique included the need for the measurement system to be operated on site by a minimum number of staff and that the procedure should be as non-invasive to the bridge traffic-flow as possible.

Initially the research investigated changes in the vibrational bending characteristics of two series of large-scale model bridge-beams in the laboratory and these included ordinary-reinforced and post-tensioned, prestressed designs. Each beam was progressively damaged at predetermined positions and its vibrational response to impact excitation was analysed. For the load-regime utilised the results suggested that the induced damage manifested itself as a function of the span of a beam rather than a localised area. A power-law relating apparent damage with the applied loading and prestress levels was then proposed, together with a qualitative vibrational measure of structural damage.

In parallel with the laboratory experiments a series of tests were undertaken at the sites of a number of highway bridges. The bridges selected had differing types of construction and geometric design including composite-concrete, concrete slab-and-beam, concrete-slab with supporting steel-troughing constructions together with regular-rectangular, skewed and heavily-skewed geometries. Initial investigations were made of the feasibility and reliability of various methods of structure excitation including traffic and impulse methods. It was found that localised impact using a sledge-hammer was ideal for the purposes of this work and that a cartridge 'bolt-gun' could be used in some specific cases. The main response monitoring programme was undertaken during periods which included the extremes of atmospheric climate typical of the Birmingham area. Air temperatures, humidities and general weather conditions measured on the day of test were noted in addition to surface temperatures present at locations on the bridge structures. From this data compilation a careful comparison of the measured variables established that the major influences on the bridge responses were related to the structural temperature. Analyses based on these data suggested that the major cause of changes in the structural stiffness due to temperature was the variability of the asphalt 'black-top' moduli. It was also suggested that thermal expansion in the transverse axes of composite constructions would modify these response changes since cracks in transformed sections would close.

Keywords:

Damage Vibration Bridges Beams Concrete Temperature

To my wife and parents:

Jayne, Iain and Connie.

" In research the horizon recedes as we advance, and is no nearer at sixty than it was at twenty. As the power of endurance weakens with age, the urgency of the pursuit grows more intense .... And research is always incomplete "

Mark Pattison (1813-1884)

Acknowledgements :

The author would like to express his sincerest thanks to the following:

Dr. John Penny, university supervisor.

Dr. Malcolm Bailey, company supervisor.

Drs Mike Friswell and John Purkiss, associate supervisors.

Mr. John Wilson, formerly Principal Engineer (Bridges) within the Structural Division of the City of Birmingham's Engineers Department.

Mr. Brian Muddyman, vibration laboratory technician.

Technical staff of the Department of Civil Engineering.

Thanks are also expressed to:

Messrs Bill Revie, Peter Baxter and Crawford Currie: present and past members of Stanger Consultants Limited (Glasgow and Elstree), Prof. John Turner of Southampton University, Dr. Tony Pretlove of Reading University, Mary Emerson of TRRL (Livingston) and Mr. F.A. Rapattoni of Vic'Roads, Kew, South Australia.

Drs Alastair Cochran and David van Rest.

Drs Colin Thornton, Ian Cole, John Maiden, Neil Short, Roger Kettle, Seamus Garvey and Messrs Bill Flint and Len Crane.

Fellow research students Al' Pilkington, Al' Roger, Andrew Carruthers, Clive Bright, Denis Greene, Helen Jones, Jason Hill, Neil Newman and Paul Edmunds.

Special thanks are expressed to Mr. Len Cole, Technical Manager (Vibrations Division) of Boxmag Rapid Ltd.; Mr. Maurice Hunt, Managing Director of T & E (Designs) Ltd. and Mr. John Montgomery, Director of J.W. Worsley (Coventry) Ltd. without whose timely financial support this research would not have been completed and submitted for examination.

Contents:

Figures:

Chapter 4: Experimental Bridge-Beam Data Analysis

Chapter 5: Experimental Testing and Monitoring of Highway Bridges

Chapter 6: Experimental Bridge Monitoring Data Analysis

Appendices:

Appendix 3: Ancilliary Beam Test Equipment

Appendix 5: Bridge-Structure Details And Dynamic Analysis Models

Appendix 6: Bridge-Site Monitoring Data Compilations

Tables:

Chapter 3: Experimental Bridge-Beam Testing

Chapter 4: Experimental Bridge-Beam Data Analysis

Chapter 5: Experimental Monitoring Of Highway Bridges

Chapter 6: Experimental Bridge Monitoring Data Analysis

Appendices

Appendix 6: Bridge-Site Monitoring Data Compilations

Nomenclature:

a	=	distance along beam to the lower bound of the damage region
A, $A(\omega)$,A_{ij}	=	Inertance (i.e. acceleration$_i$/impact force$_j$)
$\boldsymbol{A}$, $[A]$	=	stiffness matrix applied to the generalised Eigenvalue problem
A_S	=	area of reinforcement steel in tension
A_S'	=	area of reinforcement steel in compression
b	=	distance along beam to the upper bound of the damage region
B	=	width of concrete in tension zone, asphalt layer or beam width
B'	=	width of concrete in compression zone
$\boldsymbol{B}$, $[B]$	=	mass matrix applied to the generalised Eigenvalue problem
$C_{,i}$	=	constant
d	=	depth to tensile reinforcement from top face of beam
d'	=	depth to compressive reinforcement from top face of beam
$E_{,dyn}$	=	Young's elastic modulus in the undamaged state, dynamic
E_C	=	concrete Young's elastic modulus
E_S	=	steel Young's elastic modulus
$EI_{,dyn,cr}$	=	flexural rigidity of beam section, dynamic, cracked
f_{ps}	=	applied prestress over beam section
f_y	=	steel yield stress
f_{Dn}	=	linear beam frequency observed in the damaged state
F	=	visco-elastic constant
F_C	=	concrete compression equilibrium force
F_{ps}	=	tensile zone concrete prestress equilibrium force
F_{ps}'	=	compressive zone concrete prestress equilibrium force
F_S	=	tensile zone steel reinforcement equilibrium force
F_S'	=	compressive zone steel reinforcement equilibrium force
ΣF_{int}	=	sum of internal forces
H,η	=	non-linear coefficient, measure of damage
h	=	beam depth
I	=	principal second moment of beam area in the undamaged state
I_{cr}	=	principal second moment of beam area in the cracked state
I_{eff}	=	effective principal second moment of beam area

i, j	=	integer, subscript, index, superscript coefficient (i.e. power)
K_{ps}	=	effective prestress factor
$K_{slab,\ 1,\ 2,\ 3}$	=	torsional stiffness of bridge-deck substructures
K_{ij}	=	stiffness coefficient
L	=	beam span
L_{ij}	=	length between idealised masses
M	=	overall beam mass
$M_{applied}$	=	externally applied moment to beam system
M_{cr}	=	externally applied moment that creates macrocracks in beam section
ΣM_{ext}	=	sum of external moments
ΣM_{int}	=	sum of internal moments
m	=	beam mass per unit length
m_i	=	idealised beam mass
N_x, N_y	=	number of grillage beams along principal axes
n	=	observed mode of vibration
P	=	post-tensioned beam designation
Q_i	=	dynamic/static force coefficient
q, q_{ij}	=	generalised displacement
q_n	=	generalised displacement series
q''	=	second derivative of a displacement, series with respect to time
R	=	ordinary-reinforced beam designation
R_a	=	alpha ratio
$R_{m,s,c}$	=	load ratio (moment, steel, concrete)
T_{max}	=	kinetic energy of a conservative vibrating beam system
T^*	=	reference kinetic energy of the system (from $T_{max}= \omega^2.T^*$)
t	=	asphalt layer thickness
V_{max}	=	potential energy of a conservative vibrating beam system
x	=	depth to beam neutral-axis from top face of beam
x, y, z	=	displacements in principal directions, distances along principal axes
{Y}	=	abritrary displacement vector for a vibrating system
α	=	observed change in flexural rigidity
α_s	=	modular ratio
α_{ij}	=	receptance (i.e. q_i/ Q_j)
α	=	constant in expression for I_{eff}

β	=	proportion of beam span bounded by 'a' and 'b'
β	=	constant in expression for I_{eff}
δ	=	$(q_1 - q_2)$
ε	=	mechanical strain
ε'	=	mechanical strain rate (i.e. $d\varepsilon/dt$)
ε_c	=	outer-fibre concrete compressive strain
$\varepsilon_{c\ max}$	=	maximum induced concrete strain
ε_{ps}	=	prestress induced concrete strain
ε_s	=	tensile reinforcement strain
ε_s'	=	compressive reinforcement strain
σ	=	mechanical stress
ϕ	=	shape function
ϕ_n	=	shape function series
ϕ''	=	second derivative of the shape function with respect to 'x'
ω	=	rotational frequency
ω_{Dn}	=	n^{th} natural frequency of the damaged beam
ω_n	=	n^{th} natural frequency of the undamaged beam
$\{0\}$	=	zero vector

Chapter 1: Introduction

"Bridge design is the art of moulding materials we do not wholly understand into shapes we cannot precisely analyse so as to withstand forces we cannot really assess, in such a way that the community at large has no reason to suspect the extent of our ignorance"

Anon

1.1 Introduction

The research presented here concerns two areas which contribute towards the goal of a 'damage' diagnostic test for bridge structures based on vibrational responses. This chapter introduces the objectives sought, the project origins and the subsequent research programme. It also introduces the collaborating company, discusses the administrative scheme under which the research was carried out and concludes by detailing the structure of this thesis.

1.2 Research Objectives

There were two objectives identified for this programme of research. The first objective was to establish a method relating the vibrational responses of bridge-beams with their levels of induced damage and the second was to obtain test data relating any changes in the vibrational response of bridges due to ambient temperature conditions.

1.2.1 Topic Evolution

The technology of bridge design and construction originates from an early age. Design methodology has changed from 'trial and error' origins to the complex procedural codes of the present day. Methods of construction have evolved in parallel with the engineering materials available through the resource ages of stone, wood, brick and cast/wrought-iron to the steels and reinforced composites of today. Recently there has also been the need to accurately assess damage present within such structures resulting from the traffic loadings experienced.

Damage to bridge structures may be caused in one of five ways; they may be

(i) statically underdesigned (i.e. overloaded)

(ii) erected using substandard constructional techniques (i.e. poor quality work)

(iii) subject to fatiguing cyclic effects (i.e. alternating loads due to traffic or ambient air conditions)

(iv) subject to changes at the structure boundary conditions (e.g. changes in the media surrounding the bridge foundations from moisture ingress or egress)

(v) subject to substandard maintenance procedures (e.g. support bearings not replaced within the service life or weather-proofing deterioration without periodic replacement)

In practice a bridge will be subject to the effects of all the above to some degree. The problem of underdesign is not typical of present-day bridge construction unless actual traffic volumes exceed those specified for design. Resultant bridge form and, hence, behaviour has remained unpredictable even utilising the most recent bridge-design codes since completed bridges are, in the main, outside their prescribed design-tolerances and also incorporate many construction concessions (Hall *et al*, 1978).

With an engineering material such as reinforced concrete and the scale of construction in which it is employed it is understandable then that localised imperfections can (and will) occur in the erection of *in-situ* highway bridges due to the inherent nature of the construction process. Secondary effects, such as carbonation or corrosion, may subsequently act to exacerbate the problem of damage. In some cases these effects may be observed within four years of construction (Woodward, 1981).

Service loading creates its own manner of damage: fatigue. Fatigue mechanisms will always be present within a bridge-structure due to the cyclic nature of any loading originating from the motion of a vehicle traversing its bridge-deck. These mechanisms are also present in structures where prestress effectively constrains the resultant stress magnitudes to compression alone. The overall result is that cracking will occur and this leads to eventual failure if allowed to propagate throughout a structure. Cyclic loading may also be produced by wind effects. An extreme case in point is that recorded by the famous cinematographic footage of the spectacular oscillations and subsequent catastrophic failure of the Tacoma Narrows bridge (Gordon, 1978).

Soil mechanics show that for a marginal change in moisture content the density and compaction properties of most common foundation-bed materials will vary considerably. This in turn affects the dynamic properties of the supporting medium which will ultimately alter the response of a structure to the fatigue-inducing cyclic loading. The final consideration is that of substandard inspection and preventative maintenance procedures. This aspect of bridge management has given cause for concern with the result that conferences have been convened and governmental standards have been created to address this problem (IStructE, 1988)

A further consideration is that relatively recent transport legislation has allowed road-hauliers to increase the overall, static loading of their vehicles by nearly 20%. Although the nature in the design of articulated-trailers has supposedly been modified to compensate for these changes, the number of axle and bogie loadings will have risen by a greater percentage. Other legislation has dictated that certain (if not all) motorways may

be modified from six to eight-lane configurations and, hence, the overall effect is to increase both the magnitude and density of loadings over bridge structures. In certain circumstances the dynamic effect of these increased loadings will be to raise those structural fatigue rates already observed in some bridge decks (Tilley and Page, 1980).

It is of great importance that a practical technique is developed to identify potentially dangerous changes in the structural condition of bridges since many thousands in Britain are of various ages and states of repair. The purpose of this research was to build on established work whose goal was a method of damage location for bridge-structures.

1.2.2 Feasibility Study

During the mid-1980's two members of Stanger Consultants Limited, Mr. Peter Baxter and Dr. Malcolm Bailey, became aware of bridge damage research nearing completion at The University of Reading (Turner, 1984). Both were also aware of the potential of such a technique if it could be fully implemented. A basis was then prepared for furthering this avenue of research and The University of Aston in Birmingham was approached to undertake this work in early 1989. Stanger Consultants' position was that this research would represent a diversification into a new product area which, if successful, could be the basis of a large market share from a relatively small investment.

The task was then to instigate a programme of research to address the requirement of a "detection technique for damage in bridge structures". A number of investigative techniques have already been applied to road surfaces and bridge-deck structures with varying degrees of success. One method in particular showed promise, namely the variation in vibrational response of the bridges due to structural changes caused by damage.

1.2.3 Research Proposal

Earlier investigative research into the problems of both recognising and locating damage within one- and two-dimensional structures had met with considerable success with the result that a natural progression was made by attempting to implement this methodology in bridge structures. Using these advances as a foundation, the work presented here was instigated to further and broaden the area research. This research contribution would provide additional knowledge towards a workable solution in the problem of detecting damage within bridge structures using vibration techniques.

1.3 Research Methodology

The different themes of the programme were undertaken in parallel with one another. However, in common with most projects of this type there was an interdependency between each stream to varying degrees.

1.3.1 Literature Review

A comprehensive review of available literature on areas surrounding bridge damage and monitoring was instigated. Texts, Codes of Practice and other Standards were consulted in order to become familiar with bridge-structure theory and also to identify any relevant technical publications. A number of technical and conference publications sources were identified which were periodically consulted for current information of relevance to the project. Finally direct contact was established with research groups, individuals and commercial concerns who were or had been active within the "structural-dynamics" and "damage-location" fields. Thus a comprehensive compilation of past and presently available information from the project area was created.

1.3.2 Experimental Beam Investigations

The experimental work undertaken on the modelled bridge-beams was to establish the relationship between induced damage position and levels with changes in the structure response frequencies. Two series of beam designs were selected: ordinary-reinforced and post-tensioned. These were designed and manufactured to similar specifications so that the resultant data between each series would be comparable. Static load-testing procedures were also standardised so that comparative analyses could again be applied.

1.3.3 Bridge-Monitoring Programme

In order to establish the effects (if any) on the vibration responses of bridge-structures due to ambient conditions a programme of site monitoring was undertaken on several bridges. These sites were chosen due to their varied nature in both design and construction. Tests and measurements were made at approximately one week intervals between late February and early October during 1991. Resultant data from these investigations were correlated to identify the main parameters which influenced the natural frequencies of these structures.

1.3.4 Predictive Analyses

There are several methods of predictive analysis that can be applied to the dynamic behaviour of bridge-structures. In this case the response frequencies of the monitored bridges were estimated using the computer modelling technique of 'grillage' analysis. The application of this technique to establish the static behaviour of bridge-decks may be said to be the construction industry standard but little or no general use appears to have made of this method in its dynamic formulation.

1.4 Collaborating Organisation

The Stanger organisation was founded in 1874. It has built its reputation around selection, evaluation, testing and quality assurance of processes and manufactured products as well as building materials and structures. Together with their associated companies in the U.K. and overseas, they employ approximately five hundred professional and support staff covering the majority of materials technology. Recently the organisation consolidated its position by becoming part of the Tarmac multi-national company and has continued as a specialist niche within the construction engineering industry.

1.5 Interdisciplinary Higher Degrees Scheme

The research presented here has been completed under the guidance of the I.H.D. Scheme within Aston University. The scheme was established in 1968 after the ***Swann Report*** and is designed to provide advanced postgraduate training for engineers and applied scientists, which allows the project topic to combine academic research with a technical problem which has its origins in industry. Students undertake a minimum of one-hundred and twenty hours of examinable study from various taught courses in parallel with the normal research workload of a higher degree. The lecture content is not to be associated with the research topic and, here, four modules were chosen from the Aston Business School M.B.A. A more detailed text on the origins, aims, development and notable successes of the I.H.D. Scheme has been produced by Cochran (1981).

1.6 Thesis Content

The work in this thesis has been divided into a further six chapters. Chapter 2 presents a critical assessment of published work. It discusses in turn beam testing, bridge-structure monitoring and the grillage analysis method. Chapters 3 and 4 present the experimental data and analyses from the model bridge-beam test programme. Chapter 3 presents design, manufacturing and test methodologies together with a discussion of the results. Chapter 4 concentrates on the static and dynamic analyses of the Chapter 3 data.

Chapters 5 and 6 include the monitoring techniques, resultant data and their analysis for the chosen bridges in the Birmingham area. The test sites, structural excitation, response measurement methods and ambient condition variables are described in Chapter 5. Ambient condition data, bridge-structure temperature measurement and resultant statistical and predictive response techniques employed are discussed within Chapter 6, together with the relevant conclusions.

Chapter 7 presents an overall concluding discussion to the thesis content and proposes additional research. The appendices which conclude this thesis consist of a discussion of the procedural safety aspects which arose during these investigations, additional beam-testing equipment information, bridge modelling details, presents the bridge-monitoring data analysis summaries and include copies of the technical publications originating from this work. Attention now centres on the literature available in the areas of research addressed by this work.

Chapter 2: Literature Review

"Oui, cela e'tait autrefois ainsi, mais nous avons change' tout cela"

"Yes, it used to be so, but we have changed all that"

Jean Baptiste Poquelin, *i.e.* **Moliére** (1622 - 1673)

2.1 Introduction

The review presented here is divided into three principal areas of interest: damage related response changes in vibrating bridge-beams, monitoring changes in the natural frequencies of bridge-decks and the application of grillage (or grids) analysis to vibrating structures.

2.2 Beam Testing

Although static testing has been undertaken since the early developments in their construction, investigation into the dynamic characteristics of bridge beams is a relatively recent innovation. Penzien (1964) undertook a series of dynamic tests on 24 reinforced concrete beams which were nominally 0·15 x 0·15 x 2·28 m in size. The condition of the specimens varied in type and level of prestress, also in the constituent concrete properties. The reinforcement designs were based on single bars of numbers 6 and 9 high-strength, deformable steel with yield stresses of 655 N/mm^2 and 965 N/mm^2 respectively. The designs included one bar which was central or eccentric to the axial centroid of the beams and two-bar configurations which were symmetrical about the horizontal plane through the centroid. The induced axial prestress was varied in both magnitude and form over the range of test-beams. The uniform-profile prestress ranged from zero to a maximum of 20 N/mm^2 and variations on a basically triangular-profile ranged from a minimum of 6 N/mm^2 to a maximum of 28 N/mm^2. The accompanying 28 day concrete cube strengths varied between 28 N/mm^2 and 44 N/mm^2 for this series of beams.

Two methods of dynamic loading were applied in the testing of the beams. Initially the specimen was supported as a free-free beam using low-stiffness suspension springs and a steady-state, harmonic excitation was applied to the mid-span position. The system resonances were obtained by varying the excitation-frequency and ensuring that load-application and beam-response were in phase. In each case problems associated with load-measurement sensitivity limited useful data to that obtained from the fundamental mode. Measures of the Dynamic Magnification Factor (DMF) were obtained from the calculated displacements using harmonic excitations of 55 N, 110 N and 220 N: where the DMF is the ratio of dynamic to static beam deflection for a given load magnitude.

The second method of dynamic loading used a step-relaxation technique to produce decaying transient-responses in each beam. To achieve those responses each beam was statically loaded in an upward direction at the mid-span position when effectively simply-supported at each end. The magnitude of the load was varied to obtain predetermined static deflections of up to 12 mm and the free-vibration responses of the beam were recorded after the sudden removal of each load. By measuring the magnitudes of successive peaks from the resultant beam displacement histories a second measure of damping was obtained using the log-decrement technique (Thomson, 1988).

From the steady-state test results it was observed that damping was a function of prestress level. The ordinary-reinforced specimens showed the highest damping ratios, typically 2·3% for the 110 N loading, whilst comparable prestressed configurations exhibited a damping ratio of only 0·7% for the same loading. Triangular-profile prestress specimens had similar damping characteristics to those of the uniform-profile prestress beams. Free-vibration results were based on measurements over four cycles of the beam data and although broad agreement in the trend of increased damping ratio with increasing load was observed it was noted that:

> "... difficulty [of correlation between steady-state and free-vibration damping ratios] would seem to be due to the fact that in most cases the initial maximum displacements are sufficiently large to produce cracking "

The main conclusion drawn by Penzien was that the internal damping of the beams was directly related to the "history of loading" and, hence, the number and severity of cracks present throughout the structure. It followed that the magnitude of prestress present dictated any change in damping loss characteristics for a given loading.

More recently work by Hop (1991) provided much long-term data concerning the dynamic behaviour of concrete beams over a 20 year period during which changes in natural frequency and damping characteristics were investigated. Initially 4 reinforced and 19 prestressed test-beams were produced during a period from November 1959 to May 1960. The design of each series of ordinary-reinforced and prestressed beams varied reinforcement configuration, prestress levels and constituent concrete properties. Early destruction tests on 8 beams left 15 specimens of normal concrete-aggregate properties available for the long-term investigations. The design of the remaining test-beams was based on a 5·0 m length incorporating a 4·8 m span between support positions. Beam depth and width was varied with the former being either 180 mm or

Table 2.1 Long-term test-beam damping results (after Hop, 1991)

300 mm and the latter either 100 mm or 120 mm. The reinforcement regimes were varied between single symmetric or eccentric-parabolic prestress ducting arrangements and eccentric singly- or doubly-reinforced designs with some test-beams incorporating shear reinforcement in the form of stirrups or independent, fabricated lattices. The sheathed, circular prestress core which was within each duct incorporated 10 or 12 wires of 5 mm diameter steel. The ordinary axial-reinforcing steel was 5 mm, 6 mm, 8 mm or 12 mm in diameter whilst the shear-reinforcing steel was 4.5 mm or 6 mm in diameter. The 5 mm diameter prestressing wires had a tensile strength of 1800 N/mm^2 whilst the remaining steel rod had a yield strength of 360 N/mm^2. The 28 day cylindrical crush strength of the concrete used for each test-beam varied between 29 N/mm^2 and

$50N/mm^2$. Unfortunately the only data concerning the beam prestress levels were limited to the oil-pressure indicated by the apparatus used to load the tendons. The 15 test-beams were initially stored outdoors for a period of 8 years and then indoors for a further 12 years until testing.

Details of the excitation methods and apparatus arrangements used during these vibration tests were omitted from the research paper however it is assumed that some form of step-relaxation technique was applied since cracks and cracked-states were observed. Response data was acquired using a Gieger vibrograph and later a 12-channel chart recorder. The test procedure compared the frequency and logarithmic damping decrement between beams several months old and 20 years old. A selection of the results are shown in Table 2.1.

From all the data presented by Hop it was suggested that generally the dynamic moduli of the constituent concrete mixes increased by approximately 15% over 20 years whilst damping exhibited by the ordinary-reinforced test-beams reduced by as much as 75% during the same period. Prestressed beam damping was also observed to decrease by approximately 40% in the 20 year period although the majority of damping losses occurred within days of the prestress being applied to each beam.

Attempts have been made to satisfactorily quantify the observed damping characteristics of concrete elements and, for example, James *et al* (1964) investigated the modal responses of reinforced-concrete beams and plates. Initially using the standard differential equation for vibrating Euler beams (Meirovitch, 1986), James *et al* introduced the concept of a visco-elastic strain rate component in addition to the normal stress formulation of beam bending thus:

$$\sigma = E_c\varepsilon + F\varepsilon' \qquad (2.1)$$

where: E_c = Young's elastic modulus for concrete
F = visco-elastic constant
ε = mechanical strain
ε' = mechanical strain rate with respect to time (i.e. $d\varepsilon/dt$)
σ = mechanical stress

The response characteristics of a simply-supported beam subject to a mid-span, sinusoidal point-load were then derived by manipulating a Fourier-series based on a uniformly-distributed, sinusoidal loading equi-distant about the centre of the beam. By concentrating on the fundamental mode of vibration the resultant response expression was greatly simplified such that the dynamic magnification factor could be derived implicitly. Comparisons were made between this analytical DMF and the experimental value obtained directly from the measured static and dynamic load deflections. The experimental damping ratio was obtained using the measured fundamental response frequency, the experimentally derived dynamic flexural rigidity, the applied sinusoidal load and the resultant dynamic displacement.

The innovative inclusion of a visco-elastic strain rate component within the formulation for the beam vibration theory produced theoretical damping characteristics which decreased with the mode of vibration in line with observed results. This approach also produced a theoretical DMF which was independent of the amplitude of vibration, again confirming that behaviour already understood for viscously-damped systems.

The experimental programme undertaken by James *et al* involved tests on 26 concrete beams although data from only 15 were reported. Those test-beams incorporated different designs of ordinary-reinforcement, prestress arrangement and regime, also several types of concrete mix. The overall dimensions of all the beams were 101 mm wide, 203 mm deep and 3·05 m long. The test procedure was to simply-support each beam, to excite them at the mid-span position using a variable-load shaker and measure resultant displacements using a Linear Variable Differential Transformer (LVDT). The excitation frequency varied on the beam characteristics but was in the range 30 Hz to 40Hz. The damping levels were assessed applying excitations of 18 N and 36 N whilst the DMF's were estimated using excitations ranging from 4 N to 112 N, depending on the beam behaviour. The experimental data from the test-work of James *et al* are presented in Table 2.2.

One of the conclusions drawn from the results of those beam tests was that the 10% to 15% variations in natural frequency between like prestressed and ordinary-reinforced designs with similar constituent material properties

"must be attributed to a difference in elastic moduli ."

An increase in elastic modulus is expected from concrete curing under the compacting action of a compressive load and this approach of estimating changes in the effective elastic moduli does avoid problems associated with assessing levels of prestress loss

Table 2.2 Summary of test-beam data (after James *et al* , 1964)

due to tendon creep and concrete shrinkage. However any prestress losses would have been minimal since the magnitude of end-thrust in these cases should only have produced an approximately 1% reduction in the fundamental frequency. It was observed that there were changes in the dynamic response characteristics of ordinary-reinforced beams after repeated loading but not in the prestressed configurations. It was further concluded from the beam data that load-induced crack-damage suppression through prestressing was present. This supported the work of Penzien discussed earlier. James *et al* also noted that two different frequency responses could be observed in the neighbourhood of a natural mode of vibration. Each response would be dependent upon whether the sinusoidal frequency sweep approached this mode from 'above' or 'below' when trying to establish the resonance point.

The work of James *et al* continued by addressing the problem of simply-supported prestressed 'thin' plate responses. Although including the prestress in one axis by using an approximated Poisson's ratio in the formulation, the analytical derivation of the plate vibration responses did not include the strain rate contribution of the earlier beam analysis and the mid-span point-loading was modified to two parallel line-loads at the third-span positions.

A 1·2 m square, 22 mm thick concrete plate was cast from siliceous concrete which had a 28 day cylindrical crush strength of 33 N/mm^2. The plate design incorporating 2 mm diameter music wire along one axis, 9·5 mm above the lower face at 25 mm intervals and additional reinforcement was provided by a 1 mm diameter, 12·5 mm square "hardware mesh" positioned 6 mm above and below the music wire level. The music wire arrangement produced a prestress profile which varied linearly across the thickness of the plate after preloading. The extremes of this prestress distribution after losses were estimated as 2·4 N/mm^2 at the top face and 8·3 N/mm^2 at the bottom face. The total peak sinusoidal-load applied simultaneously along both line positions was 222·5 N, 445 N and 667·5 N. Peak displacements of 0·13 mm, 0·28 mm and 0·42 mm respectively were obtained using procedures similar to those of the beam tests.

After analysis of the experimentally obtained results the main conclusion stated from the second stage of the research was that the data inferred that the elastic modulus was greater in the axis of the prestress and this reflected the concrete-curing effects observed earlier in the prestressed beam cases. This conclusion concerning the elastic moduli appears to have assumed uniform second moments of area in both axes but in the practical case the unprestressed section would have been subject to some degree of

damage from cracking. Thus the calculated flexural rigidity 'EI' of the unprestressed axis will also have accommodated a differential in the Young's elastic modulus to compensate for the lowered second moment of area.

Broadening the area of research into the dynamic behaviour of concrete beams, Turner and Pretlove (1983) undertook a more detailed analysis of these types of structure by investigating effects of damage imposed on prestressing reinforcement and the result on the natural modes of vibration of a bridge-element. Their work was part of a programme of investigations into dynamic methods of bridge condition monitoring and it was hoped to incorporate a damage location technique developed by Cawley and Adams (1979) to individual bridge-beams.

The beam tested by Turner and Pretlove was a prestressed, post-tensioned 'T'-section element removed from a beam and slab design bridge-deck. The top-flange of this element was approximately 900 mm wide and 165 mm thick incorporating a total of four layers of 19mm diameter longitudinal and transverse reinforcement at 180 mm pitches. The approximate central-web dimensions were 200 mm thick for the first 405 mm of its length and then 250 mm thick for the remaining 215 mm. This web incorporated another eight 19 mm axial-reinforcing bars which were positioned at the corners and transition areas of the web-section. Two 50 mm tendons, 75 mm apart, consisting of twenty-four 7 mm diameter steel wires were located almost centrally in the lower 250 mm wide portion of the web. The entire section was simply-supported on rubber-bearings over its 12·5 m span during testing. In order to damage the tendons, access was achieved by removing a 200 mm by 50 mm 200 mm section of concrete at what appears to be the mid-span position.

The beam was excited by a step-relaxation technique which required the novel use of an ex-RAF bomb-release mechanism. In essence, the loading arrangement was a 272 kg mass supported at a one-sixth span position and this arrangement avoided any nodal positions of the lower natural frequency mode-shapes. After one or more prestressing cables were cut the beam was excited by the sudden release of the load. The resultant vibration data were recorded until the transients had decayed and the load-release procedure was repeated several times for data averaging purposes. This process of incremented tendon damage and response measurement was undertaken approximately seven times. After the experimental data had been examined it became clear that the most accurate results were obtained for the fundamental mode of vibration.

Although introducing the theoretical basis of a damage location approach to such structures (Turner, 1984), the main contribution from the work of Turner and Pretlove was the conclusion that induced damage clearly manifested itself as a change in the vibrational responses of the prestressed beam (Figure 2.1). From this conclusion it may be inferred that corrosion- or load-damaged bridge-beams should reproduce these effects.

Figure 2.1 Fundamental beam frequency versus number of severed tendon wires (after Turner and Pretlove, 1983)

At about the same period, Johns and Belanger (1981) were also actively researching vibrating concrete-beams. They investigated the relationship between the static and dynamic section properties for a series of ordinary-reinforced beams subjected to static loading. The basis of their work was in the ACI Committee 318 recommendations (fully compiled in 1983) regarding the effective second moment of area of such constructions:

$$I_{eff} = I\,(M_{cr}/M_{applied})^3 + I_{cr}\,[\,1-(M_{cr}/M_{applied})^3\,] \qquad (2.1)$$

Where: I = principal second moment of beam area in the undamaged state
I_{cr} = principal second moment of beam area in the cracked state
I_{eff} = effective principal second moment of beam area
$M_{applied}$ = externally applied moment to beam system
M_{cr} = externally applied moment that creates macrocracks in beam section

The beam dimensions were 0·20 m wide, 0·36 m wide and 6·55 m long and each was simply-supported over a span of 6·10 m. The typical cylinder crush-strength of the parent concrete was 32 N/mm^2. Axial-reinforcement design was limited to two 19 mm diameter rods of 415 N/mm^2 proof strength steel, positioned 60 mm above the lower face. No stirrups or compression reinforcement were incorporated in the design.

Using four of these beams, Johns and Belanger loaded each specimen statically in an incremental manner apparently at the third-span positions using masses. The applied bending moment induced in each beam section between the mass carriers was varied between approximately 8 kNm and 46 kNm. At each incremented load application the datum central deflection was noted and the resultant vibrational motions were then recorded after a "small intentional perturbation" was applied to the same point. The static deflection and vibrational response were both measured using a Direct Current Displacement Transducer (D.C.D.T.) connected to oscillograph. The impact/frequency measurements were repeated twice after 5 minute intervals to include any creep or settling effects, then the loads were again increased and the procedure repeated. Table 2.3 presents a summary of the static beam results evaluated from the experimental work of Johns and Belanger. Figure 2.2 illustrates a comparison between data derived for the static and dynamic flexural rigidities of beam 3 listed in Table 2.3.

Table 2.3 Summary of static flexural rigidity results (after Johns and Belanger, 1981)

By the extraction of the flexural rigidity EI from both the static load and dynamic vibration data of these beam systems, Johns and Belanger concluded that the static formulation for the mid-span deflection of the beam system was insufficient for dynamic purposes and "tentatively" proposed the following modification to (2.1):

$$(EI)_{dyn} = EI\,(M_{cr}/M_{applied})^3 + (EI)_{cr}\,[\,1-(M_{cr}/M_{applied})^3\,] \qquad (2.2)$$

In addition, they also qualified their conclusions with the important statement that:

> "Tests on a larger number of samples with different sectional geometries are indicated for further research"

Figure 2.2 Static/dynamic flexural rigidity ratio versus applied bending moment (after Johns and Belanger, 1981)

Later Jerath and Shibani (1985) continued directly from the work of Johns and Belanger using the same testing methodology and result derivation methods on three designs of beams. The designs incorporated progressively different reinforcement regimes and two beams were tested for each design.

Each beam was 125 mm wide, 255 mm deep by 3·35 m long and was simply-supported at its ends over a 3·05 m span. Cylindrical specimens taken from the concrete mixes for these beams returned average compression strengths of 28 N/mm^2. The first reinforcement design incorporated two number 4 bars 38 mm above the underside of each beam and the second design utilised two number 6 bars in the same positions. The final beam was doubly reinforced using three equi-spaced number 6 bars for tension and two number 4 bars in the compression zone, again with 38 mm concrete cover over both reinforcements.

The testing procedure was identical to that of Johns and Belanger, in this case with the two mass hangers positioned symmetrically 380 mm from the mid-span of each beam. The applied bending moment from this arrangement was varied between approximately 1·5 kNm and 12 kNm. Deflections and vibrational responses were recorded using a Linear Variable Differential Transformer (L.V.D.T.), a storage oscilloscope and a X-Y plotter.

After examination of the test results, similar data trends were found to those of the Johns and Belanger investigation and these suggested yet another interpretation of (2.1):

$$EI_{dyn} = E_{dyn} \{ I (\alpha M_{cr}/M_{applied})^{\beta} + I_{cr} [1- (\alpha M_{cr}/M_{applied})^{\beta}] \} \qquad (2.3)$$

Where α and β are constants which were found to be approximately 0·7 and 1·0 respectively for the cases studied. However Jerath and Shibani had to qualify their conclusions in the manner of Johns and Belanger with the statement that:

> "A careful evaluation of [the] α and β constants is needed ... Research is needed to define and propose formulae for determining the dynamic modulus of elasticity of concrete as a function of concrete properties. The dynamic stiffness rigidity of normal and high-strength concrete should be investigated for other shapes of beam cross-sections, wide variations in steel ratios and different support conditions"

Loo and Santos (1986) also used the ACI Committee 318 recommendations for the effective second moment of area of concrete constructions in the analysis of vibration data but for prestressed concrete beams and ordinary-reinforced box-sections. The contact law of Hertz was used here in conjunction with beam vibration theory to produce a series solution for the mid-span deflection of a simply-supported beam at any instant,

after it was subjected to an impact deflection as a method of excitation. Experimental data from previously published work on pin-ended prestressed beams and ordinary reinforced box-sections were then used to validate the solution.

The experimental data for the prestressed beams were obtained from nine specimens subjected to "maximum (below-yield)" dynamic deflections due to the impact of a 100kg mass falling between 10 mm and 600 mm. These beams were nominally 120 mm wide, seven were 180 mm deep and two were 240 mm deep. The simply-supported spans were independent of section design, varying between 2·5 m and 4·5 m, and each beam overhung the supports by nominally 150 mm. The compression strength at 28 days of specimens taken from each beam mix was between 30·9 N/mm^2 and 36·1 N/mm^2. In each case the prestress was provided by one tendon positioned on the vertical axis of each beam between 122 mm and 162 mm below the top-face. The tendon area varied between 61 mm^2 and 183 mm^2 and this was independent of the beam section dimensions. The prestress induced in the tendon was between 73·6 kN and 220·7 kN and this too was independent of the beam design.

The experimental ordinary-reinforced box-section data were obtained from four test-beams subject to mid-span impacts from a 100 kg mass, dropped from heights between approximately 100 mm and 600 mm. In each case the span was 3·8 m and the overall beam length was 4·0 m. Each beam design had a width and four wall thickness of 200 mm and 60 mm respectively with a depth of either 200 mm or 300 mm. The two areas of reinforcement were on the vertical axis in all cases with 33 mm of concrete cover between the top-face and underside of each beam. The tension and compression reinforcement areas were the same for each test-beam and either 402 mm^2 or 603 mm^2 of 450 N/mm^2 yield-stress steel rod.

The analytical investigation of that work centred on a modified version of expression (2.1):

$$I_{eff} = I\,(M_{cr}/M_{applied})^{i} + I_{cr}\,[\,1 - (M_{cr}/M_{applied})^{i}\,] \qquad (2.4)$$

where the index i is a constant prescribed for the experimental data analysis. Applying theory derived for the dynamic behaviour of a falling mass and impacted beam system in conjunction with expression (2.4), a computer program was used to iterate solutions around those data of experimental results. The theoretical basis of the analysis was involved and lengthy but statistical correlation between those analytical and experimental results (Table 2.4) suggested that $i = 3$ was an optimum value: that was in agreement

with (2.1). However regarding the analytical derivation it was stated that:

> "It should be noted that [the estimated dynamic deflection due to impact] has been found to be inadequate for predicting the impact deflection of concrete beams. This is true regardless of the formulae used to evaluate the [second moment of area]"

Index *i*	Correlation Coefficient	Standard Error of Estimate	Intercept	Slope
2	0·97177	1·05359	- 1·90298	1·23905
3	0·97480	0·99622	- 1·90352	1·21107
4	0·96628	1·14993	- 1·99221	1·17767

Table 2.4 Statistical correlation between analytical and experimental results (after Loo and Santos, 1986)

That statement in addition to the conclusions of other work discussed here suggest that the ACI Committee 318 approach to equivalent section properties should only be used in the static analysis of concrete members, where it had its basis. During the period from that work there appears to have been no research effort aimed at devising a method which relates the load-damaged condition of a concrete member to its dynamic flexural properties and it is clear that an original approach should be sought for these purposes.

2.3 Bridge-Structure Vibration Monitoring

The principal aim of 'monitoring' bridge-structures is to ensure that their load-carrying capacity is maintained. There are many methods of monitoring applied to these types of structure: visual inspection, static-load deflection, electro-potential measurement, acoustic emission, sonic reflection, infra-red thermography, radar-radiography, X-ray absorption, ultrasonic transmission, micro-siesmology, impact-echo and vibration response measurement. All of these methods are outside the scope of this work except for vibration monitoring. However an excellent review concerning these approaches has been compiled by B.P.Baxter for ETRS Pty Ltd., Australia (Vic'Roads, 1990) which indicates that the literature on these techniques is extensive.

Early research in the behavioural assessment of bridges using different vibration techniques was undertaken by the Transport and Road Research Laboratory (TRRL), now the Transport Research Laboratory (TRL). The expertise gained during experimental phases in a number of earlier investigations was condensed into one comprehensive document (Leonard, 1974). The scope of that report was extensive in that it introduced the testing philosophy and objectives for bridge assessment; excitation methods for different types of bridge structure; and the instrumentation requirements or recommendations were highlighted. Discussions of test procedures, analysis of resultant data and interpretation were supplemented by clear and concise diagrammatic aids.

Monitoring the vibration response of bridge-structures on a frequent basis has only become feasible due to the availability of small, high-powered computers and data acquisition systems since these avoid the complicated data-capture and analysis methodologies associated with the somewhat less portable equipment discussed by Leonard. Additional advances in micro-electronics have allowed transducers to be developed with in-built signal conditioners which reduce the overall complexity of the on-site instrumentation. With these new facilities for *in situ* vibrational response measurement, the task of establishing the optimum method of structural excitation has been addressed over several decades.

A number of groups have advocated ambient methods of bridge excitation after considering the potential of vehicle motion over a structure. Combining prediction with practice, work by Cambell *et al* (1979) showed that vehicle and structure 'matching' should be encouraged to excite the response modes of interest. System matching would be achieved (usually) using a heavy goods vehicle whose mass and suspension characteristics produced a natural frequency of vibration as near to the bridge-structure fundamental mode as possible. The basis of that work was tests undertaken on three longitudinally-voided, post-tensioned continuous concrete bridges that were typical of the highway structures within the Province of Ontario, Canada.

The first of these structures was 18·0 m wide, approximately 0·9 m deep and its three spans had an overall length approaching 120·0 m. The second was also 18·0 m wide however the deck was 1·3 m deep and the five-stage span of 105·5 m incorporated a 15° skew angle. The third structure was 14·6 m wide, 1·3 m deep deck and incorporated a six-stage curve of 436·0 m radius which, if developed, would be equivalent to an overall span of 205·0 m. The vehicle used as the mode of excitation was a 40 tonne, 5 axle articulated-truck.

Initially a structural dynamics computer program (STRUDL II) was used to estimate a number of the natural frequencies of this structure using beam and lumped-mass representations. Experimental data were obtained using an articulated truck driven either over the bridge at a constant velocity of between 22 m/s and 27 m/s or on to the bridge and brought to rapid halt. The former excitation method was applied to bridge 2, the latter to bridge 3 and both were applied to bridge 1. The structure displacements were measured by several, strain-gauged based "deflectometers" positioned along the deck. These deflectometers measured the excited deflections during testing then 'static' deflections when the vehicle traversed the bridge at a "crawl" speed and the dynamic deflection was taken as the nett of these data. Table 2.5 shows the comparison between the theoretical and experimental data.

Table 2.5 Comparison of theoretical and experimental frequencies (after Campbell *et al*, 1979)

Although reasonable vehicle-structure excitation matching was achieved errors as large as 25% between theory and experimental fundamental frequencies were observed. Those possible areas of error cited included limitations in both the concrete elastic modulus data and the computational facilities of the package. It has been shown earlier in Section 2.2

that the elastic modulus of concrete subject to prestress during curing is higher than its ordinary-reinforced equivalent. The STRUDL analysis package only modelled the bridges as beam elements and so all torsional properties were neglected, also it appeared that the considerable mass of the vehicle was not (or could not be) considered as part of the dynamic modelling exercise. The omission of torsional effects, vehicle masses and the modified elastic modulus from the analysis data will have contributed to those errors. Importantly, though, it was recognised that the vehicle system produced unwanted excitations within the range of structural frequencies of interest.

Single or multiple dynamic-loadings from vehicle arrivals on a deck (or 'events') are methods of excitation which are already present for the purposes of bridge-vibration monitoring. Ward (1984) undertook "exploratory" investigations primarily aimed at structural integrity monitoring. Those investigations were into the application of traffic-loading as a method of non-invasive excitation on a selection of bridge types and some of the problems which stem from this technique were highlighted.

Those bridge types monitored included viaducts, single- and multiple-span designs with main spans between 2·6 m and 75·6 m. The construction of those bridges ranged from brick, stone and cast-iron to steel, composite steel/concrete, ordinary-reinforced and prestressed concrete. Vertical response measurements were taken from each structure at mid-span using 2 individual seismometers and a FM tape recorder. For reference purposes the bridge responses were compared with vibration levels experienced by the ground in the approach to the structure and those ground vibrations were recorded by an addition pair of seismometers.

Those data obtained from all the bridge mid-spans were processed by a numerical computer using Fourier-Transform analysis methods (Thomson, 1988). Three measures of vibrational response applied to random vibrations were extracted from the data over the band-width of interest (Ewins, 1984): Autocorrelation, Peak- and Average-Spectral Density. Those measures were then compared and a summary of the results are presented as Table 2.6.

Apart from establishing an approximate relationship between length of span and the fundamental frequencies of vibration for a number of different constructions, those data illustrated the problems associated with essentially random excitation patterns since no set of three frequencies identified was the same for one bridge. There are considerable errors in some cases and accuracy and repeatability of response measurement is pivotal when considering structural integrity monitoring. It was concluded that only "geriatric"

structures would benefit from the approach since only they would show the large changes in response required of that method of vibration assessment. It was also concluded that much further work was necessary to solve some of the problems identified in the technique.

Table 2.6 Comparison of experimentally derived response frequencies (after Ward, 1984)

One subsequent research investigation tackled the problem of identifying the response frequencies of bridge-decks subject to traffic-loading, with limited success. Turner and Pretlove (1988) represented a vehicle/bridge-deck system using a beam traversed by a point-load. Experimental data obtained from bridge-site measurements were used for comparison purposes.

The analytical approach was based on the technique of 'Mode Summation' (Meirovitch, 1986) applied to a simple beam responding to the action of a point-load traversing the span at constant velocity. The deck representation was then subject to a idealised traffic loading "developed [as] a model in which the separation of vehicles having uniform mass and speed is described by a Poisson distribution". The resultant governing equation which described the system accelerations was solved using a computer-based program.

Predicted variations in system damping, vehicle event density and speed were explored and good agreement between those and experimental results was found in specific cases. Comparisons were made between predicted results and spectra data obtained from a 45·0 m span of the Burghfield Lane Bridge which carried a single vehicle across the M4 near Reading. The predicted spectrum was derived for a series of randomly distrubuted 20 tonne loads traversing the bridge at 15 m/s^2. Figure 2.3 compares the resultant data.

Figure 2.3 Comparison between predicted and experimental data trends (after Turner and Pretlove, 1988)

It was acknowledged that:

"The model used is relatively simple and has its limitations"

Although a general trend could be identified in both the predicted and measured spectra, unfortunately the work of Turner and Pretlove proved relatively inconclusive due to the problems associated with signal noise originating from 'random' vehicle arrivals. However the group hoped to develop a more sophisticated model which would be a better representation of traffic loading upon which to base future analyses.

More recently Mazurek and DeWolf (1990) undertook a laboratory study using a modelled bridge and vehicle system which compared impact and 'vehicle' excitation as a means of establishing modes of vibration of a two-span structure. An additional aspect of their investigation addressed the problem of damage detection using the comparison of vibrational data.

The test-structure consisted of eight 25 mm by 25 mm by 3·2 mm aluminium angle-sections, two 75 mm wide by 3·2 mm thick plates and a 115 mm wide by 5 mm thick cross-tie. These components were arranged to produce essentially two vertical I-sections. The overall dimensions of this section were approximately 115 mm wide by 75 mm deep. The central box-section was approximately 75 mm square. The overall length of the fabrication was 4·9 m and it incorporated two 2·3 m simply-supported spans that were symmetrical about the central support. Surface roughness was mimicked using 6 mm wide tape strips at approximately 450 mm intervals across both spans. The overall height of each strip was varied up to three tape thickness'.

A vehicle simulation whose mass varied between 0·5 % and 5 % of that of the bridge structure was towed across both spans at a typical speed of 0·12 m/s. A reference accelerometer measured responses from one span while a second was moved to various positions on both spans during the course of testing. Results concerning frequency response, mode shapes and damping were studied. Those data are summarised in Table 2.7.

Substantial amounts of data were obtained from those tests and additional investigations centred on structural responses subject to simulated damage. The modes of damage simulated included removal of one side of the two central supports and a saw-cut depth of up to 50 mm in one of the I-sections at a position of maximum bending-moment. Response frequencies, but not mode-shapes, were shown to be heavily influenced by

vehicle mass and the accelerations experienced by the structure were wholly dependent upon the vehicle approach speed. The variation in response frequency across all the observed modes was typically 2·5 % due to mass and velocity effects. Since the work of Mazurek and DeWolf ultimately addressed the problem of structural-integrity monitoring using vibrational data, there was the suggestion that the problems associated with changes in the resonant frequencies due to varying vehicle effects had not been fully addressed because almost catastrophic structural failure had to be simulated before similar changes in vibrational response were observed.

Table 2.7 Frequency, damping and modal-amplitude results summary (after Mazurek and DeWolf, 1990)

Other methods have been proposed as a means of excitation for bridge-structures. Eyre and Smith (1977) considered ambient-wind excitations and showed that the results of wind-induced responses from two of three monitored bridges were in good agreement with those frequencies predicted and measured by other means.

The two structures which were monitored for ambient-wind responses were the Cleddau and River Wye Bridges. The first of those structures is an eight-section, single box-girder construction bridge which has an overall span of 820 m between abutments. The box-girder construction of this bridge is continuous apart from a 136·5 m centre-section which is roller- and pin-supported off the main structure. The top-flange of the box-girder is an orthotropic steel deck approximately 13·4 m wide and the box-section tapers 6·1 m below carriageway level to the lower-flange width of 6·7 m. The second structure is also a box-girder design but includes cantilevered edges. The overall span of 604 m between abutments is acheived in seven stages and this cable-stayed design has a central span of 235 m, with two side spans of 87 m. The width of the orthotropic steel deck-flange is approximately 17 m and the deck cantilevers add another 14 m to the overall width. The box-section tapers 3·2 m below the crown of the carriageway to a lower-flange width of approximately 10 m.

For the Cleddau Bridge test-measurements were obtained from centre- and quarter-span positions of 213 m span section using accelerometers positioned on the bottom-flange of the box-girder section. Wind-speeds and directions were monitored for the structure using an anemometer and wind-vane mounted on a 6·0 m mast at the leading-edge of the deck. Similar data measurements were obtained from the River Wye Bridge using an accelerometer mounted at the centre of the main span and data-capture was triggered by a combination of three anemometers which also monitored wind-speed and direction. Data from both structures were processed to produce the autocorrelated frequency responses of the Cleddau Bridge, the displacement responses for the River Wye Bridge and each data set was compared either with predicted or modelled behaviour (Table 2.8).

The wind speeds required to excite the first and second bending modes of the Cleddau Bridge were between 21 m/s and 23 m/s. The results presented were very encouraging since excellent agreement was seen between predicted and measured data but it is unclear to what extent wind-loading on the structure would have affected the 'true' natural frequencies. The data from the River Wye Bridge were, however, disappointing but it was acknowledged that during the 2 months of monitoring the bridge had undergone sustained oscillations on only three occasions during this period and additional data were required to allow judgement on the technique as a result.

Table 2.8 Estimated and experimental results summary
(after Eyre and Smith, 1977)

Brownjohn *et al* (1989) conducted a similar vibrational measurement investigation on the Bosphorus Bridge using ambient-wind excitation. This cantilevered suspension design has a span of approximately 1·56 km between cable-anchorages and 1·1 km of span is between its cable-support towers. Initially the vibration response of this structure was modelled using two- and three-dimensional FEA techniques. Wind (in addition to vehicle) excitation was used to experimentally verify the transverse, lateral and torsional mode frequencies. Measurements were obtained from 3 servo-accelerometers which were positioned at various sites on the bridge so that a complete mapping of the structure responses was achieved. The response data were averaged for the purposes of accuracy, however, data-capture took over 3 minutes per event due to the resolution of frequency measurement required. This enormous experimental undertaking required 10 days of on-site testing but it is unclear what period the support data-processing and predictive analyses required, however, the resultant data showed that this slender structure has nearly 40 modes of vibration in the range of 0-1 Hz (Table 2.9).

Finally, the impulse technique has been successfully applied as a method of structural excitation and TRL have used the step-force-relaxation approach on bridge-structures during the course of major test programmes. Eyre (1976) used the strain energy suddenly released from the static deflection induced by a large load to excite the Cleddau Bridge. This bridge has been described earlier (Eyre and Smith, 1977) and the testwork was undertaken to establish levels of damping present within its structure.

Table 2.9 Selected summary of predicted and experimental results (after Brownjohn *et al*, 1989)

The main span of this bridge has an overall length of 213 m with a 136·5 m central section pin- and roller-supported off the main structure. A 33 tonne mass was suspended from the superstructure at the mid-span position and it was attached by first floating it into position under the bridge on pontoons, then lifting it free of the water using a winch *via* a pulley system. A jack was used to drop the load by freeing a dowel-pin which supported the load.

The resultant structural responses excited by the load release were recorded using six vertical accelerometers, three horizontal accelerometers and two inductive gauges to measure horizontal displacements at the centre-section support positions. Two accelerometers measured vertical responses from the centre and side of the bridge at the mid-span of the 136·5 m section. Two other accelerometers measured the vertical responses at the quarter-span positions of this section whilst an additional pair measured the mid-span responses of the adjoining 149 m bridge sections. Two horizontal accelerometers measured responses over each support-pier bearing while the third measured responses at the top of one of the piers. Results extracted from those data provided details of the fundamental frequency, logarithmic decrement and, hence, apparent damping (Table 2.10).

Table 2.10 Summary of experimental vibration results from Cleddau Bridge (after Eyre, 1976)

Some slight variations in those observed results did occur but, overall, there was repeatability of frequency measurement better than 1 %. Log-decrement and, hence, damping values obtained from the accelerometers appeared to be more consistent when compared to the displacement gauge results. However the measurement of accelerations, as opposed to dynamic displacements, has always been regarded as the more accurate method (Ewins, 1984). There is still noticeable spread over the log-decrement results obtained from the accelerometer data. With lightly damped structures the decay in any observed transients is slow and, hence, there are more response peaks to aid accurate estimation of the apparent damping but it is possible that additional, parasitic mode-responses may have contributed to those errors.

In Japan, Hara and Kawamura (1990) applied the impulse-excitation method to the vibration measurements of both a Langer-truss bridge in Nagasaki and a plate-girder bridge in Osaka. The first design is similar to that of the Sydney Harbour Bridge and it has a span of 152·0 m, whilst the second structure is almost square in plan with a 40·0m span. That work presented detailed considerations of impact exciters and their features, in addition to presenting the background procedures for averaged transfer functions and

Figure 2.4(a) Quality of imparted force spectrum
(after Hara and Kawamura, 1990)

Figure 2.4(b) Imparted force versus rubber hammer-tip thickness
(after Hara and Kawamura, 1990)

averaged time history methods of vibration data extraction. Introduction was also made to the selection of appropriate 'frequency filtering' media for impactors (Figure 2.4) and three impact force 'ranges' were accommodated by differing hammer designs. A maximum of 30 kN peak force was suggested for (what appeared to be) a sledgehammer application, 200 kN peak force for a quarter-rotation crank/mass arrangement and 500 kN for a larger, 'motorised' version of the 200 kN applicator. Unfortunately there was very little detail concerning each of the hammer designs and, although not used in the test programme, it was apparent that the largest capacity design could not be said to be truly portable. However this technique was shown to excite rigid structures of this type up to 150·0 m in span and recent work applied this method of excitation to a structure in the Birmingham area (Wood *et al*, 1991).

Figure 2.5(a) Bridge response spectrum from sledgehammer excitation (after Wood *et al*, 1991)

During initial investigations Wood *et al* demonstrated the quality of the hammer impact technique for exciting bridges using a test-structure from within the Birmingham area. Direct comparisons were made between those responses resulting from both vehicle motion and sledgehammer impacts for the same bridge structure (Figure 2.2). Figure 2.2(a) illustrates the results of a sledgehammer impact on the River Cole Bridge (described in Chapter 5) and this shows clear, unambiguous bridge responses. Although the excitation levels of Figure 2.5(b) were shown to be greater because of vehicle excitation, it was apparent that confusing parasitic responses were also present as a result of the vehicle mass and suspension systems. It was also noted that these practical levels of vehicle excitation response were only present when a very heavy truck crossed the structure.

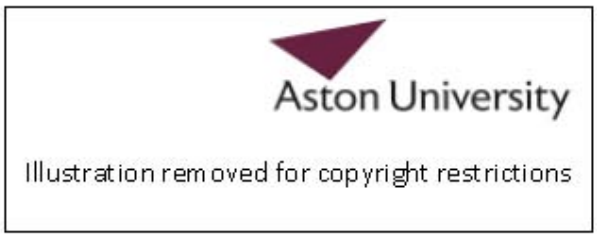

Figure 2.5(b) Bridge response spectrum from truck excitation
(after Wood *et al*, 1991)

Dynamic testing for bridge load-capacity rating was acknowledged as a viable goal by TRRL and they commissioned an "investigation of vibration methods for monitoring the integrity of bridges" (SML, 1981). The Structural Monitoring Ltd. research programme was in two parts and both predicted and observed data for three selected bridge structures were brought together for comparison purposes using finite-element (F.E.) models in conjunction with site test results.

The first of these bridges was the Westerhouse Bridge which is part of the M8 road system in Glasgow and it consists of two parallel constructions carrying two lanes of traffic over four spans. Its continuous composite concrete slab and steel beam decks are 11·8 m wide and 1·2 m deep, with overall spans of 81·5 m incorporating a skew angle of approximately 10°. The second test-site was Queens Bridge which carries traffic over the River Tay and it consists of three spans. This prestressed concrete box-section structure is 13·6 m wide with an overall span of 118·0 m and a mean deck thickness of 1·0 m. The final site was of one the Baillieston Interchange elevated sections which carries traffic between the A89 to the M8 just outside Glasgow, and it carries two lanes of traffic over seven spans which vary in length between 20 and 30 m. Its continuous reinforced deck is 11·0 m wide and 1·2 m thick. The overall developed span is approximately 170 m and it also incorporates a cross-fall of approximately 4° to produce a carriageway bank angle for the 280·0 m turn radius. SML used the random traffic and ambient wind conditions present at each structure as the excitation sources.

The damaged behaviour of each structure was predicted using bridge representations modelled by standard-section steel beams. Equivalent natural frequencies to those of the test-bridges were obtained by modifying the span lengths but the support conditions were retained. Damage was represented within the models as reduced local stiffness for a number of 1·25m long elements. The 'length' of damage was varied from major portions of the span(s) to localised 'crack' damage which used elements only 0·25 m long. It was concluded using this approach that the resolution in resultant damage measurement would be approximately 1%, whilst the predicted changes in frequencies would be about 5 %. The method of representing damage was questionable but, without any available data on what actual form damage would take within a F.E. representation, the model used should have been satisfactory for illustrative purposes. A notable conclusion originating from these investigations was that:

> "It was estimated that the natural frequencies of each bridge would be fairly insensitive to temperature variations"

The second stage of this work (SML, 1982) continued with the research initiated during the preliminary period. However with more data available from the three bridge structures described previously it was stated that:

> "The measured natural frequencies of all three bridges were stable with time, with a maximum variation from a mean value of 5 % ..... The measured mode shapes of the three bridges showed greater variations with time, and it was concluded that there was considerable scatter inherent in the [SML] method used for estimating the mode shapes"

An additional bridge structure was employed during this second stage of the research and it was used to acquire data concerning temperature effects on its construction. This addition was the Southfield Bridge near Glenrothes which consists of four spans and carries local traffic over the B921. Its reinforced concrete structure is 20·5 m wide with a mean deck depth of 0·9 m. It has a continuous overall span of approximately 60·5 m which incorporates a slight skew in plan.

Four temperature sensitivity analyses were undertaken on this structure during the last six months of 1981 in addition to similar work on the Westerhouse bridge in Glasgow. These tests included overall structure frequency measurements and temperature measurements at eight sites on the string-courses. Considering the infrequency of testing, the resolution of temperature measurement (± 1°C) and the lack of temperature data from either the blacktop or soffit of the structure, it was still concluded that temperature effects were not negligible (Figure 2.6). The suggested source of these effects was the temperature differentials between the 'blacktop' and main structure, although no definite relationsh p was established for the changes in frequency responses. It was also concluded that:

> "Measurements of the natural frequencies of a bridge for the purpose of monitoring for damage should therefore whenever possible be made in hot weather, or else suitable steps should be taken to correct the measured frequencies for temperature variations"

Figure 2.6 Southfield Bridge natural frequencies versus deck temperature (after SML, 1982)

Turner (1984) attempted to determine any correlation between temperature effects and changes in vibrational response. In that work attention was specifically given to the changes which could be directly attributed to the temperature effects present in a three span foot-bridge. The structure was composed of one central 16·0 m and two 8·0 m spans which incorporated a reinforced concrete deck approximated as 2·0 m wide, 0·8 m deep and 0·2 m thick 'T'-section. Excitation to the structure was provided (in the main) by a step-relaxation impulse technique using a 300 kg water-barrel 'bomb-released' from the mid-span position by remote control. Three transverse modes of the central span and two transverse modes of one of the side spans were monitored over a thirty month period at approximately four monthly intervals. Tests were undertaken for a range of temperatures and weather conditions. The results are presented in Table 2.11.

It was concluded that:

> "the natural frequencies of this footbridge appear to be unaffected by environmental changes"

However the same was not true for damping, but no correlation could be found between it and changes in temperature or relative humidity. Predicted response changes were proposed based on changes in the blacktop elastic modulus but definite conclusions were unable to be made due to a lack of data concerning the properties bitumen-aggregate.

Table 2.11 Experimental natural frequencies of a footbridge and test conditions (after Turner, 1984)

The long-term monitoring of bridge-structures for apparent changes in their vibrational responses due either to structural damage or the effects of ambient conditions has not guaranteed useful data in much of the cases discussed. Many researchers have expressed the wish to accelerate the process of structural degradation by inducing controlled damage in an 'expendable' bridge structure. Kato and Shimada (1986) conducted such an investigation on a prestressed concrete bridge which was designated for demolition. The availability of the bridge for the controlled destruction resulted from plans to replace it with an entry and exit interchange for the highway which it crossed.

The test bridge had overall span of 35·4 m between abutments and incorporated two support piers that were equi-spaced, at a distance of 24·0 m about the bridge centre-line. One diagonal member on each side connected the abutment to the pier base. The voided

deck was approximately 5·0 m in width and 1·0 m thick. A centre-span loading regime was applied to the upperdeck using a jacking system which was 'earthed' off the structure. The testing programme involved incrementally loading the bridge to 'failure' in six steps and noting static data such as loads, concrete strains and reinforcement prestress levels. Dynamic testing was undertaken between each load application to establish the frequencies of several of the main vibration modes of the structure. Those frequency data were then compared with predicted analyses based on progressively reduced stiffnesses for the structure in an area about the mid-span position. All the resultant data are summarised in Table 2.12. The main conclusion from this work was that major changes in the observed frequencies of the structure only occurred after the prestressed reinforcement tendons had yielded.

Table 2.12 Experimental and predicted damage responses
(after Kato and Shimada, 1986)

Agardh (1991) undertook similar destructive tests on both a prestressed-concrete and an ordinary-reinforced single-span bridge. Details regarding those structures were limited, however, the prestressed-concrete test-bridge was nine years old and constructed as a prestressed concrete frame with two straight girders, monolithic to a plate deck. The span and width were approximately 32 m and 10 m respectively but the deck depth and design was not stated. The ordinary-reinforced bridge was a "plate frame structure" constructed of reinforced-concrete. The span and width were about 21 m and 5 m respectively.

Each bridge was subjected to four central, mid-span loads varied between approximately 1 MN and 10 MN. Vibration measurements were obtained to support modal analyses of the behaviour of the bridges at each loading. Excitation of each structure was achieved by using the impact of a 60 kg mass dropped from a height of approximately 800 mm on to a load-cell positioned on the bridge. Both the impact and response data were acquired and subsequently post-processed using the modal-analysis software package *SMS-Star.*

The quality of impact excitation was broadly confirmed by Agardh and some attempt was made to linearise the increases in observed natural frequencies due to the imposed load damage. It was also stated that the damping observed in the locality of a node-line was relatively insensitive to damage. Disappointingly, however, the work did not detail the resultant frequency data but it could be inferred from the information presented that significant changes in the response modes were apparent. The final conclusion was that model-updating should be applied to damage location procedures. It was also stated that:

> "The project has given valuable experience, exposed several of the problems and also indicated requirements of equipment for future applications"

In addition to the controlled demolition of bridge-structures, pseudo-damage investigations have been undertaken. Biswas *et al* (1990) conducted simulated damage tests on a two-span, concrete slab and steel-beam structure. This bridge has an overall span of approximately 71·5 m with a 14·6 m wide deck that incorporates 9° of cross-fall. The composite deck design uses seven 2·0 m deep, welded-steel plate-girders to support a 200 mm thick reinforced concrete deck. The site was chosen for the test programme because of its typical construction nature, the low traffic volume and because its construction elements could be accessed with ease.

Damage was simulated by loosening a predetermined series of bolts in one of the beam-flange assemblies and comparisons were made between the 'damaged' and 'undamaged' vibration responses after the bridge had been impacted by a "roving" hammer. The response spectra comparisons were made for real, imaginary and sum of specific test site FRF magnitude data. Clear 'shifts' in the response spectra could be identified from the undamaged to damaged state and it was concluded that:

"changes in spectra [profiles] are detectable but are difficult to quantify"

However after the vibration data had been processed to extract the global frequency responses and mode shapes, that is results based on all the site FRF data simultaneously, it was apparent that significant structural changes had taken place since all but two, out of eight, selected modes showed average frequency reductions of 1% (Table 2.13).

Table 2.13 Experimental undamaged and simulated-damaged bridge responses (after Biswas *et al*, 1990)

Structural deterioration within bridge-structures is exacerbated by the cyclic-nature of traffic loads and so the long-term monitoring of bridges using data-logging techniques could provide an early warning of potential problems. Periodic checks on the vibrational data continuously recorded from a questionable structure should provide the basis of further action. Monitoring the dynamic behaviour of bridge structures has already been proposed as a viable method of assessing vehicle loadings (Stanger, 1990) and the

conclusions from a confidential report concerning a possible logging system were positive. For example, the work was successful in demonstrating that relatively simple equipment could be employed for monitoring bridges of the type tested. Strain, displacement and acceleration were all successfully measured at very low amplitudes of motion. Signal noise was not a significant problem when considering a battery powered system. Good consistency in the resultant data was achieved for successive traffic events. The overall success of the test was reflected by the quality of the strain gauge data and from these it was recommended that this technique should be employed rather that the more elaborate displacement and acceleration measurements.

The necessary automatic data logging instrumentation and telemetry architecture has now been developed to assist in the monitoring of major bridge structures. Deflection, mechanical strain, joint movement, temperature, wind speed and direction data were collated from the main 233·5 m span of the River Foyle bridge in Northern Ireland (Sloan *et al*, 1992). The data collection system was based around an on-site mini-computer and, apart from local (on-site) requirements, remote access to the data was facilitated by the use of a modem connection and the country-wide telephone system. These facilities allowed data processing and analysis to be undertaken at leisure by the research groups based at both Queen's University of Belfast and the Northern Ireland Department of the Environment.

In summary, the above has shown that vibration monitoring of bridge-structures is an active area of research. The overwhelming goal is to devise methods which will ensure the accurate load-capacity assessment of these structures. However the principal area of temperature effects on vibrational responses has not yet produced conclusive data.

2.4 Predictive Analyses

The available literature concerning predictive analyses applied to bridge-structures is extensive. Static analysis dominates this area and the required reading for this field is summarised by one excellent text by Hambly (1976). The interest of the work presented here centres on the dynamic analysis of bridge-structures using grillage (or grids) analysis.

Numerical modelling techniques are used to estimate the structural responses of bridges due to the complexities of their constructions. The main developments in this type of predictive analysis on bridge-structures originate from work initiated in the early 1970's. Veletsos and Huang (1970) produced a comprehensive review of work prior to this period which presented the bases of bridge-structure and vehicle dynamic idealisations, clarified the mathematical approach to resultant analyses, introduced current computer packages of the time and provided an extensive reference compilation detailing the early development of this field.

Many predictive analyses use the numerical technique of 'finite-element' analysis (FEA). Other techniques include 'grillage' analysis (GA) and this, like FEA, has its formulation basis in static analysis and recommendations for its usage are readily applicable to the vast majority of current bridge types (West, 1973). GA involves approximating a continuum by a lattice of individual beams instead of the continuous assembly of elements associated with the FEA method. The GA technique has proved its accuracy and its usefulness despite displacement continuity being maintained at the connecting nodes only, rather than uniformly along element boundaries as in FEA. The method is widely used since it is readily understood and because of the simplicity of its application. Considering that the static analysis technique may be said to be the construction industry standard there appears to be remarkably little research undertaken which applies this method to the dynamics of structures.

Ellington and McCallion (1959) were one of the first to propose the use of GA in vibration modelling using their formulation for a regular supported plate based on a lumped-mass and torsionless-beam representation. Modelling a plate as an arrangement of orthogonal, massless beams the generalised equation of motion for a lumped-mass at each node point of the resultant grillage was expressed in the form of finite-differences (Linfield and Penny, 1989). The equation of motion was expressed as the sum of the shear forces induced by the bending of each orthogonal beam, equated with the acceleration and mass at each node. The finite-difference (F.D.) formulation of the equations allowed the resultant motions to be evaluated iteratively over the domain of the grillage using a digital computer.

The grillage motions were dependent upon the constraints, or conditions, present at the domain boundaries and in each case assumed displacement patterns, or 'models', were imposed to ease the dynamic formulation. For example, the displacement model appropriate for a plate simply-supported around each of its edges was shown to be:

$$z(x,y) = C \sin (i\pi x/N_y) \sin (j\pi y/N_x) \qquad (2.5)$$

where: C = arbritrary constant
i,j = integers: 1, 2, 3 ..... N
$z(x,y)$ = vertical displacement from the X-Y plane at position (x,y)
N_x = number of beams in y-direction plus 1
N_y = number of beams in x-direction plus 1

The additional cases of plates with opposite-edges free of constraint or clamped and the general case of plate vibrations were addressed using similar displacement models.

Wah (1963) analysed grillage vibrations of regular supported plates using a distributed-mass system approach. A torsional component representing rotation of the beams connected to the node-point, at a normal to the axis considered, was incorporated in the moment-based FD formulation of Ellington and McCallion. The effects of several constraint conditions imposed on opposite boundaries of the domain were derived; including clamped, simply-supported, elastic-support and free. The lumped-mass idealisation at a typical node was replaced by the dynamic contribution of a uniformly-distributed-mass. Comparative results from each formulation were evaluated. A selection of these results is presented in Table 2.14:

It was observed that the lower modes were in good agreement, however, the higher modes did show increasing differencies in the calculated frequencies due to the omission of the torsional components. Gangarao and Cheng (1973) effectively repeated the work of Wah by comparing lumped-mass and distributed-system grillage formulations for bridges modelled as regular orthotropic plates with the opposing boundaries simply-supported or free. Gangarao and Cheng concluded that the lumped-mass grillage formulation was adequate for bridge analyses since usually only the lower modes were of interest.

Using the simpler, lumped-mass formulation Balendra and Shanmugam (1985) investigated the vibrations of plain and stiffened plate examples, also cellular structures. Initially comparisons were made between the exact theory and grillage solutions for a 203 mm square, 1·37 mm thick aluminium plate which was either clamped along all four edges or clamped and simply-supported at opposing boundaries (Table 2.15).

Table 2.14 Comparison between grillage formulation results (after Wah, 1963)

It was observed from those data of Balendra and Shanmugam that the differences between the exact and predicted frequencies were as much as 3·5 % for the simplest case considered. The comparison of the five lowest theoretical and predicted modes was repeated for rectangular plates with aspect ratios of 1·5 and 2·0 with the same boundary conditions. The apparent errors in the rectangular plate data were found to be as much as 28%.

Table 2.15 Comparison between exact theory and grillage results (after Balendra and Shanmugam, 1985)

Balendra and Shanmugam made additional comparisons of grillage data obtained from more complicated plate structures using finite-element-analysis (FEA) predictions and experimental results. The natural frequencies of square plates with clamped edges incorporating one-central or three or seven equi-spaced transverse-ribs were studied. Additional grillage and FEA analyses were undertaken on several cellular structures, however, the only experimental data presented for comparative purposes were those concerning the clamped square plate with one central, transverse rib. The dimensions of this aluminium plate were 2·037 m square and 1·37 mm thick, the rib 12·7 mm deep and 6·35 mm wide. The test and experimental results are presented in Table 2.16:

It was observed that the ribbed-plate data from the grillage analysis showed on average twice the FEA 'error' from the experimental results, but this assumes total accuracy of response measurements. In retrospect it is arguable that the simple lumped-mass approach of Balendra and Shanmugam for thin plates or membranes is ideal, also for more substantial structures where only a few of the lowest modes need to be established. However where a bridge structure is massive and additional superstructure is present on the deck then both distributed-mass and torsional considerations are extremely important when accuracy in mode prediction or model updating is necessary.

Table 2.16 Comparison between experimental, grillage and FEA results (after Balendra and Shanmugam, 1985)

Summarising, GA is a readily understood modelling technique which because of its simplicity is easily applied to bridge-structures. Its formulation is based on the accepted principles of continuum modelling and it is inherently faster as a computational solution when applied to problems of this type.

2.5 Summary

The work discussed here identifies significant omissions in current knowledge concerning bridge-structure behaviour. To date there appears to be no published data which accurately relates the load-damaged condition of a concrete member to its dynamic flexural properties. In addition the principal area of temperature effects on the vibrational response of bridges has not yet produced conclusive data. Finally, the dynamic application of the industry standard, grillage analysis, seems to have been neglected as a cost-effective alternative to finite-element analysis. The research presented in this thesis concentrates on these areas. Attention is now turned to the first of these topics: experimental testing of bridge-beams.

Chapter 3: Experimental Bridge-Beam Testing

" It is a capital mistake to theorise before one has [some] data "

Sir Arthur Conan Doyle (1859-1930)

3.1 Introduction

A programme of testing was undertaken within the laboratory to obtain data on the vibrational behaviour of two bridge-beams designs when subject to progressive levels of damage. This series of tests was made on similar ordinary-reinforced and post-tensioned designs, the preliminary results of which have already been presented (Wood *et al*, 1991).

3.2 Design and Preparation

The two series of model bridge-beams were designed and prepared to reflect the construction practices present in modern bridges. These test-beams were made as large as practicable for the test facilities available to minimise behavioural errors from scale effects such as aggregate interactions. The beam cross-section configurations and dimensions were selected for two independent reasons. The first reason was that the resultant section was representative of the many designs of bridge-beam and the methods of construction applied for a typical structure. The second was that prestress eccentricity effects should be avoided so that directly comparative analyses between the two beam designs could be made. A rectangular section was chosen since it allowed symmetrical longitudinal-reinforcement arrangements and, hence, the induced prestress would not create an internal moment.

3.2.1 Ordinary-Reinforced Beam Design

The ordinary-reinforced beam design (Figure 3.1) had an overall length of 6·3 m, of which 6·0 m was the test-span. The cross-sectional dimensions were 300 mm wide and 500 mm deep with a resultant span-depth ratio of 12. The concrete specification was a 'Portland' Grade C40 and it provided approximately 35 mm of cover around the reinforcement cage. Each cage (Figure 3.2) was fabricated from six 6·5 m lengths of 16 mm, steel axial-reinforcement. Shear reinforcement was provided by 23 equi-spaced, rectangular stirrups of 8 mm diameter steel. This reinforcement was nominally grade 460 (BS 4449: 1988) and it represented less than 4 % of the overall mass of approximately 2300 kg. End supports were two 200 mm x 100 mm x 12·5 mm thick, case-hardened steel plates and these were cast into the beam. These plates incorporated machined-V's so that a positive and repeatable location was achieved during both the static loading and vibration testing. Access to the reinforcement at the selected 'damage' positions was provided by moulded voids around the central, longitudinal reinforcing-bar (Figure 3.3).

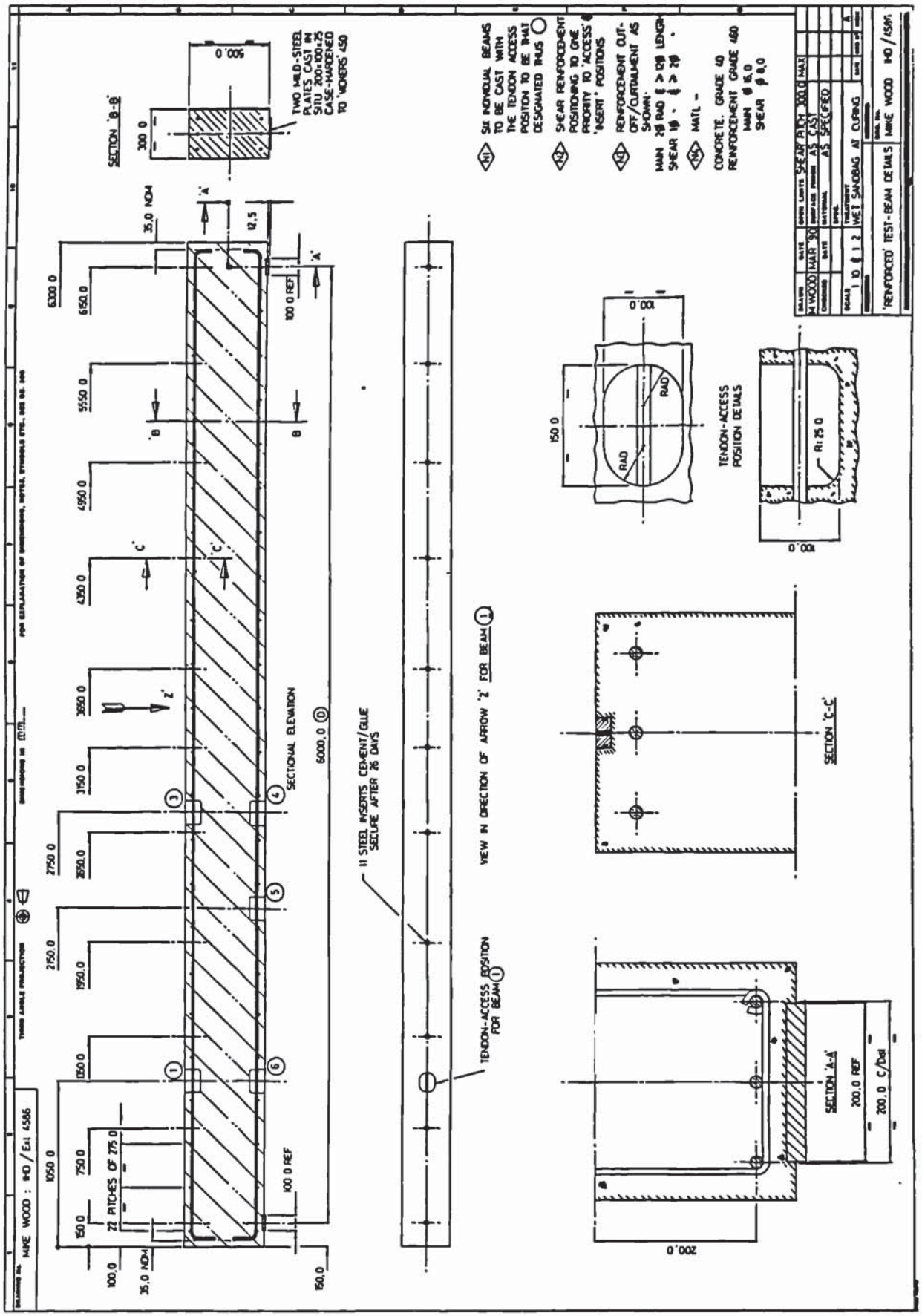

Figure 3.1 Ordinary-reinforced test-beam design

Eleven steel disks were embedded in the upper-side of the beam at prearranged span positions to allow the measurement of corresponding accelerations during vibration testing.

3.2.2 Post-Tensioned Beam Design

The post-tension beam design (Figure 3.4) was basically that of the ordinary-reinforced beam, except the design incorporated 36 mm diameter ducting instead of the six longitudinal bars. This duct dimension was typically that for systems of this type (Woodward, 1981) and the high-tensile reinforcement was inserted after casting. The post-tension reinforcement consisted of six 6·5 m lengths of nominally 16 mm diameter, grade 835 steel (BS 4486: 1980). The prestress induced in each tendon was limited to 40% of the yield strength. Additional shear reinforcement was incorporated in the first 500 mm of each end of the beam to prevent end block splitting. Two 25 mm thick steel end-plates were positioned within the mould prior to casting to provide anchorages between which to tension the tendons. The reinforcement and end-plates represented approximately 7 % of the overall mass of any post-tensioned beam.

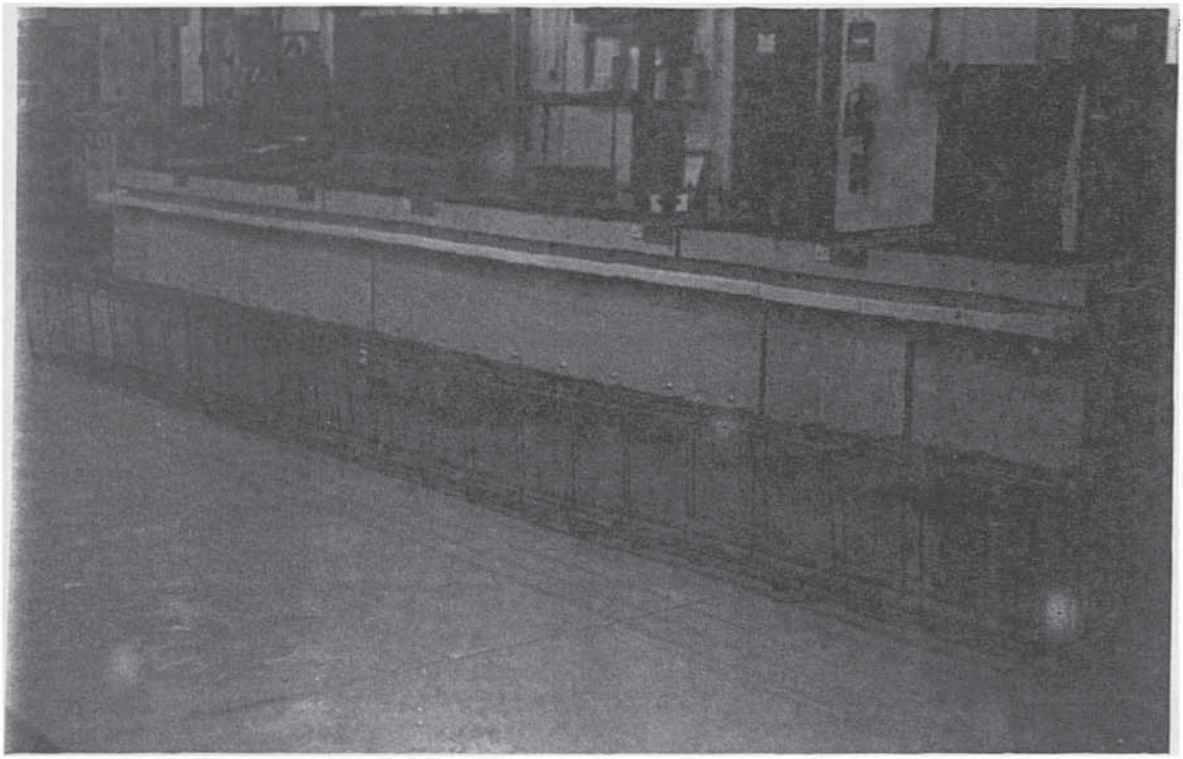

Figure 3.2 Steel reinforcement cage and beam mould

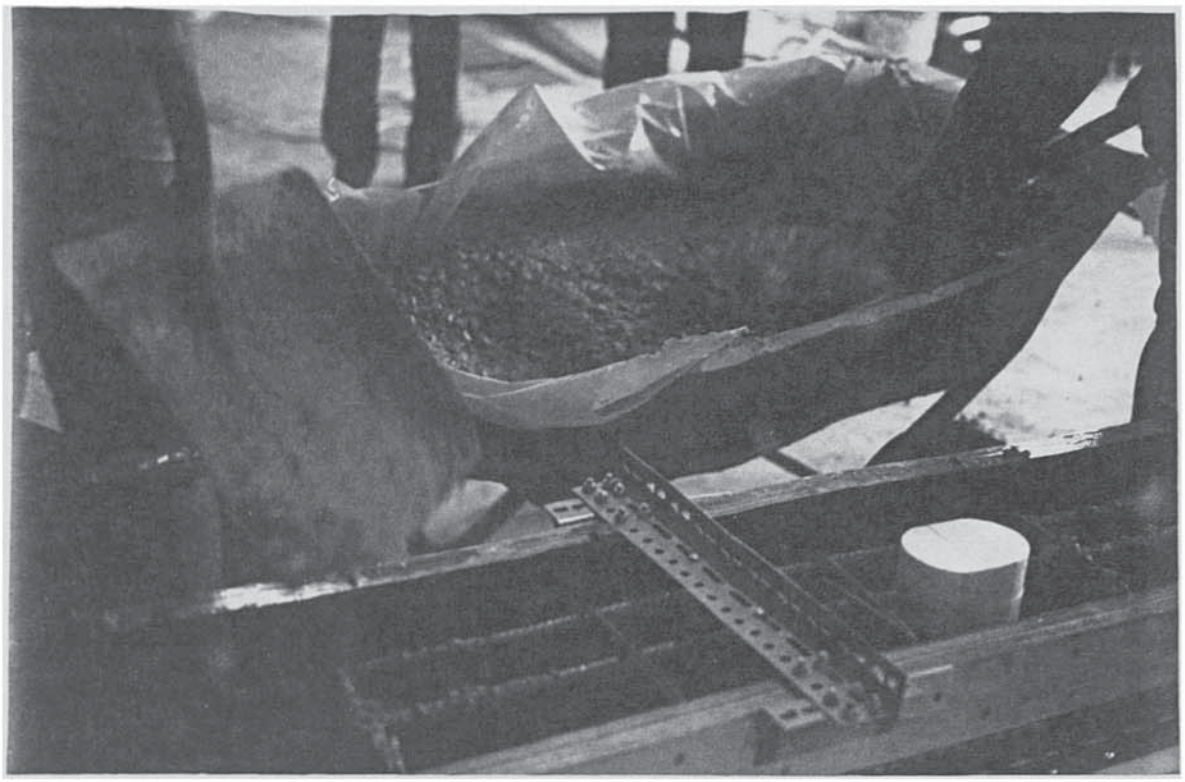

Figure 3.3 Tendon access position

3.2.3 Casting Procedures

The casting procedures used to produce each test-beam were standard and a detailed description of these is presented in Appendix 3. Atypical operations were, however, required to customise each specimen, these included creating tendon-access voids using a carefully positioned expanded polystyrene mould assembled around the central reinforcement for each test designation. The concrete was carefully placed in the mould manually and any entrained air-bubbles or aggregate concentrations were dispersed throughout the beam length using poker vibrators. Transverse ultrasonic pulse velocity (UPV) readings were made periodically to monitor the concrete quality in addition to the standard concrete cube tests. After 26 days the steel inserts were bonded into the top surface of the beam. The testing of the beam specimens commenced on day 28 after casting.

The procedure adopted for the prestressed specimens was similar to that for the ordinary-reinforced beams with the tendon-duct cores created using inflated rubber tubing (Figure 3.5). This technique avoided the difficulties in extracting taped-formers

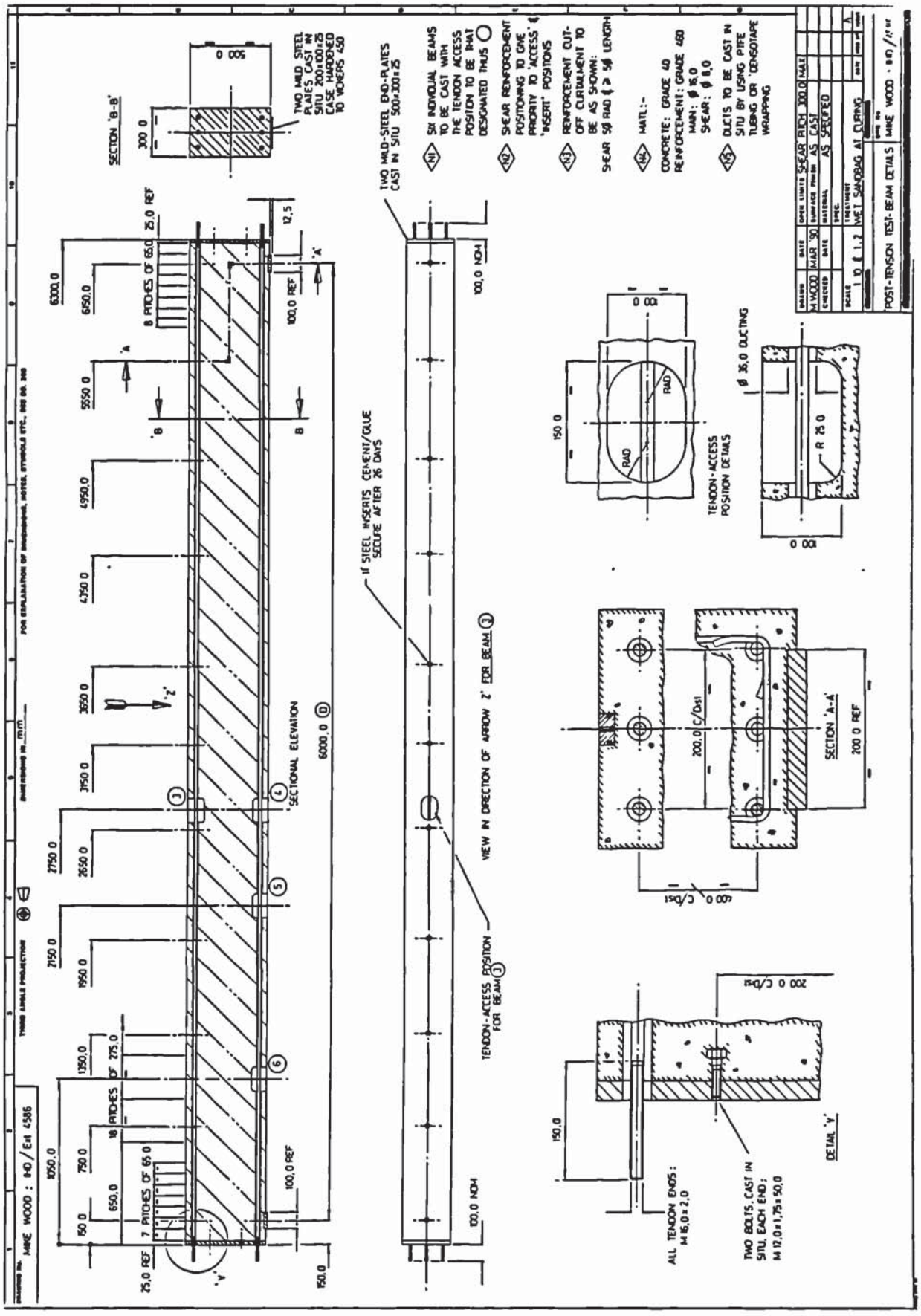

Figure 3.4 Post-tensioned test-beam design

from the beam prior to the grouting process. Pre-tensioning of each tendon was achieved using a proprietary, hydraulic stressing system until the prescribed preload was achieved. During these operations the load-cells preloads were monitored for any fluctuations. The first of these beams showed no discernible changes in the applied preload of all six tendons after overnight monitoring. Beam-testing again commenced 28 days after casting.

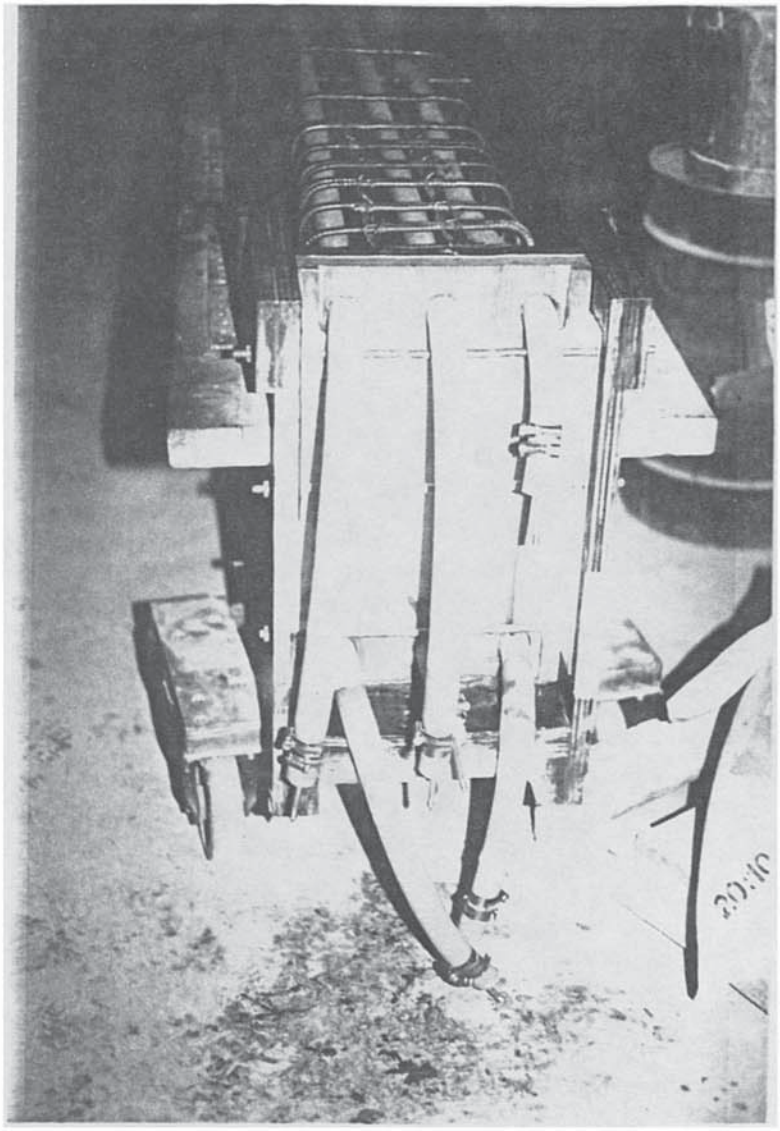

Figure 3.5 Post-tensioned beam duct tubes

3.2.4 Material Testing

Experimental data were made available for the modelling detailed in Chapter 4 by materials tests that were undertaken in parallel with the beam casting programme. Test specimens were manufactured from the tendon reinforcement 'offcuts' and standard tensile tests established the mean properties of each of the steels employed. The ordinary reinforcement material had an average proof-stress of 565 N/mm^2 and a corresponding elastic modulus of 196 kN/mm^2. The resultant proof-stress of this steel was approximately 20 % greater than its nominal grade of 460 whilst the elastic modulus was within 5 % of that accepted for steel. In comparison the post-tensioning steel returned strength values of 830 N/mm^2 and 218 kN/mm^2 respectively and these material characteristics were within 5 % of those expected.

Concrete cubes were cast at the same time as the beams and cured in accordance with BS 1881: Part 111: 1983. Compression tests on these cubes were undertaken at periodic intervals in line with Part 116 of this standard. UPV tests were made to monitor the material properties of the beams with curing-time and, after being combined with the cube density measurements and an assumed Poisson's ratio, these data broadly supported the cube strength results. The cube compression data for each beam show a range in mean value between 36 N/mm^2 and 58·5 N/mm^2 at 28 days (Table 3.1).

Beam	R1/A	R3/B	R4(a)/C	R4(b)/E	R4(c)/F	R5/G	R6/D
7 day (N/mm^2)	42	39	36	37·5	24	34	32
28 day (N/mm^2)	49	50	47	52·5	36	44	42
Beam		P3/H	P4(a)/I	P4(b)/K	P4(c)/J	P5/L	P6/M
7 day (N/mm^2)		44·5	40	38·5	41	35	34·5
28 day (N/mm^2)		58·5	51·5	47	50	45·5	44·5

Table 3.1 Test-beam cube strengths

3.3 Test Procedure

The laboratory temperatures during the curing and brief testing periods were sensibly constant. Beam testing took the form of two separate operations which required the specimens to be moved frequently between test sites. All test-beams were statically loaded within a test-rig and then repositioned on the laboratory floor for vibration response testing. The movement of these 2·5 tonne beams necessitated a number of safety considerations which are detailed in Appendix 1.

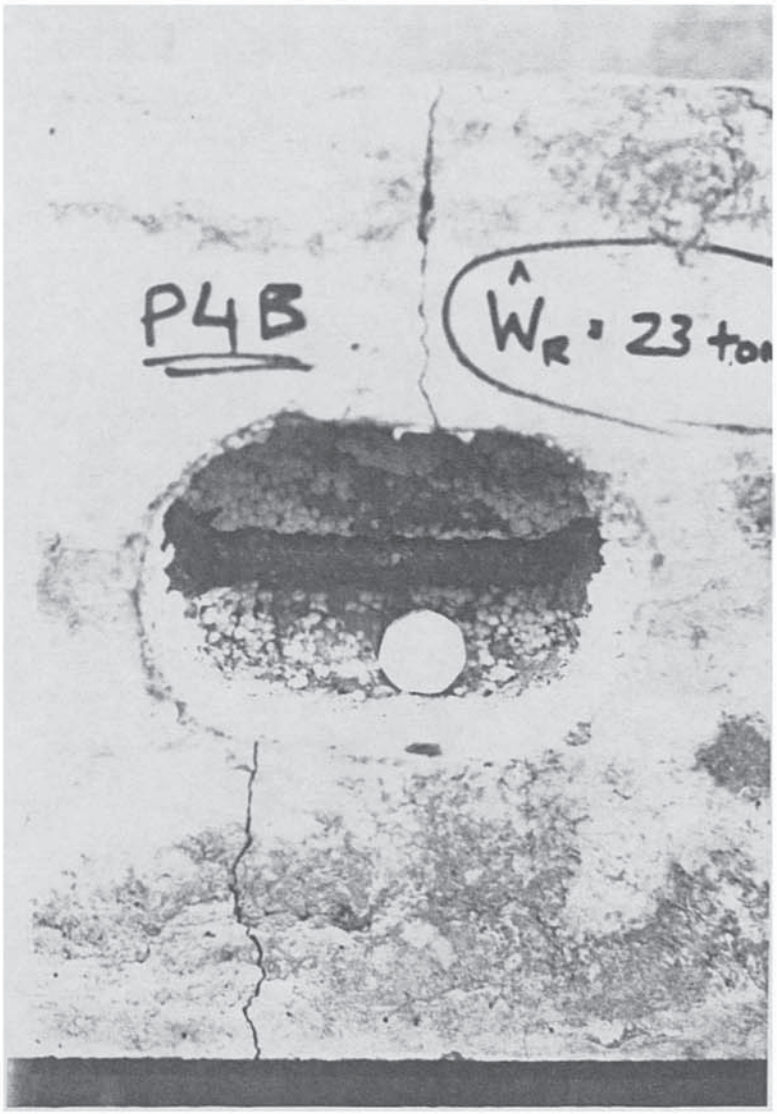

Figure 3.6 Tendon access position and induced damage

3.3.1 Damage Instigation

The specimen was first placed on the laboratory floor and, if the initial damage position was underneath the beam, it was carefully rolled on its side onto supporting wooden planks using fork-lift trucks. Access to the reinforcement was provided by removal of the expanded polystyrene void-mould. For any beam test both a position and initial level of reinforcement damage was designated. The magnitude of this damage could be complete severance, removal of half the area the reinforcing-bar or the material was left intact. Dependent upon the level of damage required either a pistol-drill was used to remove half of the reinforcement area at that point (Figure 3.6) or a hand-held mini-grinder was used to sever the tendon completely.

3.3.2 Static Loading of Beams

The test-beam was lifted into position within the loading arrangement (Figure 3.7) after the prescribed level of initial damage had been induced. The ram load was maintained for two minutes at the required level then unloaded and the beam carefully returned to the laboratory floor for vibration testing at that condition. A period of approximately 15 minutes would elapse before reponse measurement took place in order that specimen 'recovery' could take place. The load/test procedure was repeated for several prescribed loadings until the specimen could no longer sustain an increase in load and the ram-load at this point was noted. Subsequently the beam was returned to the laboratory floor and both the main and minor crack-systems were recorded for future reference after the final vibration test (Figure 3.8).

3.3.3 Vibration Response Measurement

Measurements were taken to establish the transverse modes of vibration for each of the beams during the programme of progressive load application described above. Mode shapes were also evaluated to ensure that the correct modes of vibration were identified. Impact-inertance measurements, $A(\omega)$ or 'A', were made along the beam lengths in order to identify the vibration characteristics. The impact was imparted to the beam by the use of an instrumented hammer at each of the disk positions whilst the specimen was supported on the laboratory floor by rollers. Ten bolts were firmly secured to the beam to provide unambiguous impact-points (Figure 3.9(a)). The remaining disk position allowed measurement of the resultant responses using a magnet-mounted accelerometer (Figure 3.9(b)).

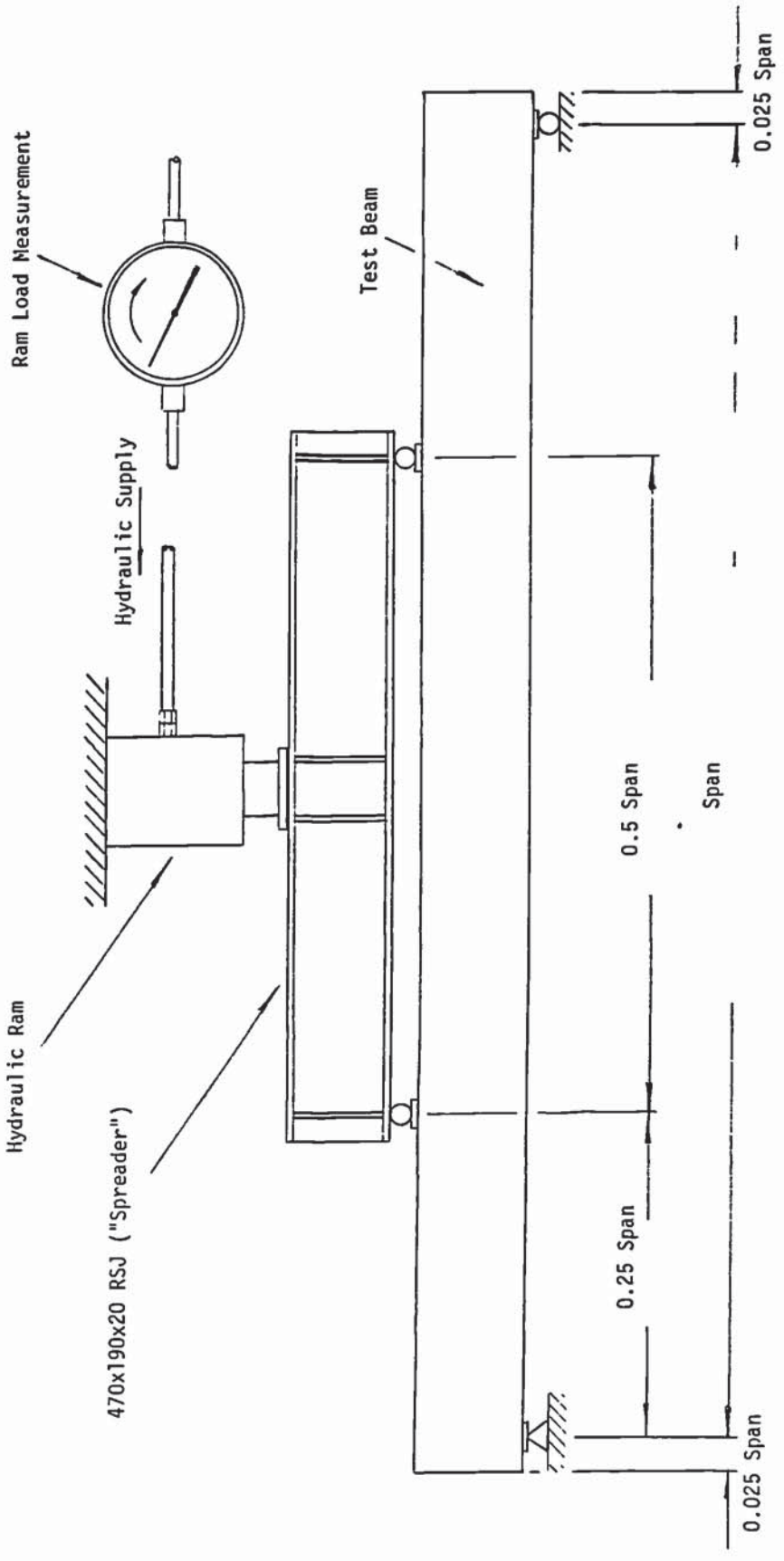

Figure 3.7 Schematic of beam test-rig

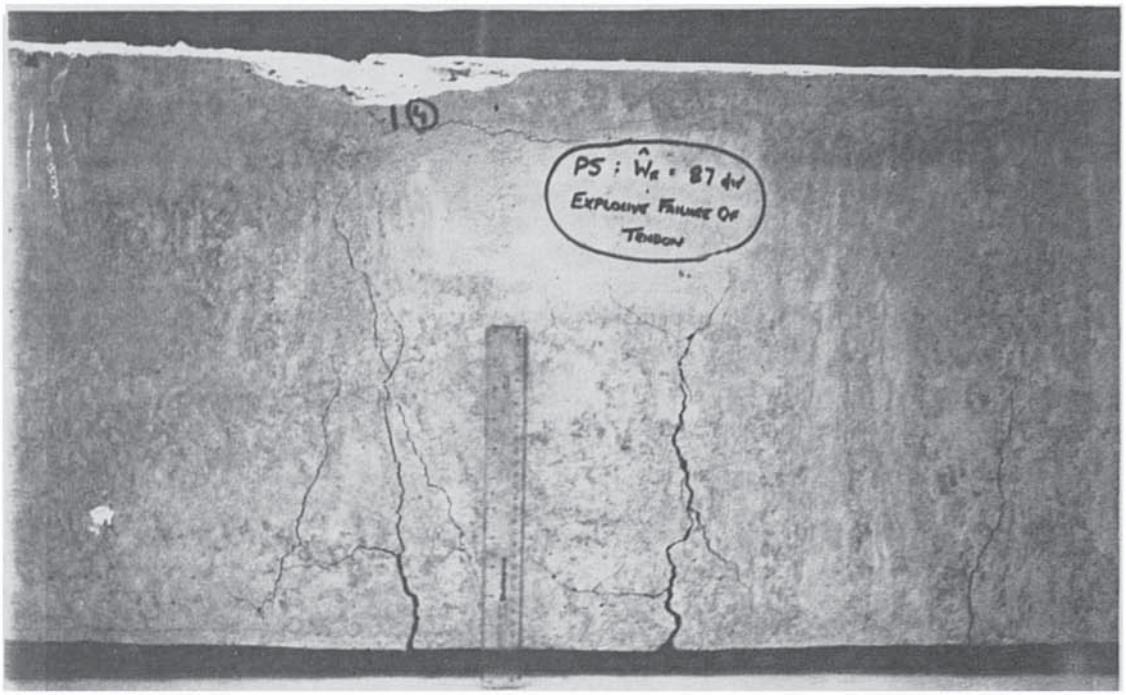

Figure 3.8 Beam failure crack mapping

The equipment used for these investigations (Figure 3.10) is typical of that generally available, full details of which are presented in Appendix 3. It is notable that the impact hammer incorporated an interchangeable strike-face and the hard-rubber striker which was selected for these tests reproduced a sensibly flat impact-spectrum over a 0-1kHz bandwidth. The impact and response signals were processed simultaneously by the analyser to gain the inertance-frequency-response-functions A_{ij} F.R.F. The inertance response $accel_i/force_j$ was measured since it is the easier of the response-function family of data to obtain.

The procedure to extract the data from each beam-test was to position the accelerometer at the initial response point and the beam was then struck at the first impact-site. There were eight impacts per site-measurement and the analyser averaged the resultant inertance data after each strike so as to minimise any noise effects which were present. The data were transferred from the analyser to the computer and this response data-aquisition procedure was repeated for each of the impact positions along the beam length including at the accelerometer site. This point-inertance, as opposed to the cross- (or transfer-) inertance of the other measurements, required careful impacts immediately adjacent to the accelerometer. This sequence of tests created a complete data-mapping of the beam from the 121 (i.e. 11 x 11) FRF measurements. The sequence was subsequently modified to three response and eleven impact positions. This minimised the test-time after data analysis had proved that the quality of results was consistent over the range of only 33 FRF's.

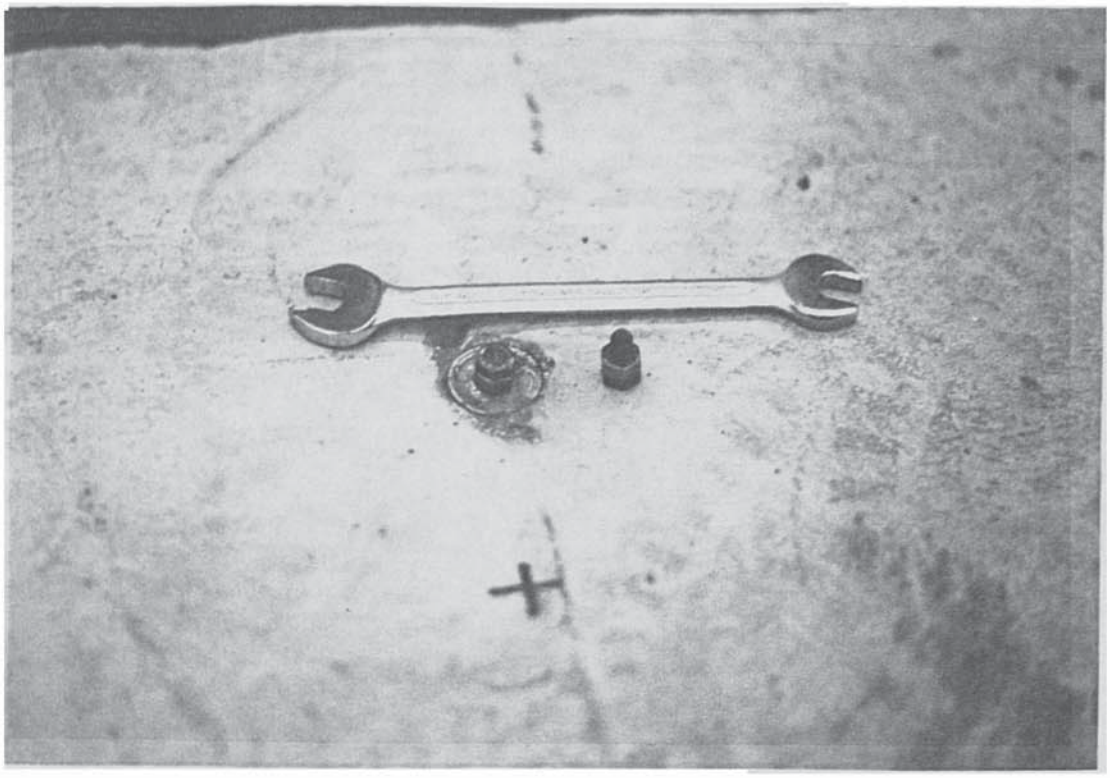

Figure 3.9(a) Beam impact position

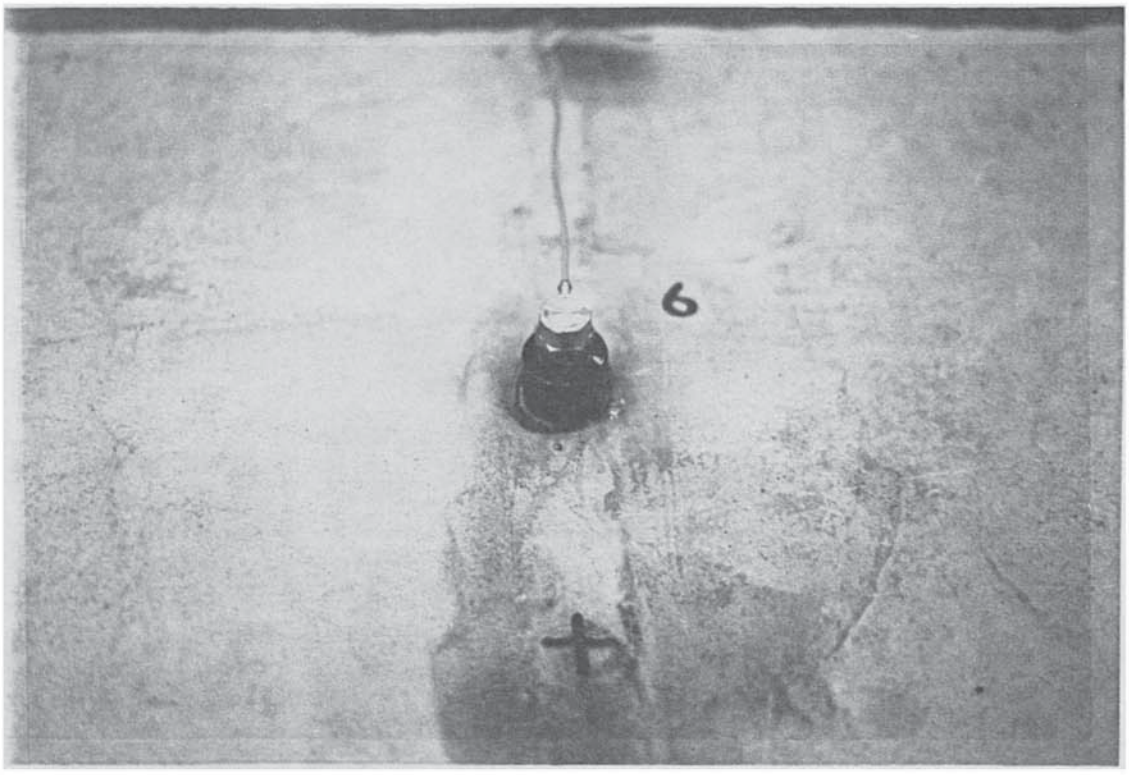

Figure 3.9(b) Beam response measurement arrangement

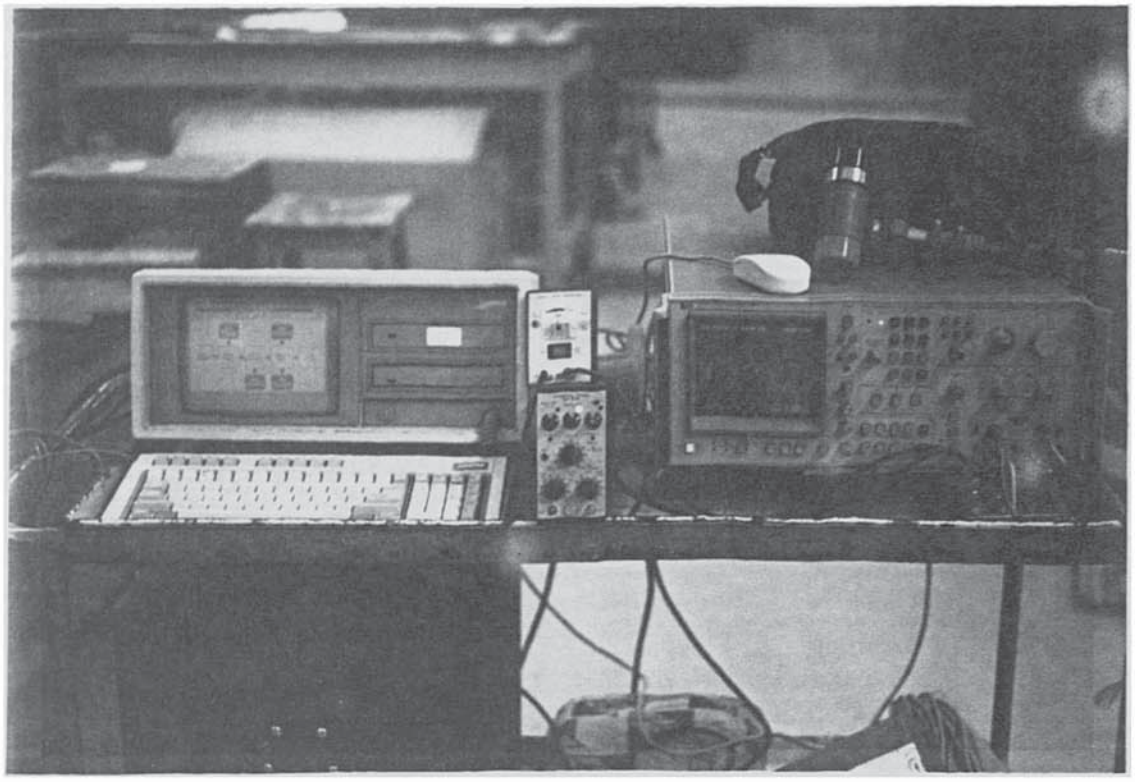

Figure 3.10 Beam response test equipment

3.4 Experimental Data Extraction

The static beam-load conditions to which the frequency data corresponded were those of unloaded 'undamaged' and initial 'damage', cracked, serviceability limit state and ultimate limit state. An additional, 'intermediate' load condition between those of serviceability and limit states was included. The two unloaded measurements of undamaged and damaged were made to ensure that no response changes occurred after the beams had been repositioned prior to the loading tests: this proved to be the case. The applied moments corresponding to these conditions were calculated using the nominal material characteristics of each type of beam design in parallel with the performance requirements of BS 5400: Part 4: 1978. Serviceability Limit State is in practice ignored by Part 4 of the code for post-tensioned concrete designs (Clark, 1983) therefore a load was estimated using a hypothetical condition which incorporated both

the ordinary-reinforced serviceability criterion 0·5 f_{cu} and the applied concrete-prestress present in the beam. These applied loadings were subsequently normalised for the individual beam properties during the damage analysis procedures of Chapter 4.

The vibrational frequency and mode-shape data were extracted for each response position and the corresponding eleven impact FRF's using a proprietary analysis package. The extracted frequencies from all the response and impact positions were then averaged for each beam condition.

3.5 Preliminary Results

Figure 3.11 is a schematic compilation of the crack-systems present at failure for both beam series. It shows initial damage locations and levels, resultant minor and major crack-features, reinforcement failure mode (if any) and comments regarding the condition of the concrete at the crush-zone.

The feature of minor or visible cracks present throughout the region between the spreader-rollers was common to all the test-beams. Modes of failure reflected the positions and levels of initial damage in the majority of cases. The method of using a simple hole drilled through the reinforcement introduced a local stress magnification factor of 2·2 in the remaining material section and this invariably led to explosive failure of the tendon at these points. It arguable that this practice of cross-section reduction would reflect conditions in the practical case but no other practical method of corrosion representation was available. Shear failures characterised beams where initial damage locations in the tensile zone were outside the region of constant bending-moment. Classical yield failure modes were shown by beams with no initial damage or if the initial damage was within the span bounded by the end-support and spreader-roller positions. Localised crushing and delamination was sometimes apparent and, since there was no common feature in initial damage condition in these cases, it suggests that this failure feature reflected local material strengths.

Figure 3.12 shows two example mode shapes typical of the responses shown by each type of beam design. The first of these can be recognised as a 'fundamental' mode of vibration whilst, although there are signs of end motion at the roller-support positions, the second suggests the sixth harmonic of the fundamental. In all cases the frequencies extracted by the computer software at each load condition were checked against the resultant mode shape. Although there was on average only 500 mm between measurement positions the resultant mode shapes typically showed clear and

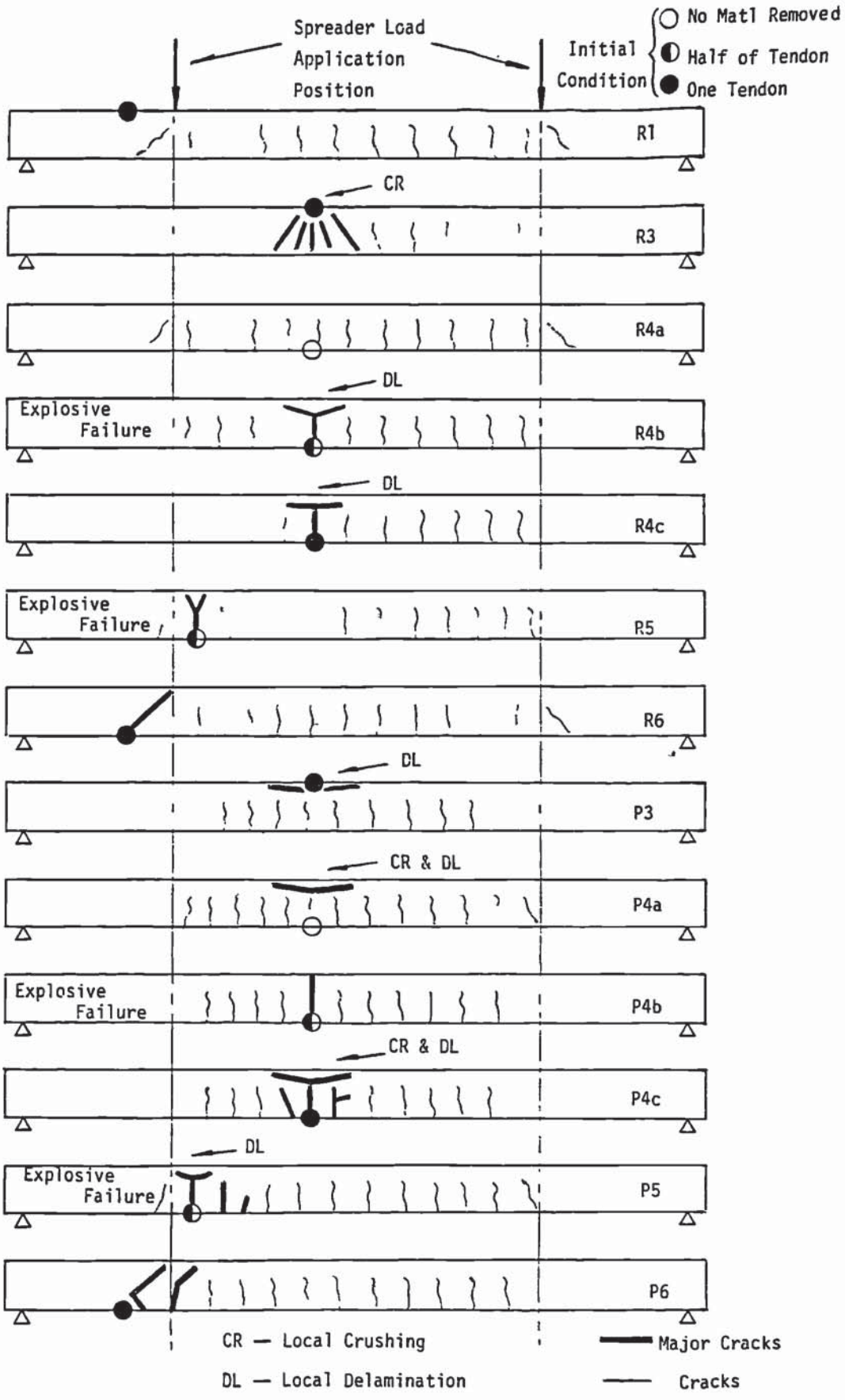

Figure 3.11 Test-beam crack systems at failure condition

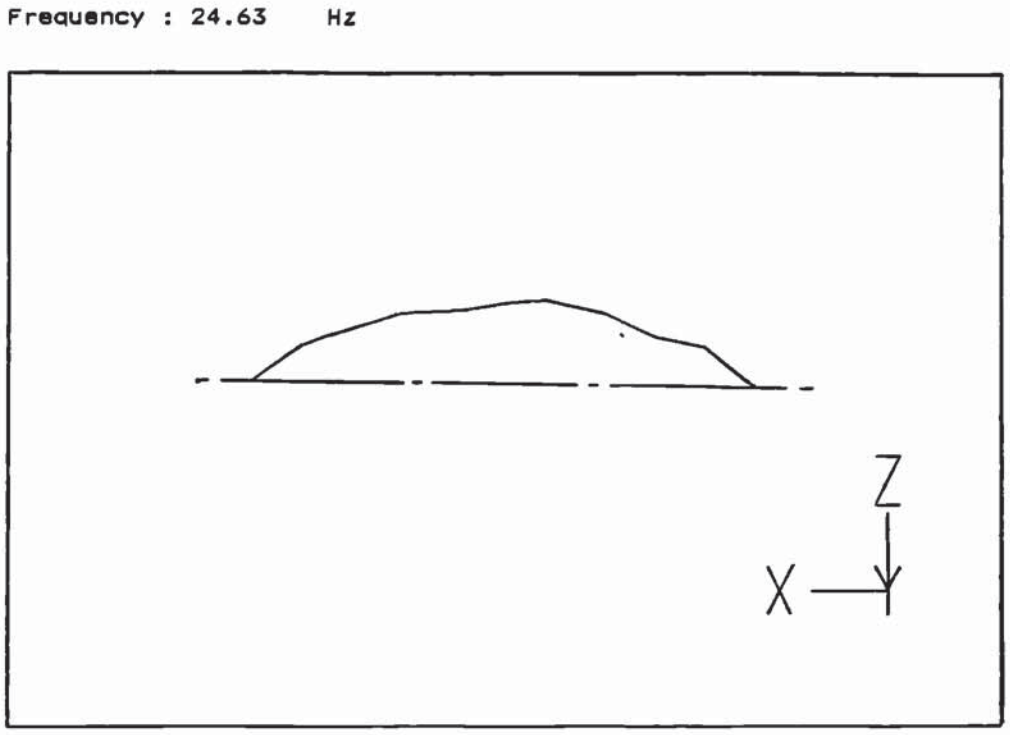

Figure 3.12 Example beam mode-shapes

unambiguous displacements, even for the highest measured frequencies. Table 3.2 presents the results of this data extraction procedure for the ordinary-reinforced test-beams and Table 3.3 does likewise for the post-tensioned beams. Omissions in these compilations show where frequencies and/or mode shapes could not be positively indentified.

It was noted that the majority of the modes shapes resulting from the data analysis showed characteristics which were not of a purely simply-supported beam system and Figure 3.13 gives examples of these. Considerable motion is present at the end-support

	R1 Undamaged	R1 Cracked	R1 Service	R1 Intermed	R1 Yield	R3 Undamaged	R3 Cracked	R3 Service	R3 Intermed	R3 Yield
1	22 55	No Data	No Data	No Data	14 97	22.18	19 86	18 78	16 91	11 37
2	69 02	No Data	No Data	No Data	57 43	62.98	60 67	62 69	60 28	56.40
3	102 03	No Data	No Data	No Data	79 72	94 67	90 32	94 22	91 09	83.93
4	168 30	No Data	No Data	No Data	120 83	156 54	146 55	140 20	130.94	101 82
5	234 80	No Data	No Data	No Data	179 13	262 47	245 31	221 38	227 80	207 20
6	393 30	No Data	No Data	No Data		402 28	379 34	339 57	330.28	301 44
7	544 25	No Data	No Data	No Data	372 11	563 44	526 28	481 02	463 56	397.10
8	710 62	No Data	No Data	No Data	482 01	735 61	683 41	632 33	598 13	541 98
9	894 88	No Data	No Data	No Data	698 15	919 42	866.76	788 64	764.83	667 49
10		No Data	No Data	No Data				963.88	940.01	942.24

	R4a Undamaged	R4a Cracked	R4a Service	R4a Intermed	R4a Yield	R4b Undamaged	R4b Cracked	R4b Service	R4b Intermed	R4b Yield
1	22 03	18 47	16 87	15 01	12 00	22 97	19 62	19 90	18 15	15 82
2	74 29	62 57	56 78	53 64	48 20	67 56	58 44	67 02	58 73	55.14
3	108 87	94 47	94 96	91 82		107 56	101 43		107 56	
4	175 70	159 19	152 55	0 10	141 80	194 55	180 57	165 66	156 97	143 04
5	262 11	235 42	217 12	213 25	172 63	280 33	256 12	243 15	227 38	198.76
6	392 54	352 04	324 28	300 58	250 98	416 66	382.41	347 76	335.29	283 89
7	592 55	485 75	435 29	413 94	301 07	579 78	535 18	503.76	485 51	356.32
8	707 00	634 78	583 22	545 51	408 55	756 66	689 81	652.70	625 68	543.18
9	890 43	306 88				943 96	875 73	820 71	791 58	741 34
10			981 96	944 55				983.59	960 82	912.85

	R4c Undamaged	R4c Cracked	R4c Service	R4c Intermed	R4c Yield	R5 Undamaged	R5 Cracked	R5 Service	R5 Intermed	R5 Yield
1	22 41	17 85	No Data	No Data	14 37	22 55	20 86	17 47	No Data	16.95
2	74 90	62 19	No Data	No Data	55 56	67 74	65 94	57 14	No Data	58.41
3	157 46	107 84	No Data	No Data	100 45	107 87	99 07	88.61	No Data	
4	191 79	169 47	No Data	No Data	144 77	184 36	162.81	153.66	No Data	142.76
5	268 29	239 84	No Data	No Data	206 53	276 68	251 01	232.03	No Data	204.63
6	396 07	339 69	No Data	No Data	306 85	408 22	375 48	343 63	No Data	296.23
7	538 33	480 17	No Data	No Data	359 40	559 64	520.31	479 91	No Data	425 20
8	690 80	606 55	No Data	No Data	539 31	734 05	688.28	641 29	No Data	579.22
9	859 92	737 63	No Data	No Data	646 44	904 58		791 59	No Data	674.04
10		920 62	No Data	No Data	876 11			964.56	No Data	935.83

	R6 Undamaged	R6 Cracked	R6 Service	R6 Intermed	R6 Yield
1	22 78	18 50	17 09	15 82	13 53
2	66.81	63 02	61 82	50 88	49 51
3	105 52	94 37	83 67	77 79	66 24
4	184 91	168 87	150 64		118 89
5	268 10	242.10	223.66	157.18	153 97
6	390 40	354 03	329.22	292.37	236.38
7	543 00	482.77	431 70	379 67	301.07
8	707 68	627 19	580 21	510.19	372.42
9	884 71		730 48	626.41	538 86
10		920.32		858.55	792.75

Table 3.2 Mean response frequencies of ordinary-reinforced beams

positions in all of the cases illustrated and this suggests interactions between the roller-support and/or laboratory-floor stiffness' and those of the beam system. Calculations based on an uncracked beam section and elastic properties derived from the average measured cube strength indicated a fundamental simply-supported beam response of approximately 25 Hz, which was comparable to a mean frequency of 23 Hz observed for all the series of tests. Estimation of a linear roller/floor interface stiffness suggested the lowest rigid-body beam mode to be 36 Hz and, on re-inspection, the FRF data from the beams showed a perceptable response in the region of this frequency. If the two characteristics of rigid-body and simple-beam vibration are combined then a composite response may be obtained (Thomson, 1988). This simple analysis suggests two frequencies for the combined system of 21 Hz and 100 Hz. The former response of

	P4a Undamaged	P4a Cracked	P4a Service	P4a Intermed	P4a Yield	P4b Undamaged	P4b Cracked	P4b Service	P4b Intermed	P4b Yield
1	24 64	23 94	23 74	22 07	12 82	23 28	22 12	21 81	No Data	20 73
2	80 95	70 58	71 79	66 83	57 80	66 59	61.10	67.66	No Data	67 98
3	126 64	119 36	117 34	110 94	87 96	114 49	109 36	113.64	No Data	99.71
4	216 50	194 57	193 04	180 10	142.33	181 08	159 57	181.93	No Data	166 69
5	270 91	272 69	265 99	263.70	187 17	267 40	259 10	263 49	No Data	239 63
6	410 59	407 40	399 97	394 36	268 45	406 60	396 00	394 84	No Data	377 00
7	569 39	566 33	558 80	553 19	397 63	564 53	553 66	545.74	No Data	520 67
8	745 66	738 73	728 49	721 34	491 24	738 31	723 88	705 19	No Data	670.78
9	937 02	921 28	908 95	904 91	706.55	929 17	912 98	890 95	No Data	832.25
10									No Data	

	P4c Undamaged	P4c Cracked	P4c Service	P4c Intermed	p4c Yield	P5 Undamaged	P5 Cracked	P5 Service	P5 Intermed	P5 Yield
1	23 59	22 47	21 67	No Data	14 62	22 81	21 70	21.04	No Data	15 85
2	77 37	64 20	64 86	No Data	57 85	71 94	67 08	67 11	No Data	59 44
3	126 21	109 10	114 59	No Data	105 82	110 83	101 54	101 74	No Data	88 56
4	189 04	170 21	168 23	No Data	156 16	168 45	141 65	178 10	No Data	151 01
5	285 49	265 02	255 07	No Data	236 95	257 45	249 68	247 37	No Data	218 76
6	422 14	403 11	387 33	No Data	349 47	396 21	388 45	380 27	No Data	324 69
7	573 91	560 88	539 22	No Data	452 21	548 97	535 49	524 47	No Data	436.70
8	748 13	728 76	699 57	No Data	574 43	716 29	698 04	685 09	No Data	
9	935 09	908 06	870 20	No Data	701 81	891 46	861 81	851.94	No Data	700 80
10				No Data	861 21				No Data	870 34

	P6 Undamaged	P6 Cracked	P6 Service	P6 Intermed	p6 Yield	P3 Undamaged	P3 Cracked	P3 Service	P3 Intermed	P3 Yield
1	21 09	21 91	20 23	17 01	12.85	24 34	23 19	No Data	No Data	14 47
2	68 05	64 97	66 82	62 33	51.24	74 70	68 69	No Data	No Data	63.53
3	105 04	107 81	99.59	95.00	98.36	112 30	108.76	No Data	No Data	107.27
4	167 07	169 83	160 59	147 42	140.10	173 80	168 01	No Data	No Data	152 26
5	266 71	262 43	243 99	213 44	188.42	272 41	262 94	No Data	No Data	255.13
6	404.83	391 81	389 38	319 44	239 93	411 41	400 79	No Data	No Data	305.24
7	555 48	541 40	531 05	460 98	352 76	573 21	561 01	No Data	No Data	417 30
8	726.73	703 88	690 65	613 55	478 35	736.77	726 44	No Data	No Data	539 11
9	916 35	882 91	863.83	748 01	602.24	944.87	931 03	No Data	No Data	683 66
10								No Data	No Data	955.35

Table 3.3 Mean response frequencies of post-tensioned beams

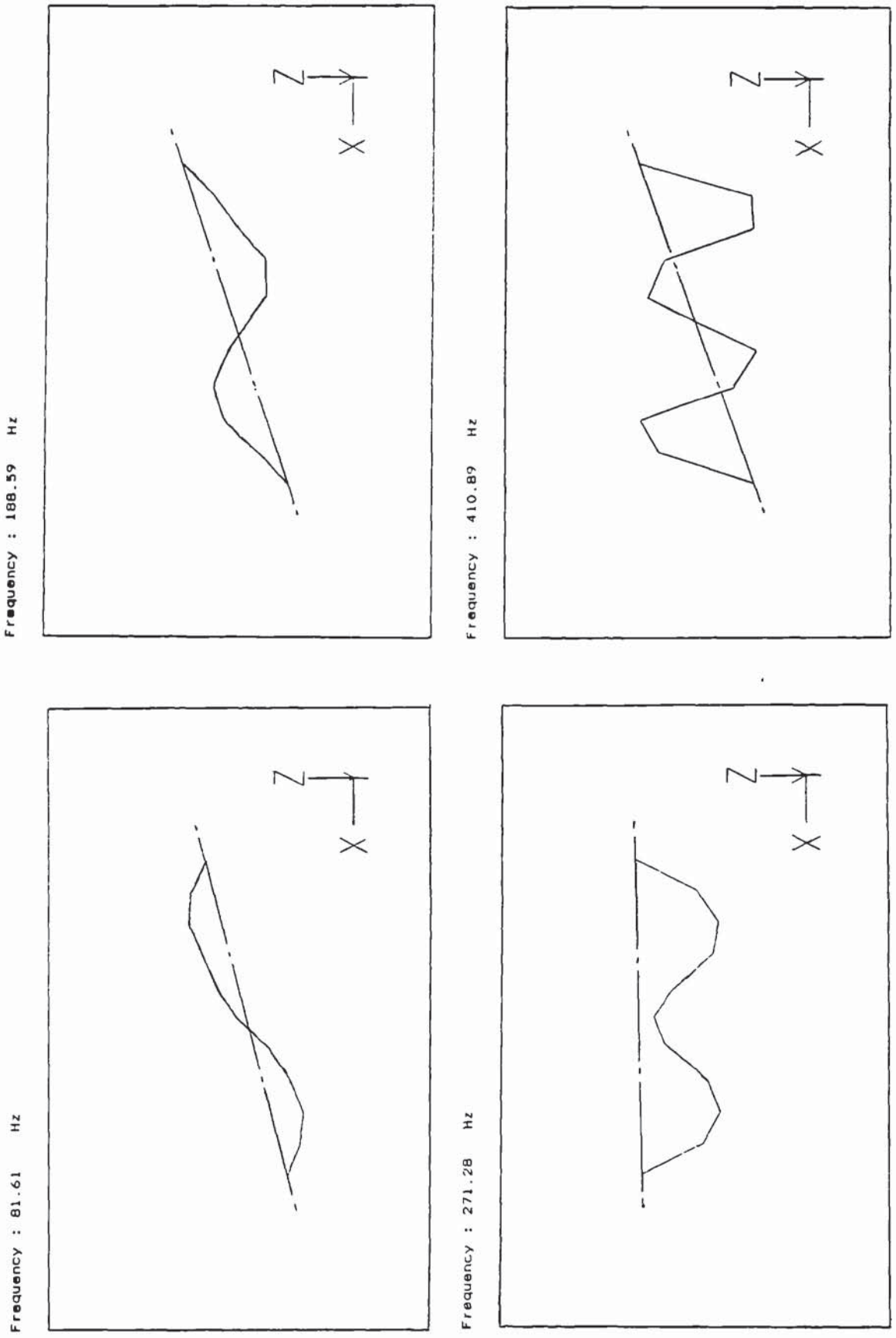

Figure 3.13 Composite beam/support mode-shapes

21 Hz is near to that of the fundamental beam mode and the 100 Hz response is almost coincident with the first harmonic. Examination of the fundamental mode shape animations showed no significant motion at the supports. Estimations of other possible beam responses were made in parallel with the combined system calculations, such as potential lateral and torsional modes, since it was conceivable that cross-coupling of the beam responses could have taken place. 100 Hz was again calculated as a possible response and so these combinations of effects are assumed to have produced the poor beam modes extracted around this frequency.

Figure 3.14 shows example curves of the mean observed frequencies against the applied-load condition for an ordinary-reinforced and a post-tensioned beam example. Gradual reduction in the beam response frequencies is observed in both cases, however, the onset of this decay is slightly delayed in the post-tensioned results. Although the majority of these results include composite system responses the characteristics are similar to those obtained by Turner (1984).

3.6 Non-Linear Behaviour

The typical data of Figure 3.14 presented a problem: it was evident that their usage would be limited in the practical case. Any potential damage condition could only be predicted if the characteristic beam responses of a specimen bridge-beam were known. Curves of this type could then be used as 'look-up' tables to establish the approximate position of the beam along the load-condition axis. However in the practical case it is highly unlikely that curves of these type would either be available or predictable due to the practicalities in obtaining useful experimental data or in accurately modelling *in situ* conditions. A method was required to identify the likely condition of the beam without requiring prior knowledge. A possible solution to this problem lay in the behaviour of the parent material(s) of the beam when subjected to loading.

At the macroscopic level, concrete is assumed to be a homogeneous material and its behaviour may be predicted using this linear idealisation. Reciprocity between load and response for two regions within the same structure requires linear material characteristics. However, at a microscopic level, local non-homogeneity occurs due to mortar/aggregate interface discontinuities such as pores, fissures and air voids. These discontinuities cause local stress-concentrations which lead to internal microcracking when the structure is at the early stages of loading. Subsequent reloading generates

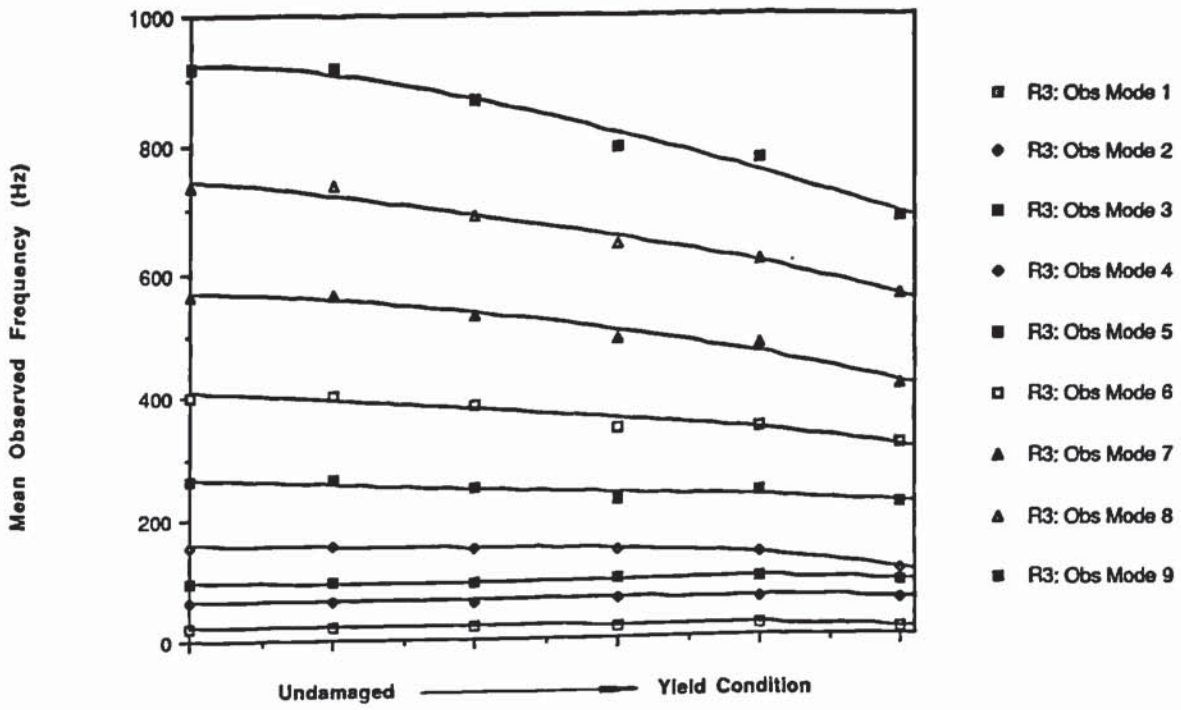

Figure 3.14(a) Ordinary-reinforced beam responses versus load-condition

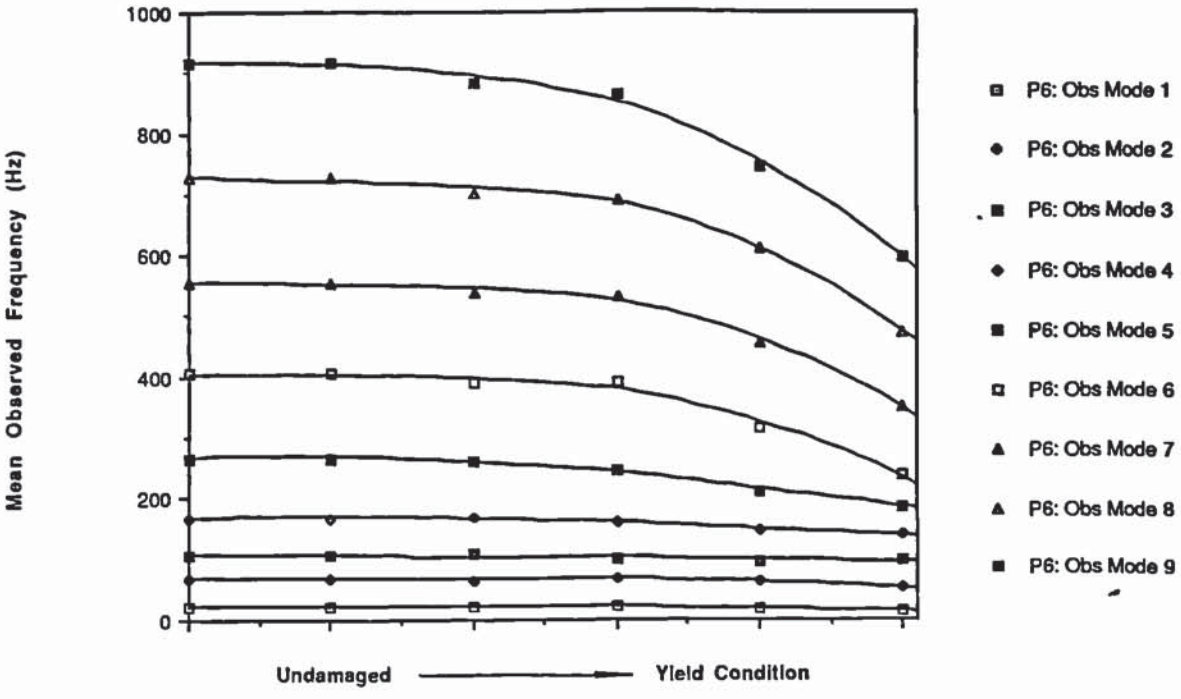

Figure 3.14(b) Post-tensioned beam responses versus load-condition

additional microcracks and macrocracks then develop from those already present. Cracks create non-linear stress-strain behaviour. Thus a crack damaged material does not retain its linearity and hence it cannot retain reciprocity between regions within the structure, $A_{ij} \neq A_{ji}$.

3.7 Non-Reciprocal Behaviour

The FRF data of ordinary-reinforced beam R3 were then re-examined. Two measurement positions (3 and 9) on different sides of the initial damage area were selected and their reciprocal inertances were compared for each load condition. Figure 3.15 shows a comparison between reciprocal inertances for the undamaged condition in the range of 0-250 Hz . It can be seen that there is very close agreement between traces, although there are signs of a definite differential between the two. Calculations using BS 8007: 1987 guidelines suggested that early thermal-microcracks up to 0·12mm in width may have been created during the curing process. Although great care was taken in moving the beams, additional calculations based on the self-weight of the beam showed that some tensile zone cracking would have taken place. Figure 3.16(a) repeats this

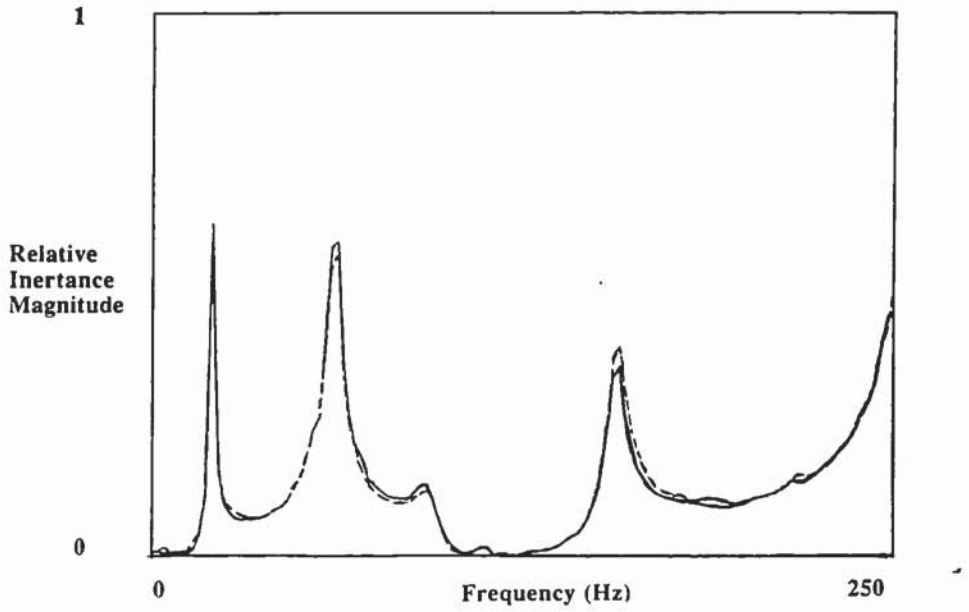

Figure 3.15 Reciprocal inertance comparison for 'undamaged' beam

procedure but at the cracked load condition. In addition to a frequency shift of the resonant responses, the differential between the magnitude of the two traces has markedly increased. Figure 3.16(b) shows the nett result of these data and it can be seen that the maxima coincide with the spectral peaks of the previous figure.

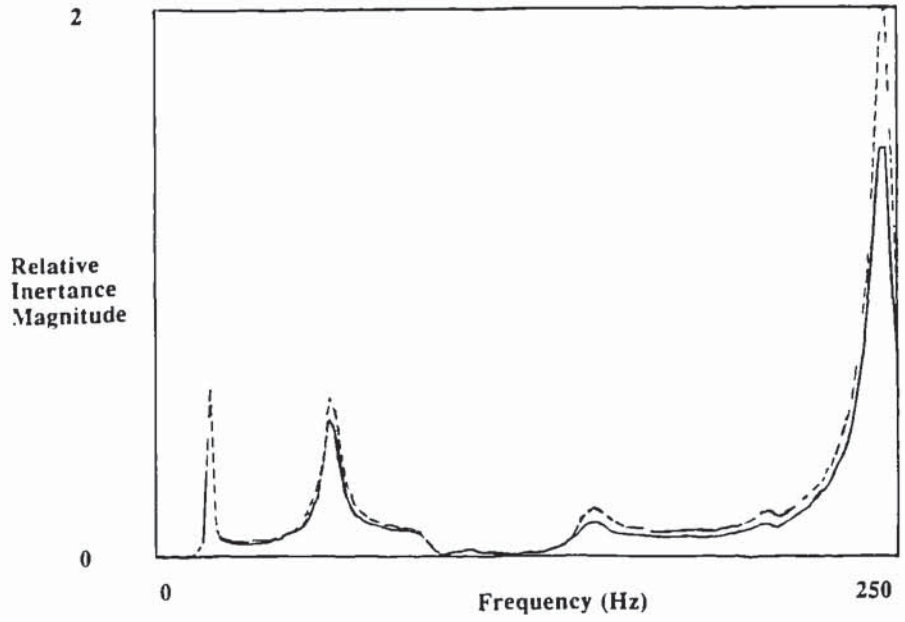

Figure 3.16(a) Reciprocal inertance comparison for 'cracked' beam

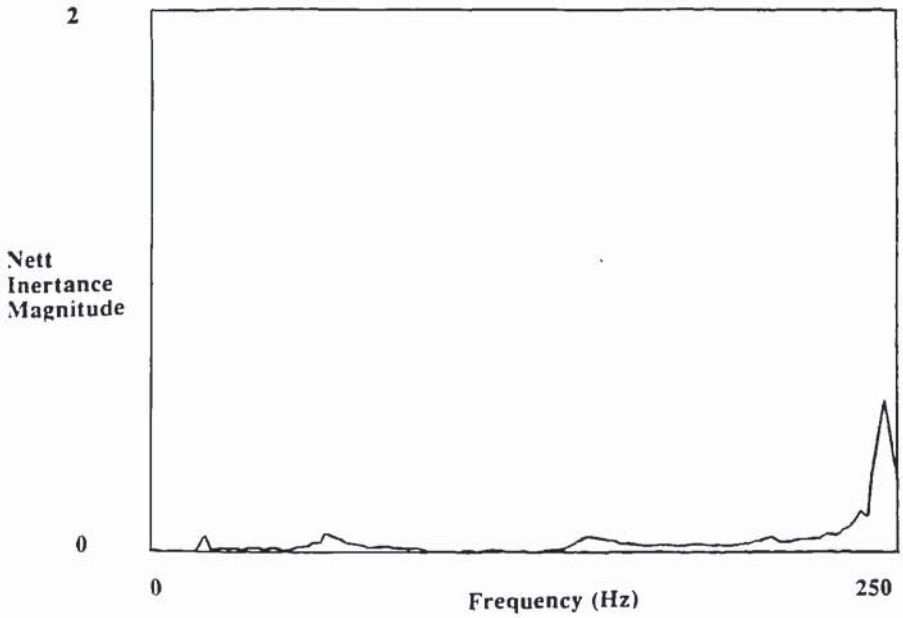

Figure 3.16(b) Nett reciprocal inertance for 'cracked' beam condition

Since the principal areas of interest were located around the spectral peaks, the inertance magnitude was then evaluated for both responses between the half-power points of the corresponding peaks and the mean value of these magnitudes was noted. The half-power points were used since they are a readily established frequency range and are a consistent feature of any spectral peak. The frequencies of the half-power points were established using the 'Real' part of the inertance FRF (Ewins, 1984) from either of the inertance magnitude data and Figure 3.17 illustrates the technique: the maxima of the data are identified and these signify the half-power points. The same evaluation was repeated for the nett magnitude of Figure 3.16(b) between the same frequency bounds and this value was normalised using the mean magnitude. A qualitative measure of the damage in a vibrating structure was then proposed as the relative differential between the two measured inertances and, hence, the expression:

$$\text{Normalised Nett Magnitude (NNM)} = \left| 2\,(A_{ij} - A_{ji}) \,/\, (A_{ij} + A_{ji}) \right| \qquad (3.1)$$

for the frequency domain bounded by the half-power points of the mode. The modulus operation ensures that the absolute value of this measure is returned.

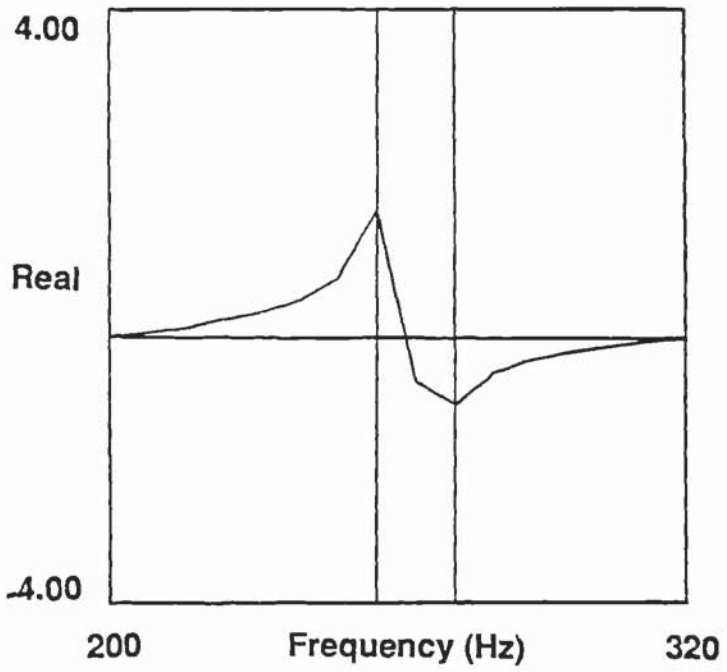

Figure 3.17 Real part of inertance FRF measurement

3.8 Normalised Nett Magnitude Results

The inertance data for ordinary-reinforced beam R3 between positions 3 and 9 were applied in expression (3.1) for all load conditions. Table 3.4 presents the resultant NNM's estimated for several observed frequencies of the beam including 1st, possible 3rd, 4th and 6th transverse modes in addition to a calculated 1st and possible 4th lateral mode. They are tabulated in order of load condition and the final column presents the 'Mean Alpha' condition. The mean alpha criterion is discussesd fully in Chapter 4 but it is presently sufficient to say that it is a measure of damage induced in the beam. Figure 3.18 presents these data graphically for the two observed modes most consistent with beam vibration theory.

There is significant data spread although it may be argued that the general characteristics of results seem consistent with the proposed trend lines, especially for the 1st transverse mode. The 6th transverse results did show some support motion in the mode shape data and so this may partially explain the level of excursion from the trend. These trends appear frequency dependent in that the response non-linearities seem to increase in line with the mode number. If the NNM data are normalised by either the mode frequency or frequency^2 the trend still persists, suggesting that the underlying non-linear mechanisms are not directly related to the excitation frequency but only to the beam condition. However it must be acknowledged that this part of the investigation was undertaken retrospectively. The testwork could not be repeated and so measurement resolutions were not able to obtain the most accurate data for the application of this technique. This aspect will have been a potential factor in the results spread shown by Figure 3.18.

Mode Number	1st Trans	1st Lateral	3rd Trans /4th Lat	4th Trans	6th Trans	Mean Alpha
1	0·079	0·021	0·057	0·117	0·557	0·000
2	0·081	0·113	0·238	0·364	0·561	0·163
3	0·121	0·081	0·101	0·182	0·297	0·278
4	0·249	0·063	0·059	0·120	0·660	0·371
5	0·254	0·209	0·233	0·202	1·670	0·620

Table 3.4 Experimental Normalised Nett Magnitude (NNM) data

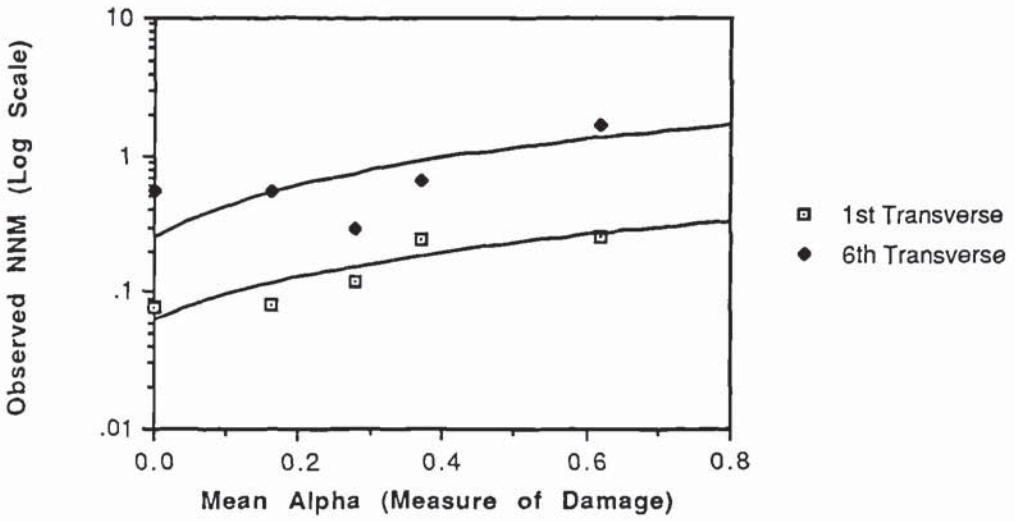

Figure 3.18 Experimental NNM data curves

3.9 Summary

Two series of modelled bridge beams were tested for their vibration response characteristics when subjected to progressive levels of damage. Their configurations were ordinary-reinforced and post-tensioned designs of nominally the same cross-section and span dimensions. The post-tensioned series included an initial preload level of 40 % of the reinforcing material yield stress. Damage was initiated at varying positions and at different levels before the vibration testing and loading procedures commenced. Results were in line with previously published work and showed that the response frequencies decreased with magnitude of load application and, hence, damage induced. These data also indicated that the beam vibration characteristics were composite responses of both the beam and its support conditions in the majority of cases.

A method was proposed to assist in determining where along the response-damage curves a specimen beam may be and this was presented as:

$$\text{Normalised Nett Magnitude (NNM)} = |2\,(A_{ij} - A_{ji}) / (A_{ij} + A_{ji})|$$

Data using this technique suggested a definite trend relating level of damage and resulting NNM. These NNM data did show spread and it was suggested that the composite system characteristics allied with the resolution of measured data available were the sources of these excursions from the trend lines. It is now necessary to analyse these experimental beam-data in order to establish the underlying relationships between each variable.

Chapter 4: Experimental Bridge-Beam Data Analysis

"There is occasions and causes why and wherefore in all things"

William Shakespeare (1564-1616)

4.1 Introduction

The static beam-loading and vibrational response data of Chapter 3 were required to be combined to create a measure of induced damage for both types of beam. This procedure initially involved accurately establishing the beam system mechanics for both designs. A precise measure was then obtained against which to compare the observed level of damage. A similar exercise was undertaken to create a representative model of damage for vibrating systems of this type.

4.2 Beam Loading Mechanics

Unlike isotropic materials such as metals, the mechanics of composites such as concrete can only be loosely approximated. The great majority of data concerning concrete is of a qualitative, rather than quantitative nature (Neville, 1981) and the behaviour of this material has two distinct limitations. The first of these limitations is that concrete has little or no strength in tension. Secondly, the latter stages of the compression and tension stress-strain relationships of concrete are highly non-linear with the result that it must be modelled accordingly (BS8110: Part 2: 1985). The problems in modelling both concrete and steel in the compressive zone using strain compatibility are such that the reinforcement 'off-loads' the concrete model under certain circumstances, otherwise the two act in tandem and it is not clear where the boundary between these states occurs.

It is generally acknowledged that the limiting strain of concrete in compression is 0·0035 and for both beam configurations the maximum strain available was less than 0·003 before yielding of the tendons occurred. It followed that the governing mechanics could be assumed to be linear until the onset of yield since there was a high level of reinforcement symmetry about both beam cross-section centroids. In addition to the assumption that the material characteristics were linear-elastic until failure occurred, the evaluation of both series of beam states assumed that any shear effects were negligible. The procedure used in evaluating stress systems of this type are well documented. For reference purposes the detailed analyses for both design models are presented in Appendix 4.

4.2.1 Ordinary-Reinforced Beam System

Figure 4.1 shows the ordinary-reinforced beam system and by observing equilibria of internal forces, internal and external moments it may be shown that the following governing expressions describe the section statics :

$$F_c = F_s \{2x - (d + d')\}/(x/3 - d')$$

$$F_s' = F_s (d - 5x/3)/(x/3 - d')$$

$$x = d - M_{applied}/(2 A_s E_s \varepsilon_s)$$

Using these equations it was possible to evaluate the associated strain levels for each of the applied moments using an iterative computer procedure. These expressions were used as the basis of the more complex post-tensioned analysis.

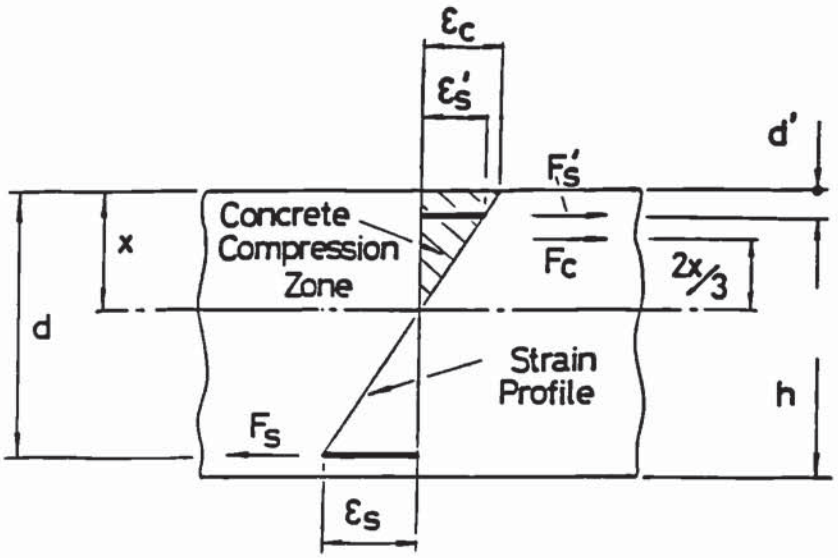

Figure 4.1 Static mechanics model of an ordinary-reinforced beam

4.2.2 Post-Tensioned Beam System

Figure 4.2 illustrates the ordinary-reinforced system incorporating a superimposed axial prestrain. With $\varepsilon_{ps} << \varepsilon_{c\,max}$ the following governing equations result after the applied bending conditions are superimposed on those created by the initial prestress:

$$F_c = F_s - F_s' + F_{ps} - \{F_s (d - 5x/3) + F_{ps} (0{\cdot}5h - 5x/3) - Fps' \, x/6\}/(x/3 - d')$$

$$F_s' = \{F_s (d - 5x/3) + F_{ps} (0{\cdot}5h - 5x/3) - Fps' \, x/6\}/(x/3 - d')$$

$$x = \left(h + \frac{A_s E_s \varepsilon_s}{f_{ps} B}\right) - \sqrt{\left(h + \frac{A_s E_s \varepsilon_s}{f_{ps} B}\right)^2 + \frac{M_{applied}}{f_{ps} B} - h^2 - \frac{2A_s E_s \varepsilon_s d}{f_{ps} B}}$$

Again, it was possible to evaluate the associated strain levels for each of the applied moments using an iterative computer procedure.

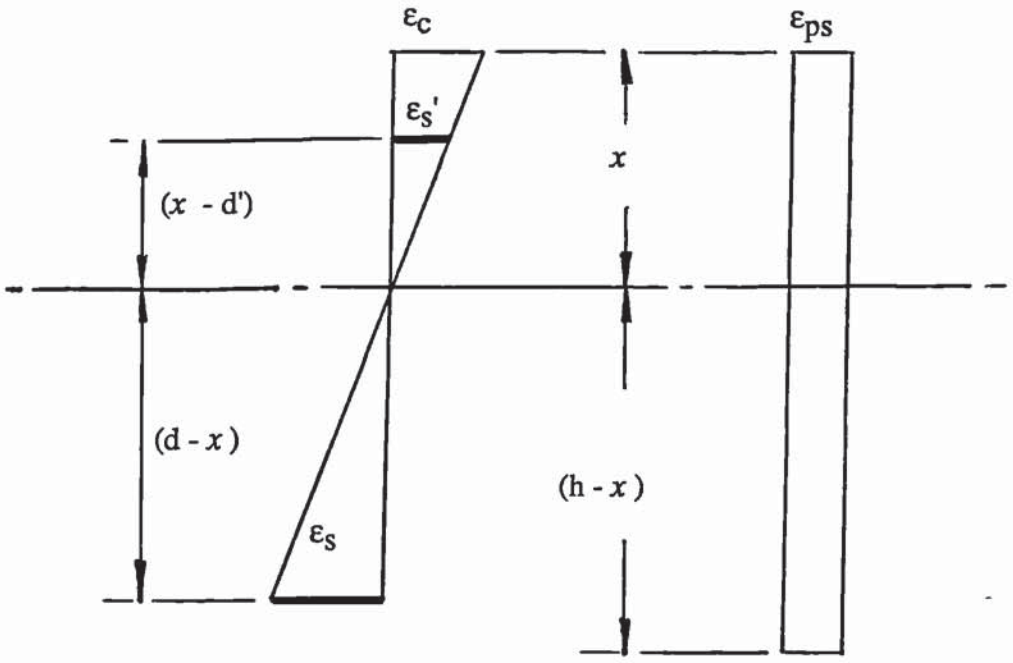

Figure 4.2 Static mechanics model of a post-tensioned beam

4.2.3 Load Ratios

The resulting strains and, hence, loads evaluated by the above procedures were normalised against those of the measured failed condition. In this way a dimensionless parameter was created to describe the beam condition under load and three specific ratios were of particular interest. These ratios were ready indicators of the operational limitations of a beam and they concerned the level of strain in the tensile reinforcement R_s, the level of strain in the compression concrete R_c and the resultant moment applied over the section R_m.

4.3 Beam Load Results

Preliminary calculations on the effects of concrete shrinkage, creep and reinforcement relaxation were made using nominal beam material properties and BS 8110: Part 1: 1985 guidelines (Martin *et al*, 1989) and these suggested that up to 25 % losses in the tendon prestress could be expected during the 28 day period until testing. Calculations of the load ratios were made incorporating this effect where applicable, and an example of the computer output from the procedure is presented in Figure 4.3. This output shows the calculated data evaluated for each load condition during the testing of post-tension beam P4a. All information pertinent to the analysis was input as two data lines prior to the calculation run. These run data included the measured cube strength, equivalent static elastic modulus, areas of tensile and compressive reinforcement, the coefficients which evaluated the applied moments at each beam condition and the ram-loads applied before each vibration response test. One of the convergence criteria within this program was that the error in equilibrium of the internal forces was less than 0·1 %. The internal and external moment equilibrium tolerance was progressively reduced, typically to less than 1%, so that the number of solutions returned was minimised. Applied moment 1 corresponds to the 'cracked' condition, 2 to 'service', 3 to 'intermediate' and 4 to 'failure'.

4.4 Beam Damage Mechanics

It has been shown previously by simple modelling (Wood *et al*, 1991) that the level of damage required at any one site in such beams would need to be considerable to reproduce a measurable change in the frequencies of vibration. In attempting to model the beams for vibration purposes the same assumptions concerning linear-elastic

```
**********************************************************

  ESTIMATION OF EXPERIMENTAL STRAINS AND APPLIED MOMENTS

  POST-TENSIONED BEAM: P4a/I : Includes Prestress Losses

   Calculated Strain Based On Internal Force And Moment
    Equilibrium, And Also External Moment Equilibrium

**********************************************************

    *****  All Ratios EXCLUDE PreStrain Components  *****

Steel Strain =  .0013              C'rete Strain =  1.420931E-03
Steel Ratio =  .4877798            C'crete Ratio =  .7658286
M =  1.092904E+08                  Calculated Moment =  1.093295E+08
Moment Ratio =  .4709218           Applied Moment =  1
              Calculated Moment Error=  3.578663E-02 %
Neutral Axis=  235                 Comp. Steel Strain=  1.118605E-03

Steel Strain =  1.950001E-03       C'rete Strain =  1.646312E-03
Steel Ratio =  .7316698            C'crete Ratio =  .8873008
M =  1.674146E+08                  Calculated Moment =  1.673173E+08
Moment Ratio =  .7206963           Applied Moment =  2
              Calculated Moment Error=  5.813837E-02 %
Neutral Axis=  206                 Comp. Steel Strain=  1.246722E-03

Steel Strain =  .00215             C'rete Strain =  1.689286E-03
Steel Ratio =  .8067127            C'crete Ratio =  .9104621
M =  1.865441E+08                  Calculated Moment =  1.864265E+08
Moment Ratio =  .8030065           Applied Moment =  3
              Calculated Moment Error=  6.306768E-02 %
Neutral Axis=  198                 Comp. Steel Strain=  1.262699E-03

Steel Strain =  .00265             C'rete Strain =  1.824671E-03
Steel Ratio =  .9943199            C'crete Ratio =  .9834298
M =  2.321606E+08                  Calculated Moment =  2.323808E+08
Moment Ratio =  1.000948           Applied Moment =  4
              Calculated Moment Error=  9.484291E-02 %
Neutral Axis=  183.5               Comp. Steel Strain=  1.327486E-03
```

Figure 4.3 Example beam-load data analysis

behaviour until failure and negligible shear effects were made. The experimental data of Chapter 3 suggested that the typical damping for both systems over the range of loadings was 3% and, hence, the system was said to be 'lightly' damped. This characteristic could have been incorporated proportionally in the mass and stiffness coefficients as Rayleigh damping. However for the purposes of this work damping was neglected since its effect was small and it would have been a further complication. Rotary-inertia effects within the beam, strain and kinetic energy effects created by the support overhangs were also assumed to be negligible since any resultant vibrational displacements were extremely small. For the post-tensioned designs, there was a final assumption that the applied axial prestress was independent of the beam condition until failure occurred.

Although the mode shapes of Chapter 3 showed small localised discontinuities at the tendon damage positions, the mode shapes for these modelling purposes were assumed to be unaffected by any induced damage. The beams were simply-supported during testing but any axial motion resulting from the transverse vibrations would have been infinitesimal and, hence, it was acceptable to model the system as pin-ended.

4.4.1 Localised Damage System

If the beam system of Figure 4.4(a) is a conservative system where the total energy present is constant, it may be shown that (Meirovitch, 1986):

$$\omega^2 = \frac{V_{max}}{T^*} = \frac{1/2 \int EI(x) \{\phi''(x)\}^2 dx}{1/2 \int m(x) \{\phi(x)\}^2 dx} \qquad (4.1)$$

If damage is assumed to have occurred in a region bounded by a and b within the span L and that the damage at this point may be represented as change in the flexural rigidity α then expression (4.1) becomes:

$$\omega_D^2 = \frac{EI [\int_0^L \{\phi''(x)\}^2 dx - \alpha \int_a^b \{\phi''(x)\}^2 dx]}{m \int_0^L \{\phi(x)\}^2 dx} \qquad (4.2)$$

where ω_D is the damaged frequency.

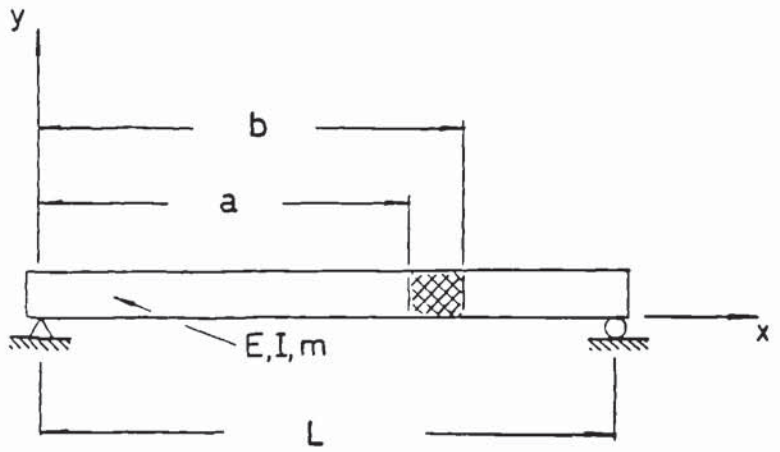

Figure 4.4(a) Dynamic model of test-beams

An admissible shape function 'ϕ' which closely approximates the boundary conditions of the test-beam system is that of:

$$\phi_n(x) = q_n \sin(n\pi x/L) \tag{4.3}$$

If the damage region bounded by a and b is small and is represented as βL then $\{\phi_n''(x)\}^2$ may be assumed to be constant between these two points by using the reasoning illustrated by Figure 4.4(b). By direct substitution of (4.3) and subsequent algebraic manipulation, the frequency for the damaged beam is given by:

$$\omega_{Dn} = \omega_n \sqrt{1 - 2\alpha\beta \sin^2(n\pi a/L)} \tag{4.4}$$

Expression (4.4) may be rearranged to establish α using the observed damaged frequencies and the flexural rigidity obtained in the undamaged state, thus:

$$\alpha = \frac{\{1 - 4\,m\,(f_{Dn})^2\,L^4 / EI\,\pi^2\,n^4\}}{2\beta \sin^2(n\pi a/L)} \tag{4.5}$$

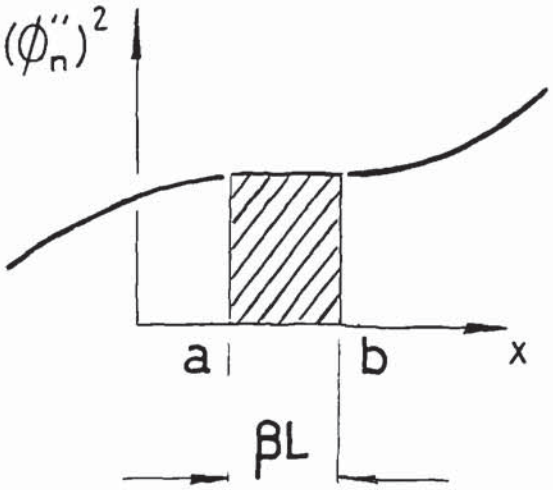

Figure 4.4(b) Function $\{\phi_n''(x)\}^2$ in the vicinity of βL

4.4.2 Significant Span-Length Damage System

Figure 4.5 illustrates the beam system assuming that the damage has occurred over a major part of the span. Since the region of damage is not localised then (4.2) may be manipulated to produce the generalisation:

$$\omega_{Dn} = \omega_n \sqrt{1 - \alpha/L \int_a^b \{1 - \cos(2n\pi x/L)\}\, dx} \qquad (4.6)$$

Again (4.6) may be rearranged to establish α using the observed damaged frequencies and the flexural rigidity obtained in the undamaged state, thus:

$$\alpha = \frac{2\{1 - 4\, m\, (f_{Dn})^2\, L^4 / EI\, \pi^2\, n^4\}}{\int_a^b \{1 - \cos(2n\pi x/L)\}\, dx} \qquad (4.7)$$

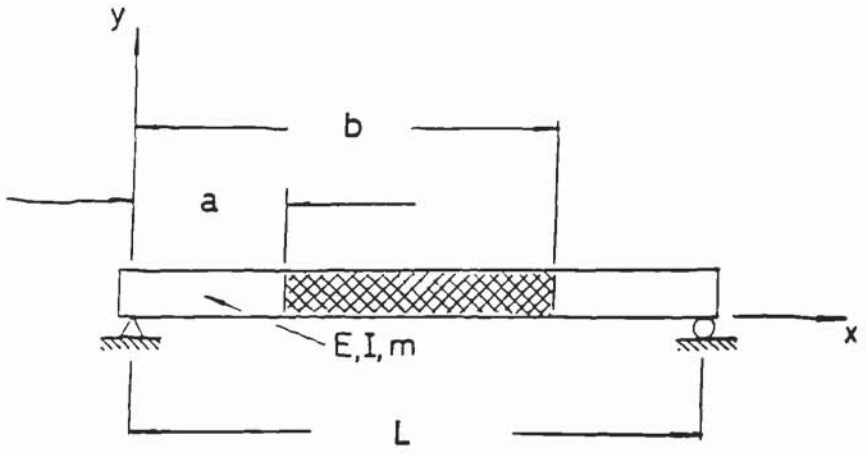

Figure 4.5 Beam system with significant span-length damage

4.4.3 Axial Prestress Considerations

If a vibrating beam is subject to an axial preload then the natural frequencies are reduced as a result of the introduction of this potential energy into the system. These effects were incorporated when the undamaged flexural rigidities were evaluated for the post-tensioned beams.

4.5 Non-Reciprocity Analysis

To provide a basis for the qualitative NNM technique of Chapter 3 it was necessary to establish at least a working model which would reflect the observed data trends. Figure 4.6(a) shows the beam system idealised as four interconnected masses supported by springs of stiffness 'k_s' and a crack located between masses 1 and 2. This concept may be represented by the very simple model illustrated as Figure 4.6(b). The behaviour between adjacent sections has been modelled by shear-springs of stiffness 'k_{ij}', where $k_{ij} = 12EI / L_{ij}^3$, and the crack by a non-linear stiffness 'k_{nl}'. Hence the classic mass-spring system of Figure 4.6(c) results.

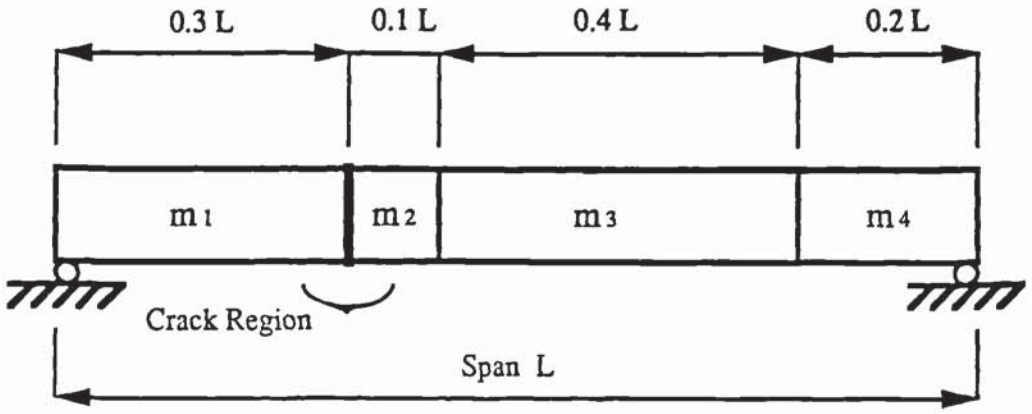

Figure 4.6(a) Test-beam idealisation

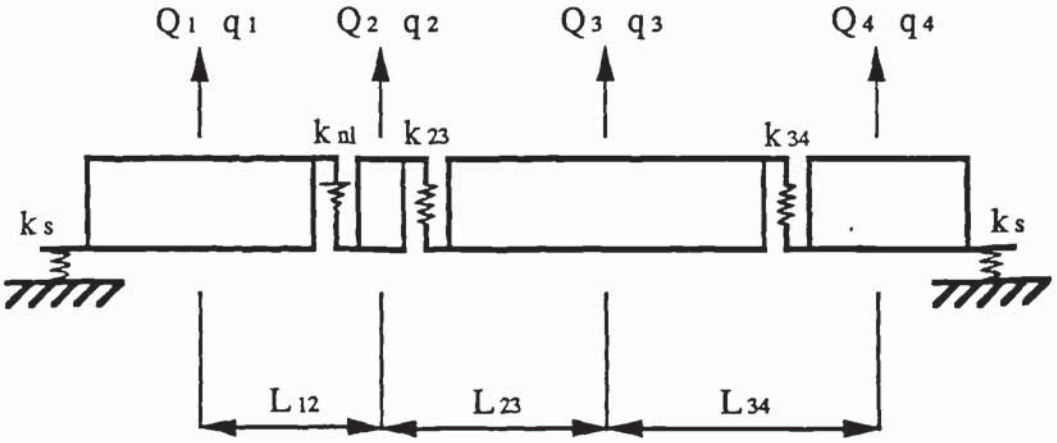

Figure 4.6(b) Test-beam model

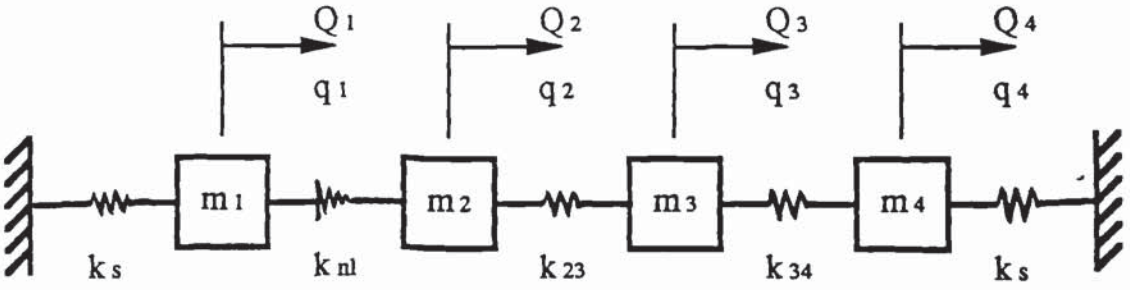

Figure 4.6(c) Classic mass-spring system

The equations of motion for this system are:

$$\begin{aligned}
m_1 q''_1 &+ k_s q_1 + k_{nl}(q_1 - q_2) &&= Q_1 \\
m_2 q''_2 &+ k_{nl}(q_2 - q_1) + k_{23}(q_2 - q_3) &&= Q_2 \\
m_3 q''_3 &+ k_{23}(q_3 - q_2) + k_{34}(q_3 - q_4) &&= Q_3 \\
m_4 q''_4 &+ k_{34}(q_4 - q_3) + k_s q_4 &&= Q_4
\end{aligned} \tag{4.8}$$

If the crack spring is represented by the non-linear characteristic:

$$k_{12} + \eta \delta^2 \qquad \text{where } \delta = (q_1 - q_2) \text{ and } \eta \text{ is a constant}$$

then (4.8) becomes:

$$\begin{aligned}
m_1 q''_1 &+ k_s q_1 + k_{12}(q_1 - q_2) + \eta (q_1 - q_2)^3 &&= Q_1 \\
m_2 q''_2 &+ k_{12}(q_2 - q_1) + k_{23}(q_2 - q_3) - \eta (q_1 - q_2)^3 &&= Q_2 \\
m_3 q''_3 &+ k_{23}(q_3 - q_2) + k_{34}(q_3 - q_4) &&= Q_3 \\
m_4 q''_4 &+ k_{34}(q_4 - q_3) + k_s q_4 &&= Q_4
\end{aligned} \tag{4.9}$$

or:

$$\begin{aligned}
m_1 q''_1 &+ (k_s + k_{12}) q_1 - k_{12} q_2 + \eta (q_1 - q_2)^3 &&= Q_1 \\
m_2 q''_2 &- k_{12} q_1 + (k_{12} + k_{23}) q_2 - k_{23} q_3 - \eta (q_1 - q_2)^3 &&= Q_2 \\
m_3 q''_3 &- k_{23} q_2 + (k_{23} + k_{34}) q_3 - k_{34} q_4 &&= Q_3 \\
m_4 q''_4 &- k_{34} q_3 + (k_{34} + k_s) q_4 &&= Q_4
\end{aligned} \tag{4.10}$$

Penny and Clark (1982) demonstrated that if the system is excited harmonically at a forcing frequency ω the harmonics resulting from the powers of q will be removed by any analyser measurement and, as a result, (4.10) may be reduced to:

$$\begin{bmatrix} (k_s + k_{12} - m_1\omega^2) & -k_{12} & & \\ -k_{12} & (k_{12} + k_{23} - m_2\omega^2) & -k_{23} & \\ & -k_{23} & (k_{23} + k_{34} - m_3\omega^2) & -k_{34} \\ & & -k_{34} & (k_{34} + k_s - m_4\omega^2) \end{bmatrix} \begin{Bmatrix} q_1 \\ q_2 \\ q_3 \\ q_4 \end{Bmatrix}$$

$$+ \begin{Bmatrix} 0{\cdot}75 \\ -0{\cdot}75 \\ 0 \\ 0 \end{Bmatrix} \eta (q_1 - q_2)^3 = \begin{Bmatrix} Q_1 \\ Q_2 \\ Q_3 \\ Q_4 \end{Bmatrix} \qquad (4.11)$$

In simplified form:

$$\begin{bmatrix} C_1 & C_2 & & \\ C_2 & C_3 & C_4 & \\ & C_4 & C_5 & C_6 \\ & & C_6 & C_7 \end{bmatrix} \begin{Bmatrix} q_1 \\ q_2 \\ q_3 \\ q_4 \end{Bmatrix} + \begin{Bmatrix} H \\ -H \\ 0 \\ 0 \end{Bmatrix} (q_1 - q_2)^3 = \begin{Bmatrix} Q_1 \\ Q_2 \\ Q_3 \\ Q_4 \end{Bmatrix} \qquad (4.11a)$$

where:

$C_1 = (k_s + k_{12} - m_1\omega^2)$ $\quad$ $C_2 = -k_{12}$

$C_3 = (k_{12} + k_{23} - m_2\omega^2)$ $\quad$ $C_4 = -k_{23}$

$C_5 = (k_{23} + k_{34} - m_3\omega^2)$ $\quad$ $C_6 = -k_{34}$

$C_7 = (k_{34} + k_s - m_4\omega^2)$ $\quad$ $H = 0{\cdot}75\eta$

When receptance measurements are made, a unit harmonic force 'Q' is applied to one position of the beam and the response 'q' is measured at a second. If Q is applied in turn to positions 1 and 2 then the force vector becomes:

$$\begin{Bmatrix} Q_1 \\ Q_2 \\ Q_3 \\ Q_4 \end{Bmatrix} = \begin{Bmatrix} 1 \\ 0 \\ 0 \\ 0 \end{Bmatrix} \; \& \; \begin{Bmatrix} 0 \\ 1 \\ 0 \\ 0 \end{Bmatrix}$$

By partitioning (4.11a) between q_2 and q_3 the lower partition shows for both states:

$$\begin{aligned} C_4 q_2 + C_5 q_3 + C_6 q_4 &= 0 \\ C_6 q_3 + C_7 q_4 &= 0 \end{aligned} \qquad (4.11b)$$

From (4.11b) it may be deduced that the following hold true for both states:

$$q_3 = \{C_4 C_7 / (C_6^2 - C_5 C_7)\} q_2 \qquad (4.11c)$$

From the upper partition of (4.11a):

$$\begin{aligned} C_1 q_1 + C_2 q_2 + H (q_1 - q_2)^3 &= Q_1 \\ C_2 q_1 + C_3 q_2 + C_4 q_3 - H (q_1 - q_2)^3 &= Q_2 \end{aligned} \qquad (4.11d)$$

Substituting for q_3, (4.11d) becomes:

$$\begin{aligned} C_1 q_1 + C_2 q_2 + H (q_1 - q_2)^3 &= Q_1 \\ C_2 q_1 + [C_3 + \{C_4^2 C_7 / (C_6^2 - C_5 C_7)\}] q_2 - H (q_1 - q_2)^3 &= Q_2 \end{aligned} \qquad (4.11e)$$

Solving (4.11e) for $Q_1 \neq 0$ and $Q_2 = 0$ returns q_{11} for q_1 and q_{21} for q_2. For $Q_1 = 0$ and $Q_2 \neq 0$ (4.11e) returns q_{12} for q_1 and q_{22} for q_2. Receptance $\alpha_{ij} = (q_i/Q_j)$, Inertance $A_{ij} = -\omega^2 (\alpha_{ij})$ and since $-\omega^2$ is common to the numerator and denominator:

$$NNM = |2 (A_{ij} - A_{ji}) / (A_{ij} + A_{ji})| = |2 (\alpha_{ij} - \alpha_{ji}) / (\alpha_{ij} + \alpha_{ji})| \qquad (4.12)$$

4.6 Beam Vibration Results

As previously stated in Chapter 3, the majority of the beam vibration data included composite effects created by the floor-support arrangements. The fundamental mode shapes showed none of these effects and so all data relating to this mode were assumed to be unaffected. All other testbeam frequency data were studied to try to establish a consistent mode close to a predicted harmonic of the fundamental. Although its mode shape animation suggested slight motion at the supports, observed mode 7 showed excellent consistency for both beam series with a mean error of less than 1·5 % about the calculated 4^{th} harmonic. No other modes were found to be suitable for further analysis due to significant differences between their observed frequencies and the predicted harmonics.

Using the above procedures it was possible to calculate the equivalent flexural rigidity EI of any specimen using the undamaged beam vibration data as bases. Overall changes in the properties of the beam flexural rigidity were established since it was not possible to distinguish to what extent these two independent characteristics were affected by the action of damage. The constant α was then evaluated for each beam condition assuming that the damage concentration was bounded by the beam depth h and the tendon access position. After consideration of these data the procedure was repeated for bounds about the access positions of $\pm h$, $\pm 2h$ and $\pm 3h$ resulting in a series of corresponding constants: α_1, α_2 and α_3.

Figure 4.7 shows the calculated change in observed flexural rigidity of post-tensioned beam P4a for both mode 1 and 5 data. The calculated mass per unit length and both the undamaged mode 1 and 5 frequencies were used to estimate the datum EI properties. The observed error between these estimated flexural rigidities was approximately 2 %. The calculated α's correspond to the damaged mode 1 and 5 frequencies for each beam condition and the span constants to the integral which is the denominator of equation (4.7).

Table 4.1 illustrates both the load ratio and calculated α's for the ordinary-reinforced specimens using the mode 1 and mode 5 data. In this case the load ratios R_m, R_s and R_c are nominally the same until nearing the beam failure condition and so no distinction has been made between them. Table 4.2 shows individual load ratios and calculated α's for the post-tensioned specimens since the initial preload on the beam sections result in a consistent differential between each load ratio.

```
************************************************************
 CALCULATION OF OBSERVED CHANGE IN FLEXURAL RIGIDITY (Alpha)
************************************************************

Beam:  P4a/I

mbar, undamaged f1 and f5:     374.8   24.64   569.39

EI( 1 ) =  1.205569E+08       Pstress= 283860
EI( 5 ) =  1.021599E+08       Pstress= 283860


Load condition 1   f1d= 23.94   and f5d= 566.33

Constants:  .6241    1.1703     1.5816

f 1 :  Alpha1= .2054747 , Alpha2= .109576  & Alpha3= 8.108041E-02

Constants:  .3015    .7218     .9363

f 5 :  Alpha1= 7.376821E-02 , Alpha2= .0308134  & Alpha3= 2.375426E-02


Load condition 2   f1d= 23.74   and f5d= 558.8

Constants:  .6241    1.1703     1.5816

f 1 :  Alpha1= .2553764 , Alpha2= .1361877  & Alpha3= .1007717

Constants:  .3015    .7218     .9363

f 5 :  Alpha1= .2470479 , Alpha2= .1031933  & Alpha3= 7.955244E-02


Load condition 3   f1d= 22.07   and f5d= 553.19

Constants:  .6241    1.1703     1.5816

f 1 :  Alpha1= .655713 , Alpha2= .34968  & Alpha3= .2587446

Constants:  .3015    .7218     .9363

f 5 :  Alpha1= .3746351 , Alpha2= .1564872  & Alpha3= .1206371


Load condition 4   f1d= 12.82   and f5d= 397.63

Constants:  .6241    1.1703     1.5816

f 1 :  Alpha1= 2.344563 , Alpha2= 1.250313  & Alpha3= .9251656

Constants:  .3015    .7218     .9363

f 5 :  Alpha1= 3.399759 , Alpha2= 1.420099  & Alpha3= 1.094764
```

Figure 4.7 Example of calculated changes in flexural rigidity

Reinforced Alpha vs Ratio

	R1 Ratio	R1 f1 Alpha1	R1 f1 Alpha2	R1 f1 Alpha3	R1 f5 Alpha1	R1 f5 Alpha2	R1 f5 Alpha3	R1 Mean Alpha
1	0.000	0.000	0.000	0.000	0.000	0.000	0.000	0.000
2								
3								
4								
5	1.007	0.594	0.564	0.559	0.871	0.616	0.533	0.546

Reinforced Alpha vs Ratio

	R3 Ratio	R3 f1 Alpha1	R3 f1 Alpha2	R3 f1 Alpha3	R3 f5 Alpha1	R3 f5 Alpha2	R3 f5 Alpha3	R3 Mean Alpha
1	0.000	0.000	0.000	0.000	0.000	0.000	0.000	0.000
2	0.417	0.635	0.339	0 251	0.846	0.353	0.272	0.163
3	0 851	0 912	0.486	0 360	1.799	0.751	0.579	0.278
4	0.922	1 342	0.716	0 530	2.143	0.895	0.690	0.371
5	1.008	2.362	1.260	0.932	3.339	1.395	1.075	0.620

Reinforced Alpha vs Ratio

	R4a Ratio	R4a f1 Alpha1	R4a f1 Alpha2	R4a f1 Alpha3	R4a f5 Alpha1	R4a f5 Alpha2	R4a f5 Alpha3	R4a Mean
1	0.000	0.000	0.000	0 000	0.000	0.000	0.000	0.000
2	0.400	0.952	0.508	0 376	2.176	0.909	0.701	0.313
3	0 843	1 325	0.707	0 523	3.054	1.276	0.983	0.437
4	0.867	1.717	0 916	0.678	3 396	1.419	1.094	0.524
5	1.008	2.254	1.202	0.889	4 921	2.056	1 585	0.723

Reinforced Alpha vs Ratio

	R4b Ratio	R4b f1 Alpha1	R4b f1 Alpha2	R4b f1 Alpha3	R4b f5 Alpha1	R4b f5 Alpha2	R4b f5 Alpha3	R4b Mean
1	0 000	0.000	0.000	0 000	0.000	0.000	0.000	0.000
2	0.452	0.867	0.462	0.342	0.981	0.410	0.316	0.209
3	0 922	0.799	0.426	0.315	1.626	0.679	0.523	0.247
4	0.991	1.204	0.642	0.475	1.982	0.828	0.638	0.337
5	1 008	1.685	0.898	0.665	4 128	1.724	1.329	0.574

Reinforced Alpha vs Ratio

	R4c Ratio	R4c f1 Alpha1	R4c f1 Alpha2	R4c f1 Alpha3	R4c f5 Alpha1	R4c f5 Alpha2	R4c f5 Alpha3	R4c Mean
1	0.000	0.000	0.000	0.000	0.000	0.000	0.000	0.000
2	0.572	1.171	0.625	0.462	1.356	0.566	0.437	0.285
3								
4								
5	1 008	1.887	1.006	0.745	3.677	1.536	1.184	0.572

Reinforced Alpha vs Ratio

	R5 Ratio	R5 f1 Alpha1	R5 f1 Alpha2	R5 f1 Alpha3	R5 f5 Alpha1	R5 f5 Alpha2	R5 f5 Alpha3	R5 Mean Alpha
1	0.000	0.000	0.000	0.000	0.000	0.000	0.000	0.000
2	0.487	0.586	0.306	0.219	0.743	0.444	0.255	0.140
3	0.987	1.624	0.849	0.607	1.449	0.866	0.498	0.332
4								
5	1.008	1.767	0.923	0.660	2.315	1.383	0.795	0.429

Reinforced Alpha vs Ratio

	R6 Ratio	R6 f1 Alpha1	R6 f1 Alpha2	R6 f1 Alpha3	R6 f5 Alpha1	R6 f5 Alpha2	R6 f5 Alpha3	R6 Mean Alpha
1	0.000	0.000	0.000	0.000	0.000	0.000	0.000	0.000
2	0.404	0.361	0.343	0.340	0.343	0.242	0.210	0.275
3	0.802	0.464	0.440	0.437	0.602	0.425	0.368	0.403
4	0.851	0.549	0.522	0.518	0.836	0.591	0.511	0.514
5	1 008	0.687	0.652	0.647	1.132	0.801	0.693	0.670

Table 4.1 Ordinary-reinforced beam load-ratios and resultant α data

PostTensioned Alpha vs Ratio

	P3 Moment	P3 Steel Ratio	P3 C'crete	P3 f1 Alpha1	P3 f1 Alpha2	P3 f1 Alpha3	P3 f5 Alpha1	P3 f5 Alpha2	P3 f5 Alpha3	P3 Mean Alpha
1	0 000	0 000	0 000	0 000	0 000	0 000	0.000	0.000	0.000	0.000
2	0.494	0.488	0.694	0 321	0 171	0.127	0.282	0.118	0.091	0.071
3										
4										
5	1.000	0.994	0.986	2 082	1.110	0.822	3.119	1.303	1.004	0.560

PostTensioned Alpha vs Ratio

	P4a Mom Ratio	P4a Steel Ratio	P4a C'crete	P4a f1 Alpha1	P4a f1 Alpha2	P4a f1 Alpha3	P4a f5 Alpha1	P4a f5 Alpha2	P4a f5 Alpha3	P4a Mean
1	0 000	0.000	0.000	0 000	0.000	0.000	0 000	0 000	0.000	0.000
2	0 471	0 488	0.766	0 205	0 110	0 081	0.074	0 031	0 024	0.038
3	0.721	0.732	0.887	0 255	0 136	0 101	0 247	0.103	0 080	0.058
4	0.803	0.807	0 910	0 656	0 350	0 259	0.375	0.156	0.121	0.131
5	1.001	0.994	0.983	2.345	1.250	0.925	3.400	1.420	1.095	0.622

PostTensioned Alpha vs Ratio

	P4b Mom Ratio	P4b Steel Ratio	P4b C'crete	P4b f1 Alpha1	P4b f1 Alpha2	P4b f1 Alpha3	P4b f5 Alpha1	P4b f5 Alpha2	P4b f5 Alpha3	P4b Mean
1	0 000	0 000	0.000	0 000	0 000	0 000	0.000	0 000	0 000	0.000
2	0 581	0.582	0.773	0 339	0 181	0.134	0.256	0.107	0 082	0.072
3	0 890	0.901	0.971	0 419	0.223	0.165	0.437	0.182	0.141	0.098
4										
5	0 999	0.994	0 988	0 688	0 367	0.272	0.993	0.415	0.320	0.182

PostTensioned Alpha vs Ratio

	P4c Mom Ratio	P4c Steel Ratio	P4c C'crete	P4c f1 Alpha1	P4c f1 Alpha2	P4c f1 Alpha3	P4c f5 Alpha1	P4c f5 Alpha2	P4c f5 Alpha3	P4c Mean
1	0 000	0 000	0 000	0 000	0 000	0 000	0 000	0 000	0 000	0 000
2	0 581	0.582	0 867	0 325	0 173	0 128	0.300	0.125	0 097	0 073
3	0 891	0.901	1.000	0 526	0 280	0 208	0.780	0.326	0.251	0.141
4										
5	1.001	0.994	0.981	1 985	1.059	0.783	2.517	1.051	0.810	0.499

PostTensioned Alpha vs Ratio

	P5 Mom Ratio	P5 Steel Ratio	P5 C'crete	P5 f1 Alpha1	P5 f1 Alpha2	P5 f1 Alpha3	P5 f5 Alpha1	P5 f5 Alpha2	P5 f5 Alpha3	P5 Mean Alpha
1	0.000	0 000	0 000	0.000	0.000	0 000	0.000	0.000	0 000	0.000
2	0.601	0 600	0.770	0.423	0.221	0 158	0.268	0 160	0 092	0.077
3	0.926	0 938	0.989	0 641	0 335	0 239	0.480	0.287	0.165	0.123
4										
5	1.001	0.944	0.985	2.120	1.108	0.792	2.012	1.202	0.691	0.445

PostTensioned Alpha vs Ratio

	P6 Mom Ratio	P6 Steel Ratio	P6 C'crete	P6 f1 Alpha1	P6 f1 Alpha2	P6 f1 Alpha3	P6 f5 Alpha1	P6 f5 Alpha2	P6 f5 Alpha3	P6 Mean Alpha
1	0 000	0 000	0.000	0.000	0.000	0.000	0 000	0 000	0 000	0.000
2	0 539	0.488	0.588				0.083	0.058	0.050	
3	0.826	0.825	0.896	0.096	0 092	0 091	0.141	0.100	0 086	0.089
4	0.920	0.938	0.998	0 379	0 360	0 357	0.510	0 360	0.312	0.334
5	1.000	0.994	0.986	0.672	0.638	0.633	0.976	0.690	0.597	0.615

Table 4.2 Post-tensioned beam load-ratios and resultant α data

Figure 4.8(a) illustrates the effect of varying the calculated region of influence centred on a localised damage position. Here, the first and fifth mode α's show convergence as the region of influence about the damage position was increased. Figure 4.8(b) also illustrates the effect of varying the calculated region of influence, however, this time centred on the generalised damage region between the spreader-rollers. Again these α's show convergence as the region of influence about the damage position was increased but the convergence was more rapid in this case.

These data inferred that the damage induced was a function of the overall rather than localised system and this conclusion was supported by observing the resultant crack system histories of Figure 3.11. The analysis procedure was repeated for changes in the properties expected over the entire length of the beams and each result was termed 'mean alpha', or simply alpha. These additional data are also presented for each beam condition in the tabulations of Tables 4.1 and 4.2 and it may be seen that they are now numerically less than unity in all cases.

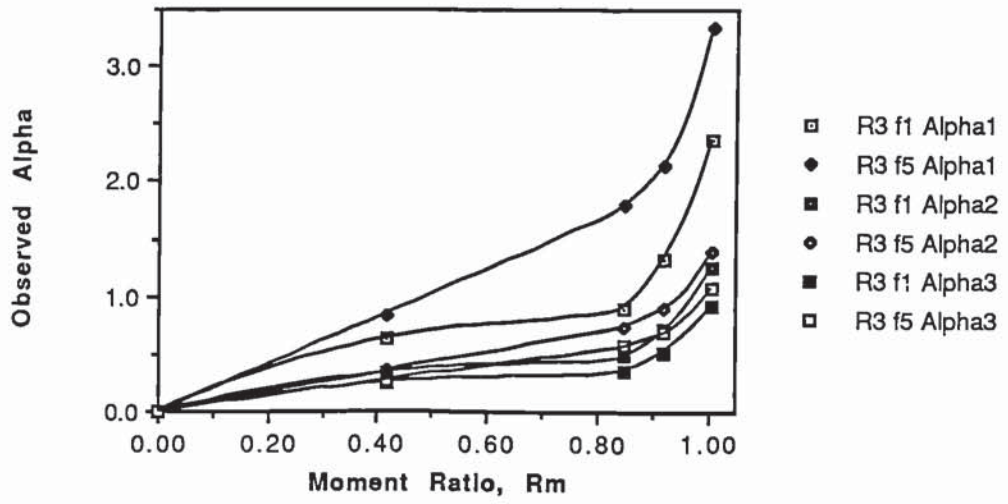

Figure 4.8(a) α_1, α_2 and α_3 data versus moment ratio for localised damage in an ordinary-reinforced beam

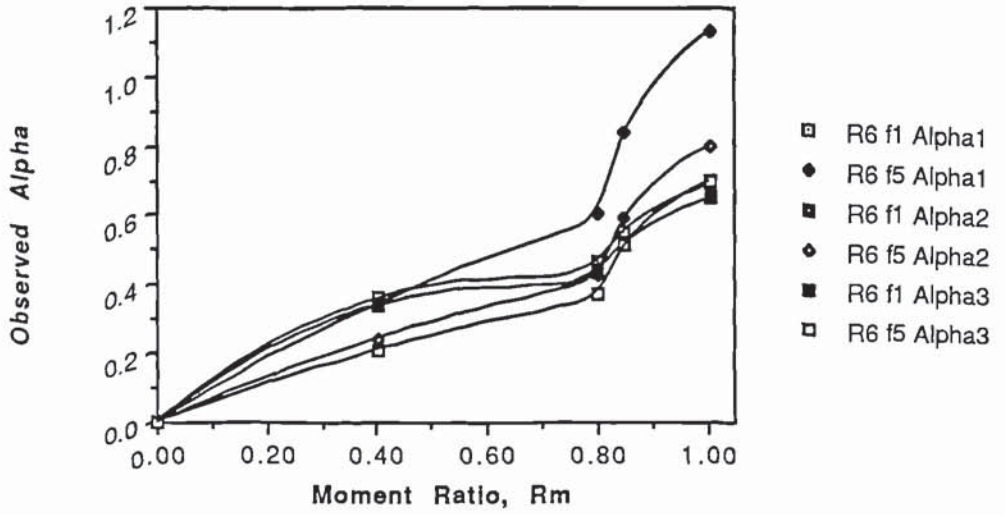

Figure 4.8(b) α_1, α_2 and α_3 data versus moment ratio for generalised damage in an ordinary-reinforced beam

4.7 Non-Reciprocity Results

A series of results were obtained for expression (4.12) using experimentally derived data. The approximate mass of typical beam 'M' was 2300 kg and by inspection m_1 = 690 kg, m_2 = 230 kg, m_3 = 920 kg and m_4 = 460 kg. The mean EI_{dyn} for the test-beams was 100 MNm^2 and the roller-support stiffness was estimated to be 60 MN/m. The overall beam span was 6·0 m and hence k_{12} = 695 MN/m, k_{23} = 355 MN/m and k_{34} = 205 MN/m. Mean observed beam frequencies of 23 Hz (144 rad/s), 137·5 Hz (864 rad/s) and 268·5 Hz (1687 rad/s) were used in the analysis. Solutions to the non-linear simultaneous equations of (4.11e) were obtained using a program applying Newtonian-based convergence criterion better than 10^{-6} (Lindfield & Penny, 1989).

Table 4.3 presents the analytically derived NNM data using the procedure outlined above. Here the coefficient 'H' provided a measure of damage and it was varied in the manner shown. Figure 4.9 shows the relationship between H and the calculated NNM and it may be seen that the resulting trends show similarity to the experimentally obtained data of Figure 3.18.

Mode Number	Damage Coefficient H	NNM: frq = 23Hz ($x10^{-6}$)	NNM: frq = 138Hz ($x10^{-6}$)	NNM: frq = 269Hz ($x10^{-6}$)
1	0·000	0	0	0
2	0·001	40	374	2041
3	0·005	114	1803	9481
4	0·010	221	3459	17491

Table 4.3 Analytically derived NNM data

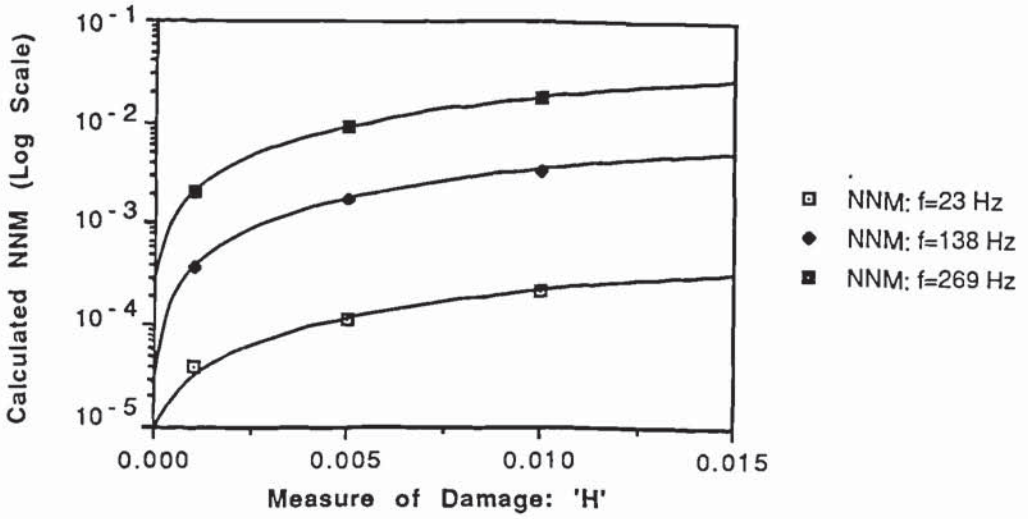

Figure 4.9 Analytical NNM data versus damage coefficient H

4.8 Results And Discussion

The load measure results from Section 4.3 provided a means to describe the relative static load condition of both beam systems. For the ordinary-reinforced case the three ratios concerning applied moment, steel and concrete strain levels were sensibly equal for all cases with an average of only 2 % difference between each of the calculated values was observed. No more than 5 % error was shown at the loads where the

concrete was near its compressive limit and 'off-loading' would be expected to occur. With the post-tensioned data, however, inclusion of the prestress in any R_s and R_c calculations created distortions in the apparent load conditions. Since there is prestrain present in both the concrete and steel then a finite load ratio would already be present without the application of a bending moment. The alternative was to use the strains nett of the prestress and this results in the behaviour illustrated in Figure 4.10. Using this approach there are distinct differentials between the concrete ratio R_c and the moment ratio R_m, although less so between R_s and R_m. It is clear that R_m is ideal as the direct indicator of the beam behaviour since it avoids the inconsistencies associated with nett prestress considerations and R_m will be used exclusively as the load ratio.

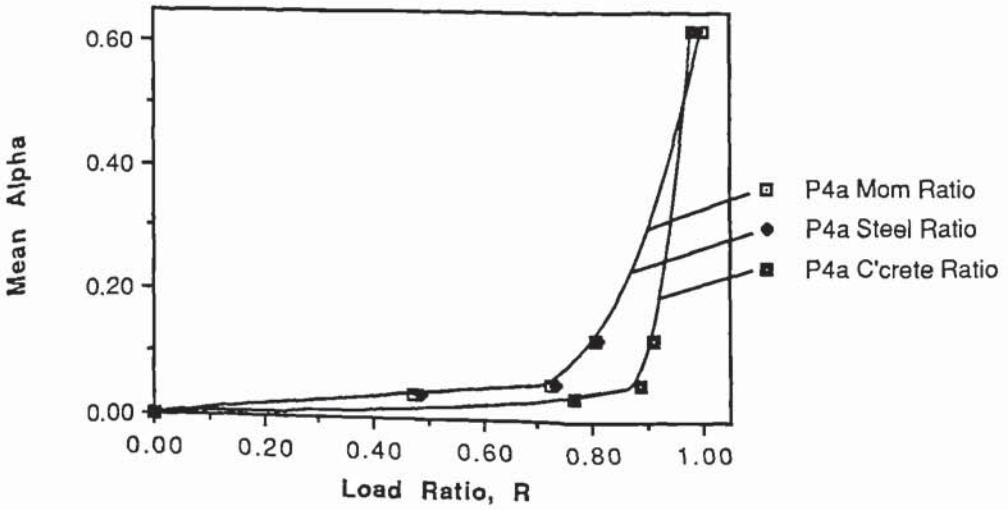

Figure 4.10 Observed α versus post-tensioned beam load-ratios

Figure 4.11(a) illustrates the relationship between the observed alpha and the moment ratio for three ordinary-reinforced beams having similar positions and initial levels of damage. The permissible crack width for beams of this type define its serviceability limit and the guidelines state that it is no more than 0·2mm (Clark, 1983). There are two interpretations of crack influence, one based on the conventional modular theory of cracked sections and the other incorporating the 'tension stiffening' action of the concrete between cracks. The gross concrete cover for both designs is nominally 50 mm and the BS 5400 equation suggests that a tensile strain equivalent to this crack width is 1225 microstrain if tension stiffening is ignored. However BS 8110 suggests that the

equivalent tensile strain should be 1100 microstrain if tension stiffening is included. The respective moment ratios for these strains are 0·422 and 0·379. Figure 4.11(a) shows the mean R_m value of 0·4 with the resulting serviceability limit, and it may be seen that a major change in flexural rigidity corresponds to this range.

Alternatively, Figure 4.11(b) illustrates the relationship between the observed alpha and moment ratio for two post-tensioned beams with the same positions and initial levels of damage as Figure 4.11(a). Ordinarily the permissible crack width for beams of this type is zero (i.e. no tensile stress is permitted). It was stated in Section 3.7 that cracking could have already taken place if the thermal or self-weight effects had been sufficient. In the ideal case, however, calculations suggest that the moment ratio required to overcome the compressive concrete stress is 0·02. Other hypothetical crack criteria are available (Clark, 1983) and they include permissible tensile stresses of 1·0 N/mm^2 for Class 1 members and 2·5 N/mm^2 for Class 2 members, with the latter based on a concrete cube strength of 50 N/mm^2 at transfer. These stresses correspond to R_m values of 0·03 and 0·05 respectively and these in addition to R_m equals 0·02 are shown in Figure 4.11(b). It can be seen that the change in flexural rigidity corresponding to this range is small and the inference is that the technique will be limited in beam systems of this kind.

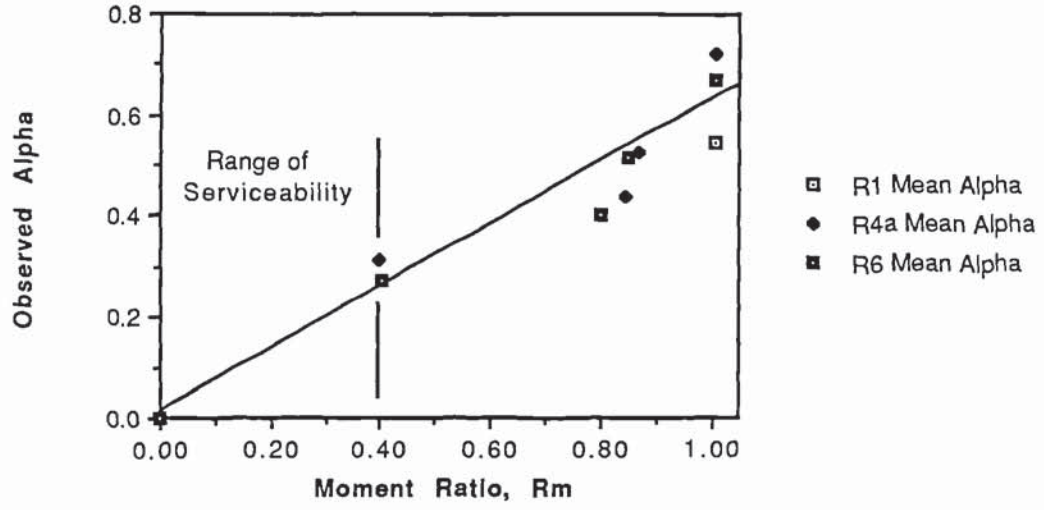

Figure 4.11(a) α versus moment ratio for similar induced damage in ordinary-reinforced beams

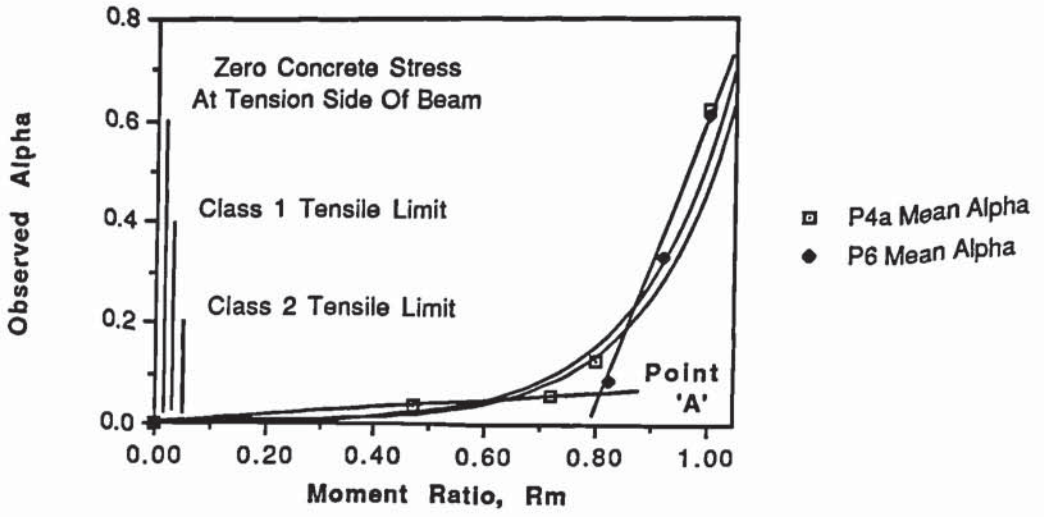

Figure 4.11(b) α versus moment ratio for similar induced damage in post-tensioned beams

The interpolated trends for both sets of data in Figure 4.11(b) show two distinctive regions. The initial gradient between moment ratio and alpha is slight until point 'A' where there is a dramatic change in trend to the failure point. Point A corresponds to approximately $R_m = 0{\cdot}8$ and examination of typical post-tensioned beam data suggest that the concrete in the compression zone has started to fail at about this point. This suggests that there is a diminishing capacity to accommodate the increasing moment within the compression concrete. Any remaining load capacity will be provided by the remaining tensile reinforcement strength until this also fails.

Comparison of trends between the moment ratio and alpha may be attempted using the data from like beams with the same initial damage induced at dissimilar span positions. Figure 4.12(a) shows the R_m and alpha data for the ordinary-reinforced beams R4b and R5 with linear regression trend-lines superimposed. These two specimens had the same initial area of tensile reinforcement but the initial damage positions were 600mm apart. Likewise Figure 4.12(b) shows the R_m and alpha data for their post-tensioned equivalents with power-law trend-lines superimposed. These data suggest that there is very little distinction between like damage for different positions, however, it would be unwise to make definite conclusions due to the sparsity of results and subsequent

research may prove that small variations do occur.

It is important to consider data spread present in all the results discussed here. It has been shown previously that the observed errors in datum flexural rigidities calculated from the frequencies observed in all the beam specimens appear small. However the occasional excursion of data points from trend lines can be considerable and there are two reasons identified for this. The first is that the imposed trend lines may not reflect the the underlying relationships, however, the data trends and the reasonable quality of the curve-fits seems to discount this. The second reason is the quality of the experimental data. It was difficult to measure accurately the exact point of beam failure with the ram-load monitoring equipment and, hence, an estimated error of approximately $\pm$ 5% is expected to be present. Another consideration is the parent material of the beams. Table 3.1 illustrated the variation in cube test data obtained from each beam specimen during the curing period. It is unlikely that these cube strengths were truly representative of the overall beam properties since they were equivalent to approximately 1% of the overall volume, however, they were the only available method of comparatively assessing the material characteristics each beam.

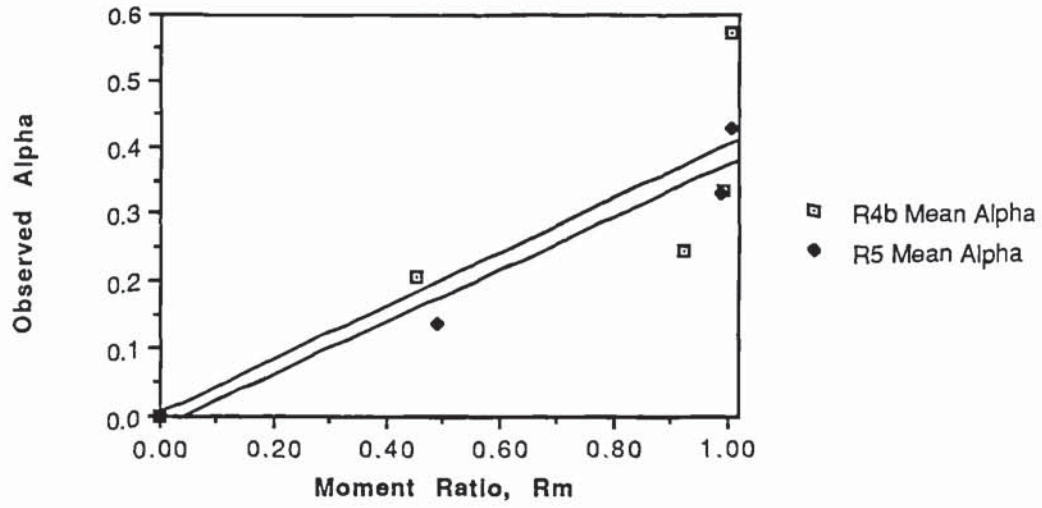

Figure 4.12(a) α versus moment ratio for like damage levels at different sites in ordinary-reinforced beams

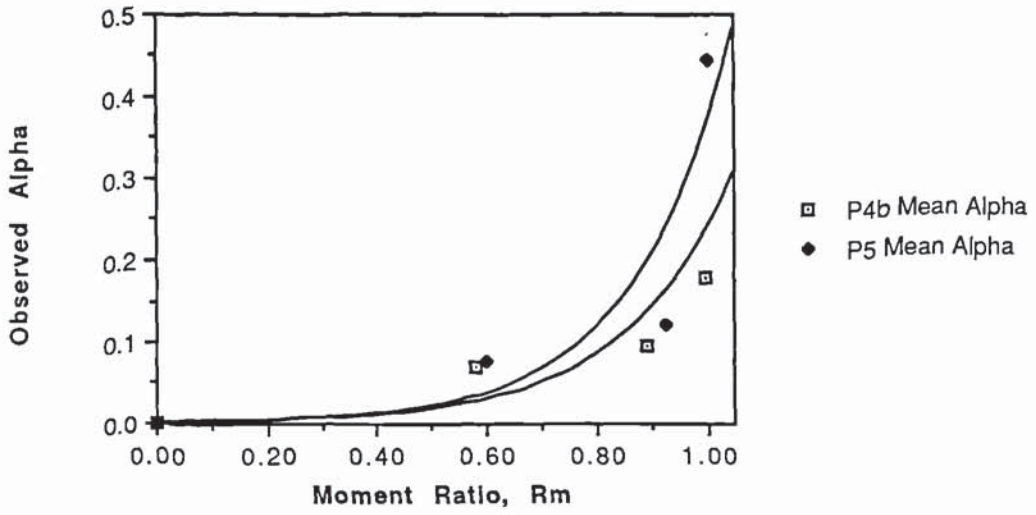

Figure 4.12(b) α versus moment ratio for like damage levels at different sites in post-tensioned beams

Using the properties of the mean alphas and moment ratios it can be established rapidly that data originates from a distinct series of beam design. Figures 4.13(a) shows the data from a series of ordinary-reinforced and post-tensioned test-beam results. All the beams had identical initial levels and positions of initial damage and it is clear that the load-damage relationships are heavily influenced by the magnitude of prestress present. The quality of the curve-fits are reflected by correlation coefficients of 0·949 for the ordinary-reinforced and 0·974 for the post-tensioned data. What is intriguing is that the alpha values at failure are 0·61 for the ordinary-reinforced and 0·65 for the post-tensioned data, representing a differential of approximately 6 %. If this differential is only (acceptable) experimental error then an assumption may be made that the alpha values at failure are the same for both beam design series.

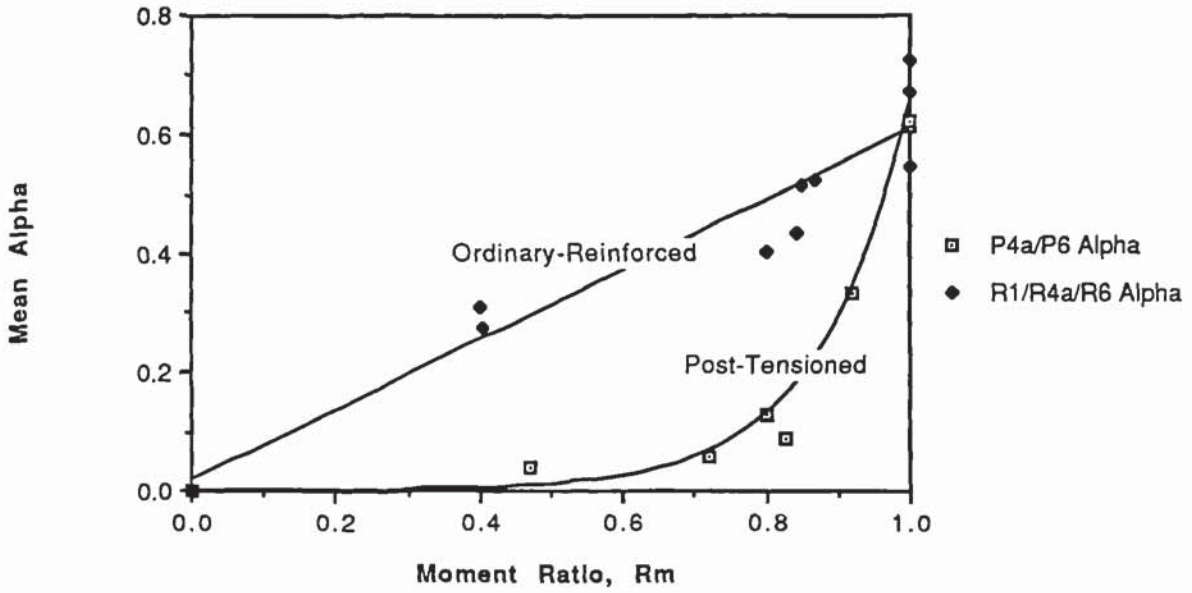

Figure 4.13(a) α versus moment ratio for like ordinary-reinforced and post-tensioned beams

If the alpha data are subsequently normalised by their values at failure another ratio 'R_a' results, and Figure 4.13(b) shows the experimental relationship between R_a and R_m. If this relationship is assumed to be a power-law which involves the level of prestrain such that:

$$R_a = R_m^{f(ps)}$$

then the experimental data suggest that the prestrain function f(ps) may be approximated by (21ps+1). Theoretical prestrain curves for $0{\cdot}1f_y$, $0{\cdot}2f_y$, $0{\cdot}3f_y$ and the BS 5400 design recommendation of $0{\cdot}7f_y$ are also presented in Figure 4.13(b), and it may be seen that there is good agreement between the experimental and theoretical results using this approach.

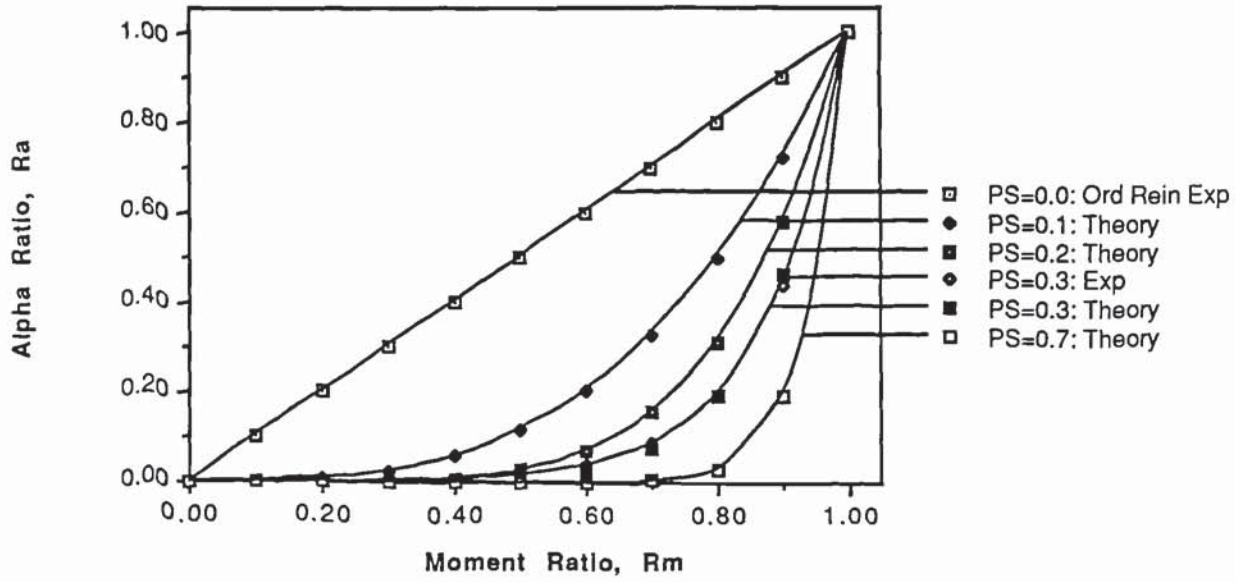

Figure 4.13(b) Experimental and theoretical alpha ratio versus moment ratio for varying levels of initial prestrain

This final application of the experimental data has suggested the behaviour of a series of beams subjected to the same load conditions may be predicted for varying levels of initial prestrain. The resultant curves also suggest that any changes in flexural rigidity due to increasing load and, hence, damage are suppressed by increased prestrain levels. It follows that for the prestressed BS 5400 design case it would be difficult to identify whether the beam serviceability criterion will have been exceeded using this approach unless the sensitivity and accuracy of measurement were available. However this approach still has merit since its purpose is to identify potential damage therefore it will be of use in the case of ordinary-reinforced designs and in the majority of post-tensioned cases where creep and shrinkage are major factors.

It must be acknowledged that the beam representation used in the NNM modelled analysis is simplistic and, hence, major assumptions regarding its vibrational behaviour have had to be made. The non-linear mechanism employed is the classical 'cubic-stiffness' model (Craig, 1981) and this is more typically associated with thin, pin-ended beam systems. However the exercise has shown the potential in using the NNM technique to establish states of damage within vibrating structures.

4.9 Summary

From a series of bridge-beam damage/response tests, ratios accurately reflecting ordinary-reinforced and post-tensioned beam load conditions have been developed from standard analysis procedures. The most representative load ratio is R_m which is the applied moment normalised by that at beam failure. A method for expressing the changes in the beam flexural rigidity due to imposed damage has been created using simple beam vibration theory as its basis. The experimental data suggest that for these loading conditions damage manifests itself as a function of the overall beam span and not localities where damage precursers are sited. Using this vibrational response technique, the ease in estimating the serviceability limits of these beam designs is dictated by the level of prestrain present.

A power-law of $R_a = R_m^{f(ps)}$ is suggested for the load-damage relationship of these beam designs and good correlation with the experimental data is obtained for the prestrain function f(ps) = (21ps+1). A working model has been produced in support of the qualitative NNM technique of Chapter 3 and it shows good agreement with the experimental data trends. Attention is now turned to the second experimental phase of this programme of research: vibration monitoring of highway bridges.

Chapter 5: Experimental Monitoring Of Highway Bridges

"Digo, paciencia y barajar"

"What I say is, patience, and shuffle the cards"

Miguel De Cervantes (1547 - 1616)

5.1 Introduction

A programme of monitoring was undertaken at several sites in the Birmingham area to obtain data on the vibrational behaviour of bridge structures subject to extremes of local ambient-air temperatures and conditions. It was important to identify the relationships between bridge construction, the ambient conditions present and the nature of any changes in vibrational response so a selection of bridge designs were sought. The location of each test-site was important with each spanning a river or canal to ensure that the only source of excitation was that present on the bridge-deck. Several sites were selected within the Birmingham area for the monitoring programme using the guidance of the Structural Division of the City Engineers Department.

5.2 Bridge Locations

The bridges were chosen for their local, a varied nature in design and construction and each had minimised 'shading' effects from surrounding buildings or trees. The structural details of each bridge are presented in Appendix 5 but brief descriptions of each are now presented.

5.2.1 Fordrough Bridge

This bridge is located in the Small Heath area of Birmingham and it spans the River Cole at the entrance to a small industrial estate. Its two north-west/south-east carriageways afford access to the main A-route between Birmingham and Coventry city centres and the bridge is subject to only occasional traffic outside normal rush-hour periods. This bridge is free of tree shading except for its southern corner which accounts for approximately 10 % of its surface area with an eastward sun.

The bridge is rectangular in plan and is 15·43 m wide, 11·43 m between bearing pads and has a 0·65 m deep deck. Its two 450 mm wide string-courses border a 7·3 m wide carriageway with nominally 2·8 m and 4·43 m wide pavements. The latter pavement dimension was checked on site and it was noted that it had been modified from that shown in the construction drawing to approximately 2·9 m wide. The carriageway surface has a mean thickness of 250 mm whilst both pavements are approximately 350 mm thick. The bridge is of composite construction consisting of *in situ* concrete infilling 28 prestressed-concrete inverted-T beams and the resultant soffit is horizontal. Each type 'T4' beam is 575 mm deep and is subject to an axial prestress of approximately 1300 kN

at an eccentricity of nominally 100 mm below the beam centroid. The structure has an overall mass of approximately 320 tonnes.

5.2.2 River Cole Bridge

This bridge is located at a T-junction in the Yardley Wood area of Birmingham and spans the River Cole (Figure 5.1). Its two north-south carriageways carry traffic between a major arterial route to and from Birmingham city centre and a large housing estate. Its traffic level is reasonably constant throughout the day at approximately 120 vehicles per hour outside rush-hour periods. This bridge is free of shading.

Figure 5.1 River Cole Bridge

The construction is similar to Fordrough bridge and River Cole bridge is again rectangular in plan. The bridge has a width of 15·58 m, a span of 12·7 m between bearing pads and the deck is 0·68 m deep. Its two 450 mm wide string-courses border a 8·6 m wide carriageway and pavements nominally 2·25 m and 4·73 m wide. The carriageway surface has a mean thickness of 175 mm whilst both pavements are approximately 300 mm thick. This design incorporates 1·4 % of longitudinal fall and a

3·5 % cross-fall over the majority of its width. The composite construction consists of *in situ* concrete infilling 30 prestressed-concrete inverted-T beams with the majority type 'T5'. The T5 beam is 615 mm deep and each includes a section prestress of approximately 1670 kN at an eccentricity of nominally 115 mm below its centroid. The structure has an overall mass of approximately 360 tonnes.

5.2.3 Old Haymills Bridge

This bridge is adjacent to the Fordrough site and its two eastbound carriageways carry the main A-route traffic from Birmingham over the River Cole in the direction of Coventry. Its traffic level is reasonably constant throughout the day at approximately 1500 vehicles per hour outside rush-hour periods and it is completely free of shading.

This structure has a 14·5° skew in plan with 11·48 m between bearing pads. The bridge is 17·0 m wide and has an overall deck depth of approximately 0·93 m. Two string-courses 550 mm wide border a 9·9 m wide carriageway and pavements nominally 2·85 m and 3·15 m wide. There are no engineering details available concerning the superstructure and the main structure dimensions had to be surveyed. The carriageway surface and pavements were estimated to be 190 mm and 300 mm thick respectively. Its turn-of-the-century steel-trough deck is horizontal and it consists of twelve 0·48 m high fabricated steel-troughs at 1·37 m centres, with a 0·61 m high and 0·45 m wide box-channel providing support at each side. An additional 460 mm thick reinforced concrete plinth and two 600 mm by 450 mm concrete string-courses were added to the deck during an upgrading in the early 1980's. The resulting structure was estimated to have an overall mass of approximately 560 tonnes.

5.2.4 New Haymills Bridge

This structure is parallel to the Old Haymills site and its two westbound carriageways carry the main trunk-route traffic from the Coventry direction to Birmingham city centre over the River Cole. It is free of shading and traffic levels are reasonably constant throughout the day at approximately those of the Old Haymills site.

The design has a 40° skew in plan with 15·09 m between bearing pads. The deck incorporates 1·4 % of cross-fall over 70 % of its 19·0 m width and it has an overall depth of 0·24 m. Its two 500 mm wide upstands border a 11·0 m wide carriageway and pavements nominally 2·8 m and 4·2 m wide. The carriageway surface has a mean thickness of 170 mm whilst both pavements are approximately 380 mm thick. It is a contiguous beam and slab construction consisting of a slab-deck incorporating 19

prestressed-concrete M-beams. The 'M2' inverted-T beam is 720 mm deep and each includes a section prestress of approximately 5250 kN at an eccentricity of nominally 60 mm below its centroid. The structure has an overall mass of approximately 365 tonnes.

5.2.5 Saturday Bridge

This bridge is situated in a city-centre location and its four north-south carriageways carry the main A-route traffic from Birmingham over the Birmingham and Fazeley Canal towards Smethwick and West Bromwich (Figure 5.2). It is completely free of shading and its traffic level is reasonably constant throughout the day at approximately 2000 vehicles per hour outside rush-hour periods.

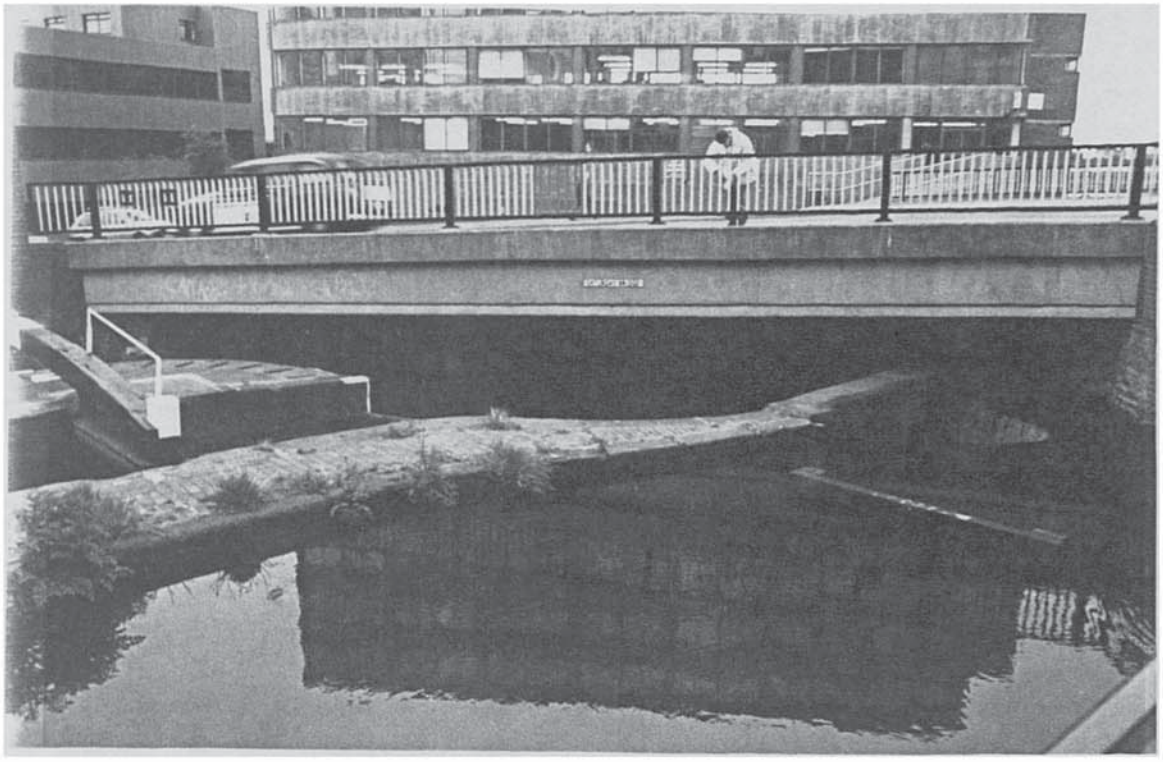

Figure 5.2 Saturday Bridge

The deck has a 35° skew and is asymmetrical in plan. It has a composite span of 15·3 m and 18·95 m between two sets of bearing pads. The width varies between 20·0 m and 20·3 m over its span(s) and the deck depth is 0·81 m over the majority of its width. Two 450 mm wide string-courses border a 14·0 m wide carriageway and two pavements nominally 2·5 m and 2·75 m wide. The carriageway surface has an approximate thickness of 200 mm whilst both pavements have a mean thickness of 300 mm. The

complex design of this bridge incorporates 4 % of fall over the entire span(s) also a composite of cross-falls and deck-offsets over its width, with the maximum cross-fall being 2 %. The composite construction consists of *in situ* concrete infilling 32 prestressed-concrete beams of varying design. The two main designs are 'T8' and 'M3D' inverted-T beams. The 'T8' beam is 735 mm deep and it was estimated from the design data that each incorporates a section prestress of approximately 1850 kN at an eccentricity of nominally 120 mm below its centroid. The 'M3D' beam is 880 mm deep and each was estimated to include a section prestress of approximately 5400 kN at an eccentricity of nominally 65 mm below its centroid.The structure has an overall mass of approximately 610 tonnes.

5.3 Bridge Response Measurement

Initial investigations into the most appropriate form of structural excitation technique for the purposes of response monitoring covered a number of aspects of structural excitation and its measurement (Wood *et al*, 1991). The method selected was easily implemented on any of the chosen structures and it minimised the required equipment resources and any inconvenience to normal road-users.

5.3.1 Excitation Technique

The chosen method of excitation involved imparting an impulse into the test bridges using a sledgehammer and this technique excited a number of the natural modes of vibration of the structure. However the energy available from a hammer impact is potentially broad-band in nature and a suitable low-pass medium had to be identified. It was found after laboratory investigation that a 150 mm x 150 mm x 20 mm thick, fibre-reinforced 'hard' rubber-mat would reproduce an optimum impact spectrum. This spectrum was sensibly flat in profile until a pronounced 'roll-off' point was reached at approximately 200 Hz. The frequency range which is excited is controlled by the stiffness of the contacting surfaces and the mass of the impactor head. The hammer-surface system resonance frequency is given by:

$$(\text{contact stiffness}/\text{impactor mass})^{1/2}$$

above which it is difficult to deliver energy to the structure (Ewins, 1984). The rear-face of the hammer incorporated an accelerometer which measured the frequency 'quality' of any impact. This signal was transferred to the computer by screened-cable via a charge-amplifier.

The impact sites were dictated by the positioning of the measurement transducers (see subsection 5.3.2). The structure was struck in turn through the mat on the pavement immediately adjacent to each accelerometer and one additional impact was made on the structure at mid-span on the opposite side of the bridge from the transducer positions. The test included only one impact since the data-acquisition software did not possess any averaging facilities. Care was taken to ensure that no vehicles were within 50 m of the site whilst exciting the structure with the hammer-blow in order to avoid parasitic excitations from traffic either approaching or leaving the immediate vicinity of the bridge.

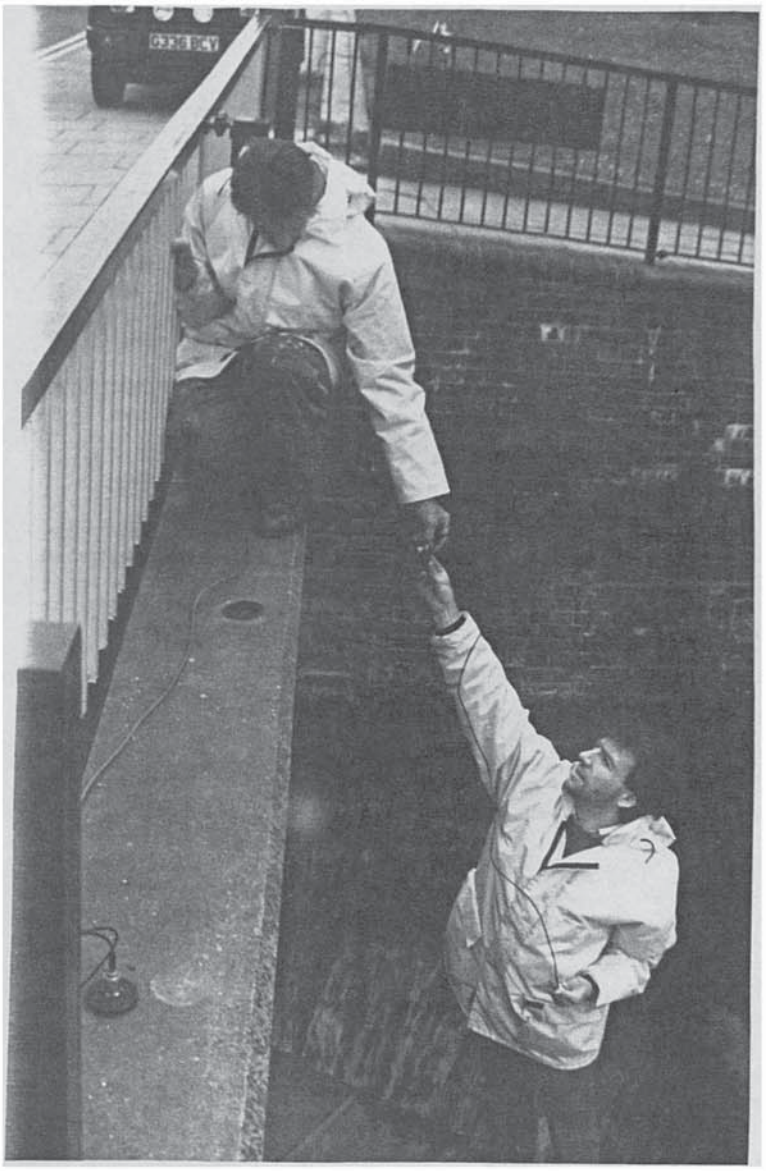

Figure 5.3 Temperature and vibration response measurement positions

5.3.2 Response Measurement Technique

The response of the bridge was measured by pre-positioned accelerometers on the main structure. The siting of these transducers was dictated by the need for direct, rather than secondary access to the resultant bridge motions. This was because most of the pavement areas had substantial layers of oily, road grit present which would have created a soft, pliable layer between structure and transducer. Each accelerometer was positioned on the concrete string-courses which form an integral part of the main structure (Figure 5.3). Three transducers were used to measure the accelerations at half-span, third-span and quarter-span positions on one side of any of the structures. The signals originating from the accelerometers were then transferred to the computer memory via screened-cabling, a power-amplifier and filter unit.

The measurement procedure was simple in that the computer operator set-up the software for manual-trigger data-acquisition from four channels. These channels included the three bridge-transducer outputs and the sledgehammer-deceleration signal. The second operator struck the bridge at the prearranged position when the bridge area was clear of traffic and pedestrians. As the hammer descended from its 'drop'-height of

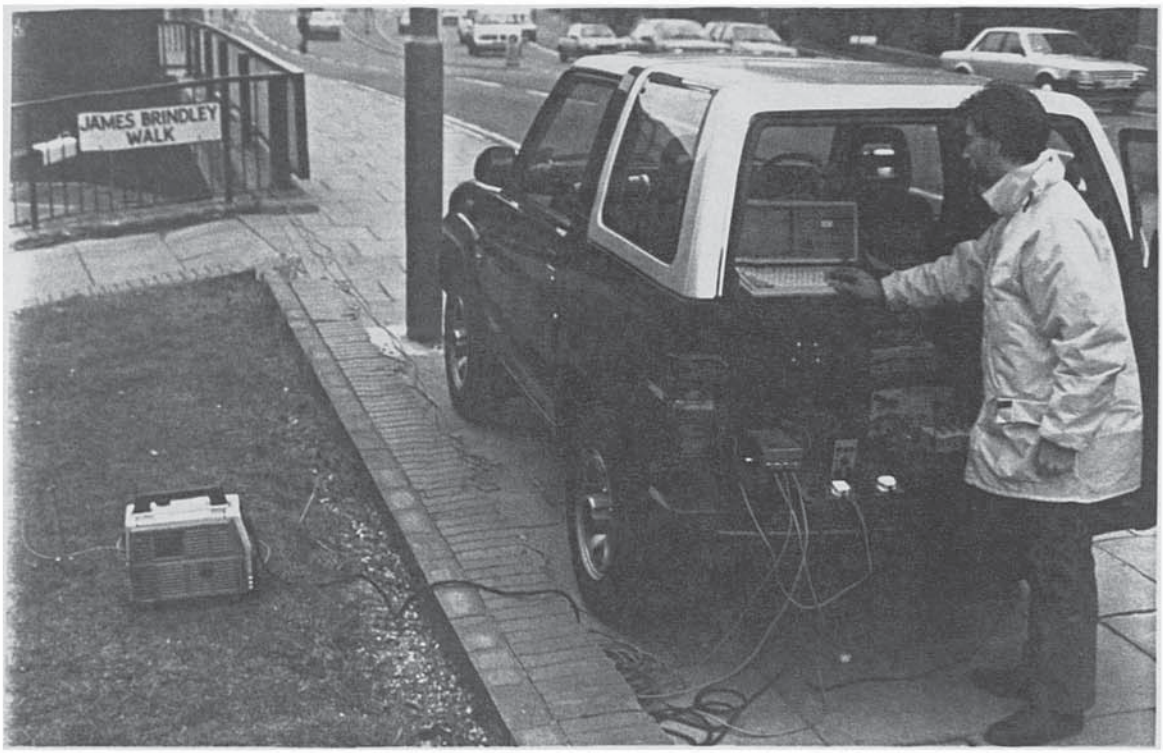

Figure 5.4 Acquiring site vibration data from one impact event

approximately 1·0 m the data-acquisition for the 'event' would be triggered (Figure 5.4). An elapse time of approximately 3 seconds would be allowed to collect the data of the decaying transients from the event before the data-acquisition was terminated and reset for the next test.

5.3.3 Equipment

The equipment used during these tests is illustrated in Figure 5.5. The sledgehammer has a mass of approximately 6·5 kg and the accelerometer attached to its rear-face was a B&K 4333 design since it was both light and robust enough to withstand the very severe decelerations.

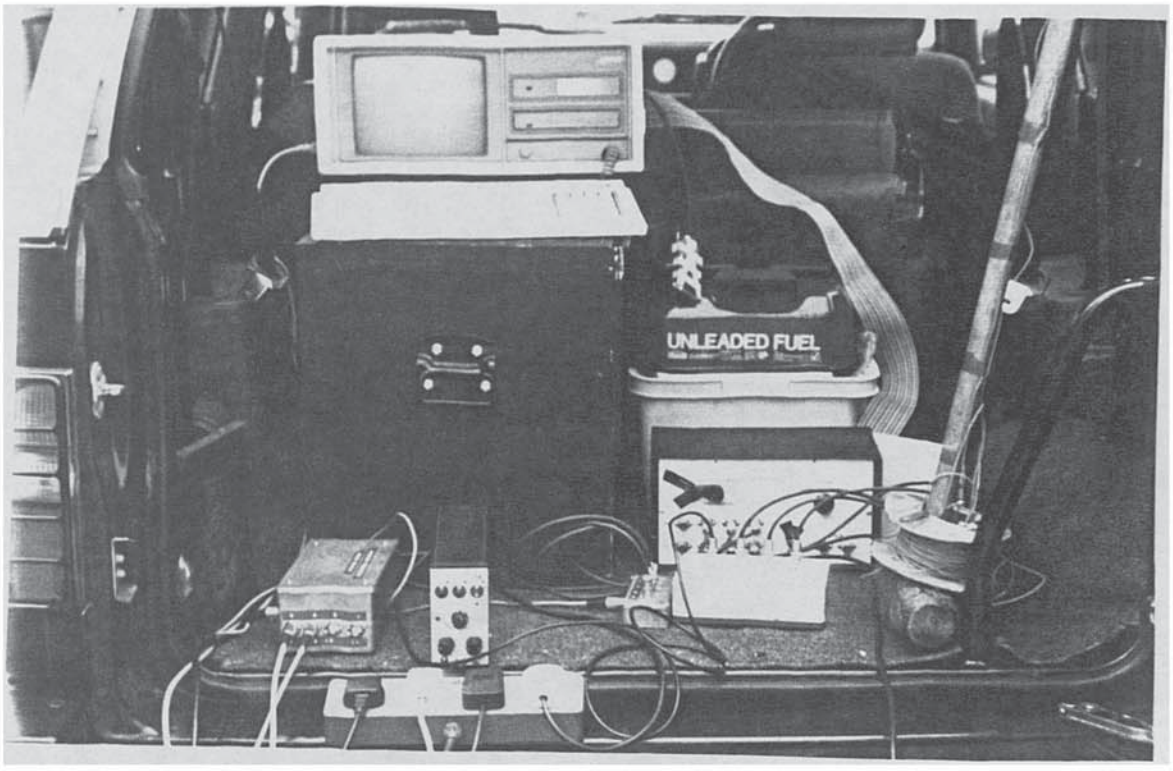

Figure 5.5 Acquisition equipment for site vibration response data

The accelerometers used were Pennwalt ACH-03's which required power-supplies of 5 volts. Their piezo-electric capacitance output is modified into a direct voltage signal by on-board electronics. This 'operational-amplifier' based signal transformation allowed

any output to be directly transferred to data-acquisition equipment by the use of standard 'analogue-to-digital' conversion (ADC) facilities. Each accelerometer with its tripod-support was independently calibrated within the laboratory and sensitivities of approximately 860 mV/g' were obtained. These responses were sensibly linear between approximately 1 Hz and 400 Hz after which the output was influenced by the inherent mechanical resonance of the instrument design. The transducers were free-standing on the bridge using the tripod-support arrangement illustrated in Figure 5.6. The transducers could be transferred from bridge to bridge with ease since they were not permanently fixed to the structure. The positioning of each transducer was guaranteed within 5 mm in both the 'X' and 'Y' planes during each bridge visit because 90 mm diameter markers had been spray-painted onto the string-courses at the designated measurement positions (Figure 5.3). The tripod support was designed to provide unambiguous measurement of the vibrational responses by using only three points of contact with the structure. Assuming purely sinusoidal excitation, it may be shown that there should be no more than a 5 % loss in motion transmission for this arrangement over the band-width considered. All the support-plates were levelled horizontally within the workshop and 'locked' in this attitude prior to use. This ensured as far as was practical that the transducer axes were normal to the surface on which these assemblies were to be placed: this measurement procedure assumed that each bridge string-course was level.

The power-amplifier for the ACH-03 units was custom-built by the Department of Mechanical and Electrical Engineering of Aston University. This unit incorporated a high-pass filter with a threshold of nominally 0·5 Hz to eliminate superfluous 'd.c.' signals. It also included a variable low-pass filter which was preset at 100 Hz for these tests.

The computer system used for the data-acquisition during these investigations was a portable COMPAQ 286 and its configuration included an ADC. The ADC system employed during these tests was tailored for the support of nCode/nSoft data-acquisition software. This system had the capability to multiplex 16 channels of incoming data simultaneously and would allow a variety of analysis operations on any one channel of information after demultiplexing. Analysis included the facility to Fast-Fourier-Transform (F.F.T.) the time domain data into the frequency domain which resulted in an Auto-Spectral-Density (A.S.D.). The sampling rate for each channel was set to 2 kHz for data acquisition purposes whilst the buffer was preset to reproduce a resolution of 0·061 Hz during any subsequent FFT analyses.

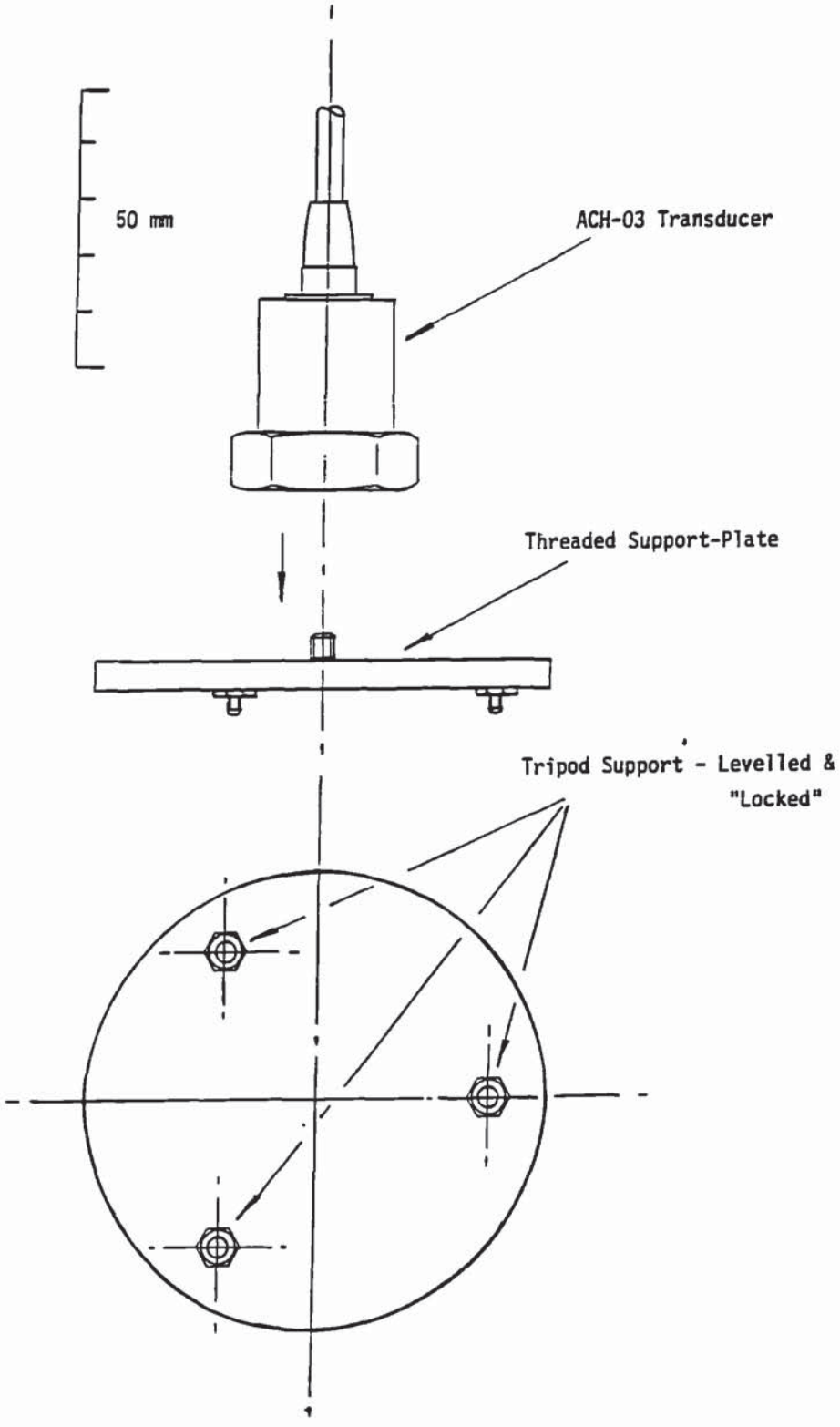

Figure 5.6 ACH-03 accelerometer and tripod-support plate

The on-site power was supplied by a portable 350 watt petrol-generator. All necessary equipment and personnel were transported in one medium-sized vehicle. Fordrough bridge was the only site where the project vehicle could not be positioned off the structure due to the dangers to traffic-flow. As a result the vehicle was carefully parked on the pavement with the off-side-rear wheel adjacent to a painted marker on the kerb since this maintained a consistent mass distribution on the structure during testing. Site-work in the vicinity of traffic and pedestrians necessitated a number of safety considerations which are detailed in Appendix 1.2.

5.3.4 Example Data

The impact time history of Figure 5.7(a) illustrates an example of the impulse imparted into a bridge structure during one test. From these data the resultant ASD of Figure 5.7(b) shows that the hammer impact was of a reasonably constant power-level over the bandwidth considered.

A FFT analysis of the time domain data from one of the subsequent bridge-transducer responses result in spectral peaks similar to those in Figure 5.8(a) and these peaks identify the natural modes of vibration of the bridge at that particular condition. Using these ASD data from all three bridge-tranducers simultaneously (Figure 5.8(b))

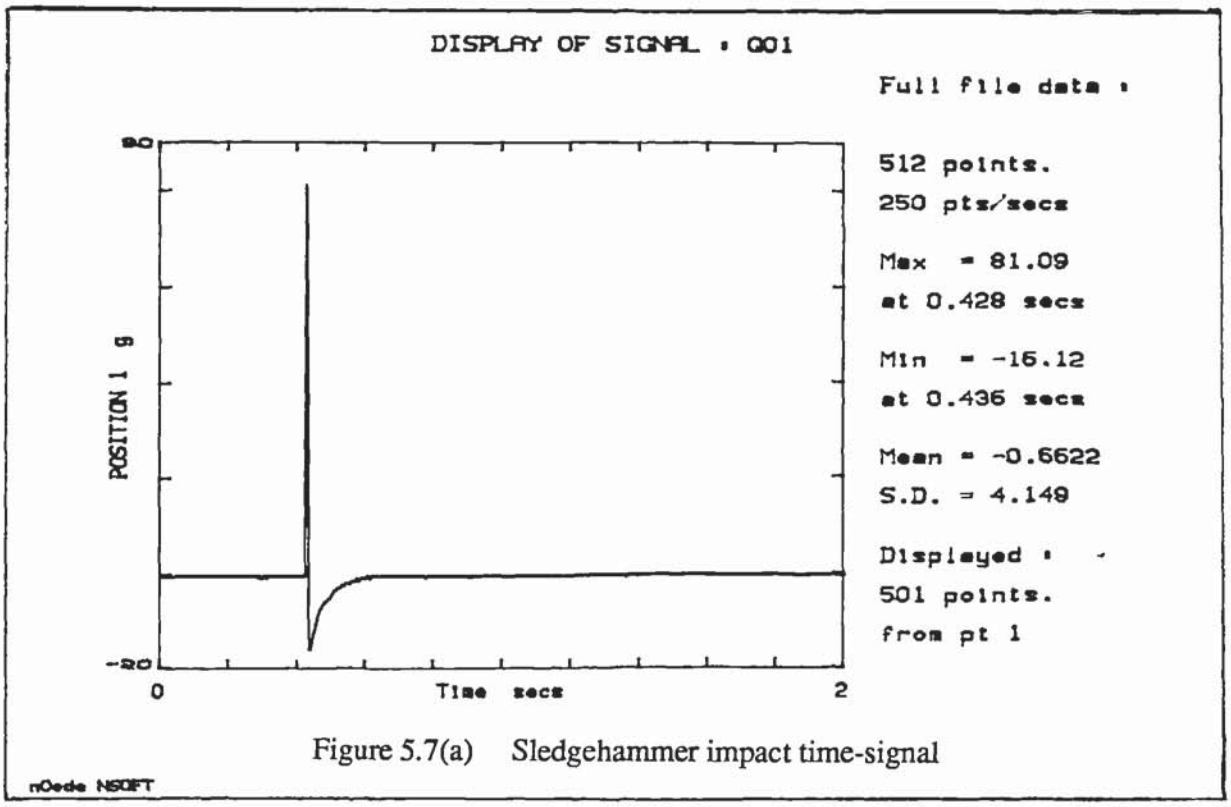

Figure 5.7(a) Sledgehammer impact time-signal

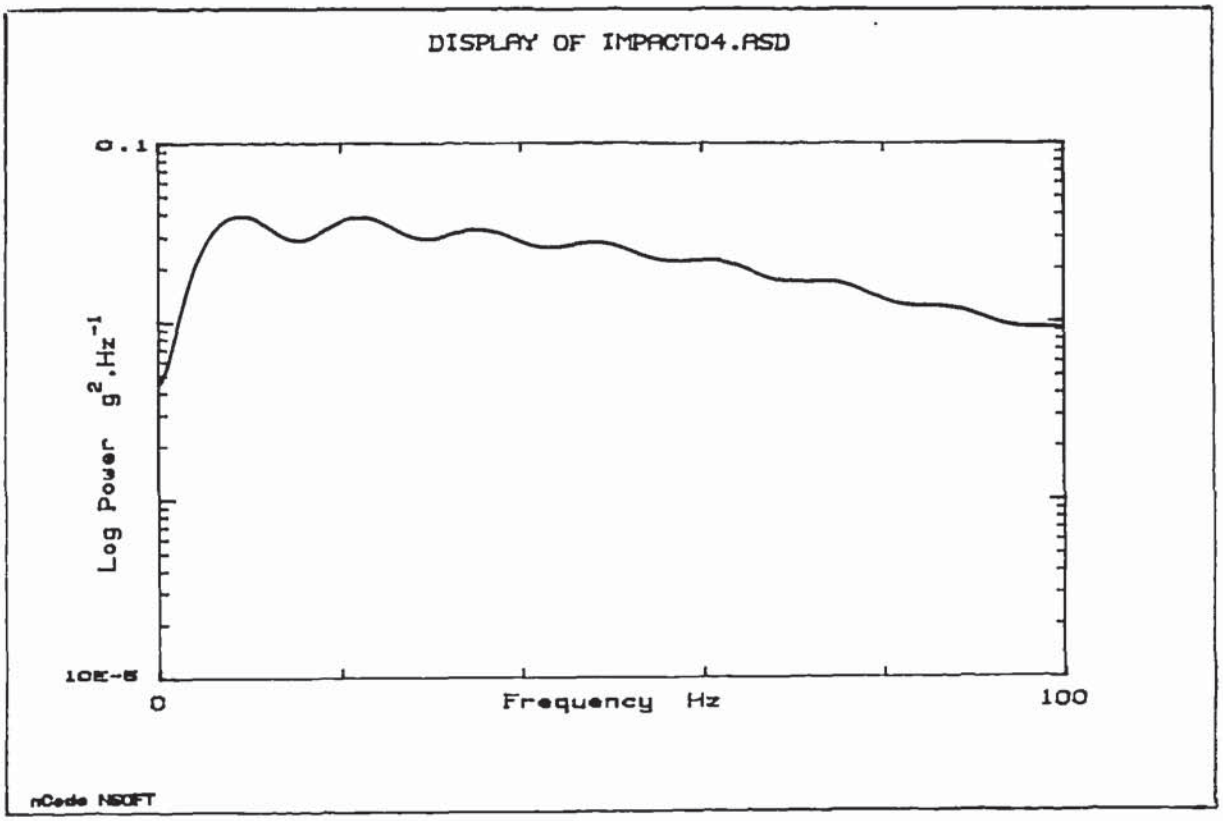

Figure 5.7(b) Sledgehammer impact Auto-Spectral-Density

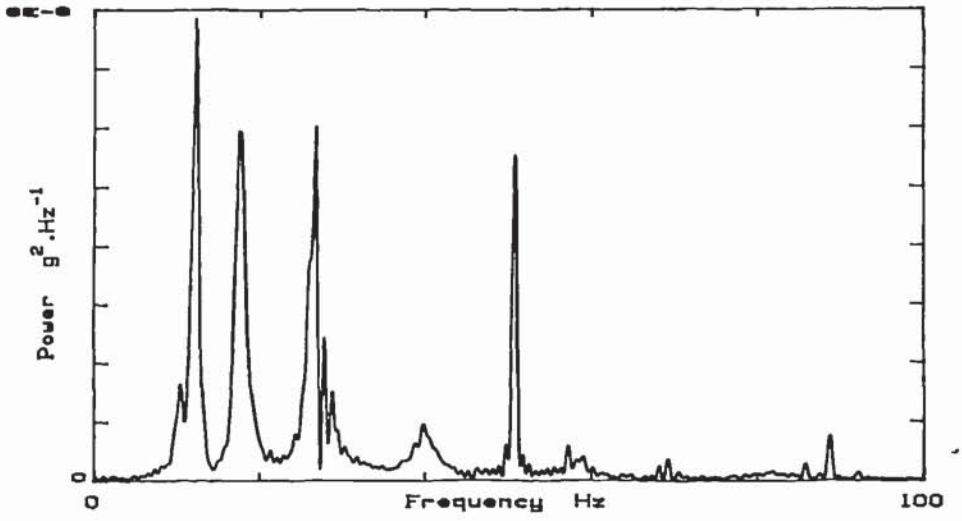

Figure 5.8(a) Response accelerometer ASD

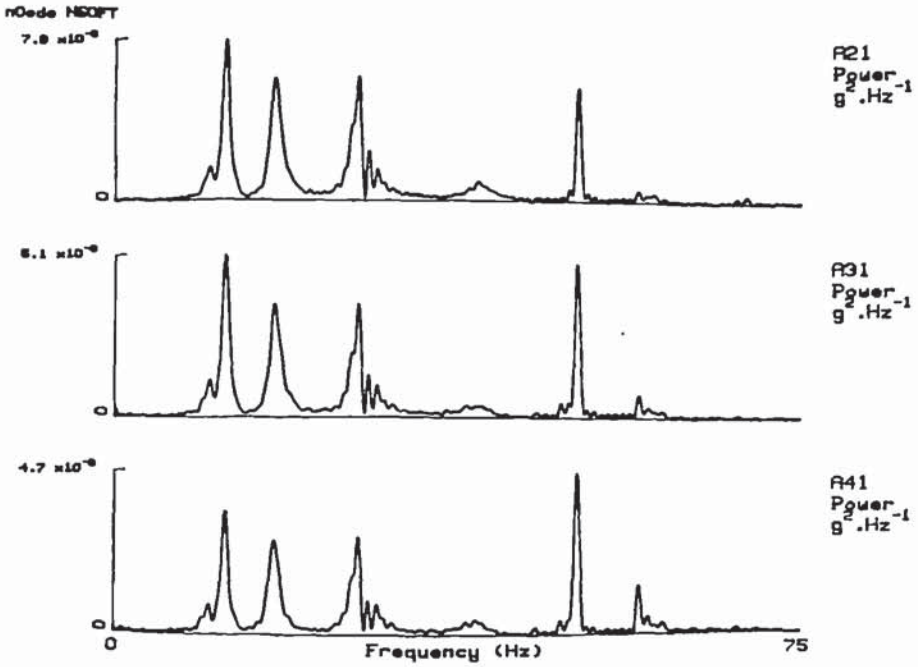

Figure 5.8(b) Simultaneous responses from 3 accelerometer positions

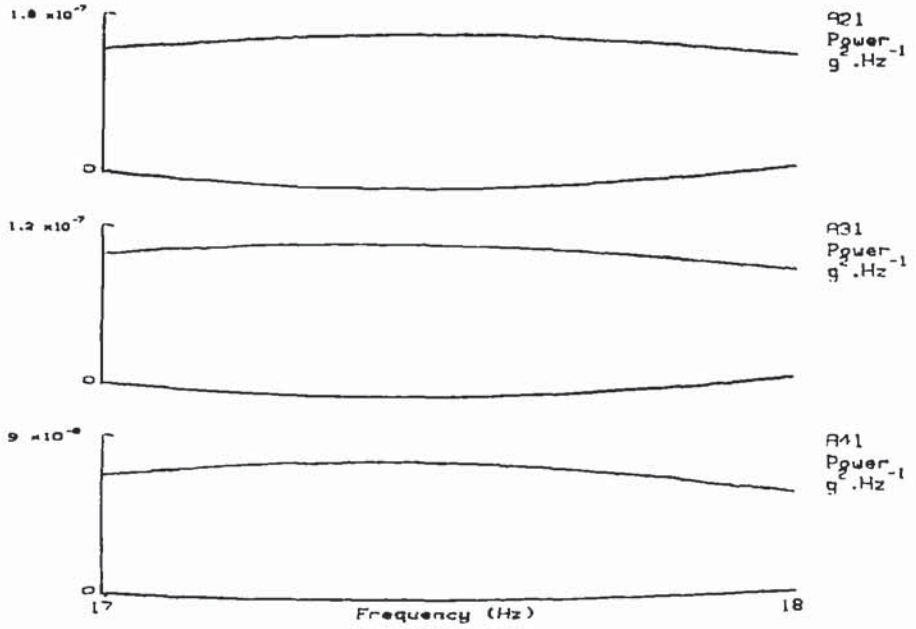

Figure 5.8(c) 'Windowed' frequency responses about one spectral peak

individual peaks were then 'windowed' to a 1·0 Hz bandwidth as shown in Figure 5.8(c). It was possible to identify the limits of the spectral peaks by using the cursor facility within the nSoft data presentation since the quanta of the display reproduced a 'peak' as a horizontal line at that resolution. This data-processing procedure was repeated for all four events which represented one bridge-test and the resultant mean frequencies were compiled as shown in Figure 5.9. The letter 'F' is abbreviated from 'Farside' and so responses obtained from the hammer impact at mid-span on the opposite side of the bridge to the transducer positions include this prefix. These impact events were remote from the instrumentation base and the hammer deceleration was not recorded since this would have required leading cable either below the bridge structure through water or over the carriageway. The hammer response of 'F01' was therefore assumed to be of similar quality to the other impacts M01, T01 and Q01. If, as in this case, the time trace from the hammer impacts was poor then all the resultant ASD's from the transducers were checked and the test was only repeated if both the time series and ASD's were of poor quality. It was established during this period of tests that the 'micro-dot' connection to the hammer accelerometer was damaged and this problem of poor quality hammer data did not occur after subsequent repair. Other event designations include 'M' for mid-span, 'T' for third-span and 'Q' for quarter-span impact positions. The response '02' identifies the signal originating from the mid-span, '03' the third-span and '04' the quarter-span position transducers. The mean mode frequencies identified from the response ASD's are shown adjacent to the 'spectral peaks' legend for each event. The overall mean frequencies from all the events are presented as the bottom line against the legend 'spectral peaks'. This value was weighted to include the 'frequency' of data obtained from the range of ASD's and, for example, if one set of transducer responses only returned two instead of three unambiguous values for one mode then this would be accommodated in the overall mean .

5.4 Bridge-Site Temperature Measurement

In parallel with the periodic bridge response measurements discussed above, the task of obtaining complementary temperature data from each bridge-site took three distinctive forms. The first included data taken directly from the structure immediately prior to the vibration measurements, the second concerned the ambient air conditions present at the bridge during the test and the third centred on general meteorological conditions for that location on the day of the test.

H

DATA FILE: FR290591	Fordrough : NCode (Blucco) Impedance ASD Analysis									
DATE: 29/5/91 TIME: 09.45	Temperature Details: T_{DB} = 10.5 °C T_{WB} = 8.5 °C : Hum = 77 % Air Barrier = 12.8 °C Air Underdeck = 10.3 °C Air Surface = 9.7 °C.									
Impact Pos'n / For Midspan	Event :	Fϕ1		Fϕ2		Fϕ3		Fϕ4		
FFT Buffer: 4096 / 0.061 Hz B/Width	Time Datums :	N		.39/1.2		.39/1.2		.39/1.2		
	ASD File :	A		A_{21}		A_{31}		A_{41}		
Spectral Peaks (Hz)		12.00	17.27	25.48	38.82		50.53	57.28		
Impact Pos'n ϕ2 / Midspan	Event :	Mϕ1		Mϕ2		Mϕ3		Mϕ4		
FFT Buffer: 4096 / 0.061 Hz B/Width	Time Datums :	Poor Signal		.64/1.2		.64/1.2		.64/1.2		
	ASD File :	Impact ϕ2		A_{22}		A_{32}		A_{42}		
Spectral Peaks (Hz)		12.25	17.19	25.62	38.69		50.74	58.70		
Impact Pos'n ϕ3 / ThirdSpan	Event :	Tϕ1		Tϕ2		Tϕ3		Tϕ4		
FFT Buffer: 4096 / 0.061 Hz B/Width	Time Datums :	As Above		.36/1.1		.36/1.1		.36/1.1		
	ASD File :	Impact ϕ3		A_{23}		A_{33}		A_{43}		
Spectral Peaks (Hz)		12.33	17.06	25.69	38.29		50.64	58.42		
Impact Pos'n ϕ4 / QuarterSpan	Event :	Qϕ1		Qϕ2		Qϕ3		Qϕ4		
FFT Buffer: 4096 / 0.061 Hz B/Width	Time Datums :	As Above		.3/.83		.3/.83		.3/.83		
	ASD File :	Impact ϕ4		A_{24}		A_{34}		A_{44}		
Spectral Peaks (Hz)		12.69	17.14	25.67	38.41		50.14	59.88		
Data Summary : 1 Hz Bandwidths About Spectral Peaks	Comments : Overcast Cool Breeze Light Wind Warm Previous Two Days									
Spectral Peaks (Hz)		12.32	17.17	25.62	38.55		50.51	58.57		

Figure 5.9 Frequency response data compilation

5.4.1 Structural Measurement Techniques

The method of structural temperature measurement had to be non-invasive to traffic flow. The technique selected for these measurements was a contact-thermocouple reading at predetermined positions on the bridge. High-conductivity metal disks were adhered to the bridge so they became integral parts of the structure and, therefore, had the same temperature of the structure at that point (Figure 5.3). These 50 mm diameter, 15 mm thick disks were manufactured from aluminium and provided a flat and conductive surface from which to obtain measurements. These disks immediately became the target of local 'collectors' even although they were painted to resemble part of the bridge superstructure. To the credit of the *Loctite* adhesive used, however, only one of these temperature 'receptors' became dislodged during the monitoring period and it was immediately replaced. These disks were firmly fixed to the four corners of each structure and the two mid-span positions on the bridge string-courses. Six more were located on the underside of the deck immediately below the string-course positions.

A further four disks were adhered to Saturday bridge because of its size. Their longitudinal positioning was altered to third-span and two-thirds span to maintain approximately equal-spacing. Fordrough bridge had an additional six disks fixed to the carriageway 'black-top' to provide additional data since its traffic-flow was infrequent and easily sighted in good time to avoid danger.

The measurement procedure included initially noting the structural temperatures at each position on the upperdeck and any carriageway positions using a Digitron meter and thermocouple surface probe. The measurement resolution of this instrument was 0·1°C and there was no recorded error in its calibration within the laboratory between temperatures of 0°C (ice-water) and 100°C (boiling water). One operator remained on the bridge-deck to record readings and the second obtained measurements from the soffit mounted receptors, entering the river if necessary. It must be noted that direct contact with inner-city canal or river water necessitated a number of safety considerations and these are detailed in Appendix 1.3.

5.4.2 Ambient Site Conditions Measurements

The ambient air conditions present at the site during the structural response investigation were recorded using a whirling-hygrometer (i.e. an aspirated psychrometer). This simple device measured both air-temperature and relative humidity. The instrument assembly consisted of two mercury thermometers in a casing which was rotated


Aston University
Illustration removed for copyright restrictions

vigorously above the head for between 15 and 20 seconds. One of the thermometers had moistened gauze surrounding its mercury bulb and measured the wet-bulb temperature. The second measured the dry-bulb, or air, temperature since this thermometer was only influenced by the ambient air conditions. The relative humidity was established from a chart listing the air temperature against the depression of, or differential in, the dry- and wet-bulb readings.

5.4.3 General Meteorological Data

The Birmingham area has a weekly climatological summary which is compiled by the School of Geography at Birmingham University. This document is the result of a series of comprehensive measurements undertaken frequently throughout the day and an example of which is illustrated in Figure 5.10. Selected information from this source was used for the comparative analyses of Chapter 6.

5.4.4 Example Data

Figure 5.11 illustrates an example of a data sheet used to record information gained from the Fordrough site prior to a series of impact response tests. It shows the relative positioning of the test vehicle on the bridge in addition to the temperature data obtained. Circles on the structure outline show the positioning of the temperature receptors. Those embedded in the carriageway are designated 'T_A' to 'T_F' and their corresponding readings are presented vertically on the right of the data sheet. The main structure receptor positions are designated 'T_1' to 'T_{12}' and their readings are presented horizontally at the bottom of the figure. The odd values measurements correspond to those positioned on the upperdeck whilst the even values are those temperatures of the soffit positions. General comments regarding the weather conditions present are made vertically to the left with the hygrometer readings and both test date and time noted at the top of the figure. The black dots illustrate the response transducer positions and, although there was no transducer positioned beside the T_3 receptor, hammer impacts were made on the pavement immediately adjacent to these points.

5.5 Statistical Correlation

Figure 5.12 shows the complete test event history of observed frequency data during the monitoring programme for Old Haymills Bridge. Table 5.1 repeats these data in tabular form but also presents the associated parametric data extracted from both the bridge-site

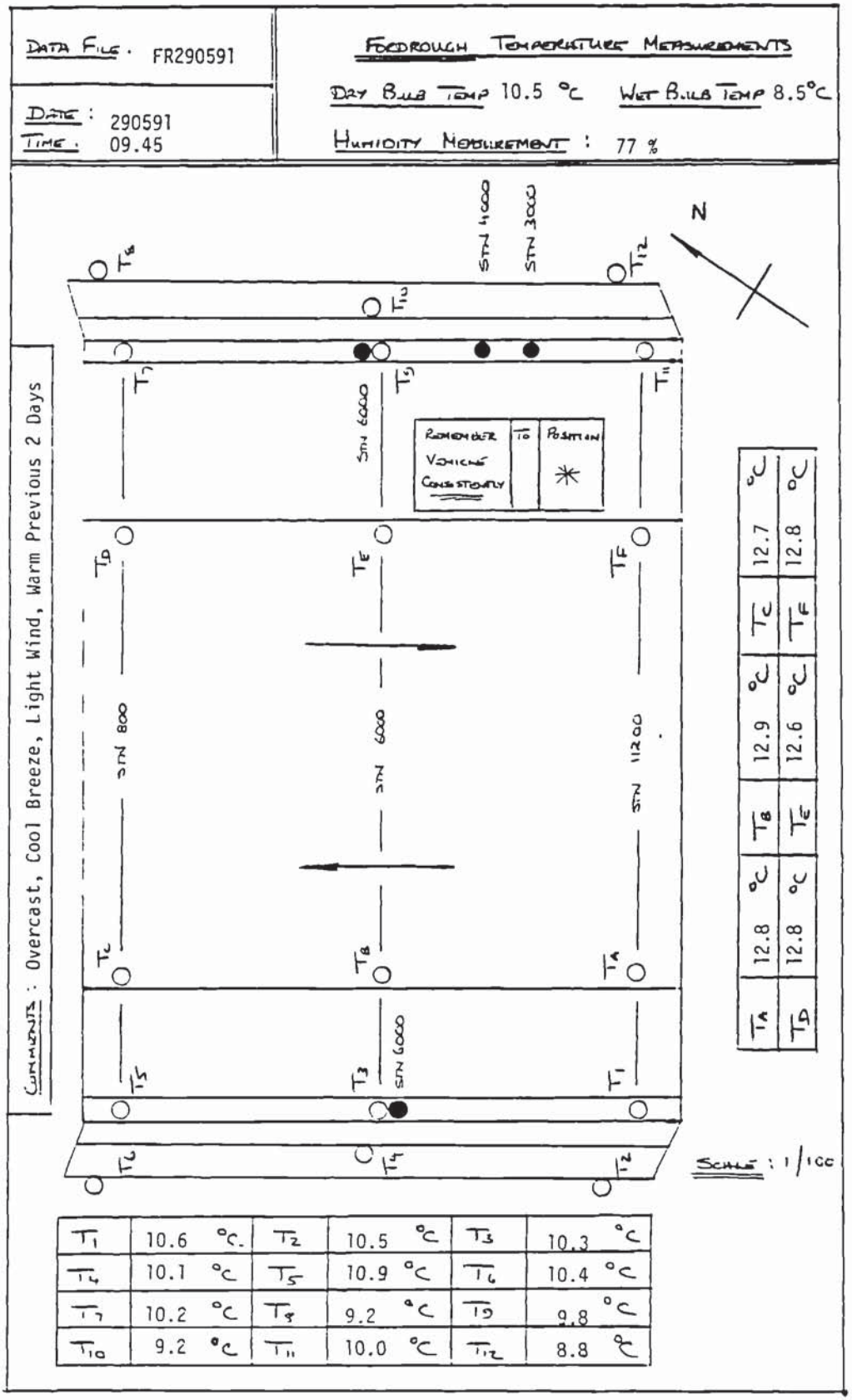

Figure 5.11 Example temperature data compilation for Fordrough site

and published ambient condition compilations. A recognised method of establishing the relationship, if any, between the data collated and the variables which could influence the vibrational response of the bridges was required. A number of choices were available but it was necessary to consider the limitations as well as the benefits of any statistical technique.

5.5.1 Technique Selection

It was unlikely that any parametric effects on the behaviour of each bridge would be linear in form after considering the mechanics of both their construction and the vibrational characteristics of orthotropic bridge decks. For this reason complex analyses

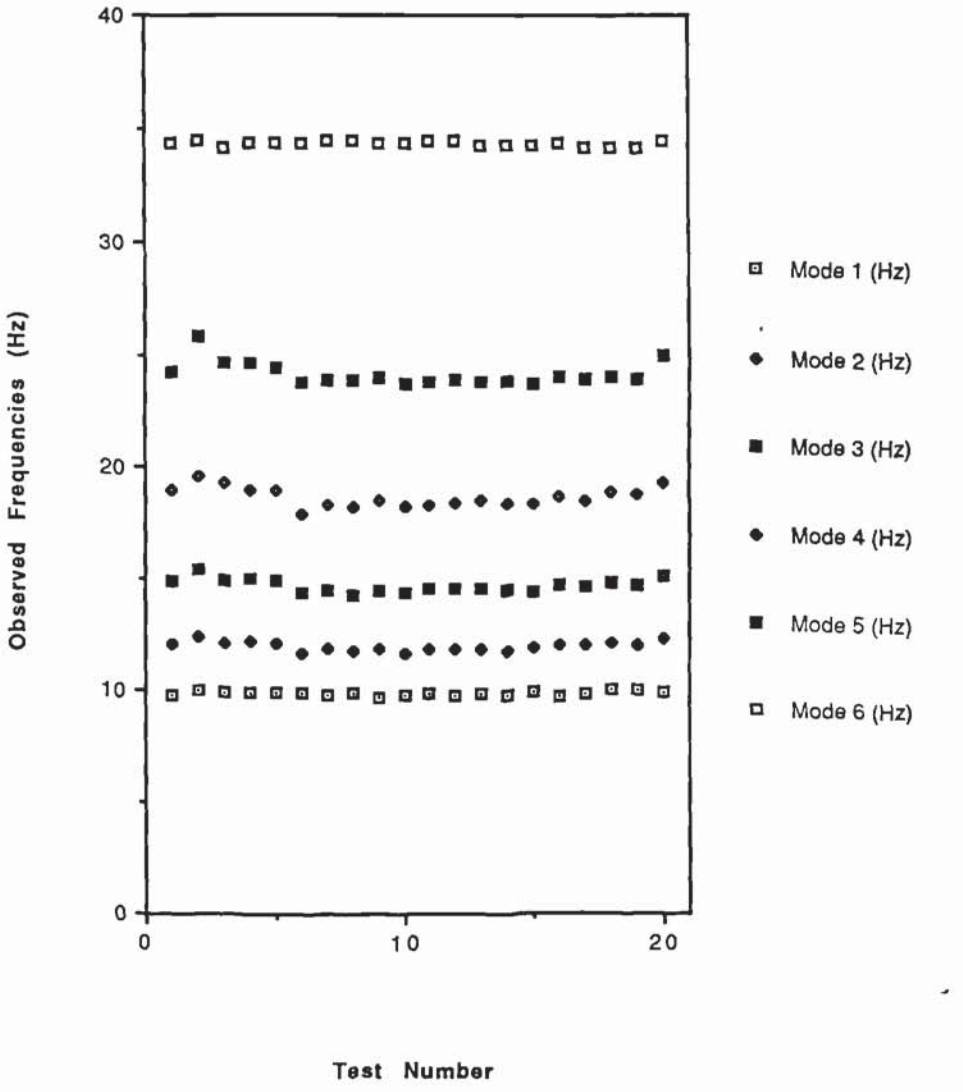

Figure 5.12 Observed bridge frequency responses versus test number

Saturday

	Event Day	Event Time	Site Temp (oC)	Site Humidity	Upperdeck (oC)	Soffit (oC)	Mode 1 (Hz)	Mode 2 (Hz)	Mode 3 (Hz)	Mode 4 (Hz)
1	107	10 25	4.5	85	5.8	4 7	9 67	13 88	21 20	30 55
2	114	10 75	13 0	59	13 6	9 3	9 59	14 15	20 61	30 16
3	129	10.25	15 0	44	15 3	10 1	9 59	13 86	20.41	29 47
4	150	11.00	11.5	83	10 8	10 1	9 96	13 84	20 71	29 90
5	168	14.50	15 0	61	17 3	12 5	10 04	13 68	19 96	29 30
6	183	9.50	17.5	77	19.2	16 7	10 02	13 69	20 62	29 06
7	189	15.50	20 0	83	18.6	18 4	10 80	14 11	20 62	30 94
8	196	9.00	17.0	81	16.5	16 4	10 37	13 66	20.38	29 83
9	200	14.75	20.0	59	20 4	17.7	10 50	13 66	19 34	29 29
10	203	8.75	20.0	70	21.5	18 5	10 61	13 93	20 22	29 40
11	205	9.00	15.0	90	14 9	14 7	10 56	13 58	20 97	30 12
12	217	14.75	20.0	83	19 9	19 0	10 54	13 97	20 20	30 05
13	221	8.75	16.0	81	14 6	14 8	10 30	13 99	20 28	29 45
14	224	14.00	20.0	59	24 5	18 8	10 62	13 78	19 72	29 02
15	231	8.75	14.0	79	14 7	14 3	9.97	14 06	20.32	29 61
16	235	14.00	17.0	81	15 5	15 1	10 18	13 65	20 42	30 33
17	260	9.25	16 0	81	16 2	15 3	10 03	13 68	20.04	29 40
18	263	14.50	18 5	53	21 6	16 8	10 45	13 41	19 57	29 45
19	267	9.25	16.0	81	13 9	13 7	9 80	14 00	20.51	29 19
20	270	14.50	11.0	94	9.9	10.4	9.72	14 00	20.94	29.96

	Mode 5 (Hz)	Mean Temp	Mean Humidity	Max Temp (oC)	Min Temp (oC)	Rainfall (mm)	Air Pressure	Upper/Soffit	Settled Rating
1	40.16	3.9	67	7.2	0 6	0.60	1029 5	1.10	2.0
2	39.99	9.5	55	12.5	6 4	0 01	1018.7	4.30	3.0
3	39.91	7.9	60	13 9	2 0	0.00	1020 8	5.20	5.0
4	40.40	10.1	87	11.5	8 8	0.01	1025 7	0.70	7.0
5	40.54	10.5	72	13.6	7 4	1.00	1015.4	4.80	5 0
6	39 82	16 8	84	22.1	11.5	19.90	1018 6	2.50	8.0
7	39.78	16.7	92	18.5	14.8	2.70	1010.5	0.20	8 0
8	39.80	16 5	74	19.3	13 8	0.30	1012.0	0.10	9 0
9	39.85	16 3	69	19.1	13.5	0.01	1010 3	2.70	6 0
10	39.49	16.3	82	23.1	9.6	0.00	1020.2	3.00	9 0
11	40 04	14.1	94	17.6	10 5	8.10	1005.6	0.20	7.0
12	39 82	17.1	85	19.8	14 5	6.00	1017.1	0.90	7.0
13	39.64	15.2	80	20.4	10.0	0.10	1024.2	-0.20	7.0
14	39.71	15.3	58	20.1	10.4	0.00	1020.6	5.70	7.0
15	39.39	14.2	78	21.4	7.0	0.30	1022.2	0.40	8.0
16	39.84	14.5	76	16.9	12.1	2.20	1006 2	0.40	6.0
17	40.23	15.5	77	20.4	10.5	0.01	1019.9	0.90	8.0
18	39.54	10.7	56	18.0	3.4	0.01	1019.1	4.80	7.0
19	39.54	15.0	73	17.0	13.0	0.40	1004.0	0.20	6.0
20	39.94	10.1	91	11.2	9.1	2.70	1006.7	-0.50	6.0

Table 5.1 Bridge frequency response and parametric data compilation

of variance were discounted. However in the majority of cases it was possible to identify sensibly linear trends in the observed responses using individual comparisons against only one measured variable. A first-order curve-fit was then employed during each of the individual comparative analyses and the quality of the 'fit' was taken as the square of the correlation coefficient R^2 (or r^2). In retrospect, complex analyses of variance could have been undertaken on these data since the response relationships appeared linear, however, the quality of the single variable approach made any additional analyses superfluous.

5.5.2 Curve-Fit Theory

The theory of least-squares linear regression and associated correlation coefficient evaluation is well documented. It is outside the scope of this thesis and so the reader is directed to a useful text for further information (Neville and Kennedy, 1964).

5.5.3 Example Results

Table 5.2 illustrates the curve-fit correlations obtained from the River Cole bridge responses and both the structural and ambient temperature data. The resultant curve-fit correlation for each observed mode of structural vibration is listed against the selected variable. The variables selected for these comparative analyses were:

(i) The event time at which the testing took place.

(ii) The site air temperature during testing, as measured by the hygrometer.

(iii) The site air humidity during testing, as measured by the hygrometer.

(iv) The mean upper-deck temperature during testing, as measured at the receptors.

(v) The mean soffit temperature during testing, as measured at the receptors.

(vi) The mean local temperature on the day of testing, from the meteorological data.

(vii) The mean local humidity at the time of testing, from the meteorological data.

(viii) The max. local temperature on the day of testing, from the meteorological data.

(ix) The min. local temperature on the day of testing, from the meteorological data.

(x) The rainfall in the day to 9.00 am prior to testing, from the meteorological data.

(xi) The mean local air-pressure on the day of testing, from the meteorological data.

(xii) The mean temperature differential between the upper-deck and soffit during testing, as measured at the receptors.

(xiii) The 'settled' rating of the local conditions for two days immediately prior to the day of testing, as observed from the general weather patterns. This rating ranged between 0 for very cold and settled conditions, through 5 for moderate and changeable conditions until 10 for very hot and settled conditions.

Fordrough Bridge had three additional variables in the form of blacktop temperature, taken as the mean of the receptor readings, also mean blacktop/upperdeck and blacktop/soffit temperature differentials due to the inclusion of the blacktop temperature as a site measurement.

The correlation values presented in Table 5.2 are the square of each of the correlation coefficients and return a modular value regardless of whether the data correlation is positive or negative. The comment in parentheses below each value is made purely as a visual judgment of the quality of the curve-fit. As mentioned previously in the text, very close agreement was found in the relationships between both site and soffit temperatures and the observed changes in structural response. The remaining data in this figure show example gradients for both the soffit and site temperature relationships with a measure of this agreement presented as the gradient ratio.

5.6 Results And Discussion

Data were obtained from each bridge using the previously described procedures on an approximately weekly basis between late February and early October of 1991. All graphical response and tabulated parametric data for each of the structures discussed are presented in Appendix 5.1 due to the volume of summarised data. Curve-fit and observed trend-quality tabulations derived from the subsequent comparative analyses are presented in Appendix 5.2 again due to the volume of resultant data.

After careful scrutiny of the resultant curve-fit analyses from all the bridge-structures, it was apparent that two variables in particular showed consistently high levels of correlation with and linearity in relation to the structural responses. These parameters were the mean soffit and upper-deck temperatures, with the soffit results marginally more consistent. Figure 5.13 shows the resultant relationship between the observed responses and the mean soffit temperature for 4 modes of vibration of Fordrough bridge. The correlation (R^2) shown in these data varies between 0·750 and 0·879 and it is characterised by the close proximity of the data about the curve-fit line. Figure 5.14 repeats this exercise for an example mode of vibration from each of the remaining sites (i.e. River Cole, Old Haymills, New Haymills and Saturday bridges) and their consistent quality show an apparent independence of the complexity in bridge-construction.

Linear Curve-fit Correlation, R^2, And Observed Trend Quality ( ): River Cole

Mode No. Parameter	1	2	3	4	5	6
Event Time	0·267 (None)	0·568 (General)	0·684 (General)	0·152 (None)	0·447 (General)	0·404 (General)
Site Temp	0·652 (General)	0·912 (V.Good)	0·971 (Excellent)	0·033 (None)	0·439 (General)	0·895 (V.Good)
Site Humidity	0·005 (None)	0·027 (None)	0·071 (None)	0·001 (None)	0·285 (None)	0·036 (None)
Upper-deck Temp	0·552 (General)	0·841 (Good)	0·927 (V.Good)	0·070 (None)	0·500 (General)	0·860 (Good)
Soffit Temp	0·713 (Good)	0·949 (Excellent)	0·962 (Excellent)	0·020 (None)	0·335 (General)	0·919 (Excellent)
Mean Temp	0·732 (General)	0·789 (Good)	0·717 (Good)	0·004 (None)	0·122 (None)	0·773 (Good)
Mean Humidity	0·000 (None)	0·034 (None)	0·070 (None)	0·122 (None)	0·303 (None)	0·040 (None)
Max Temp	0·547 (General)	0·786 (Good)	0·751 (Good)	0·070 (None)	0·320 (None)	0·652 (Good)
Min Temp	0·594 (General)	0·450 (General)	0·380 (None)	0·031 (None)	0·001 (None)	0·643 (General)

Linear Curve-fit Correlation, R^2, And Observed Trend Quality ( ): River Cole (Cont'd)

Mode No. Parameter	1	2	3	4	5	6
Daily Rainfall	0·117 (None)	0·138 (None)	0·153 (None)	0·181 (None)	0·079 (None)	0·262 (None)
Air Pressure	0·265 (None)	0·060 (None)	0·051 (None)	0·029 (None)	0·007 (None)	0·230 (None)
Upper-deck / Soffit	0·174 (None)	0·401 (None)	0·546 (General)	0·128 (None)	0·621 (Good)	0·192 (General)
Settled Rating	0·451 (General)	0·713 (Good)	0·651 (General)	0·031 (None)	0·169 (General)	0·548 (Good)
Gradient Comparisons:						
Observed Mode Gradient (Hz/°C)		2		3		6
Site Temp.		$-6{\cdot}9964 \times 10^{-2}$		-0·16301		-0·17258
Soffit Temp.		$-7{\cdot}4966 \times 10^{-2}$		-0·17046		-0·16553
Gradient Ratio (<1)		0·933		0·956		0·959
			Mean Ratio	0·950		

Table 5.2 Example curve-fit correlation and data tabulation

Other temperature-based variables (e.g. measured site and general area maxima) also showed good correlation and approximately linear relationships with the observed responses. Figure 5.15 shows the resultant relationship between observed responses and the mean site temperature for 4 modes of vibration of New Haymills bridge. The correlation (R^2) shown in these data varies between 0·692 and 0·770 and this is again characterised by the near proximity of the data about the curve-fit line. Figure 5.16 repeats this exercise for an example mode of vibration from each of the remaining sites (i.e. Fordrough, River Cole, Old Haymills and Saturday bridges). On initial inspection these results could be considered spurious because of the variability of the local climate but the data consistency suggests that a definite trend exists. Also the ambient conditions changed gradually over a period of several days and, hence, the mean bridge temperatures would have shadowed the ambient air conditions as a result of the magnitude of the structure thermal inertiae. It may then be implied that if this programme was repeated at markedly varied times, without consistent daily air conditions being present, the same high level of agreement may not have been reproduced.

Finally, one general indicator of the bridge response conditions was found in the settled rating. Defined in subsection 5.5.3, the settled rating was a value attributed to the local conditions for two days immediately prior to the day of testing. This rating ranged between 0 for very cold and settled conditions, through 5 for moderate and changeable conditions until 10 for very hot and settled conditions. Figure 5.17 shows the resultant relationship between observed responses and this rating of the local conditions prior to the test for 4 modes of vibration of River Cole bridge. The correlation (R^2) shown in these data varies between 0·451 and 0·713 and this is also characterised by the general trend of the data about the curve-fit line. Figure 5.18 repeats this exercise for an example mode of vibration from each of the remaining sites (i.e. Fordrough, Old Haymills, New Haymills and Saturday bridges). Again these data trends tend to confirm that the mean structural temperature and, hence, vibrational responses shadow the general weather conditions experienced by the bridge-site over several days.

The above highlights three measures of varying accuracy in estimating the structural response over a range of modes of vibration to changes in ambient temperature conditions. The most accurate is the soffit (or shade) temperature. If direct structural measurements are unable to be made then, if the weather conditions have been reasonably consistent for a period of two or more days, air temperature measurements between mid-morning and mid-afternoon also give good indications of the response conditions of such structures. Finally, the general weather conditions for the preceding two days may also be used to broadly estimate the potential response conditions of the structure.

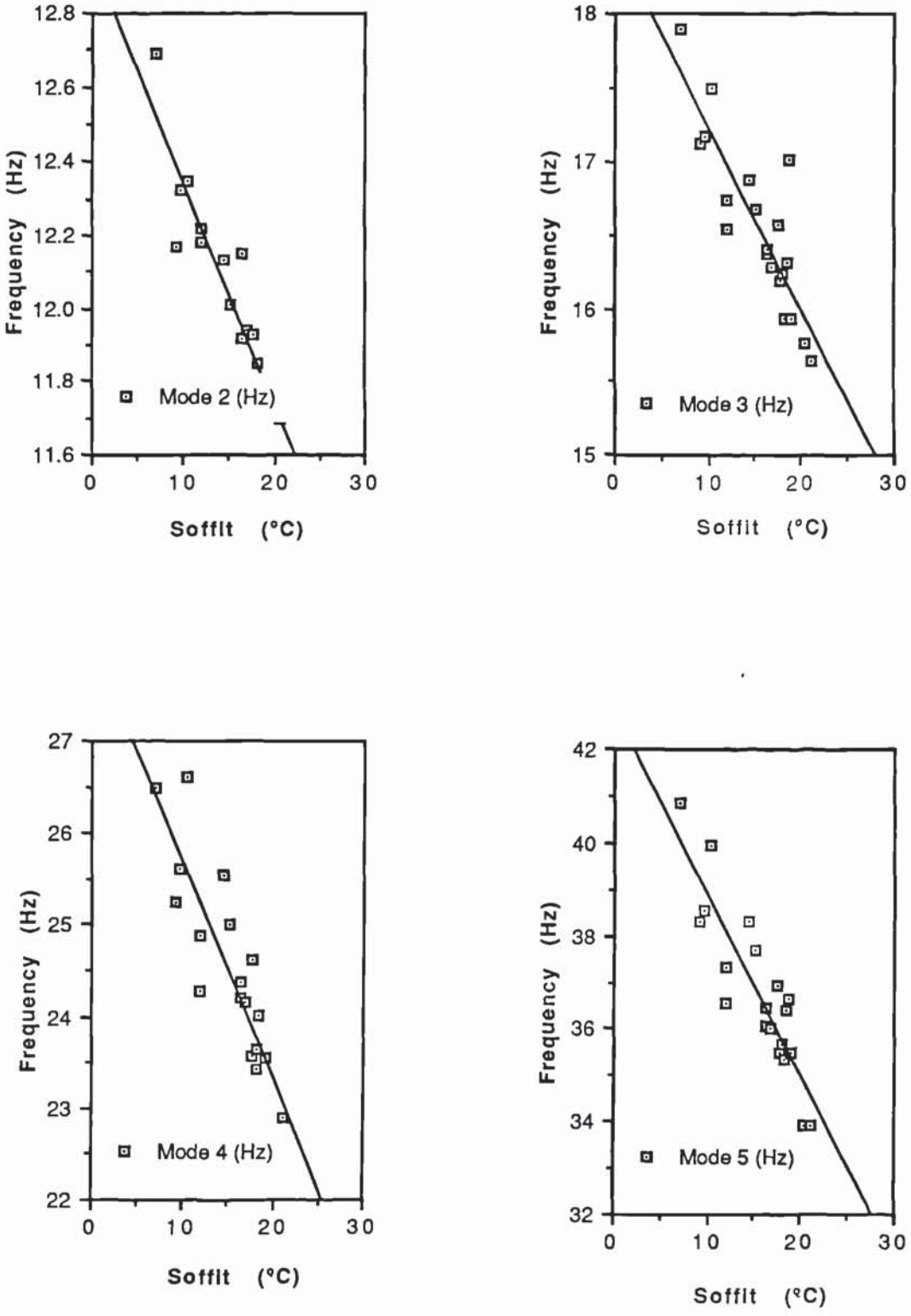

Figure 5.13 Soffit temperature versus frequency for 4 modes of response from Fordrough Bridge data

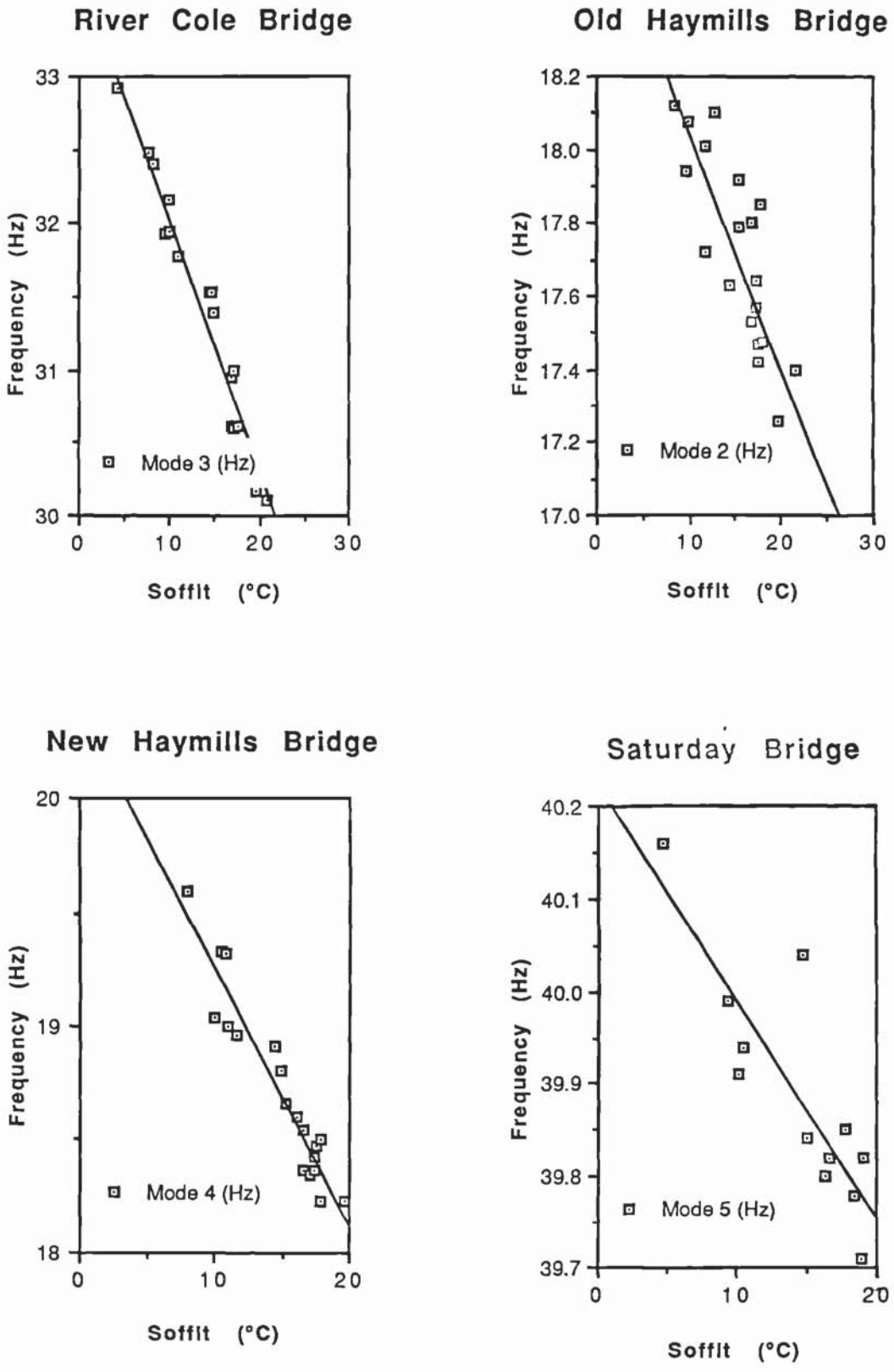

Figure 5.14 Soffit temperature versus frequency for 1 mode of response from River Cole, Old Haymills, New Haymills and Saturday Bridge data

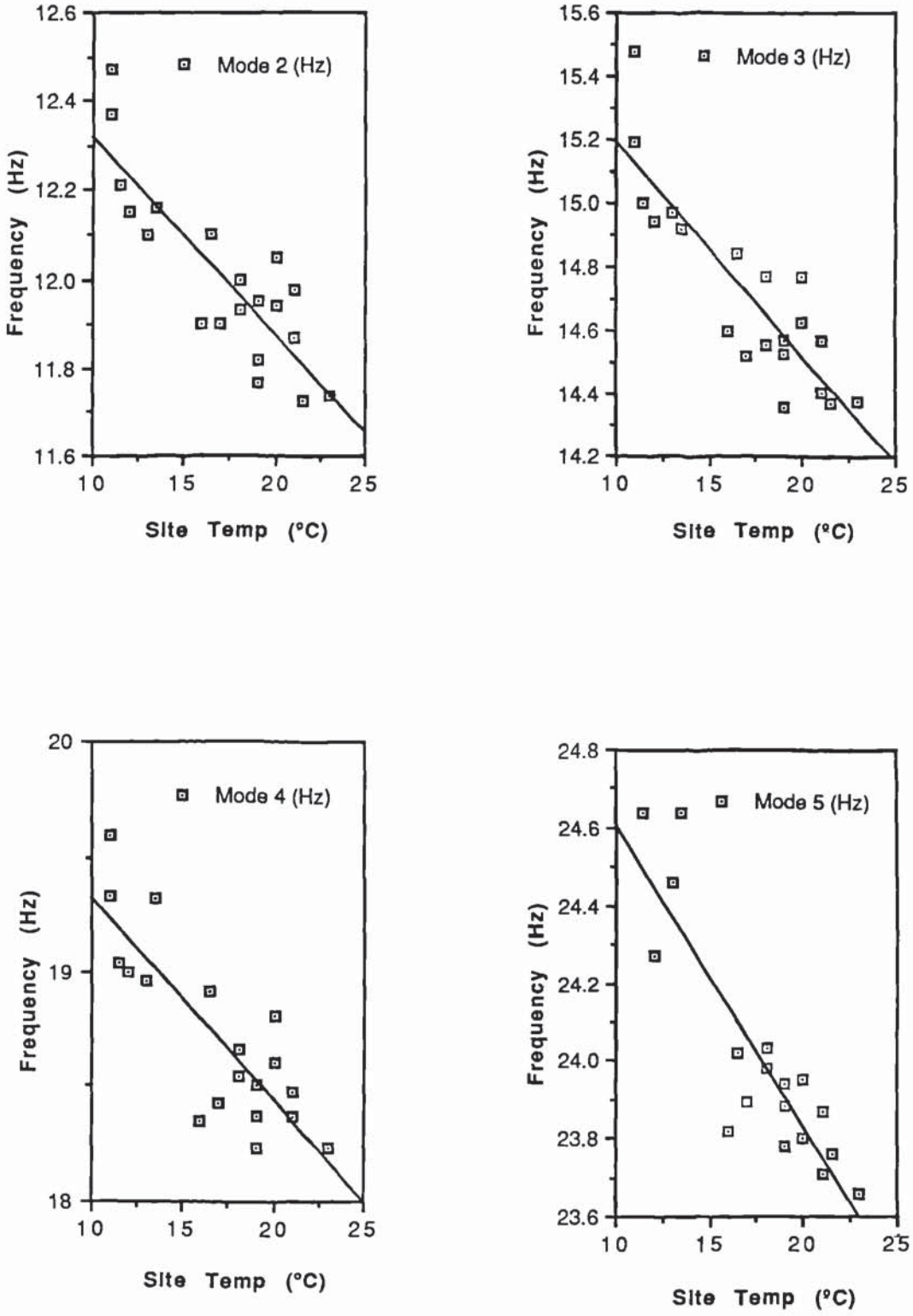

Figure 5.15 Site temperature versus frequency for 4 modes of response from New Haymills Bridge data

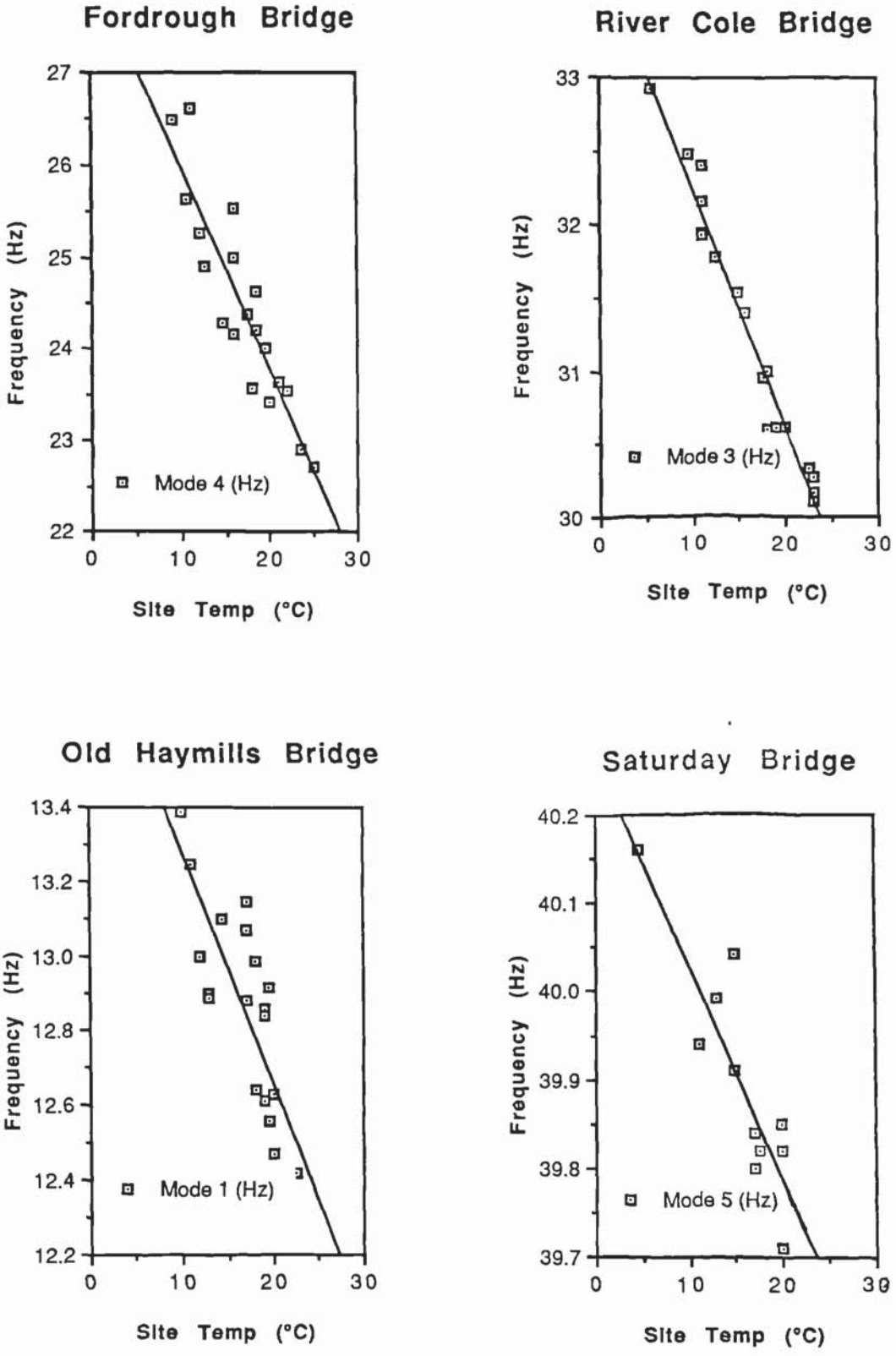

Figure 5.16 Site temperature versus frequency for 1 mode of response from Fordrough, River Cole, Old Haymills and Saturday Bridge data

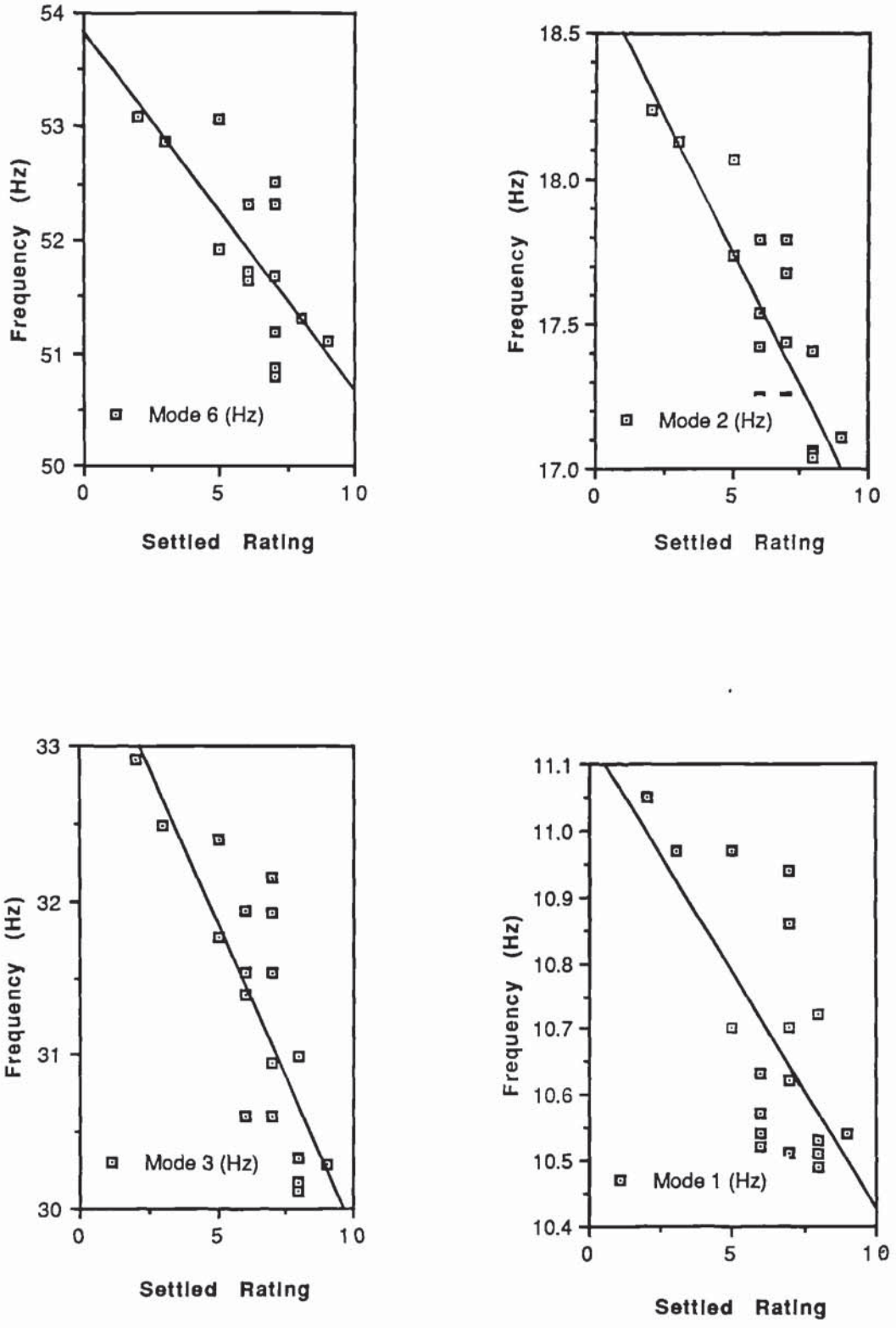

Figure 5.17 Settled rating versus frequency for 4 modes of response from River Cole Bridge data

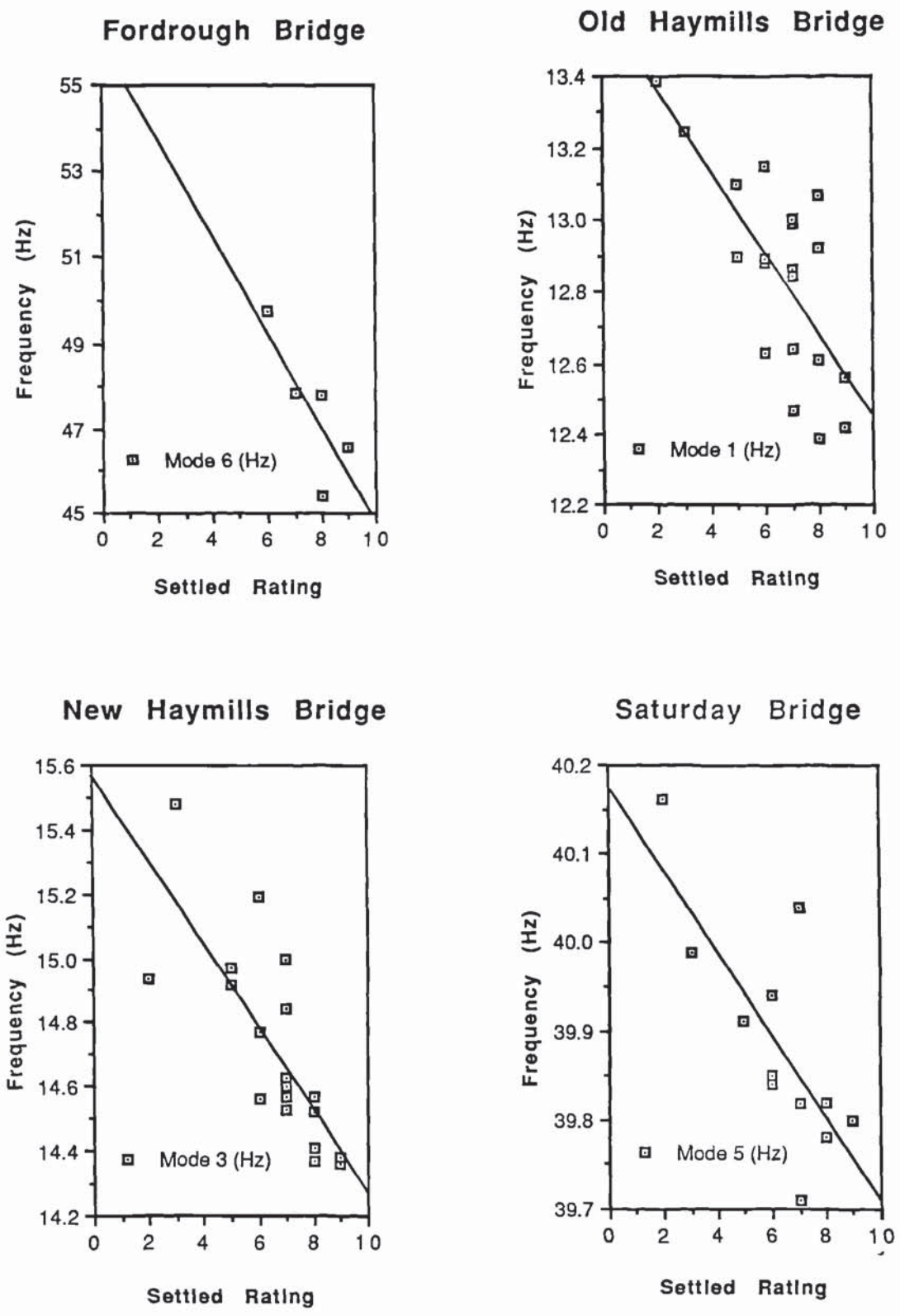

Figure 5.18 Settled rating versus frequency for 1 mode of response from Fordrough, Old Haymills, New Haymills and Saturday Bridge data

The analyses presented above utilised 'psuedo-inertance' data since it was not possible to obtain true inertance data (i.e. $accel_i$ / $impact_j$) during these bridge-monitoring investigations. Inspection of the force spectra from the hammer impacts showed great variations in both magnitude and quality: Figure 5.19(a) shows the time series history of hammer strike which was occasionally observed. The deceleration peak is approximately 300 'g' compared with the more typical 100 'g' of Figure 5.7(a). Apart from the danger of forcing the local response of the structure into non-linearity from the severity of such an impact, it is also possible to damage the bridge at the impact point. The consistency of load spectra transmitted from the hammer impact depends on the construction of the pavement at the impact point. Soft tarmac or particulate-sand supported paving-slabs do not provide the ideal transmission path from the hammer strike to the main structure and a poor impact spectrum may result (Figure 5.19(b)). In order to avoid these problems it would be necessary to impact directly onto a main structural member of the bridge and the only available position would be on the string-courses.

The dangers in using a sledgehammer in the vicinity of an unprotected drop from a bridge parapet are obvious and so a series of tests were undertaken to overcome these problems by using a 'bolt-gun'. This investigation was undertaken in both the laboratory and on-site and has recently been published (Wood *et al*, 1992). Briefly summarising; these guns are light, compact and extensively used in the Civil Engineering field to bond

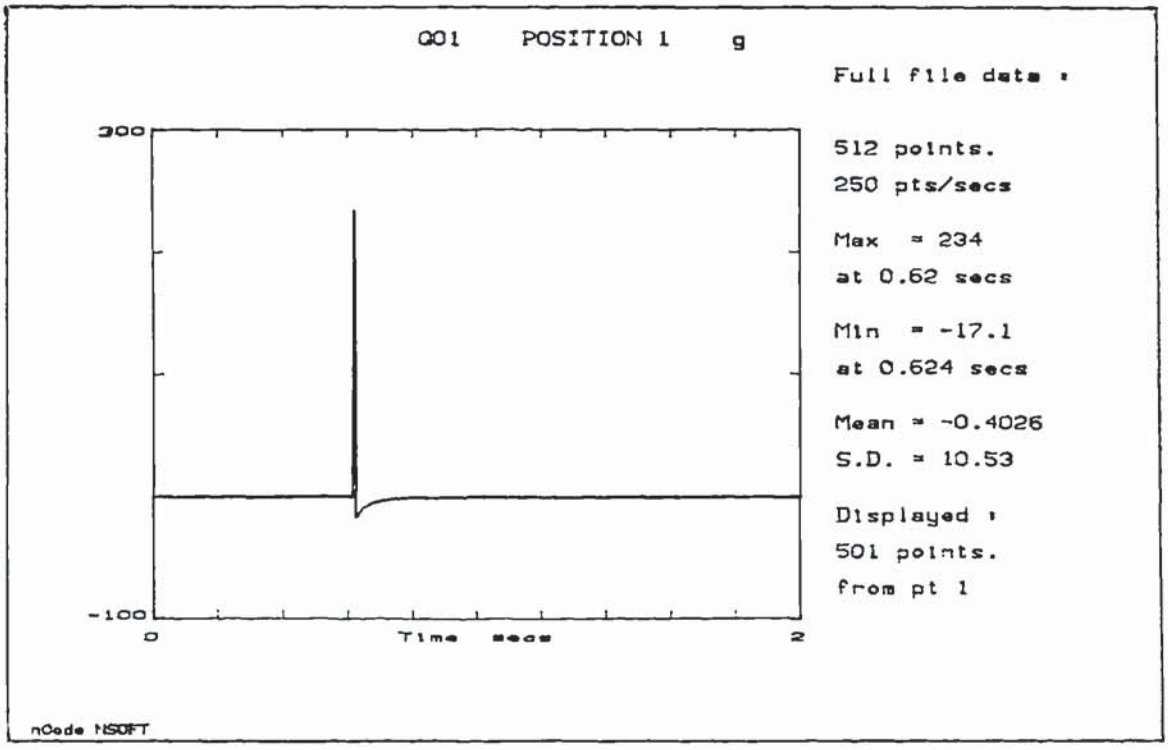

Figure 5.19(a) Atypical sledgehammer impact time-signal

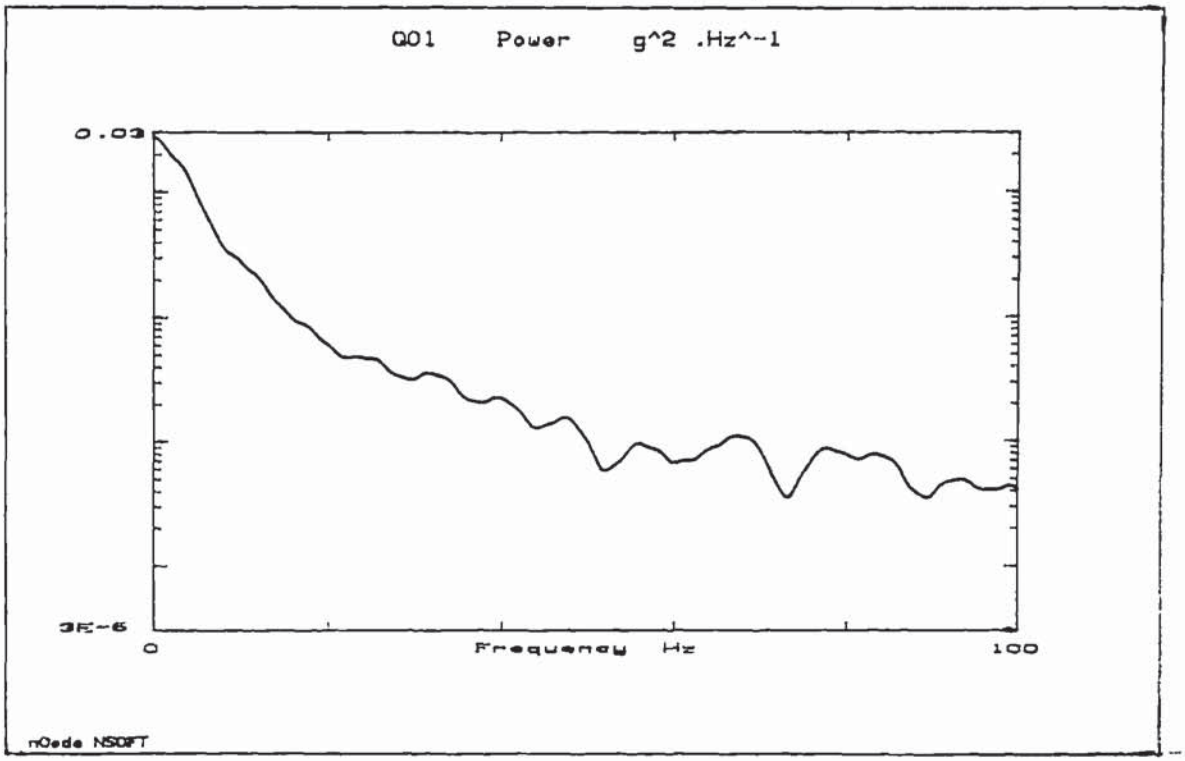

Figure 5.19(b) Poor sledgehammer impact spectrum

steels and concrete. The technique proved most useful in the excitation of these types of large structure if applied in restricted areas. In essence the investigation considered an alternative method of bridge excitation using an explosive cartridge to fire a standard nail from the gun into a small striker-plate. This plate was supported on the structure by a 'frequency filtering' mat of synthetic rubber. The technique was subsequently modified after extensive laboratory testing to use the gun's captive bolt mechanism to impact directly onto the mat without the use of the nail. Further to the on-site investigations, where the bolt-gun and sledgehammer impact spectra were found to be in good agreement, developments were proposed to identify other suitable and more durable filter materials to improve the imparted load bandwidth. It was recommended that the technique be used in conjunction with data averaging techniques in order to minimise signal noise since the site equipment used did not have this facility. Refinement of the firing procedure was proposed to eliminate the impactor 'bounce' resulting from the gun recoil and more powerful models or customised firearms were recommended for more massive structures. The use of the bolt-gun during both the laboratory and site investigations necessitated a number of safety considerations and they are fully detailed in Appendix 1.1.

5.7 Summary

Vibrational response and ambient air condition and temperature measurements were undertaken on several highway bridges of varying construction and geometry at approximately one week intervals. The ambient air conditions experienced by these structures during the testing period included extremes typical to the Birmingham area.

Structural excitation using a sledgehammer-impact was found to be an ideal method for the purposes of this investigation due to its simplicity in application and because it was non-invasive to traffic-flow. Where structure access was restricted, investigations based on an alternative excitation method using a 'bolt-gun' proved successful and developments for the future use of this tool were identified.

Ambient air condition measurements included site air-temperatures and humidities also local air-temperatures, humidities, rainfall, air-pressure and other general meteorological information. Bridge-structure data included soffit, upperdeck and (in one case) black-top temperatures. Comparisons between ambient conditions and bridge-response data showed that the natural frequencies of each of the bridges were dependent upon the mean structural temperature and in all cases the relationships between structural temperature and response frequencies were sensibly linear. It is now necessary to consider the cause of the apparently linear relationships between structural temperature and resultant vibrational responses.

Chapter 6: Experimental Bridge Monitoring Data Analysis

" All nature is but art unknown to thee;
All chance, direction which thou canst not see;
All discord, harmony not understood;
All partial evil, universal good;
And, spite of pride, in erring reason's spite;
One truth is clear, 'Whatever IS, is RIGHT "

Alexander Pope (1688 - 1744)

6.1 Introduction

From the data provided by the bridge-monitoring programme it was apparent that the temperature of each structure influenced the vibrational responses and it was considered necessary to establish which of the structural variables produced these effects. However this required a predictive technique which could be readily applied to structures of this type.

6.2 Dynamic Modelling

The method applied in the dynamic modelling of these bridges had to be a 'discrete' technique due to the complexity of the structures. Two specific methods of computer-based analysis were considered to be compatible with current structural engineering design practice: Finite Element Analysis (FEA) and Grillage Analysis (GA).

FEA is a versatile three-dimensional, continuum approximation extensively used throughout most of the engineering disciplines. It is used in applications ranging from heat- and fluid-flow solutions to static and dynamic structural analyses. In essence this technique uses variational energy methods to simulate discretised structural behaviour and applies algebraic manipulation to solve simultaneous matrix arrays which model the individual element motions. In the case of static structural analyses these motions (or displacement modes) are expressed in the form of stiffness and force products. For dynamic solutions the static case is modified to solve equilibrium equations which also include mass/inertia and acceleration products. Although not required during this work, the damping and (usually) velocity products are also incorporated into the system equation for the analysis of noticeably damped structures. The FEA technique is widely documented in Richards (1977) and Zienkiewicz (1977).

GA is also a discretised structural analysis technique using the same matrix array manipulation procedures of those described above in FEA. However it is a much simplified approach since the structure is immediately limited to two rather than three dimensions of analysis. This technique requires a methodical approach in the creation of any representation of a structure with clear guidelines as to the form that the modelled bridge-deck should take. This results in a faster and, hence, less costly technique to apply to any design under consideration. As a consequence it is probably the most widely used method in the analysis of bridge-deck behaviour and may be regarded as the industry standard. The method has been proved consistently accurate over a wide range of bridge types and configurations with Hambly (1976) presenting probably the most

informative text on its theory and application. The software package used throughout this area of the research was uncomplicated and readily applied to the structures considered.

6.3 Dynamic Analysis

Figure 6.1(a) is the main structural detail of New Haymills bridge and it shows the slab-deck and beam construction arrangement in schematic form. Using this information a representation of the structure can be established using the guidelines previously discussed (West, 1973) and the 'Grillage' idealisation of Figure 6.1(b) is obtained. The structure has been replaced by a mesh (or grid) of beam-elements and it may be seen that ends or intersections of the elements are numbered. These numbered points are termed 'nodes' and additional motion constraints or mass properties may be applied at each position. The constraints were limited in these analyses to hinged-support at the boundaries (i.e. 1, 8 ... 36, 43 and 7, 14 ... 42, 43) as this was felt to be the most representative of the actual behaviour of the structure at these points. Superstructure masses were apportioned to each node point for the inclusion of dead-load in the response analyses. The mesh is regular and symmetrical but it is a relatively crude representation in comparison with typical static analyses of this type since only the lowest response frequencies were of interest. The more elaborate a model was made the greater the computer memory requirement and, hence, more time was required to complete the analysis. This would result in higher modes of vibration being estimated but, overall, not necessarily more accurately for these purposes. Figure 6.1(b) also shows details of how the structure was idealised to establish the torsional properties of the beam mesh and this was achieved by breaking the section down into substructures and evaluating the individual torsional constants (e.g. K_{slab}, K_1, K_2 and K_3). This model and GA representations of the other bridge-structures studied are presented in Appendix 5.

The resultant data were input into the computer after the individual beam element characteristics had been calculated. The computer then created mass and stiffness matrices from the grillage model and, in this form, these data could then be used for a number of different response analyses. Since the bridge structures were to be impact-tested, the natural (free vibration) frequencies were estimated using a subroutine that applied the *Jacobi Method* solution to the resultant generalised Eigenvalue problem:

$$[\boldsymbol{A} - \boldsymbol{B}\,\omega^2]\,\{Y\} = \{0\} \qquad (6.1)$$

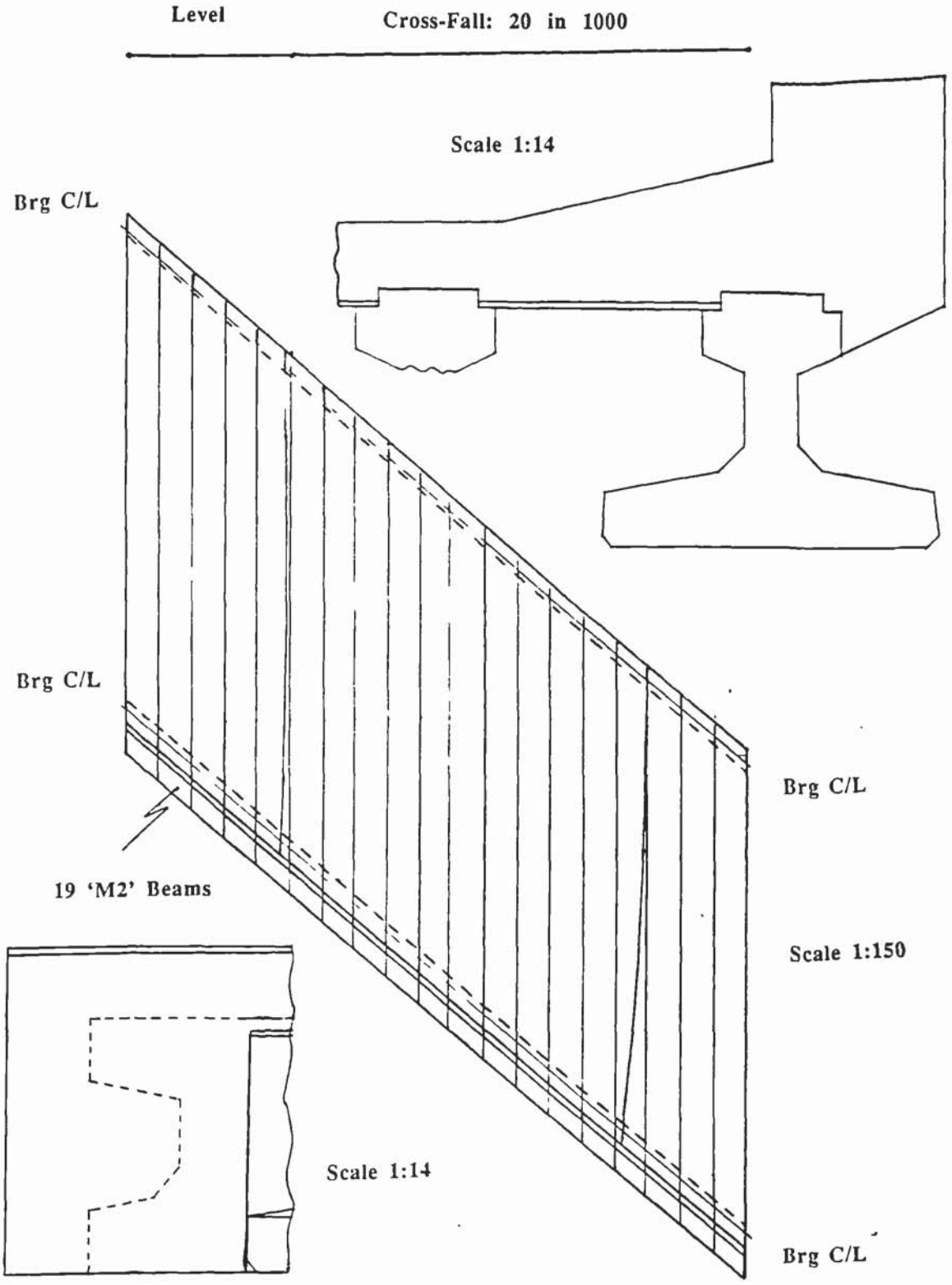

Figure 6.1(a) Structural detail schematic of New Haymills Bridge

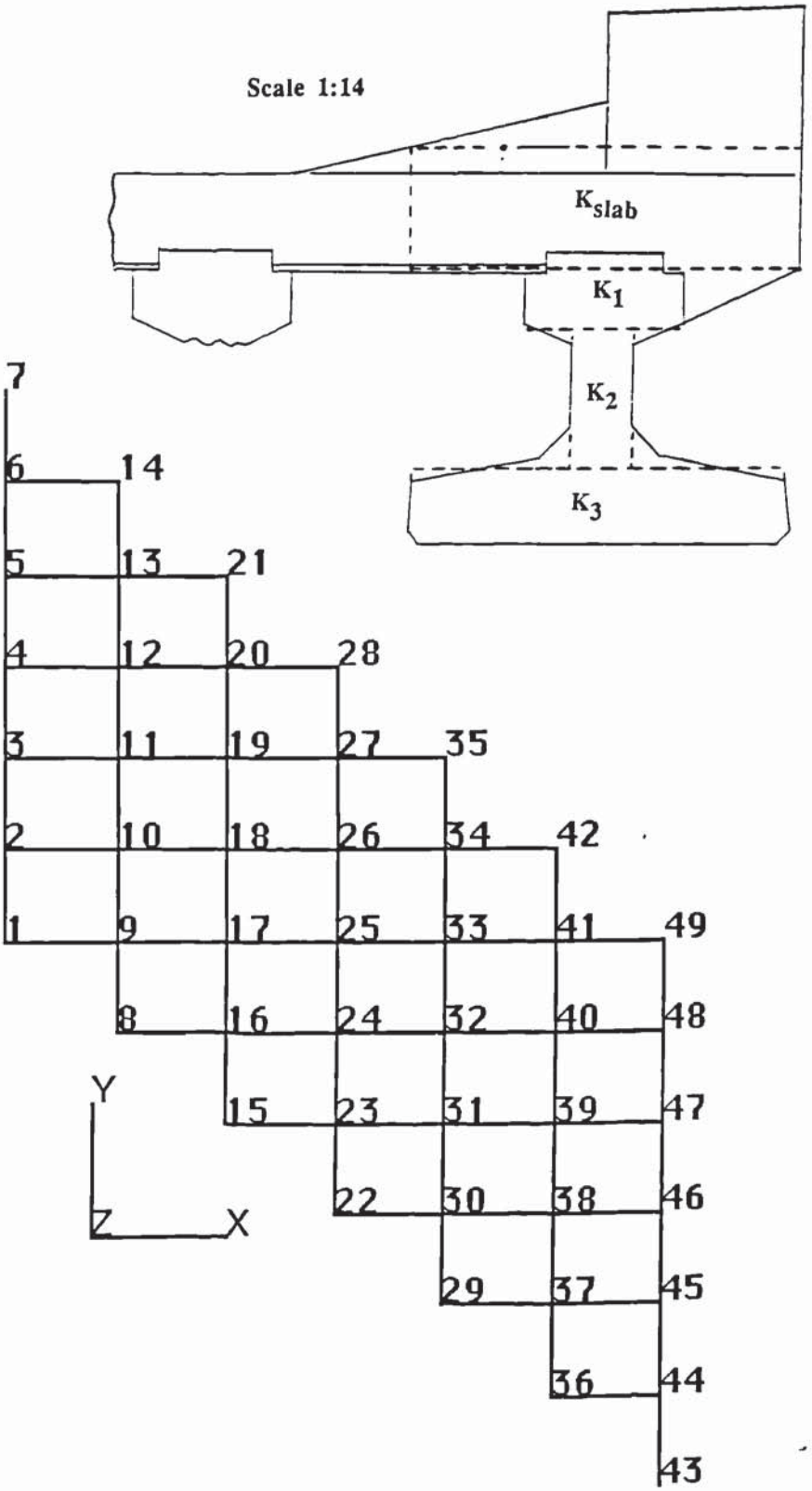

Figure 6.1(b) Grillage analysis idealisation of New Haymills Bridge

From this the system Eigenvalues (i.e. response frequencies) are evaluated in conjunction with their associated Eigenvectors (i.e. mode shapes). The latter may be animated to observe node displacement histories and these may be plotted to show maxima of the structure motion (e.g. Figure 6.2). For the purposes of this work the calculated and observed frequencies were compared to find those in agreement. Those selected which reflected the observed data were further examined to ensure that their associated mode shapes were also representative of the expected behaviour of the structure.

6.4 Vibrational Changes Induced By Structural Temperatures

Any changes in the vibrational response of a bridge structure would be described by the Eigenvalue problem equation (6.1). In this case the matrix $[A]$ corresponds to the stiffness of the structure whilst $[B]$ represents the mass. It is not envisaged that there would be a significant change in mass of each structure due to temperature effects since the bridge-decks are water-proofed and the temperature differentials are relatively small. This then implies that the changes occur in the stiffness of each structure.

The most obvious effect of temperature on a structure is thermal expansion or contraction. The bridge-bearing positions are fixed and so the span of each longitudinal vibrating element is effectively constant regardless of any expansion effects. Overall expansion in the transverse axis is again accommodated at the bearing positions in the same manner. Other transverse effects are present and these will be discussed later but, for the moment, these effects are assumed to be minimal. A temperature differential between the surface and soffit of a deck induces internal-moment at the ends of the structure. The natural frequencies of a beam subject to reactive end-moments are unaffected and the resultant radius of curvature induced would not appreciably affect the second moment of area of the element. If the mass, span and second moment of area of a vibrating beam-element are constant then the remaining variable which can change is the elastic modulus but Maréchal (1972) showed that the static and, hence, dynamic elasticity modulus of concrete is sensibly constant in the range of -25°C to +35°C. These considerations suggest that the main deck structure cannot be the source of these changes in the observed responses and so stiffness differentials must be present in the superstructure.

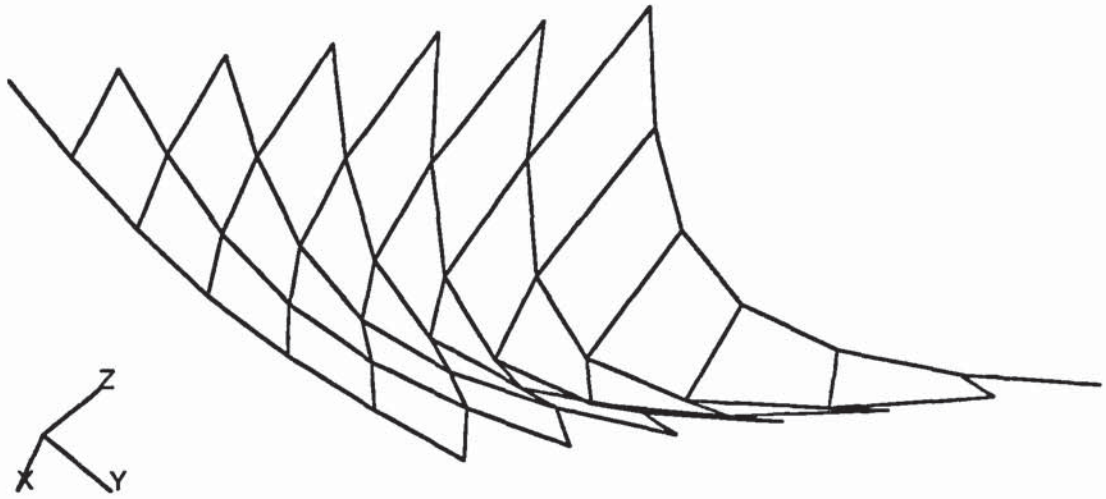

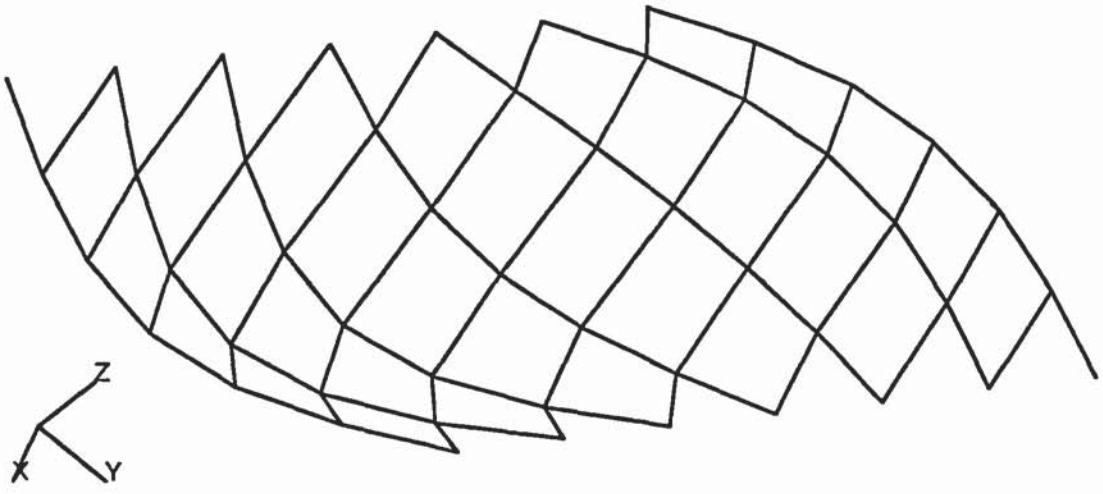

Figure 6.2 Grillage Eigenvector solutions for New Haymills Bridge

If the superstructure of a typical bridge is examined then a major component is the asphalt carriageway and pavement. The effect of temperature on this material is very apparent when considering its behaviour on cold, frosty days compared to hot, mid-summer conditions. Subject to the former temperatures asphalt appears as unyielding as concrete but on very hot days it becomes a visco-plastic fluid and, hence, here is a likely source of relatively large changes in stiffness due to relatively small changes in temperature.

6.5 Temperature-Response Analysis

Pavements and carriageways on bridge-structures will mainly consist of rolled asphalt since the need for subgrades and granular sub-bases is minimised. The performance of these bituminous materials in highly temperature dependent and stiffness is observed to decrease with increasing temperature. Potter (1977) showed that the elastic modulus for asphalt was typically 770 N/mm^2 for a variety of dynamic conditions at an effective temperature of 30°C. If the assumption is made that the pavement and carriageway moduli are similar and equal to 500 N/mm^2 at 30°C, to accommodate compaction differences, then an estimation may be made of the changes in gross material properties using the observed temperature-response trends.

$E_c|_{dyn}$ = 40 kN/mm^2 - sensibly constant between -25°C and +35°C

Modular Ratio, α_s = E_a/E_c = 0·0125 (i.e. ≈ 1%) at 30°C

This modular ratio represents a negligible contribution to the overall strength of the structure and so it is assumed that the asphalt has no effective stiffness at 30°C.

It may be assumed that the pavement/carriageway layers act independently of the main deck since shear transmission is halted at the deck/waterproof interface. Any subsequent change in the stiffness of a typical discretised beam-element due to a temperature differential may then be represented by:

$$\delta(I)_{element} = \delta\alpha_s (I)_{asphalt} \qquad (6.2)$$

where $\delta(I)_{element}$ is the change in element stiffness

$\delta\alpha_s$ is the change in modular ratio due to temperature and

$(I)_{asphalt}$ is the second moment of area of the asphalt (i.e. $Bt^3/12$)

Emerson (1977) showed that the maximum differential between soffit and black-top surfacing was constant and equal to 11°C for all thickness of deck in bridges of the types tested. If all bridges warm from a uniform temperature then a differential of 30°C at the black-top layer would be almost equivalent to a change in soffit temperature of 20°C. Thus all temperature-response analyses were made using data based on a soffit differential equal to 20°C.

6.6 Analysis Results

Figure 6.3 shows the observed frequency response data in relation to the measured soffit temperature for New Haymills bridge. Each mode shows the desired characteristic of decreasing frequency with increasing temperature and it may be observed that a general trend in these relationships is increasing gradient with mode number. Table 6.1 summarises these data:

Obs Mode	$Freq_{0°C}$ (Hz)	$Freq_{20°C}$ (Hz)	$\frac{1}{f}\frac{\partial f}{\partial T_s}$.	Curve-fit Quality (R^2)
1	10·13	9·94	-0·00094	0·738
2	12·82	11·73	-0·00425	0·869
3	15·96	14·29	-0·00523	0·897
4	20·39	18·12	-0·00557	0·917
5	25·62	23·57	-0·00400	0·904

Table 6.1 New Haymills Bridge observed data summary

It can be seen from this summary that the quality of the data is reflected by the high correlation coefficients and that when the frequency differentials are normalised against the datum mode frequency of (say) $Freq_{0°C}$ then there is also broad agreement.

For this bridge-structure a series of grillage analyses were undertaken using increasing values of $\delta\alpha_s$ and Table 6.2 illustrates the results. The mean differential for the 5 observed frequencies in Table 6.1 is -0·00400 and by using a second-order curve-fit through the differential means derived from Table 6.2 a value of $\delta\alpha_s \approx 0{\cdot}16$ was returned: this corresponds to an elastic modulus for the asphalt of 6·4 kN/mm^2 at 0°C.

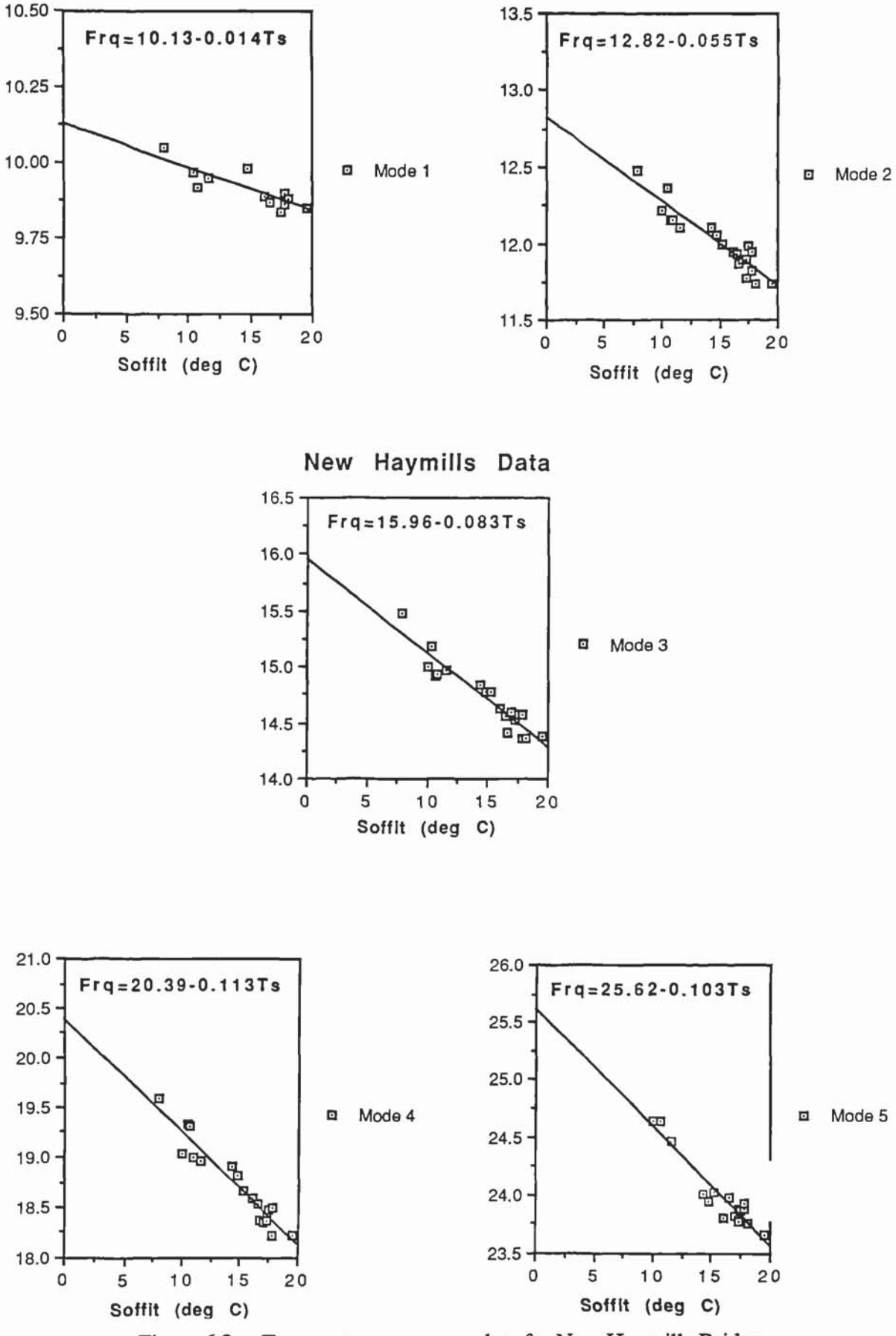

Figure 6.3 Temperature-response plots for New Haymills Bridge

Mode	$\delta\alpha_s$=0·02 $\frac{1}{f}\frac{\partial f}{\partial T_s}$	$\delta\alpha_s$=0·06 $\frac{1}{f}\frac{\partial f}{\partial T_s}$	$\delta\alpha_s$=0·1 $\frac{1}{f}\frac{\partial f}{\partial T_s}$	$\delta\alpha_s$=0·3 $\frac{1}{f}\frac{\partial f}{\partial T_s}$	$\delta\alpha_s$=0·5 $\frac{1}{f}\frac{\partial f}{\partial T_s}$
1	-0·00040	-0·00106	-0·00166	-0·00402	-0·00588
2	-0·00048	-0·00130	-0·00204	-0·00498	-0·00732
3	-0·00073	-0·00196	-0·00301	-0·00704	-0·01027
4	-0·00087	-0·00241	-0·00367	-0·00852	-0·01234
5	-0·00098	-0·00270	-0·00411	-0·00855	-0·01070

Table 6.2 New Haymills Bridge calculated data summary

This procedure was repeated for the observed and calculated data for all the bridge structures with varying degrees of success. Table 6.3 summarises the observed data and Table 6.4 the calculated data for Saturday bridge:

Obs Mode	$Freq_{0°C}$ (Hz)	$Freq_{20°C}$ (Hz)	$\frac{1}{f}\frac{\partial f}{\partial T_s}$	Curve-fit Quality (R^2)
1*	8·79	10·69	+0·01081	0·885
2	21·41	20·00	-0·00329	0·652
3	30·99	29·00	-0·00321	0·915
4	40·21	39·74	-0·00058	0·875
5	82·82	71·62	-0·00676	0·880

Table 6.3 Saturday Bridge observed data summary

The mean differential for the 5 observed frequencies in Table 6.3 is -0·00346, for the moment excluding the asterisked mode 1. Again ignoring mode 1, the second-order curve-fit through the calculated means of Table 6.4 returns a $\delta\alpha_s$ of 0·32 which suggests an error of 100% compared with the value established from the New Haymills data. The results obtained from both Fordrough and River Cole bridges produced even greater margins of error with those data of New Haymills bridge, whilst Old Haymills returned a $\delta\alpha_s$ value several magnitudes greater.

Mode	$\delta\alpha_s$=0·02 $\frac{1}{f}\frac{\partial f}{\partial T_s}$	$\delta\alpha_s$=0·06 $\frac{1}{f}\frac{\partial f}{\partial T_s}$	$\delta\alpha_s$=0·1 $\frac{1}{f}\frac{\partial f}{\partial T_s}$	$\delta\alpha_s$=0·3 $\frac{1}{f}\frac{\partial f}{\partial T_s}$	$\delta\alpha_s$=0·5 $\frac{1}{f}\frac{\partial f}{\partial T_s}$
1*	-0·00226	-0·00908	-0·01545	-0·03460	-0·04574
2	-0·00007	-0·00022	-0·00042	-0·00281	-0·00820
3	-0·00012	-0·00036	-0·00063	-0·00276	-0·00660
4	-0·00036	-0·00108	-0·00179	-0·00519	-0·00839
5	-0·00086	-0·00027	-0·00044	-0·00130	-0·00212

Table 6.4 Saturday Bridge calculated data summary

6.7 Discussion

The anomalies in the calculated values of the asphalt modulus at 0°C from the great majority of the bridge data are confusing at first sight. However mode 1 of the Saturday bridge data gives insight as to the probable cause. Figure 6.4 presents another example from the Old Haymills observed data showing that this effect is not limited to Saturday bridge alone.

It is apparent that in some cases there is an increase in stiffness due to some temperature effect which is minimal or not present in the New Haymills case. In calculating the grillage properties of New Haymills bridge it was relatively simple to model the transverse stiffness since the deck is essentially a plate in this axis with no interference from the main longitudinal beams. However each of the other structures had to be treated as cracked or transformed sections due to their composite constructions of one form or another. As stated earlier, thermal expansion will take place and in the transverse plane these transformed sections will tend to close cracks, thus, increasing the effective second moment of area in this axis. The longitudinal axis will be unaffected in this way as will the thin transverse section of New Haymills since they are uncracked. The nett effect is that whilst the softening of the asphalt tends to reduce the natural frequencies of these structures the stiffening of the transverse sections may more than compensate in some mode cases.

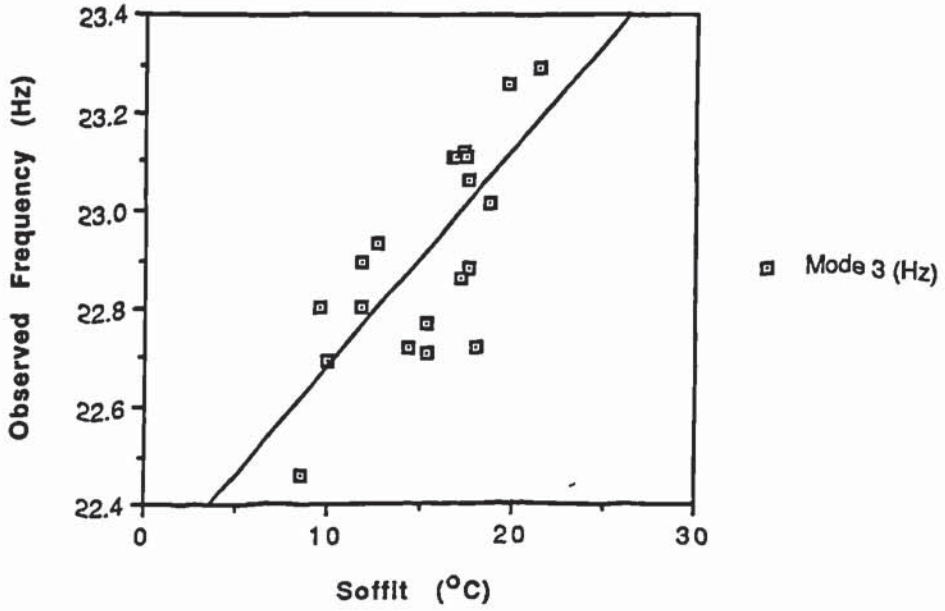

Figure 6.4 Positive response-temperature differential from Old Haymills data

Any transverse stiffening would be better indicated by soffit temperature data, however, the black-top data obtained from Fordrough bridge did show good correlation overall with the structural responses (i.e. mean $R^2 = 0{\cdot}708$). It may be that thermocouples buried in the asphalt would have reproduced better correlations since the exposed, surface contact measurements were probably overly sensitive to cloud/wind/sun conditions and hence did not truly reflect the temperature of this layer.

The exceptional errors arising from the data of Old Haymills may have a more basic cause. The design details available for this structure were at best a rough guide and at worst incorrect. The geometry of this bridge had to be surveyed on site due to the lack of information and internal details which could not be corroborated had to be taken on trust from very old drawings or simply guessed. It is unlikely then that the grillage analyses were truly representative of this structure and in addition the temperature dependent modes calculated were based on estimated pavement and carriageway thicknesses.

As a final consideration from these bridge data, during the curve-fit analyses an observed mode would on occasion show no correlation between any of the variables cited. Figure 6.5 shows observed mode 6 in relation to the mean soffit temperature for New Haymills bridge. The scatter of these data indicates that this variable has no influence on the response of the structure. However it has already been shown that the soffit temperature is pivotal when considering any structural responses. The grillage analysis undertaken on this structure indicated that modes of vibration were likely to occur at 33·2 Hz, 33·7 Hz and 35·2 Hz and, hence, it is probable that the observed mode 6 is a composite. From these data it would not be possible to identify any individual correlation and it is recommended that several distinct modes of vibration are monitored simultaneously in order to combat this problem.

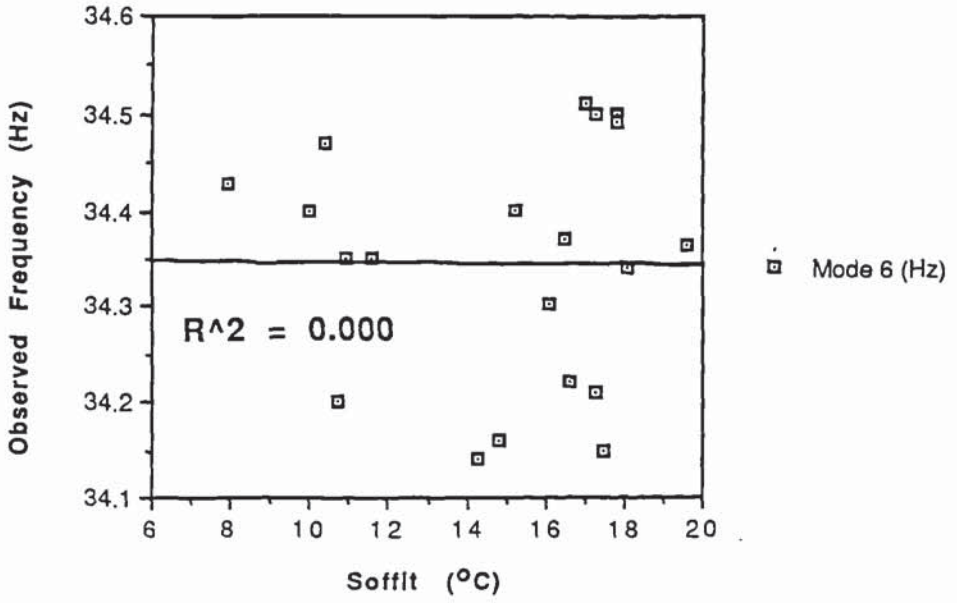

Figure 6.5 Zero correlation between observed mode frequency and soffit temperature

6.8 Summary

Analysis of the bridge monitoring data suggested that changes in the asphalt elastic modulus due to temperature effects was a major contributor to changes in the structural responses. It was estimated that the change in the elastic modulus of asphalt was approximately 6·4 kN/mm^2 for a temperature change of -30°C in the asphalt and this was equivalent to a -20°C differential in the soffit temperature.

It was also observed that increases in some mode frequencies could occur with an increase in structural temperature and this was most probably due to the transformed sections in the transverse direction closing cracks under the action of thermal expansion. The dynamic application of Grillage Analysis has been shown to be a useful tool in estimating the vibrational response characteristics of these bridge structures. All the research presented here is now summarised in the following Chapter.

Chapter 7: Concluding Discussion

" There is no more common error than to assume that, because prolonged and accurate mathematical calculations have been made, the application of the result to some fact of nature is absolutely certain "

Alfred North Whitehead (1861-1947)

7.1 Introduction

Available literature suggests that there is much active research in the fields of structural behaviour and assessment of bridge-structures. However several topics within these areas had not been successfully approached and this work was undertaken as a result. The research effort aimed at damage effects in vibrating, concrete bridge-members has been extensive but the basis for a clear and concise relationship between response and applied load for the standard case had yet to be established. In addition several groups had discussed the possible effects of ambient temperature conditions on the response frequencies of bridge-structures but they had been unable to collect usable data to support their predictions. These are the two primary areas addressed by this research and conclusions are now drawn based on the work presented here. Omissions in these investigations and future research deemed necessary to forward this area are subsequently discussed as further work.

7.2 Conclusions

i) The data obtained during the first experimental phase suggested that, for the two series of modelled bridge-beams tested, the structural damage which resulted from the applied loading-regime was not related to the position of initial, induced weakening but was more representative of a general lowering of strength over the entire specimen length.

ii) The beam test arrangement used to extract the frequencies of vibration was insufficiently isolated in order to obtain the true modes for all the observed data. However of the two modes adjudged representative of simply-supported conditions, the resultant data suggested that the changes in frequency response were identifiable as part of a family of curves whose characteristics were dictated by the prestress levels present. It was possible to recognise changes in the observed frequencies at applied load levels below half that of the failure condition for both the prestressed and ordinary reinforced designs.

iii) Using these results measures of applied loads and changes in stiffness were derived as dimensionless ratios. These ratios were used to propose a power-law relating changes in the flexural rigidity to the applied load and the levels of beam prestress present.

iv) The development of a qualitative method was made to establish the level of damage present in any beam. This method was based on the difference in measured inertance between two reciprocal positions and normalising this result against their mean values. A working model was then produced in support of this experimental technique.

v) Data obtained during the monitoring of several bridges of varying construction and geometry were used to establish which variables best indicate the vibrational response of bridge-decks under ambient conditions. For these bridges the fundamental and closely associated frequencies were shown to be sensibly linear in their relationship with the mean soffit temperature. Both site air temperature and recent weather conditions also provided a measure of the changes in vibrational response of any of the structures.

vi) Analysis of these bridge data suggested that the temperature of the asphalt black-top layer was the major cause of changes in the structural responses since its elastic modulus is highly temperature sensitive. Additional thermal expansion effects modified these changes in vibrational response since the transverse stiffness of composite constructions would increase with temperature due to cracked sections closing.

vii) It was found that for the purposes of this investigation sledgehammer impacts provided a simple method of imparting sufficient energy to excite the required number of frequencies in a controlled and repeatable manner. This method minimised interference to normal traffic flow also the need for equipment and operator manpower. In special cases where access was limited it was found that cartridge 'bolt-guns' sufficiently excited structures of this type.

viii) The monitoring procedure utilised provides a good basis upon which to develop the proposed damage-detection technique. The simplicity in response data acquisition allied with a minimum of logistics and on-site technical support provide the ideal for such a technique. However, interpretation of these resultant data requires the input of a suitably qualified engineer (at least) at a supervisory level.

7.3 Further Work

This research is aimed at supporting the development of a damage-diagnostic technique for bridge-structures. Some success has been achieved towards this goal by the development of a method which relates load damage to the changes in frequency responses of bridge-beams and a qualitative method to assess the damage level present within these constructions has been proposed. The basic relationship between the vibration responses of bridge-decks and ambient temperature conditions for a variety of constructions and planforms has been established thus providing data on how damage may be disguised by these effects. In addition the main structural causes of these response changes have also been identified. However a number of other considerations have been identified as a result of this and discussion now centres on what should be undertaken in order that progress may continue towards the eventual goal of this field of research.

i) The data presented here concerning the resultant beam responses will be further analysed and the 'simply-supported' mode frequencies will be extracted using accepted system identification techniques (e.g. Park and Blevin, 1990). This will provide additional data which should increase confidence in the conclusions already stated. It may also provide the basis of more detailed investigation of responses due to local regions and levels of damage.

ii) Testing should continue with the present beam configurations incorporating progressively higher levels of prestress until the design recommendation levels are achieved. The family of frequency damage-response curves would then be established for these section designs and reinforcement configurations, thus validating (or not) the proposed power-law relationship between flexural rigidity, applied load and prestress. These tests should also be broadened to include eccentric prestress conditions using differential loadings in the present configuration and these investigations may be supported by similar investigations using modelled 'M' or 'T' type bridge-beam configurations, hence, creating a behavioural database.

iii) The data upon which the N.N.M. analysis was based were not ideal. This approach was devised retrospectively and so the measurement of the beam responses was not made at the optimum resolutions. These measurements should be repeated using the utmost care to ensure that accurate data are available for technique validation and non-reciprocity modelling purposes.

iv) In preparation of these additional beam tests consideration should be given in devising a more 'isolated' test arrangement in order to avoid the parasitic support-effects in the resultant frequency and mode shape data. However this may prove to be too difficult in practice since these effects were previously considered and no immediate solution was identified.

v) Bridge tests should continue and further development of simple and repeatable excitation methods should be encouraged using similar impact techniques or by devising customised or custom-built apparatus based on fire-arms.

vi) The monitoring programme of bridges should be extended to include structures of high aspect ratio, steel and wood compositions to establish whether these designs and constructions also reproduce similar response frequency relationships with the ambient air conditions.

vii) Physical bridge-modelling should be attempted in order to provide the laboratory results necessary to support the damage location techniques. Where possible, consultations with the Department of Transport should be made in order to locate any bridges designated for future demolition so that controlled damage tests can be undertaken *in situ*..

viii) A series of investigations are required in the development of the most appropriate bridge-structure modelling procedure that reproduces those temperature effects observed experimentally. If this can be achieved satisfactorily then confidence may be given to inclusion of temperature effects in the proposed damage analysis techniques.

ix) More accurate modelling could be achieved by the careful application of model-updating techniques (Brandon, 1990). However care would have to be taken in reconciling the problems in accurately updating torsional-inertia coefficients within the model matrices with those behaviours observed in practice.

x) Problems will arise in the choice to update any model using either the lower or higher modes of vibration. Lower modes of vibration are readily excited and observed but higher modes of vibration can be modelled without the associated complexities of prestress effects in the construction members. The development of a finite-element incorporating frequency-dependent characteristics that would avoid this problem of prestress effects is unlikely since this would require

additional iterative operations to the already intensive processing workload of any model analysis. With the development of faster computers this additional facility could be a long-term goal. It must be noted however that static analysis facilities already include a reinforced element for structural strength purposes.

xi) More sophisticated models will be required to incorporate shear and torsional-inertia effects in bridge-elements with span to depth ratios of less than 15. This will assist in establishing more accurate relationships between the resultant frequency-response changes and the corresponding applied load states.

xii) Predictive analysis techniques should be applied to the Normalised Nett Magnitude (NNM) approach for damage level assessment so as to provide sound theoretical support to this qualitative method.

xiii) The quality of any damage location technique based on vibration responses is dependent on accurate structural modelling and constituent component degradation relationships. Therefore combining all of the above the methodology pioneered by Cawley and Adams (1979) may be applied using the superior statistical technique of Al-Tamimi and Wilson (Al-Tamimi, 1985) and an effective computer-based diagnostic tool should result.

7.4 Summary

This and previous work in this field has shown the potential for a practical damage location technique applied to bridge-stuctures and the momentum of this research must be maintained if the benefits of the final product are to be realised.

References :

ACI (1983); "Building Code Requirements for Reinforced Concrete (ACI 318-83)"; American Concrete Institute, Detroit, U.S.A.

AGARDH, L. (1991); "Modal Analyses of Two Concrete Bridges in Sweden"; *Structural Engineering International* (Science and Technology); April, pp 35 - 39.

AL-TAMIMI, A.N.J. (1985); "Damage Location in Structures by Monitoring Vibration Characteristics"; Ph.D. Thesis, University of Aston in Birmingham; February.

BALENDRA, T. and SHANMUGAM, N.E. (1985); "Free Vibration of Plated Structures by Grillage Method"; *Journal of Sound and Vibration*, Vol 99, 3, pp 333-350.

BISWAS, M.; PANDEY, A.K. and SAMMAN, M.M. (1990); "Diagnostic Experimental Spectral/Modal Analysis of a Highway Bridge"; *The International Journal of Analytical and Experimental Modal Analysis*, Vol.5, 1; January, pp 33 - 42.

BROWNJOHN, J.M.W.; DUMANOGLU, A.A.; SEVERN, R.T. and BLAKEBOROUGH, A. (1989); "Ambient Vibration Survey of the Bosporus Suspension Bridge"; *Earthquake Engineering and Structural Dynamics*, Vol.18, pp 263 - 283.

BS 970: Part 1: 1983; "General Inspection and Testing and Specification Requirements for Carbon, Carbon Manganese, Alloy and Stainless Steels"; British Standards Institution, Milton Keynes, U.K.

BS 1881: Part 111: 1983; "Method of Normal Curing of Test Specimens (20°C method)"; British Standards Institution, Milton Keynes, U.K.

BS 1881: Part 116: 1983; "Method for Determination of Compressive Strength of Concrete Cubes"; British Standards Institution, Milton Keynes, U.K.

BS 4449: 1988; "Specification for Hot Rolled Steel Bars for the Reinforcement of Concrete"; British Standards Institution, Milton Keynes, U.K.

BS 4486: 1980; "Specification for Hot Rolled and Hot Rolled and Processed High Tensile Alloy Steel Bars for the Prestressing of Concrete"; British Standards Institution, Milton Keynes, U.K.

BS 5400: Part 2: 1978; "Specification for Loads"; British Standards Institution, Milton Keynes, U.K.

BS 5400: Part 4: 1978; "Code of Practice for Design of Concrete Bridges"; British Standards Institution, Milton Keynes, U.K. (Superseded 1984).

BS 8007: 1987; "Code of Practice for Design of Concrete Structures for Retaining Aqueous Liquids"; British Standards Institution, Milton Keynes, U.K. (Supersedes BS 5337).

BS 8110: Part 1: 1985; "Code of Practice for Design and Construction"; British Standards Institution, Milton Keynes, U.K.

BS 8110: Part 2: 1985; "Code of Practice for Special Circumstances"; British Standards Institution, Milton Keynes, U.K.

CAMPBELL, T.I.; CSAGOLY, P.F. and AGARWAL, A.C. (1977); "Frequency Matching in Continuous Post-Tensioned Concrete Highway Bridges"; Symposium on Vibrations of Concrete Structures, ACI Publication SP-60; New Orleans, U.S.A.; 20th October, pp 139 - 154.

CAWLEY, P. and ADAMS, R.D. (1979); "The Location of Defects in Structures from Measurements of Natural Frequencies"; *Journal of Strain Analysis*, Vol. 14, 2, pp 49 -57.

CLARK, L.A. (1983); "Concrete Bridge Design to BS 5400"; Construction Press, London, U.K.

CRAIG, R.R. (1981); "Structural Dynamics: an Introduction to Computer Methods"; John Wiley & Sons, Chichester, U.K.

ELLINGTON, J.P. and McCALLION (1959); "The Free Vibration of Grillages"; *ASME Journal of Applied Mechanics*; December, pp 603 - 607.

EMERSON, M. (1977); "Temperature Differences in Bridges: Basis of Design Requirements"; TRRL Laboratory Report 765, Crowthorne, U.K.

EWINS, D.J. (1984); "Modal Testing: Theory and Practice"; Research Studies Press, Taunton, U.K.

EYRE, R. (1976); "Dynamic Tests on the Cleddau Bridge at Milford Haven"; TRRL Supplementary Report 200 UC, Crowthorne, U.K.

EYRE, R. and SMITH, I.J. (1977); "Wind and Traffic Induced Dynamic Behaviour of Some Steel Box Girder Bridges"; Symposium on Dynamic Behaviour of Bridges, 19th May; TRRL Supplementary Report 275, Crowthorne, U.K.

GANGARAO, H.V.S. and CHENG, FU-SHAN (1973);"Free Vibration Characteristics of Grillages"; Proceedings of The Institution of Civil Engineers, Vol. 55, 2; June, pp463 - 477.

HALL, B.O., BERRISFORD, S.J. and THOMAS, A.M. (1978); "Geometric Imperfections in In-Situ Concrete Highway Bridges"; TRRL Laboratory Report 852, Crowthorne, U.K.

HARA, T. and KAWAMURA, A. (1990); "Impulse Test Method [Applied] to the Vibration Measurement of Bridge[s]"; Proceedings of the 15th International Seminar on Modal Analysis: Part III; Katholieke Universiteit Leuven, Belgium; 19th - 21st September, pp 1 - 12.

HOP, T. (1991); "The Effect of Degree of Prestressing and Age of Concrete Beams on Frequency and Damping of their Free Vibration"; *RILEM Materials and Structures*, 24, pp 210-220.

IStructE (1988); "Assessment of Reinforced and Prestressed Concrete Bridges"; Papers presented at a seminar organised by The Institution of Structural Engineers, London, U.K.; 28th September 1988.

JAMES, M.L.; LUTES, L.D. and SMITH, G.M. (1964); "Dynamic Properties of Reinforced and Prestressed Concrete Structural Components"; *Journal of the American Concrete Institute*, Title No. 61-68; November, pp 1359 - 1381.

JERATH, S. and SHIBANI, M.M. (1985); "Dynamic Stiffness and Vibration of Reinforced Concrete Beams"; *Journal of the American Concrete Institute*, Title No. 82 - 18; March - April, pp 196 - 202.

JOHNS, K.C. and BELANGER, M.D. (1981); "Dynamic Stiffness of Concrete Beams"; *Journal of the American Concrete Institute*, Title No. 78 - 18; May - June, pp201 - 205.

KATO, M. and SHIMADA, S. (1986); "Vibration of [a] PC Bridge During Failure Process"; *ASCE Journal of Structural Engineering*, Vol.112, 7; July, pp 1692 - 1703.

LEONARD, D.R. (1974); "Dynamic Tests on Highway Bridges: Test Procedures and Equipment"; TRRL Laboratory Report 654, Crowthorne, U.K.

LINFIELD, G.R. and PENNY, J.E.T. (1989); "Microcomputers in Numerical Analysis"; Ellis Horwood, Chichester, U.K.

LOO, Y-C. and SANTOS, A.P. (1986); "Impact Deflection Analysis of Concrete Beams"; *ASCE Journal of Structural Engineering*, Vol. 112, 6; June, pp 1297 - 1312.

MARECHAL, J.C. (1972); "Variations in the Modulus of Elasticity and Poisson's Ratio with Temperature"; International seminar on Concrete for Nuclear Reactors, ACI Special Publication, Vol.1, 34; pp 495 - 503.

MARTIN, L.H.; CROXTON, P.C.L. and PURKISS, J.A. (1989); "Concrete Design to BS 8110"; Edward Arnold, London, U.K.

MAZUREK, D.F. and DeWOLF, J.T. (1990); "Experimental Study of [a] Bridge Monitoring Technique"; *ASCE Journal of Structural Engineering*, Vol. 116, 9, September, pp 2532 - 2549.

MEIROVITCH, L. (1986); "Elements of Vibration Analysis"; McGraw-Hill, London, U.K.

NEVILLE, A.M. (1981); "Properties of Concrete"; Longman Scientific and Technical, Harlow, U.K. (3rd Edn.).

PARK, K.C. and BLEVIN, W.K. (1990); "An Inverse Decomposition Technique for Dynamic Joint Characterisation"; Proceedings of the 1990 USAF/NASA Conference on System Identification and Health Monitoring, Pasadena, California, U.S.A.; 27th - 29th March, pp 223 - 243.

PENNY, J.E.T. and CLARK, A.R. (1982); "Measuring the Frequency Response of Mechanical Structures"; Transducer TEMPCON Conference, Wembley Conference Centre, London, U.K.; 29th June - 1st July.

PENZIEN, J. (1964); "Damping Characteristics of Prestressed Concrete"; *Journal of the American Concrete Institute*, Vol. 61, 9 , pp 1125-1148.

POTTER, J.F. (1977); "Deformation of Road Pavements: Correlation Between Elastic Theory and Measured Behaviour of Rolled-Asphalt Road-Bases"; TRRL Laboratory Report 784, Crowthorne, U.K.

SLOAN, T.D.; KIRKPATRICK, J.; BOYD, J.W. and THOMPSON, A. (1992); "Monitoring the Inservice Behaviour of the Foyle Bridge"; *The Structural Engineer*, Vol.70, 7; April, pp 130 -134.

SML (1981); "Investigation of Vibration Methods for Monitoring the Integrity of Bridges: Stage 1 Report"; Structural Monitoring Ltd., Glasgow, U.K; Report No. 205, September.

SML (1982); "Investigation of Vibration Methods for Monitoring the Integrity of Bridges: Stage 2 Report"; Structural Monitoring Ltd., Glasgow, U.K; Report No. 283, December.

STANGER (1990); "Trial Monitoring of the ..... Bridge: Confidential Customer Report"; Harry Stanger Ltd., The Laboratories, Elstree, UK.; 10th May, 13 pages.

THOMSON, W.T. (1988); "Theory of Vibrations With Applications"; Unwin Hyman, London, U.K. (3rd Edn).

TILLEY, G.P. and PAGE, J. (1980); "A Review of Traffic Loads and Stresses in Steel Bridges"; TRRL Supplementary Report 596, Crowthorne, U.K.

TURNER, J.D. (1984); "An Experimental and Theoretical Study of Dynamic Methods of Bridge Conditioning Monitoring"; Ph.D. Thesis, University of Reading, U.K.; February.

TURNER, J.D. and PRETLOVE, A.J. (1983); "The Effect of Damage to Prestressed Rods on the Natural Frequencies of a Prestressed Concrete Girder"; University of Reading, Unsourced Publication.

TURNER, J.D. and PRETLOVE, A.J. (1988); "A Study of the Spectrum of Traffic-Induced Bridge Vibration"; *Journal of Sound and Vibration*, Vol. 122, 1, pp 31-42.

VELETSOS, A.S. and HUANG, T. (1970); "Analysis of Dynamic Response of Highway Bridges"; *ASCE Journal of Engineering Mechanics*, Vol. 96, 5, October, pp593 - 620.

VIC'ROADS (1990); "Load Capacity of In-Service Bridges: Stage 1, Literature Search"; ETRS Pty Ltd., Consultative Report Compiled by B.P.Baxter; Vic'Roads, Kew, Victoria; May.

WAH, T. (1963); "Natural Frequencies of Uniform Grillages"; *ASME Journal of Applied Mechanics*; December, pp 571 - 578.

WARD, H.S. (1984); "Traffic Generated Vibrations and Bridge Integrity"; *ASCE Journal of Structural Engineering*, Vol. 110, 10, October, pp 2487 - 2498.

WEST, R. (1973); "C&CA/CIRA Recommendations on the Use of Grillage Analysis for Slab and Pseudo-slab Bridge Decks"; Cement and Concrete Association/Construction Industry Research and Information Association Publication, Report No. 46·017.

WOOD M.G., BAILEY M., FRISWELL M.I., PENNY J.E.T. and PURKISS J.A. (1991); "Damage Location in Reinforced Concrete Beams Using Vibration Response"; Proceedings of IMAC ***IX*** Conference, Florence, Italy; February 15th - 18th, pp 139 - 144.

WOOD M.G., FRISWELL M.I. and PENNY J.E.T. (1992); "Exciting Large Structures Using a 'Bolt-Gun'"; Proceedings of IMAC ***X*** Conference, San Diego, U.S.A; February 3rd - 7th, pp 233 - 238.

WOODWARD, R.J. (1981); "Conditions Within Ducts in Post-Tensioned Prestressed Concrete Bridges"; TRRL Laboratory Report 980, Crowthorne, U.K.

Bibliography :

BRANDON, J.A. (1990); "Strategies for Structural Dynamic Modification"; Research Studies Press, Taunton, U.K.

COCHRAN, A.J. (1981); "Vocational PhDs: Aston's IHD Scheme"; The University of Aston in Birmingham, U.K.; May.

GORDON, J.E. (1978); "Structures: Or Why Things Don't Fall Down"; Penguin Books, Harmondsworth, U.K.

HAMBLY, E.C. (1976); " Bridge Deck Behaviour "; Chapman & Hall, London, U.K.

NEVILLE, A.M. and KENNEDY (1964); "Basic Statistical Methods for Engineers and Scientists"; Intertext Books, London, U.K.

RICHARDS, T.H. (1977); "Energy Methods in Stress Analysis", Ellis-Horwood, Chichester, U.K.

ZEINKIEWICZ, O.C. (1977); "The Finite Element Method"; McGraw-Hill, London, U.K.

Appendices :

Appendix 1: Procedural Safety Aspects

A number of potentially hazardous tasks were required to be undertaken during the course of this research. It was important that the potential dangers to researchers and their technical support staff were recognised and acted upon. Those dangers identified and both the legal and medical ramifications are now briefly discussed.

A1.1 Laboratory Equipment And Tools Utilised

During the two phases of laboratory work undertaken both the equipment used and procedural logistics necessary highlighted a number of potentially hazardous operations. Bolt-gun testing was located within the confines of the Department of Mechanical and Electrical Engineering laboratory. These pseudo-firearms have the capability of inflicting serious injury through incorrect usage and, at all times, safety of the operator and additional personnel had to be observed. Before hire of the gun was possible tuition and accredited certification of competency was necessary. This training ensured that problems in, or arising from, operation should not arise: subsequent modification of the tool's usage was confirmed as safe beforehand by the technical department of the manufacturer.

The scale of construction applied in the bridge-beam experiments within the Department of Civil Engineering laboratories resulted in commercial cement vehicles being manoeuvred amongst many technical support staff. In addition the resultant beam masses required the simultaneous operation of two forklift-trucks, with one person in close attendance as a means of guidance during positioning. During the operation of casting, however industrious and distracting the environment was, all personnel involved were strenuously advised on safe practices and warned to be aware of the dangers of fellow workers around them at all times. Instruction in the use of each forklift-truck for beam transportation was given and procedural safety was observed with operator instructions confirmed at all times.

A1.2 Bridge Sitework

Experimental investigations at bridge sites involved repeated measurements of temperatures on structure parapets over (in some cases) considerable drops to rivers or canals. In the case of the Fordrough bridge site carriageway temperature measurements necessitated at least one operator to be in very close proximity to periodic traffic flow. In addition to these obstacles in obtaining structural temperatures vibration response data acquisition involved many metres of signal cable being led to the instrumentation vehicle in the very near proximity of the general public. These cables could be a hazard unless carefully positioned away from main pedestrian access and precautions were necessary when impacting the 7 kg sledgehammer onto the bridge footpaths in public areas.

In the case of parapet locations on-site temperature measurements required the conscious effort and a careful procedure to avoid the very real problem of becoming over-familiar and *blasé* with the dangers present. Carriageway measurements were undertaken with both of the operators wearing fluorescent site-jackets using the procedure that one member would face the oncoming traffic-flow at all times, warning both the vehicle and the other operator of the hazards present. Response data acquisition cables were led along the parapet behind the handrails to minimise footpath interference and each sledgehammer impact was coordinated such that no member of the public was on the bridge during each traffic-free period. All work in the vicinity of the carriageway was undertaken using the guidelines produced by the City of Birmingham Engineers Department.

A1.3 Water-Borne Hazards

With a problem vermin population within any city there are two potentially lethal by-products of such an infestation. In the majority of cases rat urine carries the virus ***Leptospirosis*** which is the cause of ***Weil's Disease*** within humans. In order to minimise such a rat population, pest controllers have to utilise the compound ***Brodifacoum*** throughout the sewer systems. Unfortunately this "potent rodenticide" is also a powerful anti-coagulant within humans. Both of these agents can enter the bloodstream, the former through unbroken skin tissue, and are present at some level of concentration within the waterways of the Birmingham city area. Water-borne hazards were minimised by the use of 'wellington-waders' and rubber gloves during the procedures which required water contact under the bridge structures. Only the author would carry-out these procedures to minimise the exposure to such agents, also he was supplied with the appropriate documentation for the benefit of his general-practitioner by Birmingham City Engineers Department.

A1.4 Summary

It became apparent during the background research to the proposed experimental work that training which would encompass all of the above safety considerations would be required. A day course at a local training centre was attended where the legal, as well as practical, ramifications arising from the supervision of such work were emphasised. In all cases the Health and Safety at Work Act (1974) states that the burden of prosecution would fall on the author, above all others, since he is **THE** supervisor of this work and in the eyes of the law would be to blame if an accident were to occur: this fact would not have gained attention otherwise.

Appendix 2: Research Papers

A2.1 WOOD M.G., BAILEY M., FRISWELL M.I., PENNY J.E.T. and PURKISS J.A. (1991); "Damage Location in Reinforced Concrete Beams Using Vibration Response"; Proceedings of IMAC *IX* Conference, Florence, Italy; February 15th - 18th, pp 139 - 144.

A2.2 WOOD M.G., FRISWELL M.I. and PENNY J.E.T. (1992); "Exciting Large Structures Using a 'Bolt-Gun'"; Proceedings of IMAC *X* Conference, San Diego, U.S.A; February 3rd - 7th, pp 233 - 238.

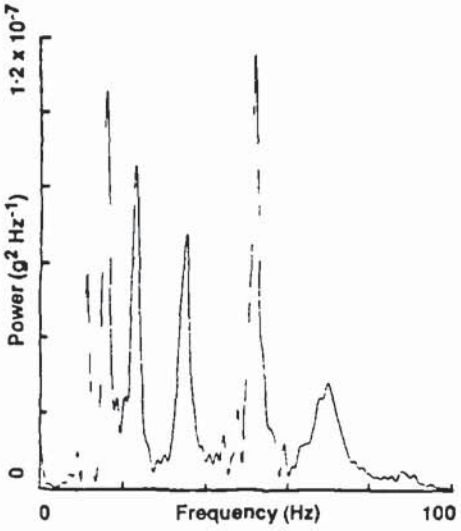

Figure 8 Bridge Response ASD (Sledgehammer Impact)

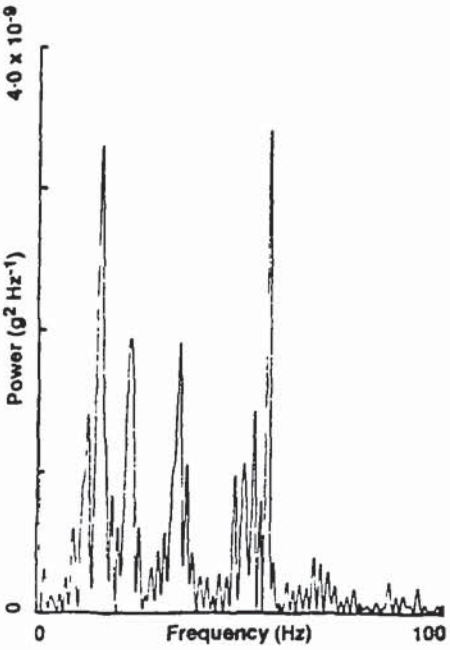

Figure 10 Bridge Response ASD (Bolt-gun Impact)

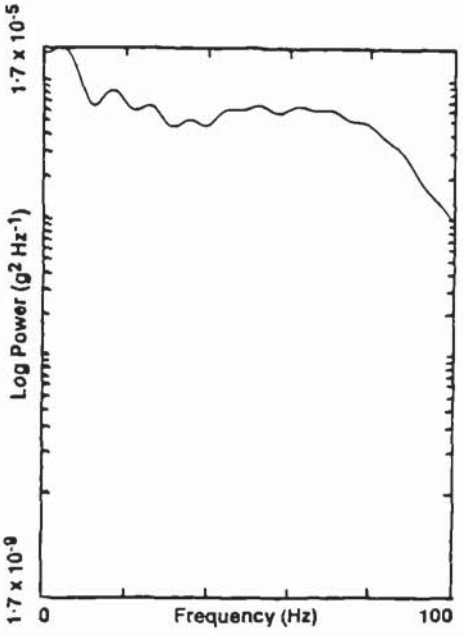

Figure 9 Sledgehammer Acceleration ASD

Appendix 3: Ancilliary Beam Test Equipment

Two areas of interest on beam testing which were not covenient to discuss in Chapter 3 are now presented: prestress load-cell and response measurement equipment details.

A3.1 Prestress Load-Cells

The load-cells employed to monitor the tendon preloads were designed and manufactured specifically for this task (Figure A3.1). Having a nominal overall length of 100 mm and a major diameter of 45 mm, each load-cell had a 17 mm diameter axial hole throughout to accommodate tendon access and was manufactured from EN 16 medium-tensile steel (BS 970: Part 1: 1983). The design incorporated a 30 mm central shank of 36 mm diameter on which the measurement strain-gauges were bonded. The strain-gauge grid arrangement consisted of an fully-active and temperature-compensated, four element Wheatstone-bridge. The 350 Ω foil-gauges used the action of both the hoop and axial strains under loading and they provided a sensibly linear response of approximately 185 μV/kN. Using a Dennison compression-tester, each load-cell was cycled 5 times through to 125 % of the design load to minimise any mechanical hysteresis effects. Calibration was undertaken using the same compression-tester and this was repeated after each beam manufacture, until it became apparent that the calibrated responses did not change. The load-cells were located accurately and securely by the use of a circular register which mated precisely in a counterbore within the end-plates. Digital readout from the individual load-cell bridges was provided by a Tinsley 5794, six-channel switch and balance unit (see Figure A3.2).

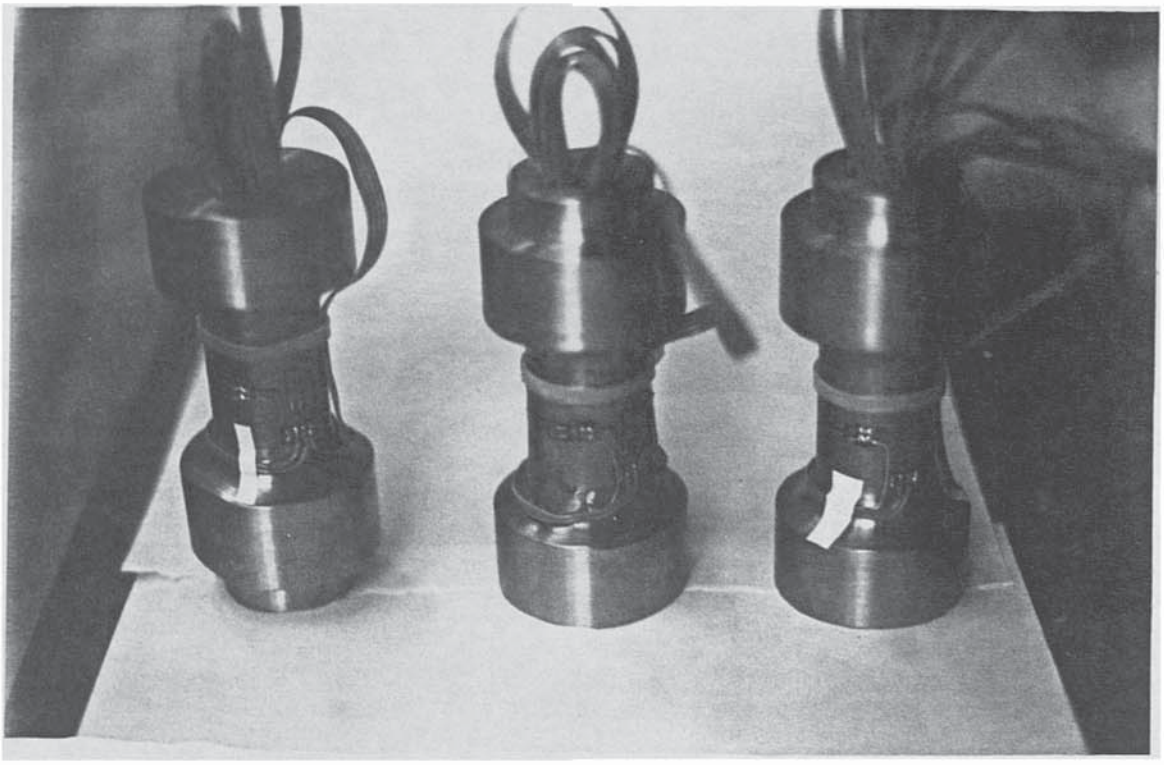

Figure A3.1 Tendon-prestress transducers

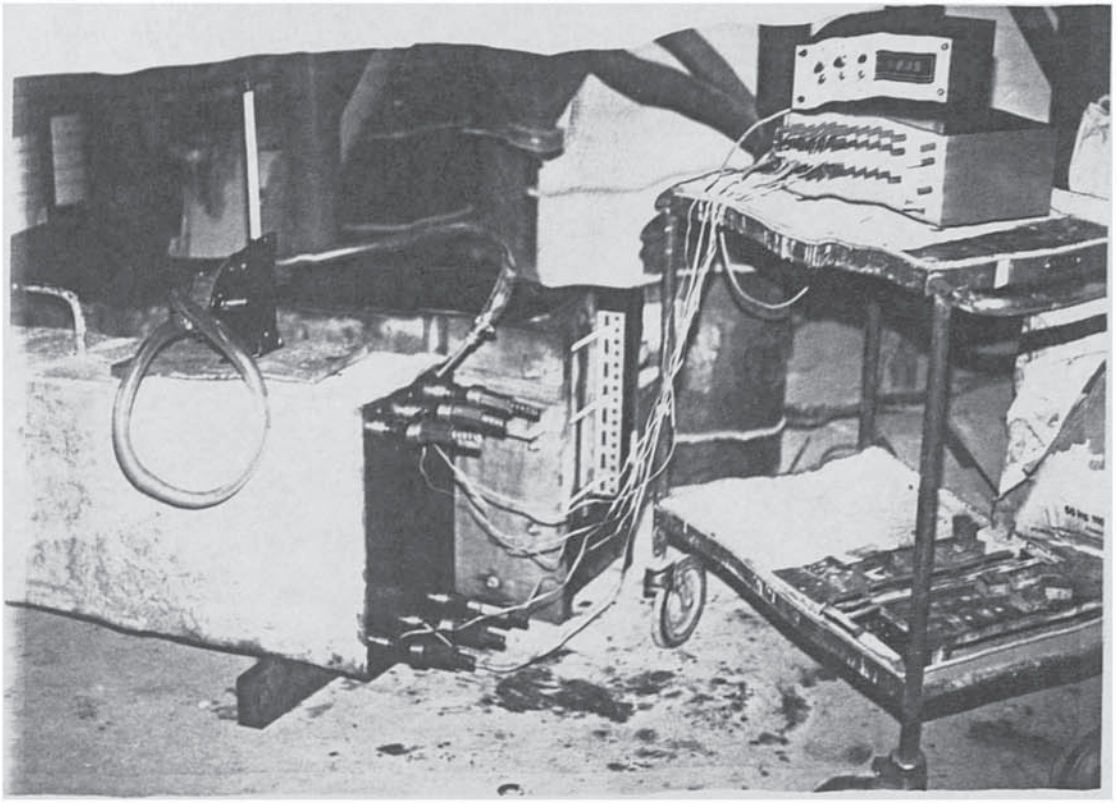

Figure A3.2 Post-tensioning instrumentation and grout-pump

A3.2 Response Measurement Equipment

The equipment used for these investigations (Figure 3.10) included a PCB Piezotronic SP205 impact-hammer and accompanying model 480 power-unit. This hammer incorporated an interchangeable strike-face and the hard-rubber striker which was selected for these tests reproduced a sensibly flat impact-spectrum over the 0-1kHz bandwidth. Additional equipment included a B&K 4333 response accelerometer and its signal was transferred to a HP 3582A analyser via a B&K charge-amp. The impact and response signals were processed simultaneously by the analyser to display the resultant inertance-frequency-response-function (i.e. A_{ij} F.R.F.). These data were then transferred to a portable COMPAQ 286 computer which hosted a SMS 'Star' data-analysis suite via a National Instruments general purpose interface-board.

Appendix 4: Static Analysis Beam Model Derivations

Here the static mechanics of the beam section are derived from first principles for both the ordinary-reinforced and prestressed systems. The symbols used are standard notation and they are detailed below:

A_s	=	area of reinforcement steel in tension
A_s'	=	area of reinforcement steel in compression
B	=	width of concrete in tension zone
B'	=	width of concrete in compression zone
d	=	depth to tensile reinforcement from top face of beam
d'	=	depth to compressive reinforcement from top face of beam
E_c	=	concrete Young's elastic modulus
E_s	=	steel Young's elastic modulus
f_{ps}	=	applied prestress over beam section
f_y	=	steel yield stress
F_c	=	concrete compression equilibrium force
F_{ps}	=	tensile zone concrete prestress equilibrium force
F_{ps}'	=	compressive zone concrete prestress equilibrium force
F_s	=	tensile zone steel reinforcement equilibrium force
F_s'	=	compressive zone steel reinforcement equilibrium force
ΣF_{int}	=	sum of internal forces
h	=	beam depth
K_{ps}	=	effective prestress factor
$M_{applied}$	=	externally applied moment to beam system
ΣM_{ext}	=	sum of external moments
ΣM_{int}	=	sum of internal moments
x	=	depth to beam neutral-axis from top face of beam
ε_c	=	outer-fibre concrete compressive strain
$\varepsilon_{c\ max}$	=	maximum induced concrete strain
ε_{ps}	=	prestress induced concrete strain
ε_s	=	tensile reinforcement strain
ε_s'	=	compressive reinforcement strain

A4.1 Ordinary-Reinforced System

With reference to Figure 4.1 which shows the ordinary-reinforced system, for any condition the following must hold for strain compatibility:

$$\varepsilon_c = \varepsilon_s x/(d - x)$$
$$\varepsilon_s' = \varepsilon_s (x - d')/(d - x) \qquad \text{(A4.1)}$$

The constitutive relations for the forces are as follows:

$$F_c = 0{\cdot}5\, B' x\, E_c \varepsilon_c$$
$$F_s' = A_s' E_s \varepsilon_s' \qquad \text{(A4.2)}$$
$$F_s = A_s E_s \varepsilon_s$$

The following must hold for static equilibrium of forces:

$$\Sigma F_{int} = 0 = F_s - F_s' - F_c \quad (\text{i.e. } F_c = F_s - F_s') \qquad \text{(A4.3)}$$

Similarly, for moments:

$$\Sigma M_{int} = 0 = F_s (d - x) - F_s'(x - d') - 2F_c x/3$$

Hence, using the substitution of (A4.3):

$$F_s' = F_s (d - 5x/3)/(x/3 - d') \qquad \text{(A4.4)}$$

Also, (A4.3) becomes:

$$F_c = F_s \{2x - (d + d')\}/(x/3 - d') \qquad \text{(A4.5)}$$

Now:

$$\Sigma M_{int} + \Sigma M_{ext} = 0 = F_s (d - x) - F_s'(x - d') - 2F_c x/3 - M_{applied}$$

Finally, using the substitution of (A4.4) and (A4.5):

$$x = d - M_{applied}/(2 A_s E_s \varepsilon_s) \qquad \text{(A4.6)}$$

A4.2 Post-Tensioned System

With reference to Figure 4.2 which illustrates the ordinary reinforced system incorporating a superimposed axial prestress, the additional constitutive relations for stress and forces are:

$$\begin{aligned} f_{ps} &= K_{ps}\{2 A_s f_y/(B h)\} \\ F_{ps}' &= f_{ps} B' x \\ F_{ps} &= f_{ps} B (h - x) \end{aligned} \qquad \text{(A4.7)}$$

Using the same procedure of solution as that of Section A4.1 since $\varepsilon_{ps} << \varepsilon_{cmax}$ the following governing equations result:

$$F_c = F_s - F_s' + F_{ps} - \{F_s (d - 5x/3) + F_{ps} (0{\cdot}5h - 5x/3) - F_{ps}' x/6\}/(x/3 - d') \qquad \text{(A4.8)}$$

$$F_s' = \{F_s (d - 5x/3) + F_{ps} (0{\cdot}5h - 5x/3) - F_{ps}' x/6\}/(x/3 - d') \qquad \text{(A4.9)}$$

$$x = \left(h + \frac{A_s E_s \varepsilon_s}{f_{ps} B}\right) - \sqrt{\left(h + \frac{A_s E_s \varepsilon_s}{f_{ps} B}\right)^2 + \frac{M_{applied}}{f_{ps} B} - h^2 - \frac{2 A_s E_s \varepsilon_s d}{f_{ps} B}} \qquad \text{(A4.10)}$$

Appendix 5: Bridge-Structure Details And Dynamic Analysis Models

Presented here are the structural details and grillage analysis idealisations for each of the bridge structures discussed within this work.

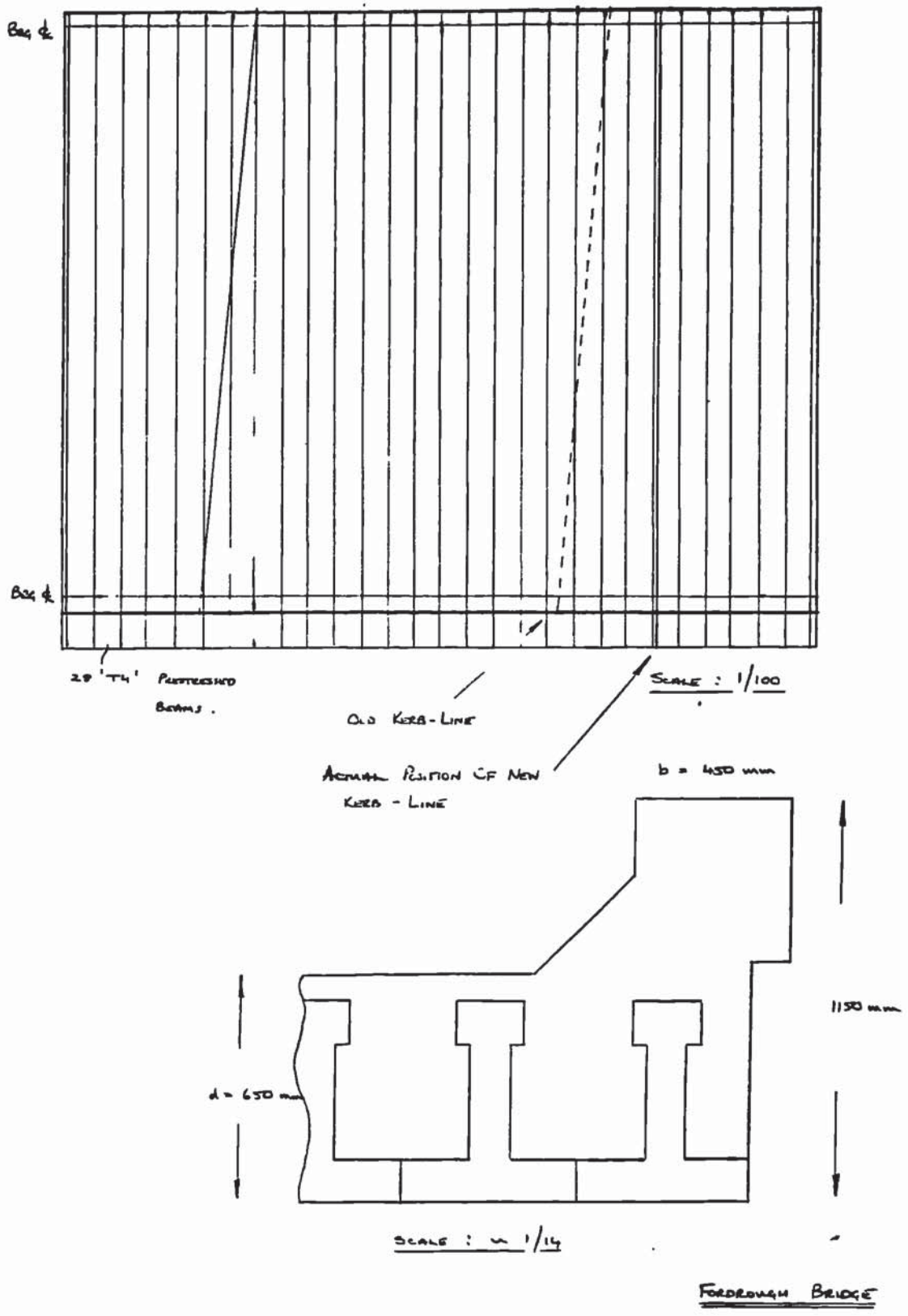

Figure A5.1(a) Fordrough Bridge structural details schematic

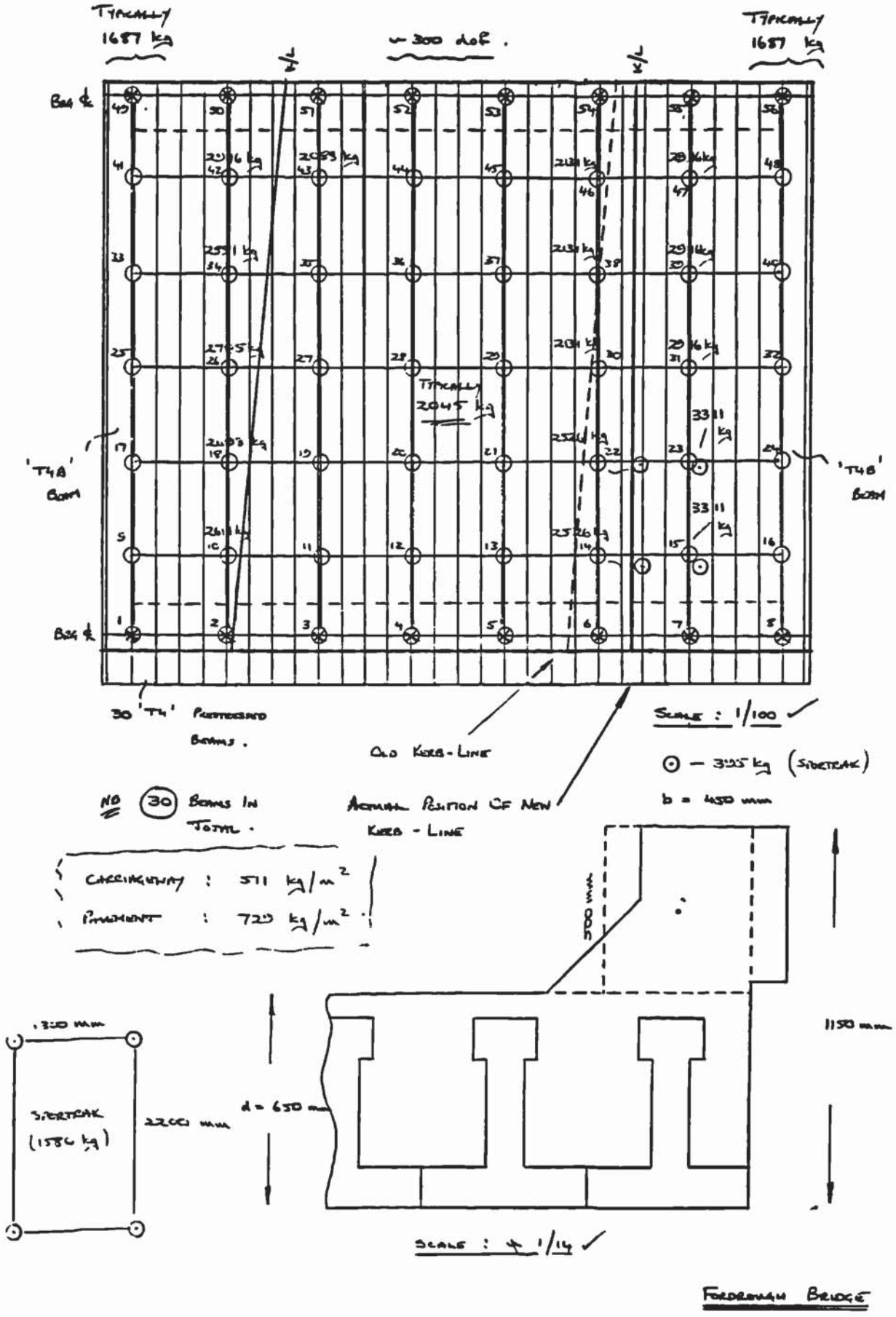

Figure A5.1(b) Fordrough Bridge Grillage Analysis idealisation

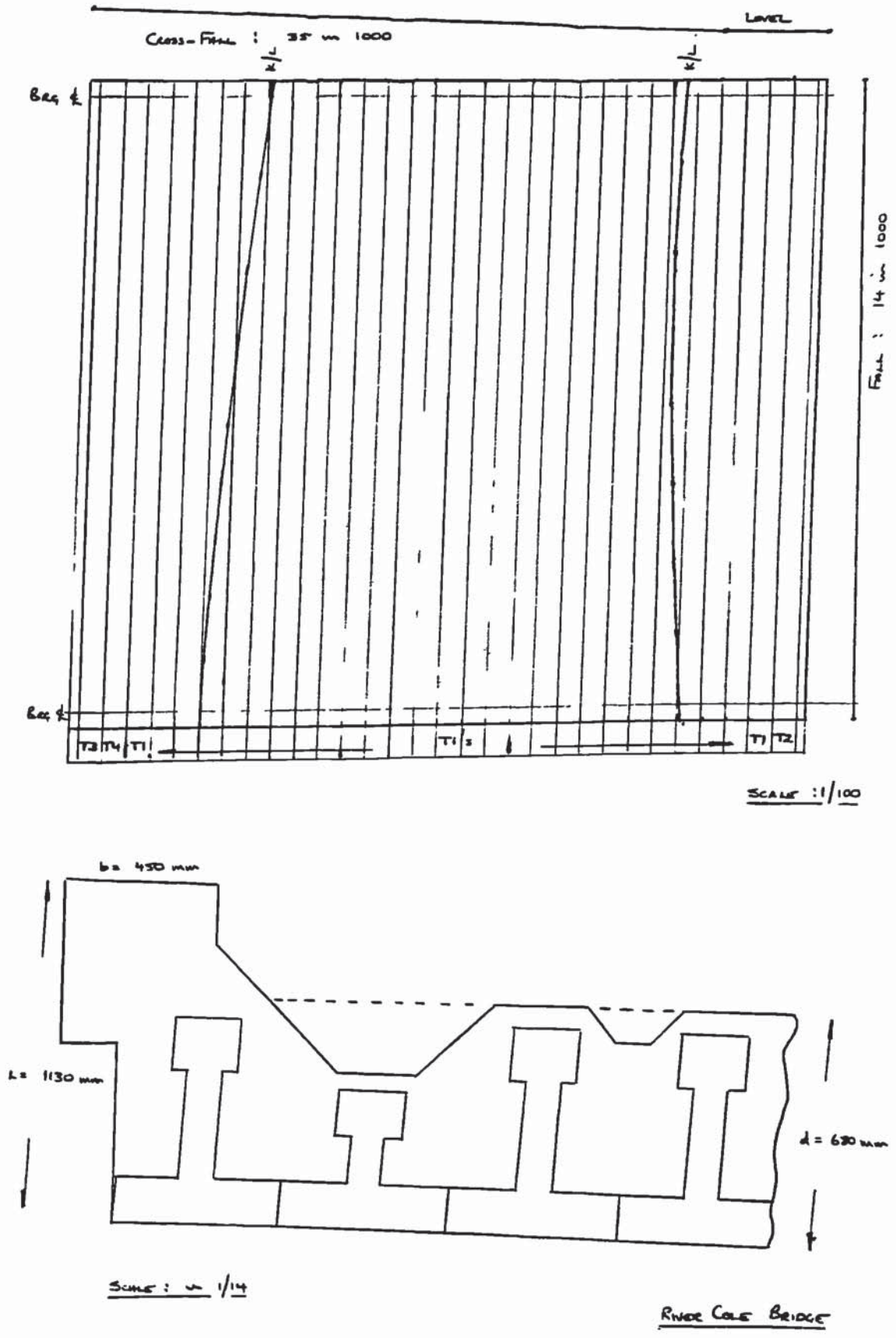

Figure A5.2(a) River Cole Bridge structural details schematic

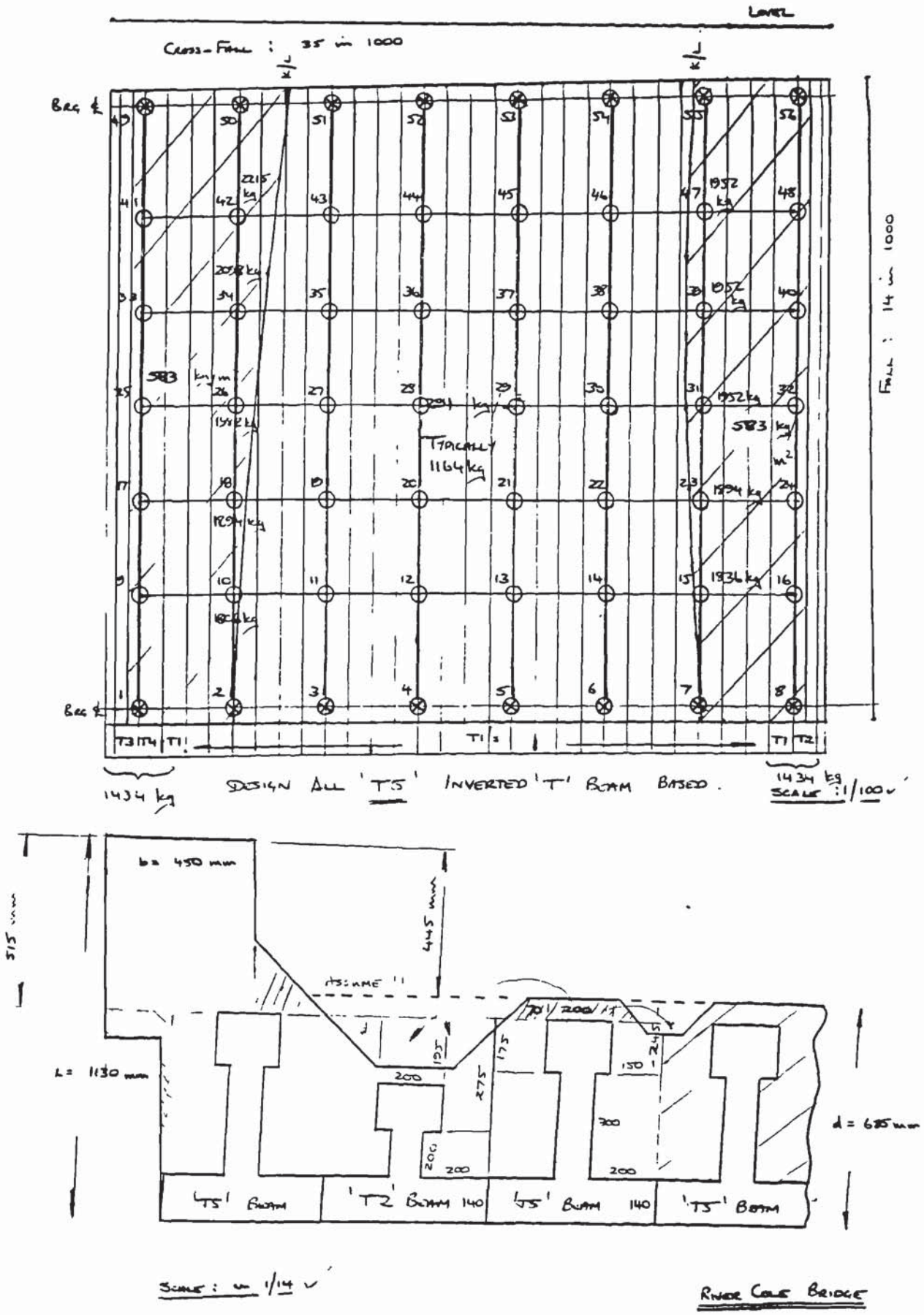

Figure A5.2(b) River Cole Bridge Grillage Analysis idealisation

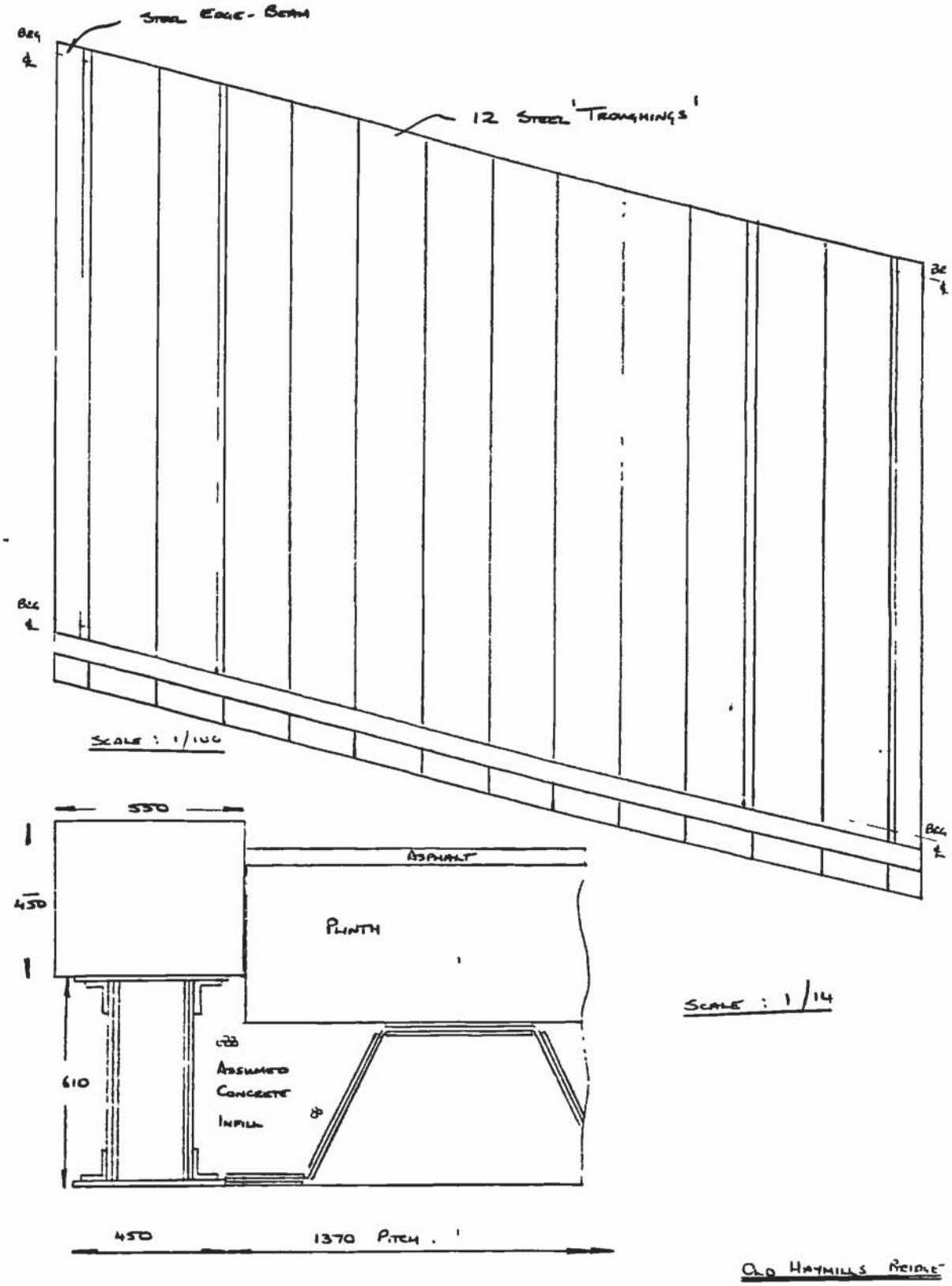

Figure A5.3(a) Old Haymills Bridge structural details schematic

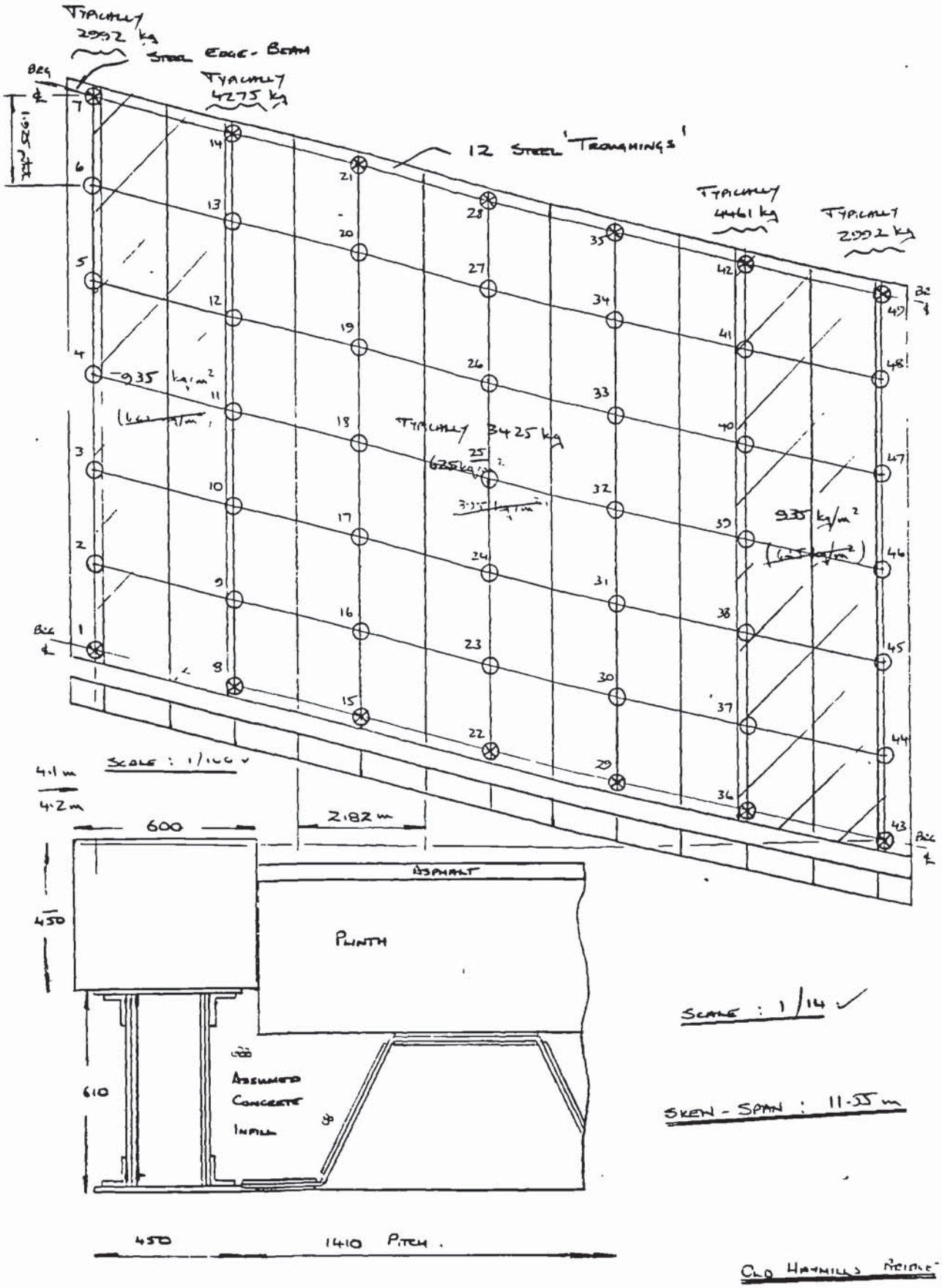

Figure A5.3(b) Old Haymills Bridge Grillage Analysis idealisation

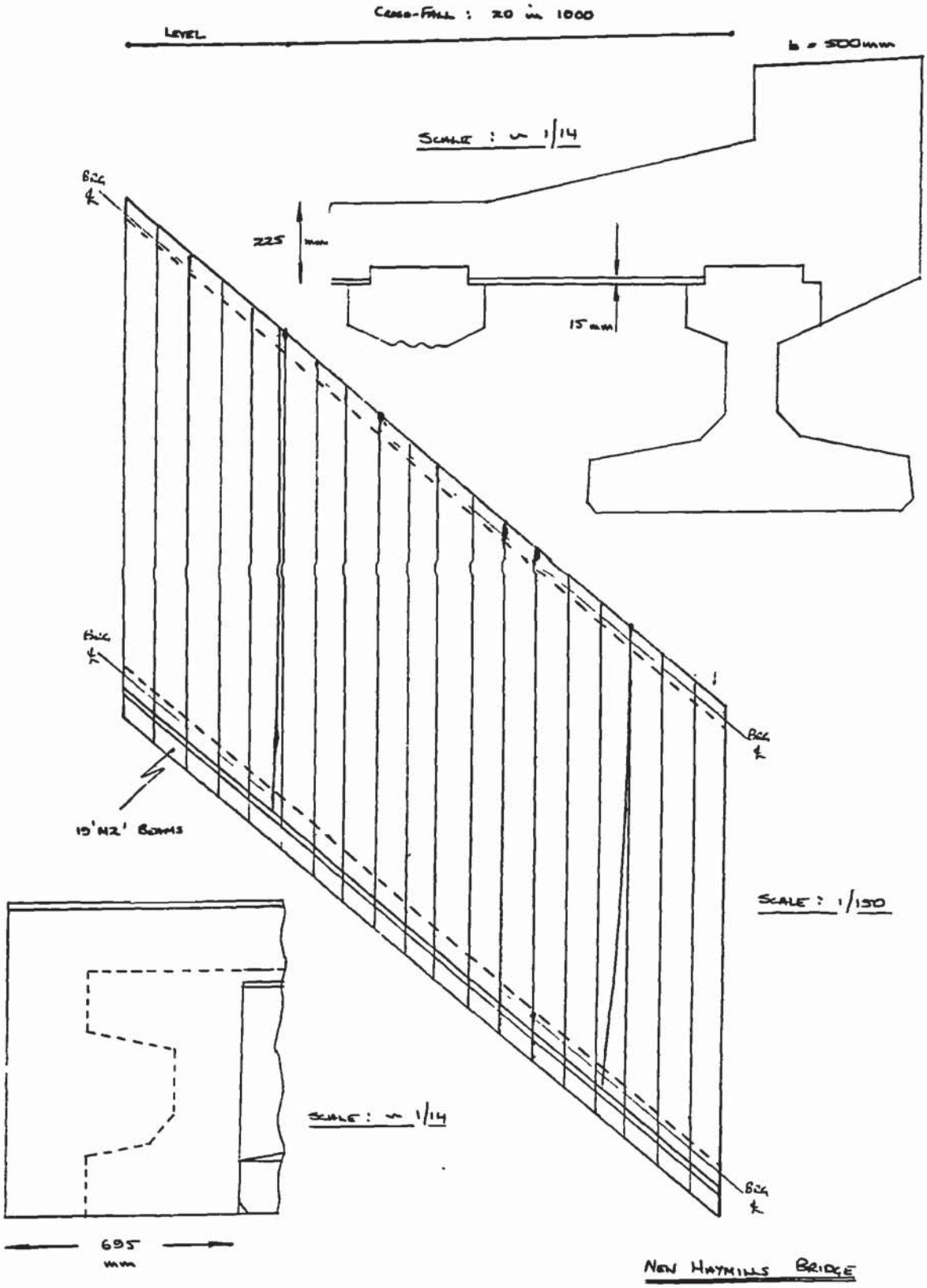

Figure A5.4(a) New Haymills Bridge structural details schematic

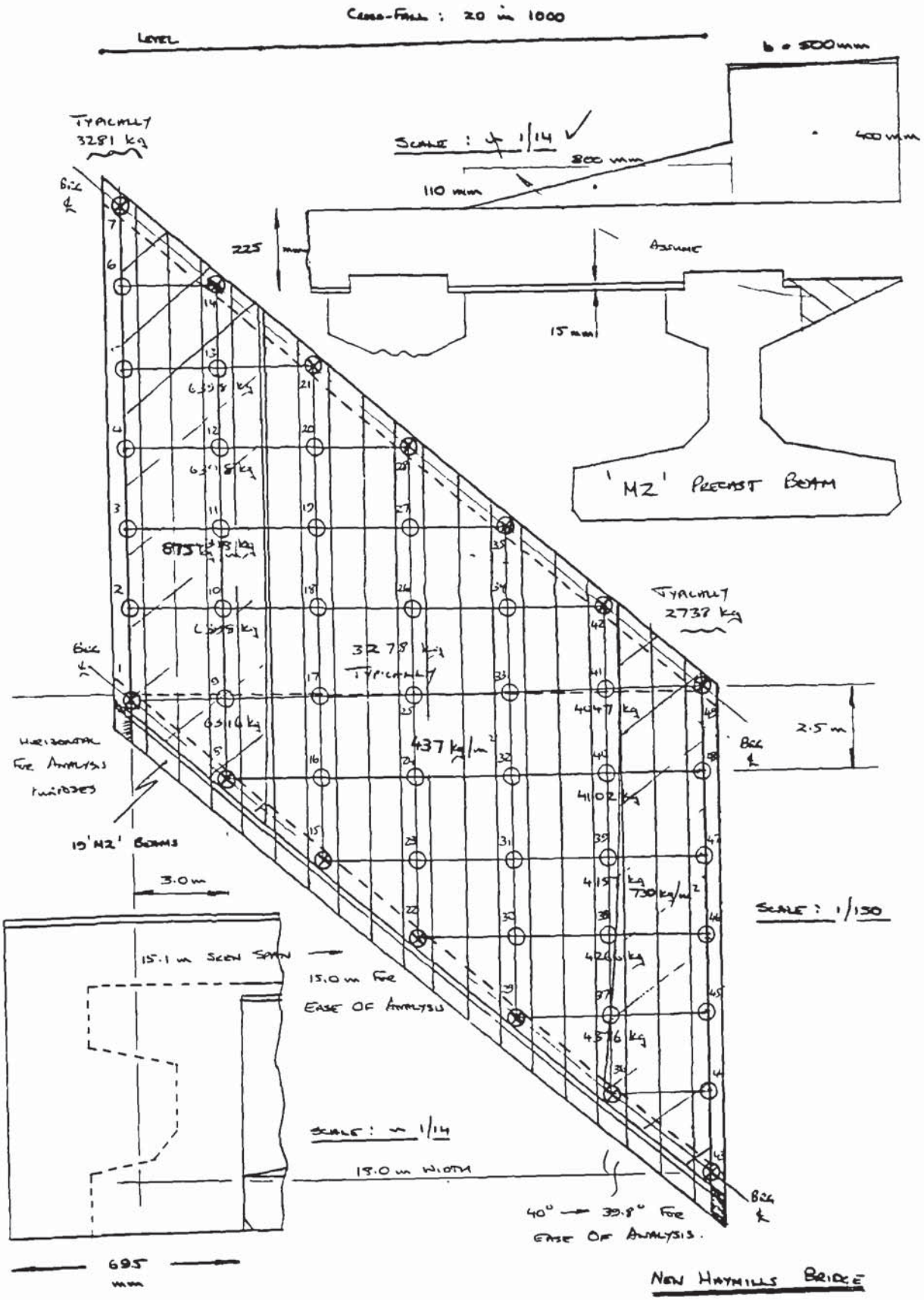

Figure A5.4(b) New Haymills Bridge Grillage Analysis idealisation

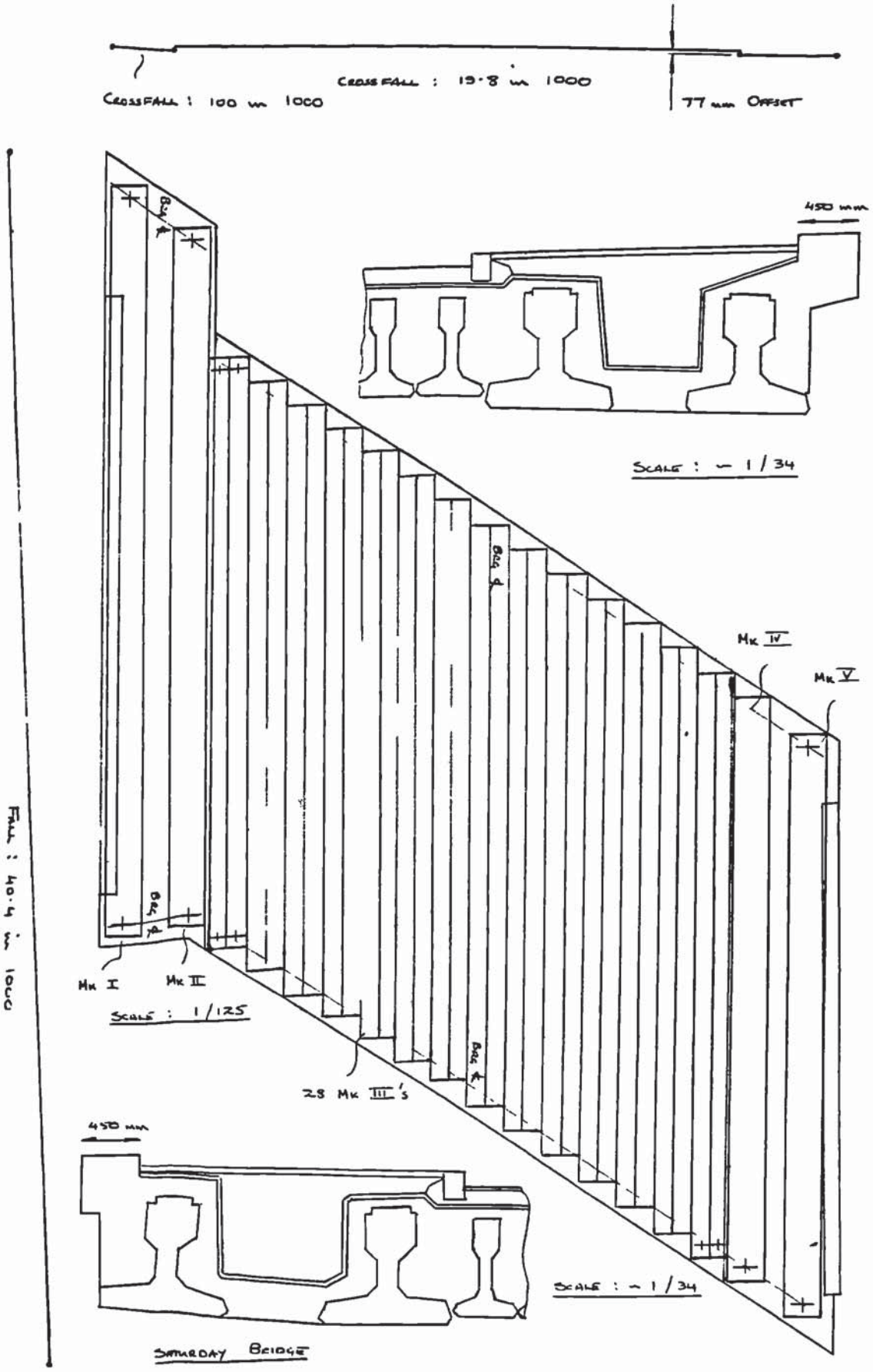

Figure A5.5(a) Saturday Bridge structural details schematic

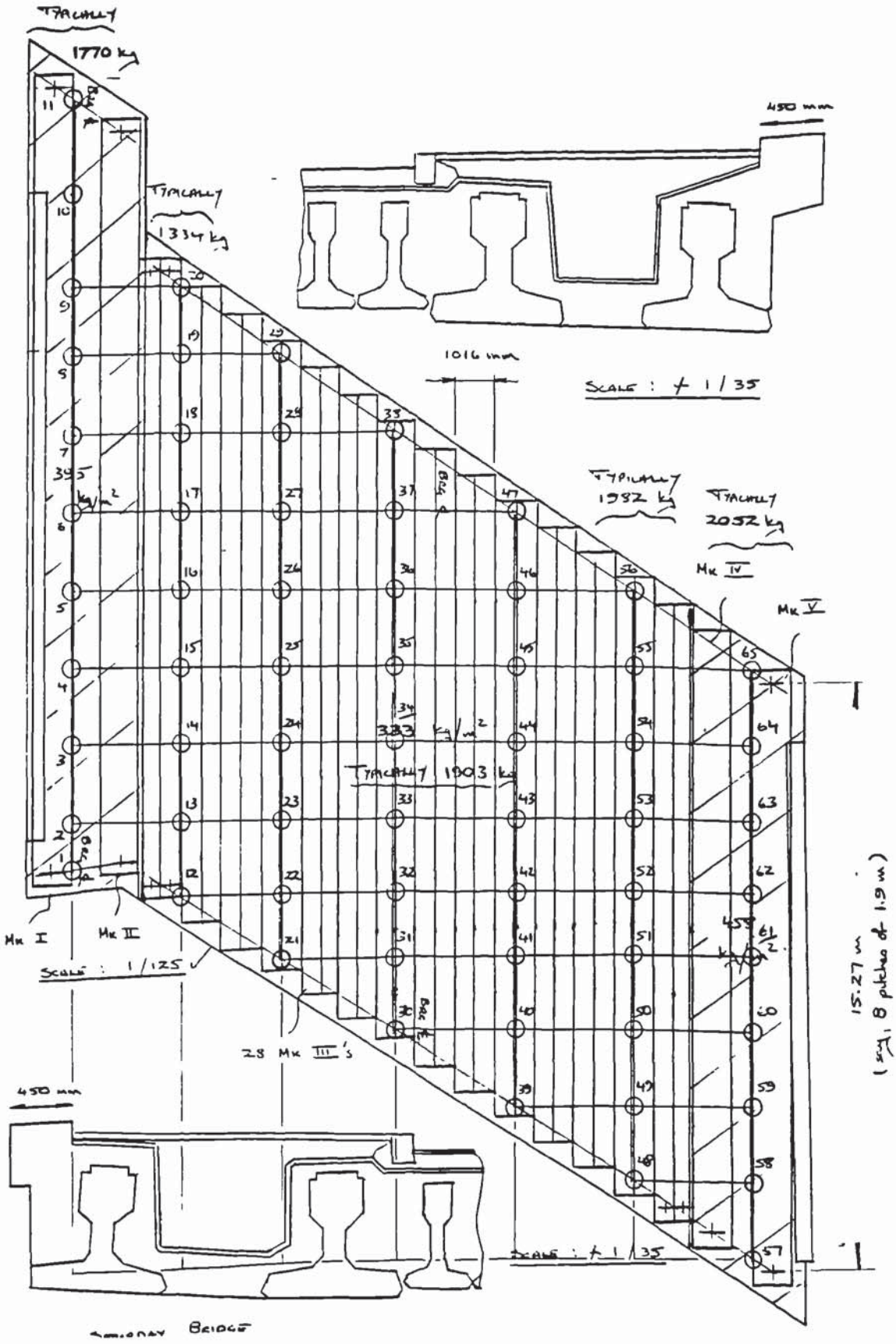

Figure A5.5(b) Saturday Bridge Grillage Analysis idealisation

Appendix 6: Bridge-Site Monitoring Data Compilations

Presented here are the experimental frequency and associated parametric data for the bridges discussed within this work. In addition the parametric frequency curve-fit correlation results are also tabulated for these bridge-sites.

A6.1 Frequency And Parametric Data

Presented here in both graphical and tabular form are the frequency and associated parametric data for each of the five bridge-sites discussed.

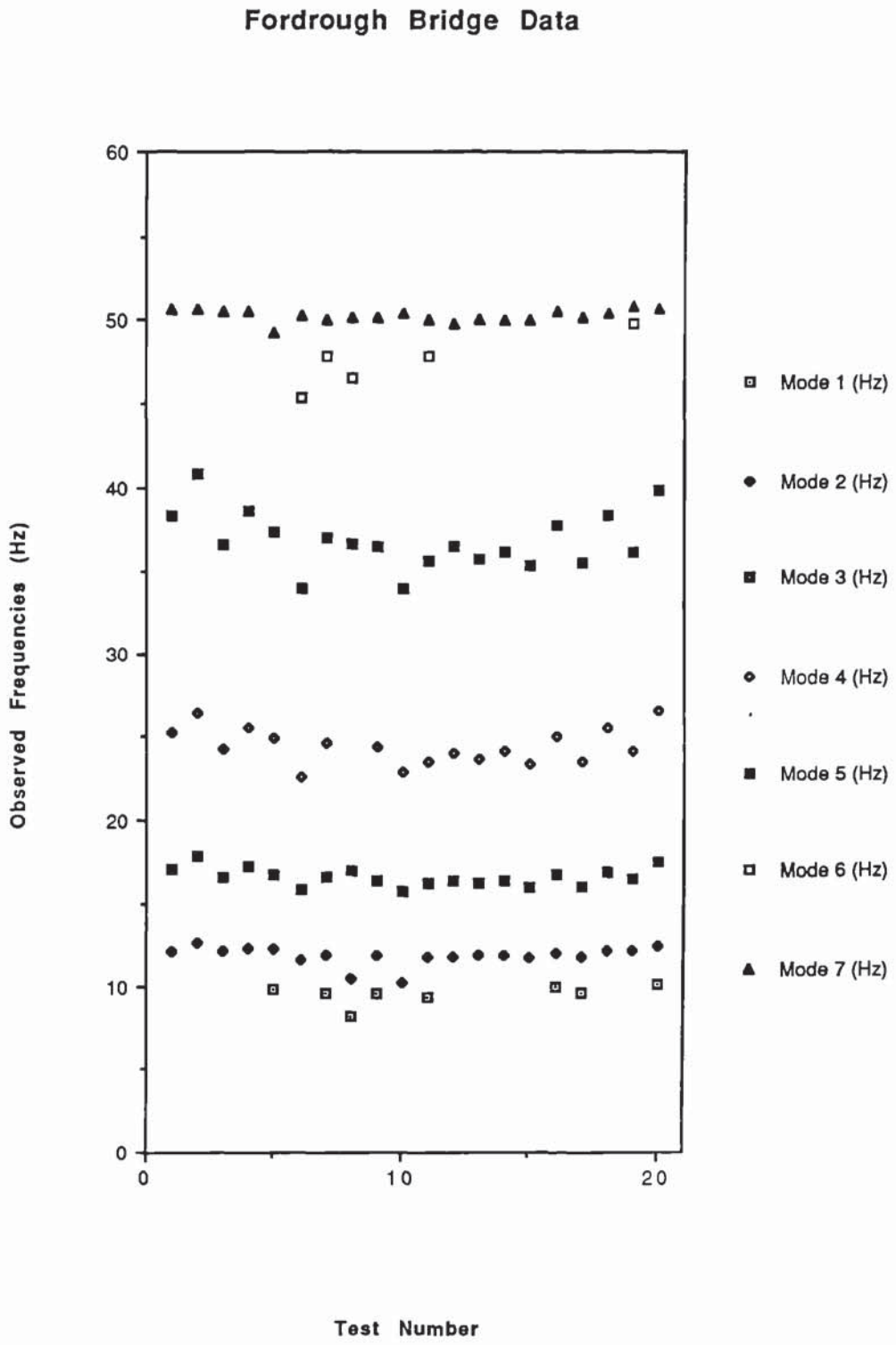

Figure A6.1 Observed response frequencies of Fordrough Bridge

Fordrough

	Event Day	Event Time	Site Temp (oC)	Site Humidity	BlackTop (oC)	Upperdeck (oC)	Soffit (oC)	Mode 1 (Hz)	Mode 2 (Hz)	Mode 3 (Hz)
1	106	12.00	12.0	57	19.9	16.5	9.2		12.17	17.12
2	113	9 50	9.0	58	10 5	9.5	7.0		12 69	17.90
3	129	14 50	14 5	43	20 0	17 1	12.0		12.18	16.54
4	149	9.75	10 5	77	12.8	10 3	9.7		12.32	17 17
5	168	10.25	12.5	74	17.0	15 2	11.9	9.88	12.22	16.75
6	183	14 50	25.0	44	38 7	29 1	20.5		11.70	15.77
7	189	10.50	18.5	73	21.9	20 4	17.6	9.59	11.93	16.58
8	196	14.25	20.0	59	27 2	23.1	18.7	8.23	10.53	17.02
9	200	10.00	17.5	72	19.3	17.7	16.4	9.60	11.92	16.37
10	203	14.00	23.5	55	32 4	27.9	21.0		10.26	15.64
11	205	14.50	18 0	82	22.2	20 5	17.7	9.43	11.81	16.19
12	217	10 00	19.5	78	21.8	20 2	18.4		11.80	16.32
13	221	12.00	21.0	67	26.9	23 5	18.1		11.85	16.24
14	224	9.75	16.0	71	22 4	19.6	16.9		11.94	16.29
15	231	12.50	20.0	59	29.4	24.1	18.2		11.79	15.93
16	235	10.75	16.0	71	16 6	15.7	15.1	9.96	12.01	16.68
17	260	14.25	22.0	54	30.2	23.2	19.0	9.59	11.80	15.93
18	263	10.25	16.0	71	18 7	16 9	14.4		12.13	16.89
19	267	13.00	18 5	60	24.0	20.9	16.4		12.15	16.41
20	270	10.50	11.0	100	10.4	10.0	10.3	10.09	12.35	17.50

Fordrough

	Mode 4 (Hz)	Mode 5 (Hz)	Mode 6 (Hz)	Mode 7 (Hz)	Mode 8 (Hz)	Mode 9 (Hz)	Mode 10 (Hz)	Mode 11 (Hz)	Mode 12 (Hz)	Mean Temp
1	25.26	38 33		50 61		58.89	58.69	62.84	77.59	7.5
2	26 48	40 84		50 60			58.05	60.04	82.59	5.5
3	24 27	36 55		50 53	53.36		58 67			7 9
4	25.62	38 55		50.51		56.84	58.57		78.05	9.9
5	24.89	37 31		49 18	52.75	54.66	58.77		75.51	10.5
6	22 72	33.91	45.42	50.21			58.74			16.8
7	24 63	36.92	47 81	50 05	53.96		58.33		73.49	16.7
8		36 64	46.58	50.17		56.86	58.86		73.30	16.5
9	24 37	36.44		50.17	52.50					16.3
10	22.90	33 91		50 35						16.3
11	23.58	35.51	47.84	49.99	51 60				71.49	14 1
12	24.02	36.40		49 76	52.39					17.1
13	23.64	35.67		50 01	51.30	56.51				15.2
14	24 15	36.04		49 99	52.80					15 3
15	23 43	35 37		50 05	51.80	57 15				14.2
16	25 00	37.68		50 45		55 95				14 5
17	23.55	35 47		50 12		56 49				15.5
18	25 54	38 32		50.36		57.02				10.7
19	24.20	36.05	49.76	50.72		55 85				15.0
20	26.62	39.93		50.64		56.62				10.1

Fordrough

	Mean Humidity	Max Temp (oC)	Min Temp (oC)	Rainfall (mm)	Air Pressure	BTop/Upper oC	BTop/Soffit oC	Upper/Soffit	Settled Rating
1	52	11.1	3 8	0.01	1033 3	3 4	10.7	7.3	2
2	71	11 1	0 0	0 00	1023.7	1 0	3.5	2.5	3
3	46	13.9	2 0	0 00	1020.8	2 9	8 0	5 1	5
4	77	12 3	7.5	0.01	1026.7	2.5	3.1	0.6	7
5	73	13.6	7.4	1.00	1015.4	1.8	5.1	3.3	5
6	68	22.1	11.5	19.90	1018.6	9.6	18.2	8.6	8
7	93	18 5	14.8	2 70	1010.5	1.5	4.3	2.8	8
8	63	19 3	13 8	0.30	1012 0	4 1	8 5	4 4	9
9	75	19 1	13.5	0 01	1010 3	1.6	2.9	1 3	6
10	64	23.1	9.6	0 00	1020.2	4.5	11.4	6 9	9
11	84	17.6	10.5	8 10	1005.6	1 7	4.5	2.8	7
12	89	19.6	14.5	6.00	1017.1	1.6	3.4	1.8	7
13	75	20.4	10.0	0.10	1024.2	3 4	8.8	5.4	7
14	70	20.1	10.4	0.00	1020.6	2.6	5.5	2.9	7
15	64	21.4	7.0	0.30	1022.2	5.3	11.2	5.9	8
16	73	16 9	12.1	2.20	1006.2	0.9	1.5	0 6	6
17	64	20.4	10 5	0 01	1019.9	7.0	11.2	4.2	8
18	63	18 0	3.4	0.01	1019.1	1.8	4.3	2.5	7
19	57	17.0	13 0	0 40	1004.0	3 1	7.6	4.5	6
20	93	11.2	9.1	2.70	1006.7	0.4	0.1	-0.3	6

Table A6.1 Parametric data compilation for Fordrough Bridge

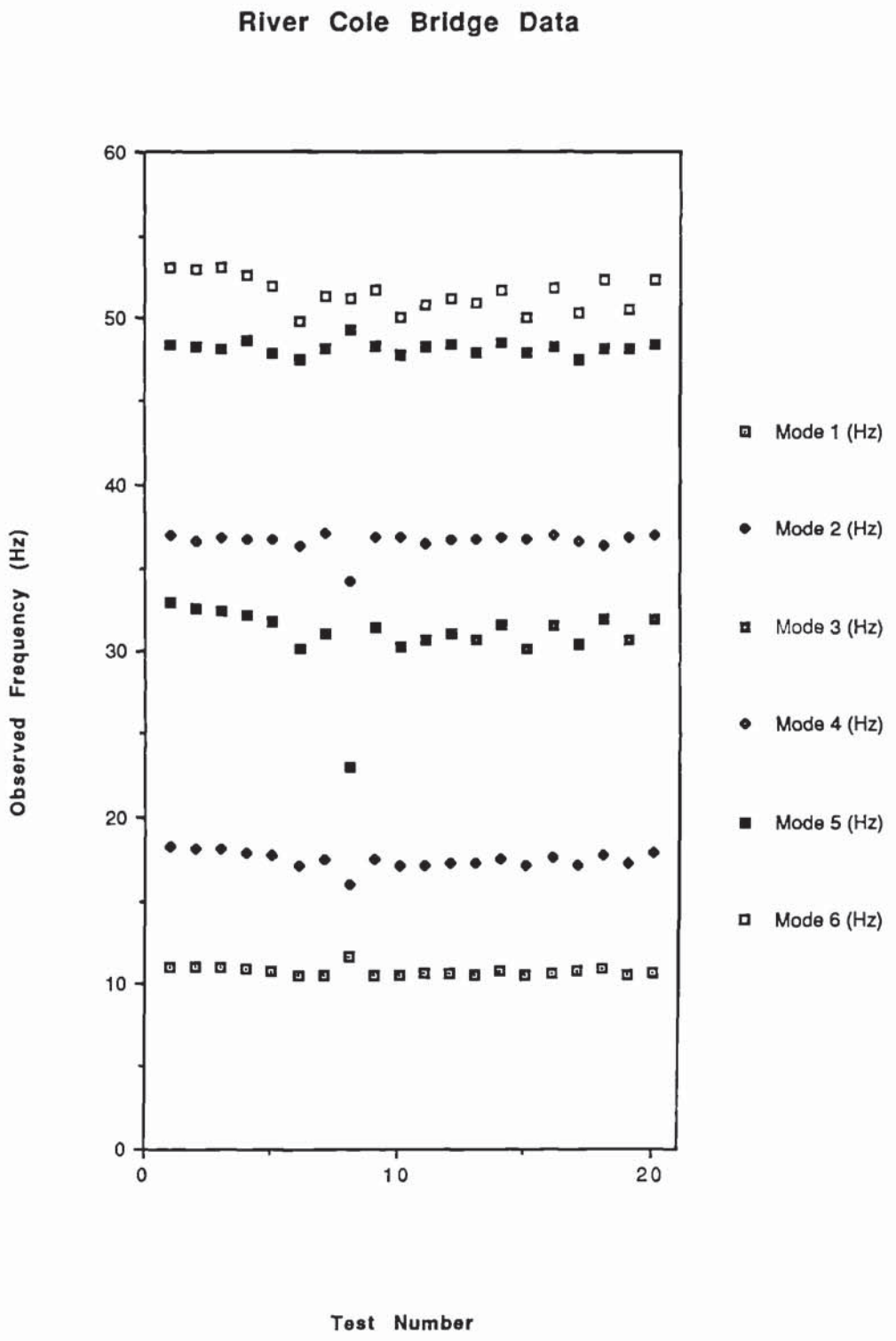

Figure A6.2 Observed response frequencies of River Cole Bridge

River Cole

	Event Day	Event Time	Site Temp (oC)	Site Humidity	Upperdeck (oC)	Soffit (oC)	Mode 1 (Hz)	Mode 2 (Hz)	Mode 3 (Hz)	Mode 4 (Hz)
1	107	8.75	5 5	59	4 2	4 3	11 05	18 24	32 92	36 93
2	114	9 00	9 5	76	9 9	7 7	10 97	18 13	32 48	36 56
3	129	8 75	11 0	56	9 4	8 1	10 97	18 07	32 40	36 83
4	150	9.00	11.0	83	9 9	10 0	10 94	17 79	32 16	36 74
5	168	9.00	12 5	74	13 2	10 9	10 70	17 74	31 77	36 70
6	183	16.00	23 0	65	30 0	20 9	10 49	17 04	30 11	36 36
7	189	9.00	18 0	82	17 6	17 1	10 53	17 41	30 99	37 05
8	196	15.75	20 0	59	23 5	19 2	11 65	15 91	23 09	34 19
9	200	8.75	15.5	80	14 8	14 9	10 54	17 42	31 39	36 84
10	203	15.50	23 0	55	27 4	20 9	10 54	17 11	30 28	36 83
11	205	15.75	18 0	73	20.4	17 1	10 62	17 13	30 60	36 50
12	217	8.75	17.5	86	17 4	16 8	10 62	17 25	30 95	36.68
13	221	14.00	20 0	83	20 1	17 6	10 51	17 24	30 61	36 75
14	224	8.50	15 0	80	15.1	14 7	10 70	17 44	31 53	36 87
15	231	14.50	23 0	62	25.7	19 6	10 51	17 06	30 17	36 70
16	235	9.00	15.0	80	14 0	14.3	10 57	17 54	31 53	36 99
17	260	15.25	22 5	55	25 3	20 0	10 72	17 05	30 33	36 56
18	263	9.00	11 0	94	8.5	9.3	10 86	17 68	31 93	36 29
19	267	14.75	19 0	65	20.5	16.9	10 52	17 25	30 61	36 81
20	270	8.75	11.0	100	8.5	9.8	10.63	17 79	31.94	36.94

River Cole

	Mode 5 (Hz)	Mode 6 (Hz)	Mean Temp	Mean Humidity	Max Temp (oC)	Min Temp (oC)	Rainfall (mm)	Air Pressure	Upper/Soffit	Settled Rating
1	48.38	53.09	3.9	72	7.2	0.6	0.60	1029 5	-0 1	2
2	48.25	52.88	9.5	67	12.5	6.4	0.01	1018 7	2.2	3
3	48.07	53.06	7.9	70	13 9	2.0	0.00	1020 8	1.3	5
4	48.67	52.52	10.1	88	11.5	8.8	0.01	1025 7	-0 1	7
5	47.80	51.92	10.5	76	13.6	7.4	1.00	1015.4	2.3	5
6	47.53	49.78	16.8	64	22.1	11.5	19.90	1018.6	9.1	8
7	48.09	51.30	16.7	91	18.5	14.8	2.70	1010.5	0.5	8
8	49.29	51.11	16.5	61	19.3	13.8	0.30	1012.0	4.3	9
9	48.21	51.65	16.3	79	19.1	13.5	0.01	1010 3	-0 1	6
10	47.73	49.98	16.3	65	23.1	9.6	0.00	1020.2	6 5	9
11	48.22	50.79	14.1	81	17.6	10.5	8.10	1005 6	3 3	7
12	48.37	51.18	17.1	89	19.6	14.5	6.00	1017.1	0.6	7
13	47.90	50.88	15.2	78	20 4	10.0	0.10	1024 2	2.5	7
14	48.53	51.69	15.3	72	20.1	10.4	0.00	1020 6	0.4	7
15	47.81	49.94	14.2	66	21.4	7.0	0.30	1022.2	6.1	8
16	48.24	51.73	14.5	78	16.9	12.1	2.20	1006 2	-0.3	6
17	47.48	50.26	15.5	65	20.4	10.5	0.01	1019.9	5.3	8
18	48.06	52.31	10.7	73	18.0	3.4	0.01	1019.1	-0.8	7
19	48.15	50.47	15.0	59	17.0	13.0	0.40	1004.0	3.6	6
20	48.40	52.32	10.1	95	11.2	9.1	2.70	1006.7	-1.3	6

Table A6.2 Parametric data compilation for River Cole Bridge

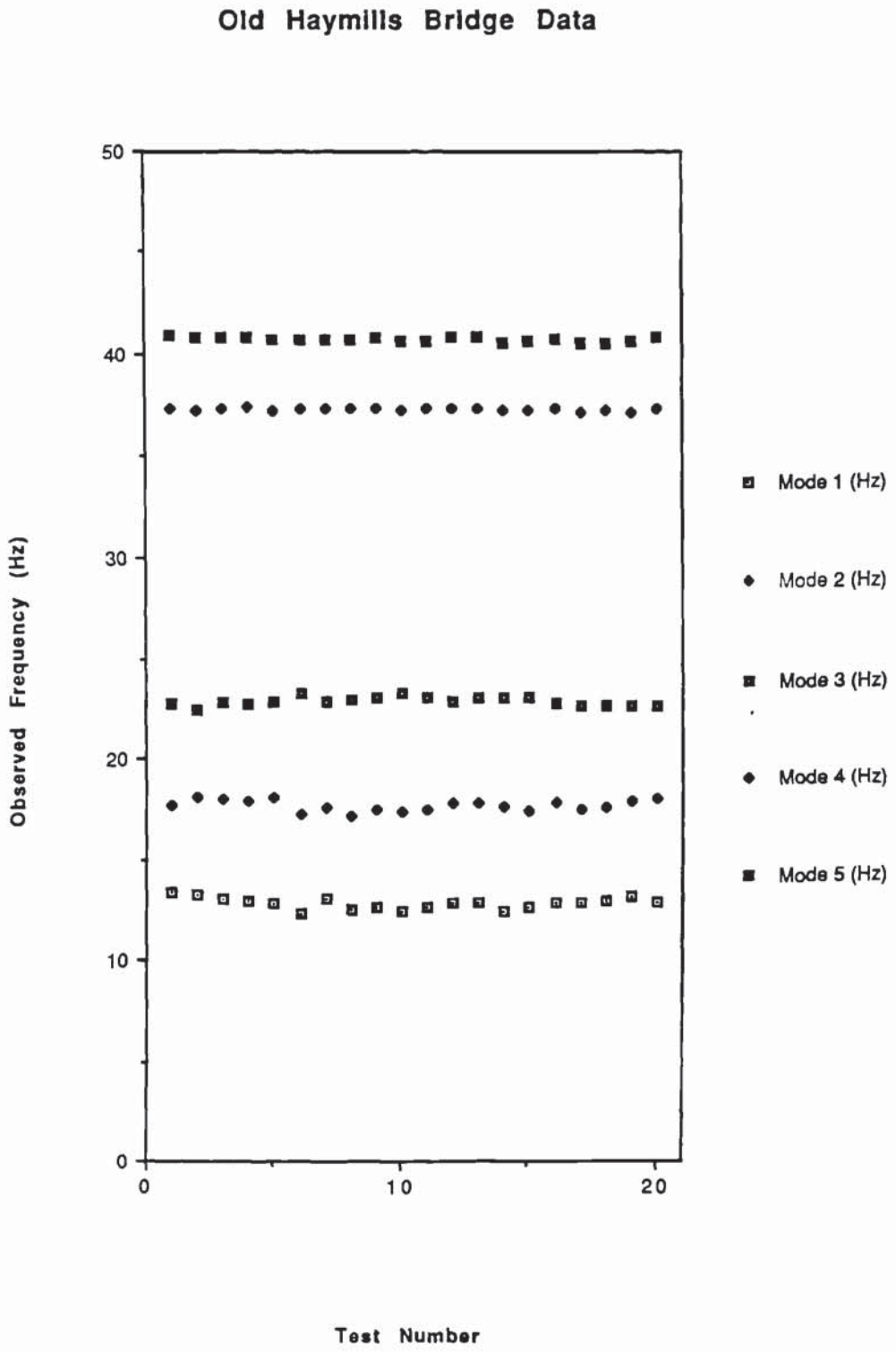

Figure A6.3 Observed response frequencies of Old Haymills Bridge

Old Haymills

	Event Day	Event Time	Site Temp (oC)	Site Humidity	Upperdeck (oC)	Soffit (oC)	Mode 1 (Hz)	Mode 2 (Hz)	Mode 3 (Hz)	Mode 4 (Hz)
1	106	15 50	10 0	65	13 9	11 8	13 39	17 72	22 80	37 30
2	113	11 25	11 0	66	10 9	8 5	13 25	18 12	22 46	37 25
3	128	14 75	14 5	56	16 3	11 8	13 10	18 01	22 89	37 31
4	149	11 75	12 0	78	11 5	9 5	13 00	17 94	22 80	37 44
5	168	12 25	13 0	74	14 2	12 7	12 90	18 10	22 93	37 24
6	183	12 25	21 5	68	28 9	19 8	12 39	17 26	23 26	37 39
7	189	12 75	17 0	90	17 4	17 2	13 07	17 64	22 86	37 31
8	196	10 75	19 5	65	21 2	18 8	12 56	17 19	23 01	37 29
9	200	12 50	20 0	59	19 2	16 8	12 63	17 53	23 11	37 38
10	203	10 50	22 5	57	25 9	21 5	12 42	17 40	23 29	37 24
11	205	10.75	18 0	73	22 8	17 6	12 64	17 47	23 06	37 35
12	217	12 75	19 0	86	18 7	17 7	12 86	17 85	22 88	37 29
13	221	10 25	19 0	74	19 8	16 9	12 84	17 80	23 11	37 30
14	224	12 25	20 0	66	23 3	17 4	12 47	17 57	23 12	37 19
15	231	10 50	19 0	65	22 7	17 5	12 61	17 42	23 11	37 22
16	235	13 00	17 0	72	16 9	15 4	12 88	17 79	22 77	37 29
17	260	11 25	19 5	65	20 9	18 1	12 92	17 48	22 72	37 12
18	263	12 25	18 0	65	18 8	14 3	12 99	17 63	22 72	37 19
19	267	11 25	17 0	72	16 4	15 3	13 15	17 92	22 71	37 17
20	270	12 25	13 0	95	9 4	9 9	12 89	18 08	22 69	37 32

Old Haymills

	Mode 5 (Hz)	Remarks	Mean Temp	Mean Humidity	Max Temp (oC)	Min Temp (oC)	Rainfall (mm)	Air Pressure	Upper/Soffit	Soiled Rating
1	40 97		7 5	52	11 1	3 8	0 01	1033 3	2 10	2 0
2	40 85		5 5	68	11 1	0 0	0 00	1023 7	2 40	3 0
3	40 85		9 3	59	13 1	5 4	0 00	1018 9	4 50	5.0
4	40 78		9 9	76	12 3	7 5	0 01	1026 7	2 00	7 0
5	40.72		10.5	69	13 6	7.4	1 00	1015 4	1.50	5 0
6	40 72		16 8	73	22 1	11 5	19.90	1018 6	9 10	8 0
7	40 73		16.7	94	18 5	14 8	2.70	1010 5	0 20	8 0
8	40 68		16 5	69	19 3	13.8	0 30	1012 0	2 40	9 0
9	40.84		16 3	69	19 1	13 5	0 01	1010 3	2 40	6.0
10	40.57		16 3	72	23 1	9.6	0 00	1020 2	4.40	9.0
11	40.64		14 1	91	17 6	10 5	8 10	1005 6	5 20	7 0
12	40 81		17.1	88	19 6	14 5	6 00	1017 1	1 00	7 0
13	40 80		15.2	78	20 4	10 0	0 10	1024 2	2 90	7.0
14	40.50		15 3	58	20.1	10 4	0 00	1020 6	5 90	7 0
15	40 61		14 2	70	21.4	7.0	0 30	1022 2	5.20	8 0
16	40 71		14 5	73	16 9	12.1	2 20	1006 2	1 50	6 0
17	40.51		15 5	67	20 4	10 5	0 01	1019 9	2 80	8 0
18	40.52		10.7	48	18 0	3.4	0 01	1019 1	4 50	7 0
19	40.62	Shot-Blasting	15.0	61	17.0	13 0	0 40	1004 0	1.10	6.0
20	40.83		10.1	91	11 2	9.1	2.70	1006 7	-0.50	6.0

Table A6.3 Parametric data compilation for Old Haymills Bridge

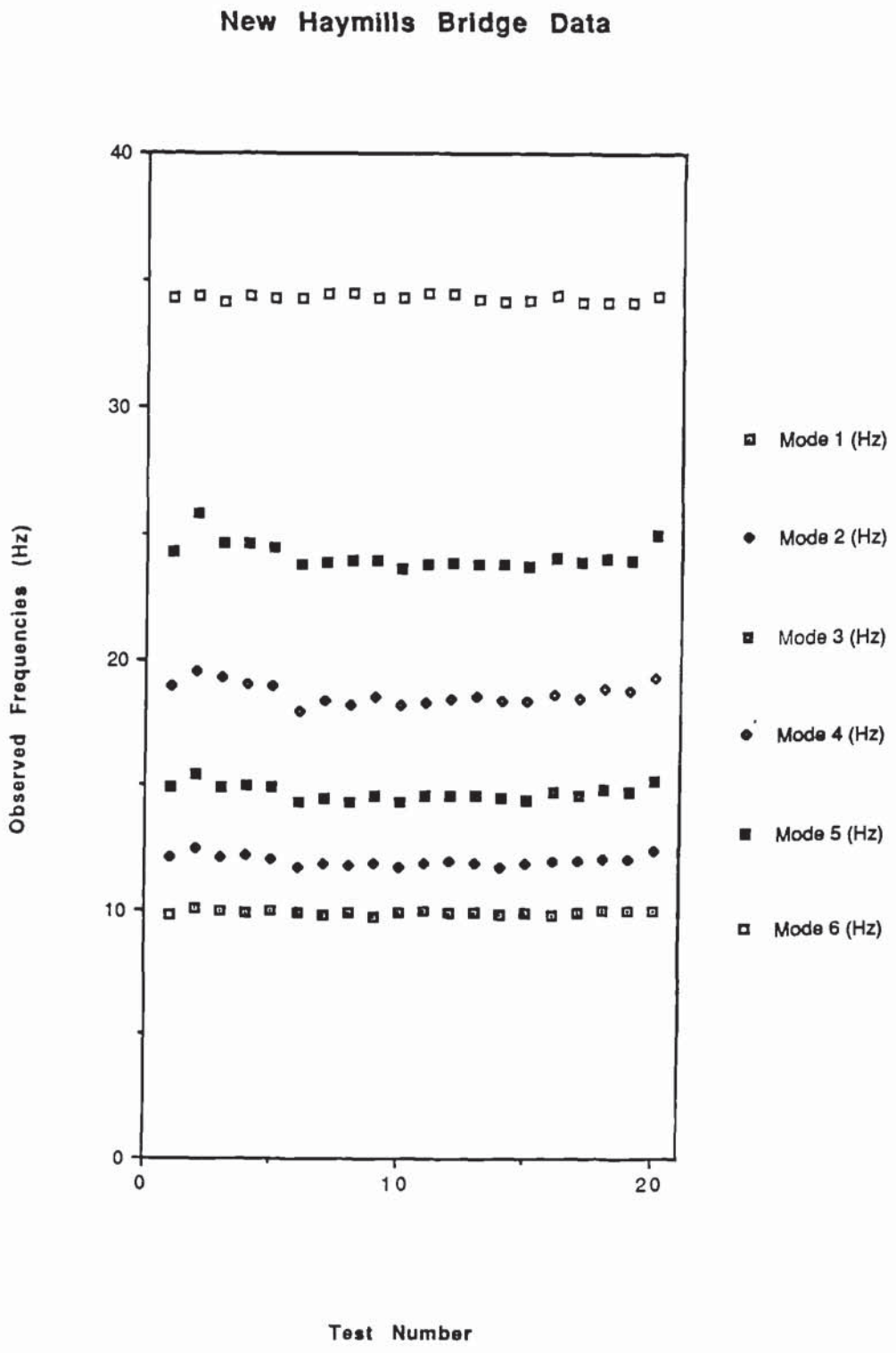

Figure A6.4 Observed response frequencies of New Haymills Bridge

New Haymills

	Event Day	Event Time	Site Temp (oC)	Site Humidity	Upperdeck (oC)	Soffit (oC)	Mode 1 (Hz)	Mode 2 (Hz)	Mode 3 (Hz)	Mode 4 (Hz)
1	106	14 50	12 0	48	16 3	10 9	9 79	12 15	14 94	19 00
2	113	10 50	11 0	66	10 5	7 9	10 05	12 47	15 48	19 59
3	128	13 75	13 5	60	16 7	10 7	9 92	12 16	14 92	19 32
4	149	10 75	11 5	78	11 3	10 0	9 91	12 21	15 00	19 04
5	168	11 50	13 0	74	14 0	11 6	9 95	12 10	14 97	18 96
6	183	11 50	21.5	68	26 4	18 1	9 88	11 73	14 37	17 95
7	189	12 00	17.0	90	17 2	17 3	9 82	11 90	14 52	18 43
8	196	12 00	19 0	65	22 0	17 8	9 90	11 82	14 36	18 23
9	200	11.50	18 0	73	18 3	16 5	9 74	11 93	14 56	18 54
10	203	12 25	23 0	55	27 8	19 6	9 85	11 74	14 38	18 23
11	205	12 25	16.0	81	21 8	17 0	9 97	11 90	14 60	18 35
12	217	12 00	19 0	82	18 5	17 8	9 86	11 95	14 57	18 50
13	221	11 50	20 0	74	19 2	16 1	9 89	11 94	14 63	18 60
14	224	10 50	19 0	74	21 2	17 3	9 82	11 77	14 53	18 37
15	231	11 75	21 0	60	20 3	16 6	9 87	11 87	14 41	18 37
16	235	12 00	18 0	65	16 6	15 2	9 75	12 00	14 77	18 66
17	260	12 50	21.0	60	20 9	17 5	9 84	11 98	14 57	18 48
18	263	11 25	16 5	67	17 6	14 3	9 98	12 10	14 84	18 91
19	267	12 25	20 0	59	16 7	14 8	9 98	12 05	14 77	18 81
20	270	11 50	11.0	94	10 1	10 4	9 97	12 37	15 19	19 33

New Haymills

	Mode 5 (Hz)	Mode 6 (Hz)	Mean Temp	Mean Humidity	Max Temp (oC)	Min Temp (oC)	Rainfall (mm)	Air Pressure	Upper/Soffit	Settled Rating
1	24.27	34.35	7.5	52	11.1	3 8	0 01	1033 3	5 40	2.0
2	25.79	34.43	5.5	69	11 1	0 0	0 00	1023 7	2 60	3 0
3	24.64	34.20	9 3	61	13.1	5 4	0 00	1018 9	6 00	5 0
4	24.64	34 40	9.9	77	12 3	7.5	0 01	1026 7	1 30	7 0
5	24.46	34 35	10.5	70	13 6	7 4	1 00	1015 4	2 40	5 0
6	23.76	34.34	16.8	76	22.1	11 5	19 90	1018 6	8 30	8 0
7	23.89	34.50	16.7	95	18 5	14 8	2.70	1010 5	-0 10	8.0
8	23.94	34.50	16.5	66	19.3	13 8	0 30	1012 0	4 20	9.0
9	23.98	34.37	16.3	70	19.1	13.5	0 01	1010 3	1 80	6 0
10	23 66	34.36	16.3	64	23.1	9.6	0.00	1020 2	8 20	9.0
11	23.82	34.51	14 1	89	17.6	10 5	8 10	1005 6	4 80	7.0
12	23.88	34.49	17.1	90	19.6	14.5	6.00	1017 1	0 70	7 0
13	23.80	34.30	15.2	76	20.4	10.0	0 10	1024 2	3 10	7.0
14	23.78	34.21	15.3	66	20.1	10.4	0 00	1020 6	3.90	7 0
15	23.71	34.22	14.2	64	21.4	7.0	0 30	1022.2	3.70	8.0
16	24.03	34.40	14.5	70	16 9	12.1	2 20	1006 2	1.40	6.0
17	23.87	34.15	15.5	63	20 4	10.5	0 01	1019.9	3.40	8.0
18	24.02	34.14	10.7	53	18.0	3.4	0.01	1019.1	3.30	7.0
19	23.95	34.16	15.0	56	17.0	13.0	0.40	1004.0	1.90	6.0
20	24.99	34.47	10.1	92	11.2	9.1	2.70	1006 7	-0.30	6.0

Table A6.4 Parametric data compilation for New Haymills Bridge

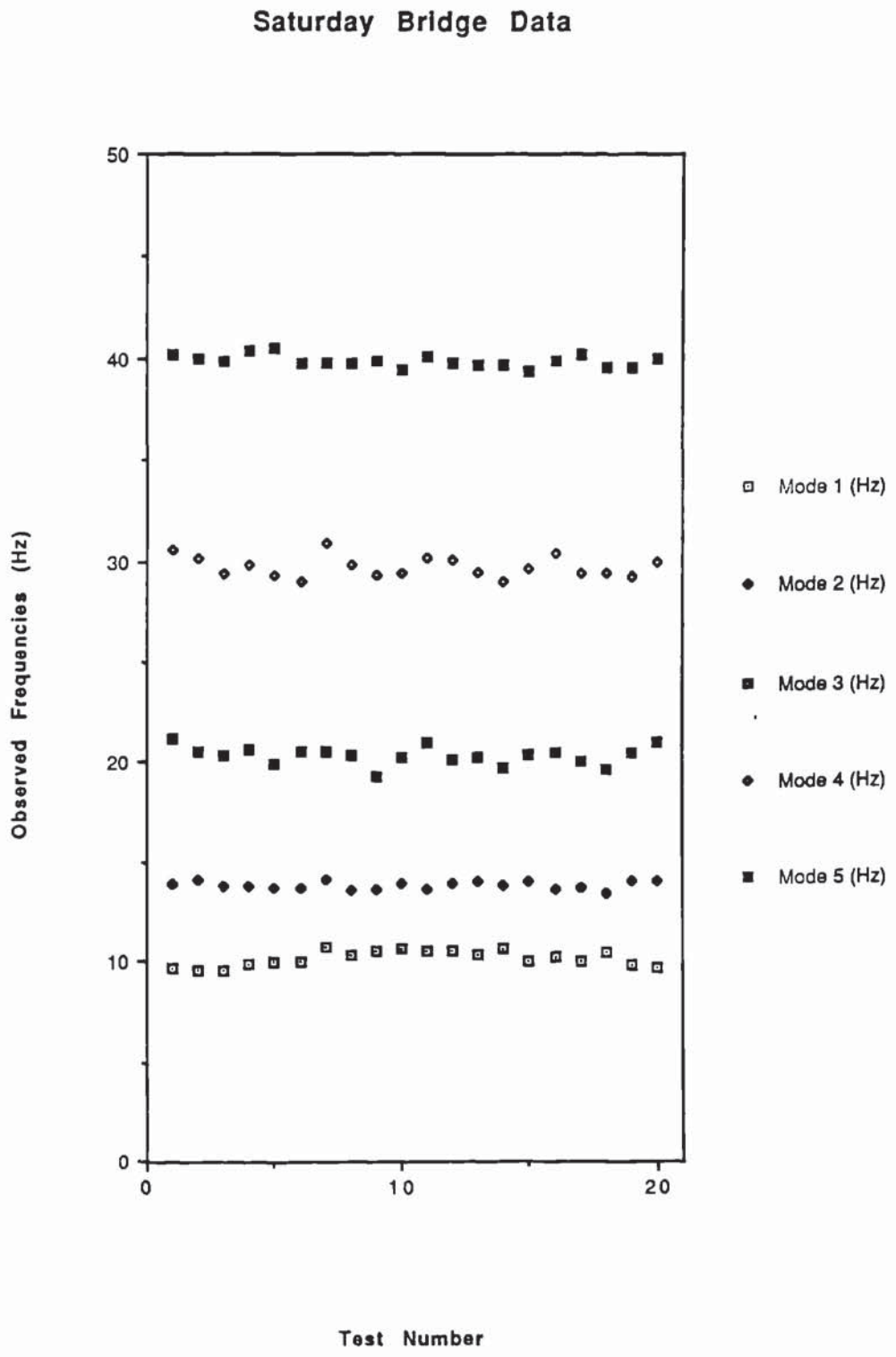

Figure A6.5 Observed response frequencies of Saturday Bridge

Saturday

Event Day	Event Time	Site Temp (oC)	Site Humidity	Upperdeck (oC)	Soffit (oC)	Mode 1 (Hz)	Mode 2 (Hz)	Mode 3 (Hz)	Mode 4 (Hz)
1 107	10 25	4 5	85	5 8	4 7	9 67	13 88	21 20	30 55
2 114	10 75	13 0	59	13 6	9 3	9 59	14 15	20 61	30 16
3 129	10 25	15 0	44	15 3	10 1	9 59	13 86	20 41	29 47
4 150	11 00	11 5	83	10 8	10 1	9 96	13 84	20 71	29 90
5 168	14.50	15 0	61	17 3	12 5	10 04	13 68	19 96	29 30
6 183	9.50	17 5	77	19 2	16 7	10 02	13 69	20 62	29 06
7 189	15.50	20 0	83	18 6	18 4	10 80	14 11	20 62	30 94
8 196	9.00	17 0	81	16 5	16 4	10 37	13 66	20 38	29 83
9 200	14.75	20 0	59	20 4	17 7	10 50	13 66	19 34	29 29
10 203	8.75	20 0	70	21 5	18 5	10 61	13 93	20 22	29 40
11 205	9.00	15 0	90	14 9	14 7	10 56	13 58	20 97	30 12
12 217	14.75	20 0	83	19 9	19 0	10 54	13 97	20 20	30 05
13 221	8.75	16 0	81	14 6	14 8	10 30	13 99	20 28	29 45
14 224	14 00	20 0	59	24 5	18 8	10 62	13 78	19 72	29 02
15 231	8.75	14 0	79	14 7	14 3	9 97	14 06	20 32	29 61
16 235	14 00	17 0	81	15 5	15 1	10 18	13 65	20 42	30 33
17 260	9.25	16 0	81	16 2	15 3	10 03	13 68	20 04	29 40
18 263	14.50	18 5	53	21 6	16 8	10 45	13 41	19 57	29 45
19 267	9.25	16 0	81	13 9	13 7	9 80	14 00	20 51	29 19
20 270	14.50	11.0	94	9.9	10.4	9 72	14 00	20 94	29 96

Mode 5 (Hz)	Mean Temp	Mean Humidity	Max Temp (oC)	Min Temp (oC)	Rainfall (mm)	Air Pressure	Upper/Soffit	Settled Rating
1 40.16	3.9	67	7.2	0 6	0 60	1029 5	1.10	2 0
2 39 99	9 5	55	12.5	6 4	0 01	1018 7	4.30	3 0
3 39 91	7.9	60	13 9	2 0	0 00	1020 8	5 20	5 0
4 40.40	10.1	87	11 5	8 8	0.01	1025.7	0.70	7 0
5 40.54	10 5	72	13.6	7 4	1.00	1015 4	4 80	5 0
6 39 82	16 8	84	22.1	11.5	19.90	1018 6	2 50	8.0
7 39 78	16 7	92	18 5	14.8	2.70	1010 5	0 20	8 0
8 39 80	16 5	74	19 3	13 8	0 30	1012 0	0 10	9 0
9 39.85	16 3	69	19.1	13 5	0 01	1010.3	2.70	6 0
10 39 49	16.3	82	23.1	9.6	0 00	1020 2	3 00	9 0
11 40 04	14 1	94	17.6	10 5	8 10	1005 6	0 20	7.0
12 39 82	17.1	85	19 8	14 5	6 00	1017.1	0.90	7.0
13 39 64	15.2	80	20.4	10 0	0.10	1024 2	-0.20	7 0
14 39.71	15.3	58	20.1	10.4	0.00	1020 6	5 70	7.0
15 39.39	14.2	78	21.4	7.0	0.30	1022.2	0.40	8 0
16 39.84	14.5	76	16.9	12.1	2.20	1006.2	0.40	6.0
17 40.23	15.5	77	20.4	10.5	0.01	1019 9	0.90	8.0
18 39.54	10.7	56	18.0	3.4	0.01	1019 1	4.80	7.0
19 39 54	15.0	73	17.0	13.0	0 40	1004 0	0 20	6.0
20 39.94	10.1	91	11.2	9.1	2.70	1006.7	-0.50	6.0

Table A6.5 Parametric data compilation for Saturday Bridge

A6.2 Curve-Fit Correlation Data

Tabulated here are the parametric frequency curve-fit correlation results for all the bridge-sites.

Linear Curve-fit Correlation, R^2, And Observed Trend Quality ( ): Fordrough

(Cont'd.

Mode No. / Parameter	1	2	3	4	5	6	7
Daily Rainfall	0·097 (None)	0 200 (None)	0·111 (None)	0·153 (None)	0·141 (None)	0·470 (None)	0·021 (None)
Air Pressure	0 035 (None)	0 021 (None)	0 004 (None)	0 000 (None)	0 005 (None)	0 856 (Good)	0 002 (None)
Black-Top / Upper-deck	0·178 (None)	0·278 (General)	0·374 (General)	0·483 (General)	0·450 (General)	0·512 (General)	0·002 (None)
Black-Top / Soffit	0·312 (General)	0·222 (General)	0·354 (General)	0·504 (General)	0·459 (General)	0·459 (General)	0·001 (None)
Upper-deck / Soffit	0·429 (General)	0·132 (General)	0·263 (None)	0·416 (General)	0·370 (General)	0·384 (General)	0·000 (None)
Settled Rating	0·390 (General)	0·488 (General)	0·377 (None)	0·390 (General)	0·415 (General)	0·620 (General)	0·074 (None)

Gradient Comparisons:

Observed Mode Gradient (Hz/°C)	2	3	4	5
Site Temp.	-5·3182 x10·2	-0·11395	-0·22083	-0·36017
Soffit Temp.	-6·0435 x10·2	-0·12429	-0·23737	-0·38935
Gradient Ratio	0·880	0·917	0·930	0·925

Mean Ratio 0·913

Linear Curve-fit Correlation, R^2, And Observed Trend Quality ( ): Fordrough

Mode No. / Parameter	1	2	3	4	5	6	7
Event Time	0·347 (None)	0·207 (General)	0·287 (General)	0 475 (General)	0 421 (General)	0 165 (None)	0 011 (None)
Site Temp	0·634 (General)	0·815 (V.Good)	0·755 (V.Good)	0·824 (V.Good)	0·810 (V.Good)	0 635 (General)	0 065 (None)
Site Humidity	0 222 (None)	0·020 (None)	0·125 (None)	0·240 (None)	0·187 (None)	0·239 (None)	0 030 (None)
Blacktop Temp	0·610 (General)	0·670 (Good)	0·710 (Good)	0 855 (Good)	0 820 (V.Good)	0·584 (General)	0 048 (None)
Upper-deck Temp	0·776 (General)	0·777 (V.Good)	0·760 (Good)	0 896 (V.Good)	0·867 (V.Good)	0·645 (General)	0·075 (None)
Soffit Temp	0·753 (Good)	0·879 (Excellent)	0·750 (V.Good)	0·785 (V.Good)	0·790 (V.Good)	0·949 (V.Good)	0·130 (None)
Mean Temp	0·499 (General)	0·731 (General)	0·536 (General)	0·534 (General)	0·565 (General)	0·381 (General)	0·139 (None)
Mean Humidity	0·014 (None)	0·010 (None)	0·017 (None)	0·043 (None)	0·037 (None)	0·005 (None)	0·105 (None)
Max Temp	0·633 (General)	0·789 (Good)	0·739 (Good)	0·729 (Good)	0·734 (Good)	0·849 (Good)	0·122 (None)
Min Temp	0·191 (None)	0·421 (General)	0·207 (None)	0·204 (None)	0·242 (None)	0·034 (None)	0·095 (None)

Table A6.6 Curve-fit correlations for Fordrough Bridge

Table A6.7 Curve-fit correlations for River Cole Bridge

Linear Curve-fit Correlation, R^2, And Observed Trend Quality ( ): River Cole

Mode No. / Parameter	1	2	3	4	5	6
Event Time	0·267 (None)	0·568 (General)	0·684 (General)	0·152 (None)	0·447 (General)	0 404 (General)
Site Temp	0·652 (General)	0 912 (V.Good)	0·971 (Excellent)	0 033 (None)	0 439 (General)	0 895 (V.Good)
Site Humidity	0·005 (None)	0·027 (None)	0·071 (None)	0 001 (None)	0 285 (None)	0 036 (None)
Upper-deck Temp	0·552 (General)	0·841 (Good)	0·927 (V.Good)	0·070 (None)	0 500 (General)	0·860 (Good)
Soffit Temp	0·713 (Good)	0·949 (Excellent)	0·962 (Excellent)	0·020 (None)	0·335 (General)	0·919 (Excellent)
Mean Temp	0·732 (General)	0·789 (Good)	0·717 (Good)	0·004 (None)	0·122 (None)	0·773 (Good)
Mean Humidity	0·000 (None)	0·034 (None)	0·070 (None)	0·122 (None)	0·303 (None)	0·040 (None)
Max Temp	0·547 (General)	0·786 (Good)	0·751 (Good)	0·070 (None)	0·320 (None)	0·652 (Good)
Min Temp	0·594 (General)	0·450 (General)	0·380 (None)	0·031 (None)	0·001 (None)	0·643 (General)

Linear Curve-fit Correlation, R^2, And Observed Trend Quality ( ): River Cole (Cont d

Mode No. / Parameter	1	2	3	4	5	6
Daily Rainfall	0·117 (None)	0·138 (None)	0·153 (None)	0 181 (None)	0·079 (None)	0·262 (None)
Air Pressure	0·265 (None)	0 060 (None)	0·051 (None)	0 029 (None)	0·007 (None)	0·230 (None)
Upper-deck / Soffit	0·174 (None)	0·401 (None)	0·546 (General)	0·128 (None)	0·621 (Good)	0·192 (General)
Settled Rating	0·451 (General)	0·713 (Good)	0·651 (General)	0·031 (None)	0·169 (General)	0·548 (Good)

Gradient Comparisons:

Observed Mode Gradient (Hz/°C)	2		3	6
Site Temp.	-6·9964 x10^{-2}		-0·16301	-0·17258
Soffit Temp.	-7·4966 x10^{-2}		-0·17046	-0·16553
Gradient Ratio (<1)	0·933		0·956	0·959
		Mean Ratio	0·950	

Linear Curve-fit Correlation, R^2, And Observed Trend Quality ( ): Oldhaymills

Mode No. Parameter	1	2	3	4	5
Event Time	0·244 (None)	0·048 (None)	0·062 (None)	0·044 (None)	0·481 (General)
Site Temp	0·646 (Good)	0·573 (General)	0·493 (General)	0·034 (None)	0·386 (General)
Site Humidity	0·042 (None)	0·145 (None)	0·094 (None)	0·055 (None)	0·009 (None)
Upper-deck Temp	0·625 (Good)	0·724 (Good)	0·646 (Good)	0·014 (None)	0·338 (General)
Soffit Temp	0·541 (General)	0·679 (Good)	0·545 (Good)	0·033 (None)	0·392 (Good)
Mean Temp	0·460 (General)	0·437 (General)	0·393 (General)	0·002 (None)	0·326 (General)
Mean Humidity	0·041 (None)	0·001 (None)	0·013 (None)	0·198 (None)	0·041 (None)

Linear Curve-fit Correlation, R^2, And Observed Trend Quality ( ): Oldhaymills (Cont'd

Mode No. Parameter	1	2	3	4	5
Upper-deck / Soffit	0·338 (None)	0·330 (None)	0·367 (None)	0·001 (None)	0·084 (None)
Settled Rating	0·531 (General)	0·444 (General)	0·304 (General)	0·003 (None)	0·525 (General)
Max Temp	0·559 (General)	0·600 (General)	0·498 (General)	0·054 (None)	0·404 (General)
Min Temp	0·213 (None)	0·161 (None)	0·166 (None)	0·020 (None)	0·159 (None)
Daily Rainfall	0·157 (None)	0·107 (None)	0·125 (None)	0·174 (None)	0·018 (None)
Air Pressure	0·040 (None)	0·000 (None)	0·002 (None)	0·000 (None)	0·191 (None)

Table A6.8 Curve-fit correlations for Old Haymills Bridge

Linear Curve-fit Correlation, R^2, And Observed Trend Quality ( ): Newhaymills

Mode No. / Parameter	1	2	3	4	5	6
Event	0·030	0·001	0·011	0·000	0 059	0 008
Time	(None)	(None)	(None)	(None)	(None)	(None)
Site	0·388	0·728	0·755	0·692	0·770	0 085
Temp	(General)	(Good)	(Good)	(General)	(Good)	(None)
Site	0·000	0·014	0 011	0 001	0 002	0 296
Humidity	(None)	(None)	(None)	(None)	(None)	(None)
Upper-deck	0·330	0·825	0·773	0·729	0·593	0·021
Temp	(General)	(Good)	(Good)	(Good)	(General)	(None)
Soffit	0·500	0·869	0·897	0·917	0·860	0 000
Temp	(Good)	(V.Good)	(V.Good)	(Excellent)	(V.Good)	(None)
Mean	0·556	0·752	0·806	0·797	0·638	0·003
Temp	(General)	(Good)	(Good)	(Good)	(General)	(None)
Mean	0·022	0·000	0·001	0·010	0·032	0·537
Humidity	(None)	(None)	(None)	(None)	(None)	(General)
Max	0·474	0·808	0·824	0·790	0·816	0 037
Temp	(General)	(Good)	(Good)	(Good)	(Good)	(None)
Min	0·366	0·406	0·465	0·479	0·228	0·085
Temp	(None)	(Good)	(Good)	(Good)	(None)	(None)

Linear Curve-fit Correlation, R^2, And Observed Trend Quality ( ): Newhaymills (Cont'd

Mode No / Parameter	1	2	3	4	5	6
Daily	0·006	0·116	0·088	0 049	0·079	0·073
Rainfall	(None)	(None)	(None)	(None)	(None)	(None)
Air	0·055	0 014	0 019	0 039	0·053	0·067
Pressure	(None)	(None)	(None)	(None)	(None)	(None)
Upper deck	0 026	0·201	0·138	0·048	0 031	0·069
/ Soffit	(None)	(None)	(None)	(None)	(None)	(None)
Settled	0·521	0·515	0·605	0·573	0·354	0·000
Rating	(General)	(General)	(General)	(General)	(General)	(None)

Gradient Comparisons:

	2	3	5
Observed Mode Gradient (Hz/°C)			
Site Temp.	-4·4257 x10^{-2}	-6·7680 x10^{-2}	-7·7665 x10^{-2}
Soffit Temp.	-5·4658 x10^{-2}	-8·3335 x10^{-2}	-9·6660 x10^{-2}
Gradient Ratio	0·810	0·812	0·803
		Mean Ratio 0·808	

Table A6.9 Curve-fit correlations for New Haymills Bridge

Linear Curve-fit Correlation, R^2, And Observed Trend Quality ( ):					Saturday
Mode No. Parameter	1	2	3	4	5
Event Time	0·098 (None)	0 014 (None)	0 024 (None)	0 001 (None)	0·215 (General)
Site Temp	0·567 (General)	0·041 (None)	0·494 (General)	0·353 (General)	0·780 (Good)
Site Humidity	0·002 (None)	0·049 (None)	0·102 (None)	0·202 (None)	0 050 (None)
Upper-deck Temp	0·520 (General)	0·104 (None)	0·481 (General)	0·417 (General)	0·751 (Good)
Soffit Temp	0·721 (Good)	0·055 (None)	0·406 (General)	0·281 (General)	0·729 (Good)
Mean Temp	0·477 (General)	0·003 (None)	0·398 (General)	0·208 (General)	0·636 (General)
Mean Humidity	0·078 (None)	0·029 (None)	0·014 (None)	0·033 (None)	0·001 (None)

Linear Curve-fit Correlation, R^2, And Observed Trend Quality ( ):					Saturday (Cont'd)
Mode No. Parameter	1	2	3	4	5
Max Temp	0 414 (General)	0·021 (None)	0·534 (General)	0 338 (General)	0·655 (Good)
Min Temp	0·326 (None)	0·003 (None)	0·145 (None)	0·044 (None)	0·506 (General)
Daily Rainfall	0·005 (None)	0·031 (None)	0·040 (None)	0·009 (None)	0·007 (None)
Air Pressure	0·042 (None)	0·017 (None)	0·008 (None)	0·000 (None)	0·063 (None)
Upper-deck / Soffit	0·001 (None)	0·065 (None)	0·017 (None)	0·182 (None)	0·034 (None)
Settled Rating	0·395 (General)	0·032 (None)	0·315 (General)	0·207 (General)	0·567 (Good)

Table A6.10 Curve-fit correlations for Saturday Bridge